

**RECOVERY AND KINETICS
STUDY OF ISOELECTRIC
PRECIPITATION OF SUNFLOWER
PROTEIN IN A TUBULAR
PRECIPITATOR**

A Thesis Submitted to the College of
Graduate Studies and Research
in Partial Fulfilment of the Requirements
for the Degree of Doctor of Philosophy
in the Department of Chemical Engineering
University of Saskatchewan
Saskatoon

By
Matheo Lue Raphael
Fall 1997



National Library
of Canada

Acquisitions and
Bibliographic Services

395 Wellington Street
Ottawa ON K1A 0N4
Canada

Bibliothèque nationale
du Canada

Acquisitions et
services bibliographiques

395, rue Wellington
Ottawa ON K1A 0N4
Canada

Your file Votre référence

Our file Notre référence

The author has granted a non-exclusive licence allowing the National Library of Canada to reproduce, loan, distribute or sell copies of this thesis in microform, paper or electronic formats.

The author retains ownership of the copyright in this thesis. Neither the thesis nor substantial extracts from it may be printed or otherwise reproduced without the author's permission.

L'auteur a accordé une licence non exclusive permettant à la Bibliothèque nationale du Canada de reproduire, prêter, distribuer ou vendre des copies de cette thèse sous la forme de microfiche/film, de reproduction sur papier ou sur format électronique.

L'auteur conserve la propriété du droit d'auteur qui protège cette thèse. Ni la thèse ni des extraits substantiels de celle-ci ne doivent être imprimés ou autrement reproduits sans son autorisation.

0-612-23969-1

UNIVERSITY OF SASKATCHEWAN
College of Graduate Studies and Research
SUMMARY OF DISSERTATION
Submitted in partial fulfilment
of the requirements for the
DEGREE OF DOCTOR OF PHILOSOPHY
by
Matheo Lue Raphael
Department of Chemical Engineering
University of Saskatchewan
Fall 1997

Examining Committee:

Dr. D.J. Carrier	Dean/Associate Dean, Deans's Designate, Chair College of Graduate Studies and Research
Dr. J. Postlethwaite	Chair of Advisory Committee, Department of Chemical Engineering
Dr. S. Rohani	Supervisor, Department of Chemical Engineering
Dr. F. Sosulski	Co-supervisor, Department of Crop Science and Plant Ecology
Dr. D. G. MacDonald	Department of Chemical Engineering
Dr. G. Hill	Department of Chemical Engineering
Dr. P. R. Chang	Canada Agriculture Research Station

External Examiner:

Dr. D. Kirwan
Chemical Engineering Department
University of Virginia
Charlottesville, VA 22903-2442

Recovery and Kinetics Study of Isoelectric Precipitation of Sunflower Protein in a Tubular Precipitator

Defatted sunflower meal contains substantial amount of nutritious protein which is recoverable by extraction and precipitation methods. For effective recovery of the solid proteins from the solids-liquid suspension, it is imperative to have large particles with a narrow spread in their size distribution and high solids concentration.

In this research, up to 97 % w/w and 65 % w/w of the proteins in the laboratory and industrially defatted sunflower meals, respectively, were extracted using aqueous alkaline solutions at pH 10.0. Up to 84 % of these soluble proteins were recovered as solids when the pH was lowered to isoelectric pH using aqueous HCl acid.

Three types of the precipitator configuration were used in this study, the batch, mixed suspension mixed product removal (MSMPR), and the tubular precipitators. The batch precipitator was found to produce precipitates with high solids concentrations (yield), but small mean particle sizes ($< 10 \mu\text{m}$) with narrow spread in the particle size distribution (PSD). The MSMPR precipitator produced low solids yields and medium particle sizes (ca. 10 to 20 μm) with a wide spread in the PSD. High concentrations of the protein in the feed solution resulted in bimodal PSD. The tubular precipitator operating in turbulent flow regime produced precipitates similar to the batch precipitator. In the laminar flow regime, the tubular precipitator produced large particles (aggregates) which increased in size with increases in the mean residence time and protein concentration in the feed solution.

A population balance equation (PBE) describing the precipitation of sunflower proteins in the tubular precipitator was developed. The equation included the growth of protein particles by the molecular mechanism and by the aggregation. Also, the breakage of protein particles by turbulent collisions and hydrodynamic forces (Glatz et al., 1986) was included. The flow dispersions along the tubular precipitator were introduced in the equation as a dimensionless group, Pe number. The resulting steady state PBE was a non-linear integral-differential equation. This model equation was solved numerically using the Orthogonal Collocation-Multiple Shooting Method. Determination of the precipitation kinetic parameters from the experimental data is described. In addition, a comparison between the model predictions and the experimental data is presented.

PERMISSION TO USE

In presenting this thesis in partial fulfilment of the requirements for a Postgraduate degree from the University of Saskatchewan, I agree that the Libraries of this University may make it freely available for inspection. I further agree that permission for copying of this thesis in any manner, in whole or in part, for scholarly purposes may be granted by the professor or professors who supervised my thesis work or, in their absence, by the Head of the Department or the Dean of the College in which my thesis work was done. It is understood that any copying or publication or use of this thesis or parts thereof for financial gain shall not be allowed without my written permission. It is also understood that due recognition shall be given to me and to the University of Saskatchewan in any scholarly use which may be made of any material in my thesis.

Requests for permission to copy or to make other use of material in this thesis in whole or part should be addressed to:

Head of the Department of Chemical Engineering
University of Saskatchewan
Saskatoon, Saskatchewan, S7N 5C9.

ABSTRACT

Oilseed sunflower is one of the major vegetable oil sources. The residue after the extraction of oil (defatted meal, DM) contains a substantial amount of nutritious protein which is recoverable by extraction and precipitation methods. For effective recovery of the solid proteins from the solids-liquid suspension, it is imperative to have large particles with a narrow spread in their size distribution and high solids concentration.

In this research, up to 97 % w/w and 65 % w/w of the proteins in the laboratory and industrially defatted sunflower meals, respectively, were extracted using aqueous alkaline solutions at pH 10.0. Up to 84 % of these soluble proteins were recovered as solids when the pH was lowered from 10.0 to 4.0 (isoelectric pH) using aqueous HCl acid. The amount of proteins recovered as solids decreased with decreasing concentrations of the acid.

Three types of precipitator configuration were used in this study: the batch, mixed suspension mixed product removal (MSMPR), and the tubular precipitators. Factors affecting the particle size distributions and the solids yield were studied. The batch precipitator was found to produce precipitates with high solids concentrations (yield), but small mean particle sizes ($< 10\ \mu\text{m}$) with narrow spread in the particle size distribution (PSD). The MSMPR precipitator produced low solids yields and medium particle sizes (ca. 10 to 20 μm) with a wide spread in the PSD. High concentrations of the protein in the feed solution resulted in bimodal PSD. The tubular precipitator operating in turbulent flow regime produced precipitates with small particles and a narrow size distribution similar to the batch precipitator. In the laminar flow regime, the tubular precipitator produced large particles (aggregates) which increased in size with increases in the mean residence time and protein concentration in the feed solution. These sizes increased from ca. 10 μm to ca. 40 μm . The solids yield for the tubular precipitator increased with mean residence time at both flow regimes. Solids yields in the laminar flow regime were

as high as those obtained from the batch precipitator.

Solutions of the population balance equations describing the batch and MSMR precipitators have been developed extensively for several precipitating systems. Before this study, there have been only two studies documenting the population balance equation for protein precipitation in the tubular precipitator. These previous studies dealt with simplified models which neglected particle aggregations and particle breakages which are the prevalent mechanisms for protein particle growth. A model (population balance equation) equation describing the precipitation of sunflower proteins in the tubular precipitator was developed. The model included the growth of protein particles by the molecular mechanism and by the aggregation method. Also, the breakage of protein particles by turbulent collisions and hydrodynamic forces (Glatz et al., 1986) was included in the model. The decreases in protein concentration as the solution flowed down the tubular precipitator were included in the molecular particle growth and in the nucleation model equations. The flow dispersions along the tubular precipitator were introduced in the model equation as a dimensionless group, Pe number. The resulting steady state population balance equation was a non-linear integral-differential equation. This model equation was solved numerically using the Orthogonal Collocation-Multiple Shooting method. This method transformed the non-linear integral-differential equation into a set of ordinary differential equations. Simulation parameters showed that this solution method was flexible to fit the two sets of boundary condition data using a wide range (different values) of model parameters. Based on the experimental results from the tubular precipitator, the global optimization method was used to determine the optimum parameters for the model equations. A total of 11 parameters describing the precipitation kinetics of sunflower proteins in a tubular precipitator were obtained.

The developed model equations were used to predict the experimental data (mean particle size) from the tubular precipitator. The differences between the model predictions and the experimental data were about 25 % for particles with small mean sizes ($< 10 \mu\text{m}$) and less for large particles. With these model parameters, it is possible to predict the length of the tubular precipitator required to obtain precipitates with the desired PSD and solids concentration. The required inputs to the model are the precipitator geometry (diameter of the tubular precipitator and the length) and the

operating conditions (flow velocity, protein feed concentration, and starting PSD at a known location close to the static mixers).

ACKNOWLEDGMENTS

I would like to express my sincere appreciation to my supervisor, Dr. S. Rohani and the co-supervisor Dr. F. Sosulski, for their patient instructions and continued interests in this research. I thank Dr. J. Postlethwaite for chairing my graduate committee, Dr. D. G. Macdonald, Dr. G. Hill, and Dr. P. R. Chang for participating on my graduate committee.

I am indebted to the faculty and graduate students of the Chemical Engineering Department at University of Saskatchewan for their cooperation. Mr. H. W. Braitenbach of Crop Science Department, Mr. W. Woodward of Engineering Workshop, Mr. T. Wallentiny, Mr. T. Redman, and Ms. K. Burlock of Chemical Engineering Department provided valuable assistance for which I am very thankful.

I must also thank the University of Saskatchewan, TAN047 Project, UDSM, and the Chemical and Process Engineering Department of the University of Dar-Es-Salaam, for the fellowship they provided during my graduate studies. Finally, my sincere thanks to my family for their continued support.

DEDICATION

Dedicated to F.R.E.D.

TABLE OF CONTENTS

	Page
COPYRIGHT	i
ABSTRACT	ii
ACKNOWLEDGEMENTS	v
DEDICATION	vi
TABLE OF CONTENTS	vii
LIST OF TABLES	xii
LIST OF FIGURES	xv
NOMENCLATURE	xx
 CHAPTER 1. INTRODUCTION	
1.1 Background	1
1.2 Research Objectives	3
 CHAPTER 2. LITERATURE REVIEW	5
2.1 Oilseed Proteins	5
2.1.1 Composition of Oilseed Proteins	5
2.1.2 Solubility of Proteins in Aqueous Solutions	7
2.1.3 Sunflower Proteins and Their Composition	11
2.2 Recovery Process of Oilseed Proteins by Precipitation	15
2.3 Previous Studies on Oilseed Protein Precipitation	21
2.3.1 Precipitation Studies Using Batch Precipitators	21
2.3.2 Precipitation Studies Using Mixed-Stirred Precipitators	22
2.3.3 Precipitation Studies using Tubular Precipitators	23
2.3.4 Precipitation Kinetics	26

2.4	Other Related Studies on Crystallization and Precipitation	32
2.4.1	Studies on Particle Aggregation and Breakage	32
2.4.2	Studies on Precipitation in Batch Precipitators	33
2.4.3	Precipitation Studies in Mixed Suspension Mixed Product Removal Precipitators (MSMPRP)	34
2.4.4	Precipitation Studies in Plug Flow and Dispersed Flow Precipitators	37
2.5	Particle Size Distribution (PSD)	38
2.6	Population Balance Equation (PBE) and Solution Methods	39
CHAPTER 3. EXPERIMENTAL METHODS		44
3.1	Preliminary Experiments	44
3.1.1	Sunflower Protein Solubility and Solids Yield	44
3.1.2	Functional Properties of Sunflower Protein Isolates	47
3.1.3	Inhibition of Discoloration of Sunflower Protein Isolates	47
3.1.4	Effects of HCl Concentration (Volumetric Ratio) and Precipitation Temperature on Protein Solubility	48
3.2	Isoelectric Precipitation of Sunflower Protein in a Tubular Precipitator	50
3.2.1	Description of the Experimental Set-up	50
3.2.2	Residence Time Distribution (RTD) Studies	53
3.2.3	Selection of Precipitation Conditions and Experimental Design	53
3.2.4	Preparation of Sunflower Protein Feed Solutions	54
3.2.5	Effect of Fluid-Induced Shear on Particle Size Distribution	55
3.2.6	Effect of the Precipitator Length	55
3.2.7	Effect of Static Mixers	57
3.3	Comparison With MSMPR and Batch Precipitators	57
3.3.1	Experimental Set-up for the MSMPR and Batch Precipitators	57
3.3.2	Residence Time Distribution (RTD) Studies	62

3.4	Precipitation of Sunflower Protein Using Calcium Acetate	62
3.5	Experimental Measurements	62
3.5.1	Protein Concentration Measurement	62
3.5.2	Solid Protein Concentration Measurement Using Turbidimeter	63
3.5.3	Protein Particle size Distribution Measurement Using Coulter Counter	63
3.5.4	pH Measurement	64
3.5.5	Measurements of Feed Flow Rate	64
3.5.6	Density of Solid Sunflower Protein	65
3.5.7	Estimation of the Experimental Errors	65
CHAPTER 4. EXPERIMENTAL RESULTS AND DISCUSSION		67
4.1	Preliminary Experimental Results	67
4.1.1	Solubility of Sunflower Protein as a Function pH	67
4.1.2	Solubility of Sunflower Protein as Function of NaCl Concentrations	72
4.1.3	Precipitation Yields of Sunflower Protein by Aqueous HCl and Calcium Acetate	72
4.1.4	Effect of Temperature on the Mean Particle Size and Precipitation Yield	78
4.1.5	Some Functional Properties of Sunflower Defatted Meal and Isolate	82
4.1.6	Inhibition of Discoloration of Sunflower Protein Isolates	82
4.1.7	Effects of HCl Concentration and Precipitation Temperature on Protein Solubility	84
4.1.8	Solids Concentration Measurements Using Turbidimetry Method	88
4.2	Tubular Precipitator Results	88
4.2.1	Residence Time Distribution (RTD) Studies	88
4.2.2	Effect of the Static Mixers	89
4.2.3	Effect of the Precipitator Length	93
4.2.4	Effect of the Protein Concentration in the Feed Stream	98

4.2.5	Effects of the Mean Residence Time and Flow Velocity (Flow Regime)	98
4.2.6	Effect of Volumetric Flow Ratio of Feed Solutions	104
4.2.7	Effect of Fluid-Induced Shear on Particle Size Distribution	108
4.3	Comparison Studies of the Tubular Precipitator With the MSMPR and the Batch Precipitators	110
4.3.1	Residence Time Distribution Studies for the MSMPR Precipitator	110
4.3.2	Comparison Between the Tubular and the MSMPR Precipitators: Effects of the Mean Residence Time and the Protein Feed Concentration on the Mean Particle Size and the Solids Concentration	110
4.3.3	Comparison Between the Tubular and the Batch Precipitators: Effects of the Precipitation Time and Protein Feed Concentration on the Mean Particle Size and the Solids Concentration	116
4.3.4	Scanning Electron Micrographs of the Precipitates	123
4.4	Estimation of the Experimental Errors	123
CHAPTER 5. MATHEMATICAL MODELLING		130
5.1	MSMPR Precipitator	130
5.1.1	Fitting of the Aggregation-Breakage Model to the Experimental Data	130
5.1.2	Model Fitting Results	133
5.2	Modelling of a Tubular Precipitator With Particle Aggregation and Breakage	139
5.2.1	Population Balance Equation for the Tubular Precipitator	139
5.2.2	The Solution of the Population Balance Equation	144
5.2.3	Node by Node Calculations	152
5.2.4	Simulation of the Model Solution	155
5.2.5	Determination of Precipitation Kinetic Parameters from Experimental Data	164
5.2.6	Model Predictions of the Experimental Results	169

CHAPTER 6. CONCLUSIONS AND RECOMMENDATIONS	173
6.1 Conclusions and Recommendations on the Three Types of Precipitators and Precipitants Used in This Study for Protein Recovery	173
6.2 Conclusions on Precipitation Kinetic Parameters Obtained From the MSMPR Precipitator Data	174
6.3 Conclusions and Recommendations on the Results of the Tubular Precipitator Modelling	174
REFERENCES	176
APPENDIX A. ESTIMATION OF THE ISOELECTRIC POINT OF SUNFLOWER PROTEIN	185
APPENDIX B. CALIBRATION OF THE TURBIDIMETER FOR ON-LINE MEASUREMENTS OF SOLIDS CONCENTRATION	188
APPENDIX C. MEASUREMENTS OF PSD USING COULTER COUNTER	194
C.1 Determination of the Number of Particles in the Sample (Number Count)	194
C.2 Calculations of the Mean Particle Size and the Coefficient of Variation From the Coulter Counter Data	194
C.3 Calculations of the Population Density From the Coulter Counter Data	195
APPENDIX D. COMPUTER ALGORITHMS FOR SOLVING THE TUBULAR PRECIPITATOR MODEL	199
D.1 Determination of the Optimum Model Parameters From the Experimental Data (Figure D.1)	199
D.2 Model Predictions of the Experimental Data (Figure D.2)	201
VITA	205

LIST OF TABLES

	Page
Table 2.1 Essential amino acid composition of major oilseeds (g/16gN) (Viroben and Bertrand, 1985)	6
Table 2.2 Solubility of proteins (Powrie and Nakai, 1981)	8
Table 2.3 Average composition of sunflower meal as compared with cottonseed and soybean meals (Salunkhe and Desai, 1986)	12
Table 2.4 Amino acid composition of defatted sunflower meal (Sosulski and Fleming, 1977)	13
Table 2.5 Previous studies on preparations of colourless sunflower meals and isolates	14
Table 2.6 Types of precipitants used in protein precipitation (Bell et al., 1983)	19
Table 3.1 Experiments performed in the batch precipitator to determine the effects of volumetric feed ratio and precipitation temperature on protein solubility	49
Table 3.2 List of precipitation experiments performed in the tubular precipitator at a fixed pH 4.0	52
Table 3.3 List of experiments for studies of the effect of fluid-induced shear in the tubular precipitator	56
Table 3.4 List of precipitation experiments performed in the MSMR precipitator at a fixed pH 4.0 and mixer speed at 600 rpm	60
Table 3.5 List of isoelectric precipitation experiments performed in the batch precipitator at a fixed pH 4.0	61
Table 4.1 Properties of samples used in preparations of sunflower protein solution	68
Table 4.2 Nitrogen (protein) balance for precipitates (isolates) obtained at pH 4.0 and 6.0 from alkaline extracts of defatted confectionery-type sunflower meal	76

Table 4.3	Nitrogen (protein) balance for precipitates (isolates) obtained at pH 4.0 and 6.0 from alkaline extracts of defatted oil-type sunflower meal	77
Table 4.4	Some functional properties of sunflower defatted meal from confectionery-type seeds and isolate obtained at pH 4.0	83
Table 4.5	Efficiency of membrane filtration experiments to remove discolouring pigments in the sunflower protein (molecular weight of CA = 354.3 kg/kmol)	85
Table 4.6	Summary of RTD results for the tubular precipitator using KCl solution as a tracer	90
Table 4.7	Calculated local Pe numbers for the tubular precipitator at increasing flow Re numbers used in this study	92
Table 4.8	Comparison between the calculated and the experimental mean residence times for the MSMPR precipitator using PVC particles as a tracer	111
Table 4.9	Experimental results from the MSMPRP: Effects of the mean residence time and the protein feed concentration on the mean particle size, solids concentration, and the coefficient of variation (protein feed concentrations: Runs MS2_series = 11.6 kg/m ³ and Runs MS3_series = 2.9 kg/m ³)	112
Table 4.10	Experimental results of isoelectric precipitation of sunflower protein in a tubular precipitator at pH 4.0: Effects of protein feed concentration, flow Re number, and feed ratio on the mean particle size and solids concentration	126
Table 4.11	Estimations of the experimental errors for the mean particle size and the solids concentration for runs performed in the tubular precipitator	128
Table 5.1	Calculated parameters for the MSMPR precipitator model with protein particles aggregation and breakage (protein feed concentrations: runs MS2_series = 11.6 kg/m ³ and runs MS3_series = 2.9 kg/m ³)	135
Table 5.2	Values of parameters used in the model simulation (reference data)	158
Table 5.3	Summary of the runs in the tubular precipitator used in the determination of precipitation kinetic parameters: experimental conditions and measured mean particle size and CV of samples from ports 2 and 3	165
Table 5.4	Initial estimates of kinetic parameters, the search range used in optimization, and the final optimum values	167

Table 5.5	Deviations between the model calculated (fit using optimum parameters) mean particle sizes and the experimental mean particle sizes from runs used in optimization	170
Table 5.6	Comparison between the model predicted (using optimum parameters) mean particle sizes and the experimental mean particle sizes	171
Table A.1	Values of pK_R and charges of ionizable amino acid groups (Lehninger, 1982)	187
Table C.1	Sample data sheet for calculations of the PSD (particle count, mean particle size, CV, and the population density) from the experimentally measured data using Coulter Counter	197

LIST OF FIGURES

	Page
Figure 2.1 Steps occurring during folding of a polypeptide chain to form a native protein structure (Anfinsen and Scheraga, 1975)	9
Figure 2.2 Approximate distribution of sunflower proteins in defatted meal (Kabirullah and Wills, 1983)	16
Figure 2.3 Flow diagram for preparation of dry protein isolate	18
Figure 2.4 Process flowsheet for solid protein recovery from defatted oilseed meals	20
Figure 3.1 Experimental setup for the tubular precipitator	51
Figure 3.2 Geometrical configuration of an MSMPR precipitator (used also as a batch precipitator)	58
Figure 3.3 Experimental setup for an MSMPR precipitator	59
Figure 4.1 Effect of pH on protein extractability from laboratory and industrially defatted sunflower meals	69
Figure 4.2 Solubility of sunflower proteins from confectionery-type seeds in aqueous solutions at pH 1.0 to 10.0	71
Figure 4.3 Solubility of sunflower proteins in increasing concentrations of aqueous NaCl solution at pH 6.5	73
Figure 4.4 Effects of pH on precipitated protein yields for extracts from laboratory and industrially defatted sunflower meals	74
Figure 4.5 Effects of Ca^{2+} on precipitated protein and mean particle size at pH 6.5 using calcium acetate in a batch precipitator for protein conc. = 10.8 kg/m^3 with 1 M NaCl and feed ratio = 1.0 v/v	79
Figure 4.6 Effects of precipitation time and temperature on the mean particle size and solids concentration in a batch precipitator: mixer speed = 600 rpm and protein feed concentration = 2.8 kg/m^3	80

Figure 4.7	Effects of precipitation time and temperature on the mean particle size and solids concentration in a batch precipitator: mixer speed = 600 rpm and protein feed concentration = 11.8 kg/m ³	81
Figure 4.8	Effects of volumetric feed ratio and initial protein concentration on the final protein concentration in the solution during isoelectric precipitation (protein feed solution at pH 10.0 and final solution at pH 4.0)	87
Figure 4.9	Linear fit for the experimental RTD data: 1/Pe versus flow velocity in the tubular precipitator	91
Figure 4.10	Effects of static mixer and mean residence time on the mean particle size and solids concentration in the tubular precipitator: protein feed conc. = 11.5 kg/m ³ , flow Re no. = 800 and volumetric feed ratio = 1.0 v/v	94
Figure 4.11	Effects of static mixer and mean residence time on the mean particle size and solids concentration in the tubular precipitator: protein feed conc. = 11.5 kg/m ³ , flow Re no. = 5,000 and volumetric feed ratio = 1.0 v/v	95
Figure 4.12	Effects of precipitator length and mean residence time on the mean particle size and solids concentration in the tubular precipitator: protein feed conc. = 2.8 kg/m ³ , flow Re no. = 800 and volumetric feed ratio = 1.0 v/v	96
Figure 4.13	Effects of precipitator length and mean residence time on the mean particle size and solids concentration in the tubular precipitator: protein feed conc. = 11.8 kg/m ³ , flow Re no. = 5,000 and volumetric feed ratio = 1.0 v/v	97
Figure 4.14	Effects of protein feed concentration and mean residence time on the mean particle size and solids protein concentration in the tubular precipitator: flow Re no. = 800 and volumetric feed ratio = 1.0 v/v	99
Figure 4.15	Effects of protein feed concentration and mean residence time on the mean particle size and solids protein concentration in the tubular precipitator: flow Re no. = 5,000 and volumetric feed ratio = 1.0 v/v	100
Figure 4.16	Effects of flow Re number and mean residence time on the mean particle size and solid protein concentration in the tubular precipitator: protein feed conc. = 11.8 kg/m ³ and volumetric feed ratio = 1.0 v/v	101

Figure 4.17	Effects of flow Re number and mean residence time on the mean particle size and solid protein concentration in the tubular precipitator using 0.05 M aq. calcium acetate as a precipitant: protein feed conc. = 12.0 kg/m ³ with 1.0 M NaCl, feed ratio = 1.0 v/v, and precipitation pH 6.5	102
Figure 4.18	Effects of flow Re number and mean residence time on the population density of protein particles in the tubular precipitator: protein feed conc. = 11.8 kg/m ³ and volumetric feed ratio = 1.0 v/v	103
Figure 4.19	Effects of flow Re number and mean residence time on CV (based on volume distribution) for precipitates from the tubular precipitator: protein feed conc. = 11.8 kg/m ³ and volumetric feed ratio = 1.0 v/v	105
Figure 4.20	Effects of volumetric feed ratio and mean residence time on the mean particle size in the tubular precipitator with flow Re no. = 5,000: (A) protein feed conc. = 2.8 kg/m ³ (B) protein feed conc. = 11.6 kg/m ³	106
Figure 4.21	Effects of volumetric feed ratio and mean residence time on protein solids concentration in the tubular precipitator with flow Re no. = 5,000: (A) protein feed conc. = 2.8 kg/m ³ (B) protein feed conc. = 11.6 kg/m ³	107
Figure 4.22	Effects of the flow regime (fluid-induced shear) and the mean residence time on the mean particle size: (A) laminar flow regime Re no. = 440 (B) turbulent flow regime Re no. = 5,000	109
Figure 4.23	Population density of sunflower protein aggregates in an MSMR precipitator as a function of mean residence time: protein feed concentration = 2.9 kg/m ³ and volume feed ratio = 1.0 v/v	114
Figure 4.24	Population density of sunflower protein aggregates in an MSMR precipitator as a function of mean residence time: protein feed concentration = 11.6 kg/m ³ and volume feed ratio = 1.0 v/v	115
Figure 4.25	Effects of precipitation time (for the batch precipitator) and the mean residence time (for the MSMR and the tubular precipitators) on the mean particle sizes of precipitates for protein feed conc. = 2.8 kg/m ³ and volume feed ratio = 1.0 v/v	117

Figure 4.26	Effects of precipitation time (for the batch precipitator) and the mean residence time (for the MSMPR and the tubular precipitators) on the mean particle sizes of precipitates for protein feed conc. = 11.8 kg/m^3 and volume feed ratio = 1.0 v/v	118
Figure 4.27	Comparison of the population densities of precipitates from the batch, MSMPR, and the tubular precipitators for protein feed conc. = 2.8 kg/m^3 and volume feed ratio = 1.0 v/v	119
Figure 4.28	Comparison of the population densities of precipitates from the batch, MSMPR, and the tubular precipitators for protein feed conc. = 11.8 kg/m^3 and volume feed ratio = 1.0 v/v	120
Figure 4.29	Effects of precipitation time (for the batch precipitator) and the mean residence time (for the MSMPR and the tubular precipitators) on the coefficient of variation (CV) for protein feed conc. = 11.8 kg/m^3 and volume feed ratio = 1.0 v/v	121
Figure 4.30	Effects of precipitation time (for the batch precipitator) and the mean residence time (for the MSMPR and the tubular precipitators) on the solids concentration (yield) for protein feed conc. = 11.8 kg/m^3 and volume feed ratio = 1.0 v/v	122
Figure 4.31	SEM of washed precipitates from the tubular precipitator for protein feed conc. = 11.8 kg/m^3 and volume feed ratio = 1.0: v/v (A) laminar flow regime (B) turbulent flow regime	124
Figure 4.32	SEM of washed precipitates (A) from the batch precipitator (B) from the MSMPR precipitator: protein feed conc. = 11.6 kg/m^3 and volume feed ratio = 1.0 v/v	125
Figure 5.1	The algorithm for calculating the aggregation and breakage rates parameters from the MSMPR precipitator experimental data	134
Figure 5.2	Population density of sunflower protein aggregates in an MSMPR precipitator: comparison of the experimental data with the model fitting for protein feed concentration = 2.9 kg/m^3	136
Figure 5.3	Population density of sunflower protein aggregates in an MSMPR precipitator: comparison of the experimental data with the model fitting for protein feed concentration = 11.6 kg/m^3	137
Figure 5.4	Ratio of the breakage and the growth rate constants as a function of protein feed concentration and mean residence time in an MSMPR precipitator	138

Figure 5.5	Node points scheme for orthogonal collocation-multiple shooting method for solving the population balance equation for the tubular precipitator	146
Figure 5.6	Simulated reference PSD along the tubular precipitator using parameters shown in Table 5.2	157
Figure 5.7	Simulated PSD along the tubular precipitator with a high breakage rate parameter, $\beta = 3.5$	159
Figure 5.8	Simulated PSD along the tubular precipitator for high nucleation rate constant ($k_B = 0.98$)	160
Figure 5.9	Simulated PSD along the tubular precipitator for a low nucleation rate constant ($k_B = 0.0$)	161
Figure 5.10	Simulated PSD along the tubular precipitator for high growth rate exponent ($g = 3.5$)	162
Figure 5.11	Simulated PSD along the tubular precipitator for high flow velocity ($u_z = 3.0$ m/s)	163
Figure 5.12	Calculation algorithm for determination of the optimum kinetic parameters from the tubular precipitator experimental data	168
Figure B.1	Experimental setup for the calibration of the turbidimeter	190
Figure B.2	Fit of Beer-Lambert's law to experimental data: $\ln(\text{Tr})$ as a function of protein solids concentration for a photo-cell with $l = 2.66$ cm	192
Figure B.3	Polynomial fit ($\ln(\text{Tr})$ as a function of $\ln(C_s)$) for protein particles suspension	193
Figure D.1	The flow sheet of the computer programs used in the calculation of the optimum model parameters from the experimental data	202
Figure D.2	The flow sheet of the computer programs used in the predictions of the experimental data from the model	204

NOMENCLATURE

a	= nucleation parameter
aa	= exponential parameter (Equations 2.3 and 2.17a)
ab	= homogenous nucleation parameter (Equation 2.8)
a_g	= growth rate parameter
a_p	= acceleration due to gravity or centrifugal (m/s^2)
A	= aggregation rate (no./ μm mL s)
A_T	= total solids surface area per volume of solid free liquid (m^2/m^3)
b	= growth rate parameter
bb	= exponential parameter (Equation 2.17a)
bs	= secondary nucleation parameter (Equation 2.9)
B	= net rate of population density change due to particle breakage (no./ μm mL s)
B_a	= birth rate due to aggregation (no./ μm mL s)
B_b	= birth rate due to breakage (no./ μm mL s)
B_{con}	= parameter defined in Equation (5.39)
B^o	= nucleation rate (no./mL s)
B^o_o	= initial nucleation rate (no./mL s)
cc	= exponential parameter (Equation 2.3)
C	= protein concentration (g/mL or kg/m^3 of solid free liquid)
C_i	= protein concentration in the solution (g/mL or kg/m^3)
Co	= protein concentration in the feed stream (g/mL or kg/m^3)
C_p	= protein concentration in the solution (g/mL or kg/m^3)
Cs	= solids concentration (g/mL or kg/m^3 of solid free liquid)
CV	= experimental coefficient of variation based on volume distribution
CV_e	= coefficient of variation at exit
CV_{ij}	= coefficient of variation based on volume distribution for run i at the jth port

CV_m	= calculated coefficient of variation based on volume distribution
$CV_{m_{i,j}}$	= coefficient of variation based on volume distribution for run i at jth port
C^*	= solute or equilibrium protein concentration (g/mL or kg/m ³)
d	= mean particle size ($\mu\text{m}^4/\mu\text{m}^3$)
dd	= exponential parameter (Equation 2.3)
df_i	= degrees of freedom
d_i	= mean particle size from ith run ($\mu\text{m}^4/\mu\text{m}^3$)
d_{ij}	= mean particle size for run i at jth port
d_m	= calculated mean particle size ($\mu\text{m}^4/\mu\text{m}^3$)
$dm_{i,j}$	= calculated mean particle size ($\mu\text{m}^4/\mu\text{m}^3$)
d_p	= mean particle size (m or μm)
d_t	= diameter of the tubular precipitator (cm or m)
D	= particle death rate (no./ $\mu\text{m mL s}$)
D_a	= death rate due to aggregation (no./ $\mu\text{m mL s}$)
D_b	= death rate due to breakage (no./ $\mu\text{m mL s}$)
$D_{i,j,k}$	= particle diffusivity (cm ² /s or m ² /s)
D_z	= axial dispersion coefficient (cm ² /s or m ² /s)
DM	= defatted meal
ee	= exponential parameter (Equation 2.3)
e_i	= voltage (volt)
E_b	= activation energy (kJ/kmol)
E_G	= activation energy (kJ/kmol)
E_N	= activation energy (kJ/kmol)
f	= number of daughter particles (Equation 2.16c)
$f(\epsilon, \zeta)$	= function defined in Equation (5.36a)
f_f	= Fanning friction factor
ff_R	= fraction of specie that has deprotonated
F_{ij}	= frequency of orthokinetic collisions
g	= growth rate parameter
G	= particle growth rate ($\mu\text{m/s}$)
G_a	= aggregate growth rate ($\mu\text{m/s}$)

G_s	= average shear rate (1/s)
G_o°	= initial particle growth rate ($\mu\text{m/s}$)
h	= general function
H	= objective equation to be minimized
HM	= objective equation to be minimized
I	= intensity of the emerging beam
IS	= ionic strength (mol/L)
I_o	= intensity of the source
Ix_k	= function defined in Equation (5.37)
I_∞	= function defined in Equation (5.38)
js	= secondary nucleation parameter (Equation 2.9)
k	= homogeneous nucleation parameter (Equation 2.8)
k_a	= specific area shape factor
k_b	= nucleation rate constant (Equation 2.17a)
k_B	= nucleation parameter
k_{Bo}	= nucleation parameter
k_d	= breakage rate parameter
k_D	= model parameter, death rate constant
k_{ER}	= constant (Equation 3.3b)
k_g	= growth rate constant (Equation 2.17b)
k_G	= growth rate parameter
k_{Go}	= growth rate parameter
k_m	= nucleation parameter (Equation 2.7)
k_n	= primary nucleation parameter (Equation 2.7)
k_p	= parameter in Equation (2.3)
k_s	= secondary nucleation parameter (Equation 2.9)
k_v	= volume shape factor
k_1	= constant in Equation (3.3b)
k_2	= constant in Equation (3.3b)
k_3	= constant in Equation (3.3b)
K	= aggregation kernel

K_B	= nucleation rate parameter
K_D	= particle death rate parameter
K_e	= model parameter
K_{fi}	= conversion factor (Equation C.3)
K_G	= particle growth rate parameter
K_i	= dissociation constant
K_o	= model parameter
K_R	= dissociation constant
K_s	= precipitation constant (Equation 3.3b)
l	= travel path of the beam (cm or m)
l_i	= location of measuring point i along the precipitator (cm or m)
L	= particle or aggregate size (μm)
L_c	= particle size scaling factor (μm)
$L_{i,j,k}$	= particle or aggregate size at the ith, jth, or kth size interval (μm)
L_o	= nuclei particle size (μm)
m	= number of experimental sets
M_i	= mole fraction
M_s	= the weight of dry defatted meal (g or kg)
M_T	= solid protein concentration (g/mL or kg/m^3 of solid free liquid)
n	= number of node points used in defining the PSD
nc	= number of measuring channels in the Coulter Counter
nr_i	= number of replications
N	= particle concentration (no./mL)
$N_{i,j,k}$	= particle concentration in the size range i, j, or k (no./mL)
NR	= speed of mixer (rpm)
N_s	= number density scaling factor (no./mL)
NT	= particle concentration in the undiluted sample (no./mL)
p	= population density (no./ μm mL)
p_i	= population density of particles in the size range i (no./ μm mL)
pK_i	= $-\log K_i$
p^o	= initial number density (no./ μm mL)

p_o	= nuclei density (no./ $\mu\text{m mL}$)
P	= matrix of parameters to be optimized
P_A	= parameter in Equation (5.19)
Pe	= Peclet number (zu/D_z)
Pe_i	= Peclet number in the i th port
pK_R	= $-\log K_R$
q	= total liquid flow rate (mL/s , mL/min or m^3/s)
Q	= total liquid feed flow rate (mL/s , mL/min or m^3/s)
r	= volumetric feed ratio (precipitant : protein solution) (v/v)
r_i, r_j	= mean radius of particles in the size range i or j (μm)
R	= universal gas constant (kJ/mol K)
R^2	= coefficient of regression
R_a	= aggregation rate (no./ $\mu\text{m mL s}$)
Re	= flow Reynolds number ($\rho u d/\mu$)
R_i	= relative number
s_i	= nucleation rate parameter
s_j	= nucleation rate parameter
s_g	= growth rate parameter
S	= supersaturation ratio
Se	= pooled estimate of the standard error
Se_i	= standard error for the experimental set i
S_o	= initial supersaturation ratio
t	= time (s or min)
t_{ij}	= mean residence time between points i and j
t_m	= mean residence time (s or min)
T	= temperature (K)
Tr	= transmission = I/I_o (%)
u	= superficial liquid velocity (cm/s or m/s)
u_p	= settling velocity of the particle (cm/s or m/s)
u_z	= superficial liquid velocity (cm/s or m/s)
v_i	= total volume fraction of particles at the i th channel or interval

V	= precipitator volume (mL or m ³)
V_{ci}	= equivalent volume of sphere with diameter as the channel size (μm ³)
V_i	= volume of protein solution (mL or m ³)
V_p	= total volume of protein solution (mL or m ³)
w_i	= weighting factors of Gaussian-Laguerre quadrature
W	= dimensionless concentration
W_i	= total mass of particles in the in the size range i (g or kg)
W_s	= protein content of the dry defatted meal (g/g or kg/kg)
x	= dimensionless particle size
$x_{e,o}$	= dimensionless particle sizes at exit and entrance
X	= ln(Cs)
y	= dimensionless population density
y_n	= (n-1)th order trial function
Y	= ln(Tr)
z	= precipitator length (cm or m)
z_T	= total length of the precipitator (cm or m)
Z	= net charge

Greek letters

α_i	= weighting function
β	= model parameter, breakage power
β_o	= collision frequency (mL/s or m ³ /s)
β_o°	= secondary nucleation rate (no./μm mL s)
γ	= parameter in Equation (2.13)
$\gamma_{i,k}$	= elements of matrix
δ_{ij}	= Kronecker delta ($\delta_{ij} = 0$ if $i \neq j$; $=1$ if $i = j$)
ϵ	= dimensionless particle size less than x
$\hat{\epsilon}$	= absorbance coefficient (cm ² /g or m ² /kg)
κ	= Beer-Lambert's law constant (mL/g or m ³ /kg)
η	= rate of energy dissipation per unit mass (W/kg)

Λ_{ij}	= parameter (Equation 2.5)
λ	= growth rate parameter
λ_{ij}	= weighting factors (Equation 2.18)
λ_o	= wavelength of the source (cm or m)
μ_e	= model parameter
μ_L	= liquid viscosity (g/mL.s or kg/m.s)
μ_o	= model parameter
ζ	= dimensionless distance along the precipitator
ζ_o	= dimensionless location (distance) of the entrance or starting port
ζ_f	= dimensionless location (distance) of the exit or end port
ρ	= liquid density (g/mL or kg/m ³)
ρ_a	= density of protein aggregates (g/mL or kg/m ³)
ρ_s	= solids density (g/mL or kg/m ³)
σ	= apparent relative supersaturation
σ_{ti}^2	= variance of distribution (min ²)
σ_{12}^2	= variance of distribution between points 1 and 2 (min ²)
σ_{θ}^2	= dimensionless variance of distribution (min ²)
τ	= mean residence time of solid-free liquid (s or min)
Υ	= turbidity (cm ⁻¹ or m ⁻¹)
ν	= kinematic viscosity (cm ² /s or m ² /s)
ν_L	= kinematic viscosity of liquid (cm ² /s or m ² /s)
κ	= travel distance of the light beam (cm or m)
Φ	= matrix
Φ_i	= ith term of exponentially weighted Laguerre function
Θ_{io}	= mean flow time (s or min)
$\phi_{i,k}$	= elements of matrix
ψ_i	= ith term in Laguerre polynomial
ω	= speed of the mixer (1/s or rpm)

Acronyms

B.C.	= boundary condition
CA	= chlorogenic acid
CC	= Coulter counter
CMC	= carboxymethylcellulose
CSD	= crystal size distribution
CSTR	= constant stirred tank reactor
CV	= coefficient of variation
db	= dry basis (no water)
DIF	= differential volume fraction
DM	= defatted meal
FAC	= fat absorption capacity
HMP	= hexametaphosphate
IC	= initial condition
Ip	= isoelectric point (pH)
MSM	= multiple shooting method
MSMPR	= mixed suspension mixed product removal
MSMPRC	= mixed suspension mixed product removal crystallizer
MSMPRP	= mixed suspension mixed product removal precipitator
MWR	= method of weighted residue
NETLIB	= www.netlib.org (data base of numerical, scientific, and computing softwares)
OCM	= orthogonal collocation method
OCMSM	= orthogonal collocation multiple shooting method
ODE	= ordinary differential equation
PBE	= population balance equation
PEG	= polyethylene glycol
PSD	= particle size distribution
PSP	= problem specific polynomial
RTD	= residence time distribution

SEM = scanning electron micrograph

TNT = pentaerythritol tetranitrate

WHC = water hydration capacity

Subscript

cal = calculated value

exp = experimental value

CHAPTER 1

INTRODUCTION

1.1 Background

Defatted meals from vegetable oil mills are known to contain high contents of vegetable proteins, up to about 58 %w/w in association with indigestible fibre, oligosaccharides, antinutrients, toxic compounds, and adverse color and flavor constituents. Oilseed proteins in their native state are readily soluble in aqueous alkaline solutions and sparingly soluble in the pH range between 3 and 6.5 (isoelectric pH). Thus, they can be extracted from defatted meals using an aqueous alkaline solution and then recovered as pure solid proteins at lower pH. Eighty percent of these proteins can be recovered by this precipitation process.

Vegetable proteins have many desirable nutritional properties and their main uses are as protein supplements or functional ingredients in meat products, bread and bakery products, confectionery, and milk-like products (Uzzan, 1988). Currently, industries for isolation or concentration of soybean proteins are well established, but are almost non-existence for the other two major oilseeds, cottonseed and sunflower seeds. Products containing soybean protein have a beany flavour and limited applications to certain people who are allergic to legumes. Therefore, there is a need for development of new sources of vegetable proteins. Sunflower seeds show a great potential as a new protein source; it is the third most important oilseed (Lusas, 1985; Uzzan, 1988); it has the highest protein content among oilseeds, and, unlike soybean protein, it has no toxic constituents (Clandinin, 1958; Sosulski, 1979a). Furthermore, there has been extensive studies on the characterization of sunflower proteins. Therefore, sunflower protein was chosen for this study.

There are several methods of precipitating proteins from alkaline extracts such

as: heating, adjusting the pH using mineral acids, and the addition of organic solvents, neutral salts, non-ionic polymers, polyelectrolytes or metal ions. Most of these precipitants have to be removed from the final product by washing. Unlike other precipitants, mineral acids are normally used in small quantities and result in higher solids yield. Moreover, their residue is nontoxic and is acceptable in food industries. Therefore, precipitation by adjusting the pH (isoelectric precipitation) was chosen for this study. Isoelectric precipitation of protein is characterized by a rapid formation of solids from the solution followed by aggregation of small particles to form larger particles. Formation of the larger particles depends on the mixing of the feed solutions (protein solution and the precipitant) in the precipitator, concentrations of the feed solutions, precipitation pH, shear forces exerted on the solid particles by the surrounding fluid, particle collisions with the precipitator walls and the mixer, and the mean residence time in the precipitator. Traditionally, protein precipitation has been carried out in batch precipitators. However, batch processes are not economical when processing large volumes, due to down time and variations in batch quality. Also, the mean particle size of the precipitate is normally small due to prolonged mixing. The well-mixed precipitator, with continuous feed and product withdrawal, is also used to recover proteins from the solution. Unlike the batch precipitator, the mean residence time of solids can be controlled by adjusting the flow rates. However, the presence of newly formed solid particles among the aged particles results in a precipitate with a wide spread of particle size distribution (PSD) and protein losses into the whey. Another alternative is the use of the tubular precipitator. The tubular precipitator operating near the plug flow regime resembles a series of moving batch precipitators. Thus, the product will have a uniform mean residence time, less particle breakages because there is no mechanical mixer, and the mean residence time can be varied by changing the precipitator length or the feed flow rates.

For a given precipitator, the solids yield and the mean particle size of the precipitate can be estimated beforehand using the population balance equation (PBE) together with the precipitation kinetics data (nucleation rate, particle growth rate, aggregation rate, and breakage rate). Precipitation kinetics data for a particular protein are evaluated from experimental data using empirical correlations. The solution of the

resulting PBE can be evaluated analytically for a simple equation or by an iterative method for a complex set of equations. There are no reports in the literature on kinetics data or solutions of the PBE involving sunflower protein precipitation, although these studies have been done for soybean protein precipitation.

A subsequent process after protein precipitation is solids-liquid separation. The efficiency of this process depends on the particle size, spread of the particle size distribution, and the solids concentration. For efficient recovery it is desirable to have a precipitate with large particles and a narrow spread in the particle size distribution.

1.2 Research Objectives

The objectives of this research were:

1. To perform experimental studies on isoelectric precipitation of sunflower protein in a continuous flow tubular precipitator. The goal was to determine the operating parameters which will maximize the yield (recovered solid protein), maximize the mean particle size of the protein particles, and minimize the spread of PSD. The operating parameters which were studied include the effects of: feed flow rate, protein concentration in the feed stream, volumetric feed ratio of the precipitant (concentration of aqueous HCl solution) to protein solution, and the precipitator length.
2. To compare the solid protein yields and particle size distribution of the precipitate from the tubular precipitator and two other types of precipitators, namely, the mixed suspension mixed product removal precipitator (MSMPRP) and the batch precipitator.
3. To compare the solid protein yields and the particle size distributions of the precipitates obtained by isoelectric precipitation and by Ca^{2+} precipitation (calcium acetate).
4. Determination of the isoelectric precipitation kinetic parameters (nucleation rate, particle growth rate, aggregation rate, and breakage rate) of the sunflower proteins in the tubular precipitator.

5. Determination of the solution of the population balance equation and the model predictions for the tubular precipitator with particle aggregation and breakage terms.
6. Evaluation of the best method to prohibit discolouration of the sunflower protein isolate.

CHAPTER 2

LITERATURE REVIEW

2.1 Oilseed Proteins

2.1.1 Composition of Oilseed Proteins

Oilseed proteins are composed of about 22 α -amino acid each with the L configuration (i.e., the amino group is present on the α -carbon atom). The composition of these amino acids determines the properties of the protein (denaturation, nutritional value, and physical properties). The general chemical structure of the amino acids is:



where R is the side chain group. The side chain group determines the properties of the individual amino acid. Also the charge properties of the protein molecules are determined by the ionization of the side chain. In a protein molecule the amino acids are joined together by a peptide bond (-CO-NH-). This bond is formed by the condensation of α -COOH of one amino acid with α -NH₂ of the other amino acid to form a low molecular weight polymer, primary structure (polypeptide). Theoretically, for the 22 naturally occurring amino acids there are almost unlimited possible combinations, but functional proteins in animals and plants must have very specific amino acid sequences, even in storage proteins of seeds. Table 2.1 shows the composition of essential amino acids found in major oilseed proteins.

Table 2.1 Essential amino acid composition of major oilseeds (g/16 gN)
(Viroben and Bertrand, 1985).

Amino acid	Soybean	Cottonseed	Sunflower	Rapeseed	Groundnuts
Threonine	3.7 - 4.2	3.4	3.5	4.0	2.5 - 3.0
Valine	4.9 - 5.4	5.0	5.1	4.6	4.2 - 4.7
Isoleucine	4.8 - 5.5	3.2	4.2	3.3	3.4 - 3.8
Leucine	7.5 - 8.3	5.8	6.3	6.2	6.3 - 6.9
Phenylalanine	4.7 - 5.3	5.8	4.6	3.5	4.8 - 5.3
Methionine	1.5 - 1.6	0.7	4.2*	1.8	1.3 - 1.5
Cysteine	1.5 - 1.8	1.9		2.8	1.3 - 1.6
Lysine	5.8 - 6.5	4.3	3.3	5.3	3.3 - 3.6
Tryptophan	1.2 - 1.4	1.2	1.3	---	0.9 - 1.2

*methionine + cysteine

Proteins are classified according to their solubilities (Table 2.2) and by the shape of their molecules. The native structures of the protein molecules are either globular or fibrous. The former have sphere-like shapes formed by folding one or more protein monomers, and the latter are rod shaped (thread-like) and composed of polypeptides subunits. A globular protein can be polymerized into a fibre form. According to Wall and Huebner (1981) albumins and globulins are highly compact protein molecules. Their folding nature is maintained by internal hydrogen and hydrophobic bonds as well as by the disulphide bonds.

2.1.2 Solubility of Proteins in Aqueous Solutions

A native protein molecule remains in solution by folding in such a way that it achieves a minimum free energy. The folded molecule turns the hydrophobic groups towards the interior of the coiled structure such that the hydrophilic groups interact most with water molecules (Whitaker, 1977; Valentas et al., 1991). For example, in aqueous solution (not at isoelectric pH), protein solubility is a result of hydrogen bonding between water and protein molecules. Proteins can undergo reversible denaturation (renaturation) which involves unfolding and refolding of the protein molecule structure. Unfolding and refolding of the protein molecules depends on changes in the environment surrounding these molecules. During refolding a portion of a unfolded (random coiled) polypeptide chain (Figure 2.1a) forms α -helices along its axis (globulin proteins i.e., albumins, caseinogen, and gluten) and β -pleated sheets, a zig-zag structure of polypeptide chain (Figure 2.1d). These join with other polypeptides to form a periodic 3-dimensional structured native protein (Figure 2.1f).

Decreases in protein solubility (precipitation) are caused by the protein associations at the molecular level, followed by aggregation which involves the formation of larger particles. The association process involves the bonds between active groups of the polypeptide, bonds such as: electrostatic interaction, hydrogen bonds, hydrophobic interaction, covalent bonds, disulphide bonding, and dipole-dipole interaction. Furthermore, these associations depend on the type of functional group in the protein molecule participating in the associative interaction, and the agent that disrupts

Table 2.2 Solubility of proteins (Powrie and Nakai, 1981).

Proteins	Solubility characteristic
Albumins	Soluble in water and aqueous solutions.
Globulins	Slightly soluble in water, very soluble in aqueous salt solutions.
Prolamines	Soluble in 70%-80% ethanol, insoluble in water or salt solutions.
Glutelins	Soluble in alkaline or acid solutions.
Scleroproteins	Insoluble in aqueous solutions.

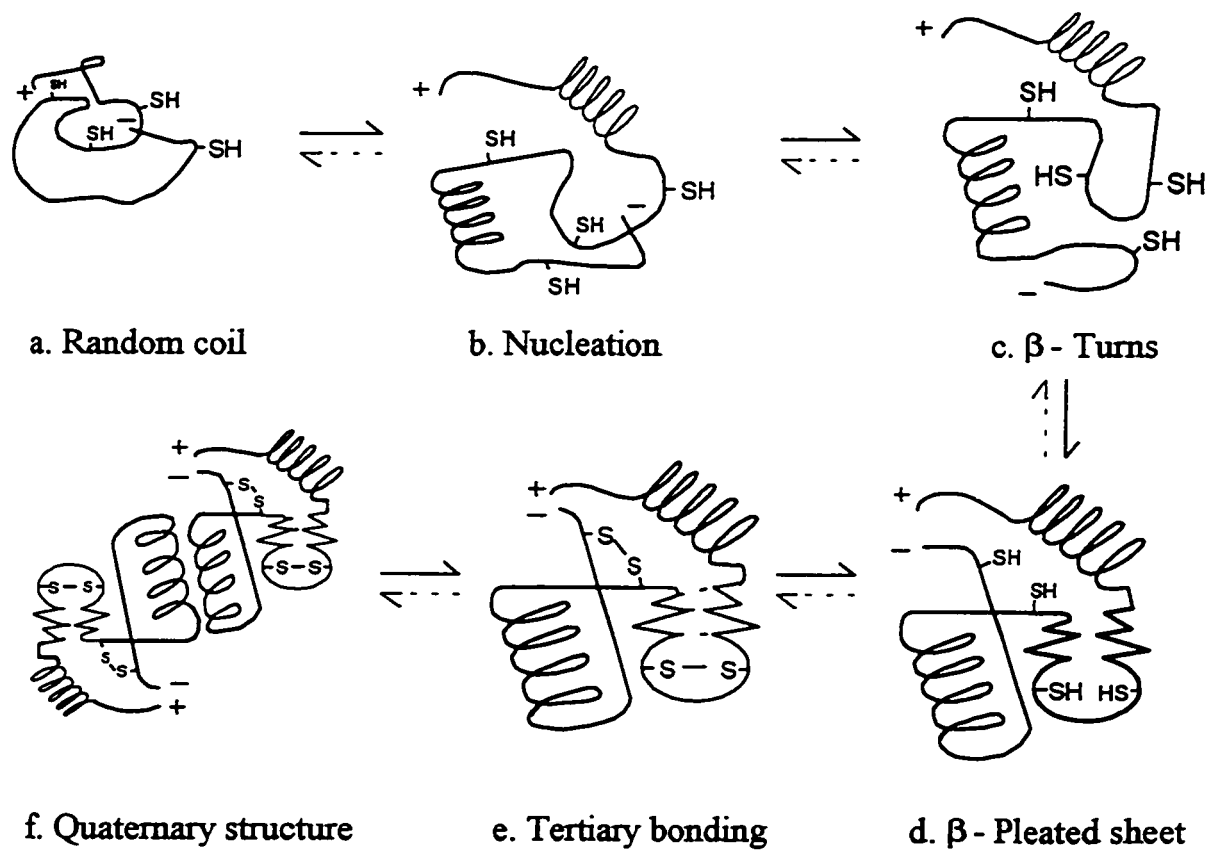


Figure 2.1 Steps occurring during folding of a polypeptide chain to form a native protein structure (Anfinsen and Scheraga, 1975).

the bond (Wall and Huebner, 1981). For example: The electrostatic bond, $\text{COO}^- - ^+\text{NH}_3$, is disrupted by concentrated salt solutions or extreme pH values; reducing agents (sulphite) tend to disrupt the covalent bond -S-S- (disulphide bond) in functional groups of cystine (this bond maintains the intramolecular bonds, crosslinks, and quaternary structure between protein chains); organic solvents and detergents are known to disrupt the hydrophobic bonds, which are found in functional groups with long aliphatic chains or aromatic groups; salts like urea disrupt the hydrogen bond found in hydroxyl, amide, and phenol functional groups.

In the solution, native protein molecules are amphoteric compounds which can have negative, positive, or zero net charge depending on the ionization of the side chain group of the amino acids. The less soluble proteins can be dissolved at extreme pH (acidic or basic) due to the excess of similar repelling charges which causes protein structure to unfold. The solubility of proteins is minimal at the isoelectric pH (neutral charge). At this point the solubility is minimal because dipole-dipole attraction and the electrostatic attraction between neighbouring protein molecules increases, allowing the molecules to pack together. Hydrogen bonding also influences the packing. This reduces solvent-protein molecule interaction, and hence overall solubility decreases. At the isoelectric point (I_p), the packed protein molecules no longer repel one another due to lack of net charges. Therefore, the molecules have more chances of aggregating. However, the solubility depends also on the temperature and the presence of other organic and inorganic ions in the solution.

During protein precipitation from the solution, hydrogen bonds, hydrophobic bonds, covalent bonds, and electrostatic bonds are broken down, resulting in unfolding of the protein chains with large regions of random coil structure which are less soluble in aqueous solutions. Further modifications of these secondary and tertiary structures (by extreme pH, heat or salt concentrations) of the proteins, which does not involve peptide bonds leads to protein denaturation (an irreversible change).

Shen (1981) reported that the solubility of soy protein isolate is very much dependent on the path used (e.g., mixing of solid proteins with water followed with concentrated NaCl solution results in higher solubility than mixing of solid protein with diluted NaCl, albeit the final NaCl concentrations are the same). This is because the

thermodynamic equilibrium criteria are different. Thus, it is necessary to adhere to the same procedure each time in order to obtain comparable experimental results.

2.1.3 Sunflower Proteins and Their Composition

Sunflower (*Helianthus annuus*) is one of the major oilseed crops in the world, it ranks third after soybeans and cottonseed (Lusas, 1985; Uzzan, 1988). Sunflower seed contains between 25 and 48 %w/w oil (Salunkhe and Desai, 1986). The protein content of the seed varies from 15 to 20 %w/w depending on the variety and the location of growth. After extraction of oil, the high protein meal can be used for protein extraction. Table 2.3 compares the compositions of the defatted meals from the three major oilseeds. Also, Sosulski and Bakal (1969) reported that defatted sunflower meal has higher protein content than other oilseed meals. Previous studies by Clandinin (1958) and by Sosulski (1979a) have reported that sunflower seed proteins has many desirable nutritional properties and no known anti-nutritional factors. Therefore, sunflower protein could be used as a primary source of vegetable proteins for human consumption. Table 2.4 (Sosulski and Fleming, 1977) shows the amino acids compositions of sunflower meal and the WHO recommended requirements for human consumption. Defatted sunflower meal and protein isolate have low contents of lysine and leucine. These deficiencies suggest that sunflower products have to be supplemented with high lysine proteins. Another drawback of sunflower products is the presence of phenolic acids (chlorogenic, caffeic, and quinic acids) which compose 3-3.5 %w/w of defatted meal (Sosulski, 1979a; Dabrowski and Sosulski, 1984). These phenolic acids bind covalently with low molar mass proteins (Smith and Johnsen, 1948; Sosulski and Bakal, 1969; Sabir et al., 1974; Sosulski, 1979b) to produce discoloration. The colour changes from milk-white to cream yellow, to deep green, and finally to dark brown when the pH is raised above neutrality. This discoloration is caused by chemical or enzymatic oxidation of phenolic acids (Cater et al., 1972). Once the green or brown colour is formed, it is not easily removed. Several methods of producing colourless products have been published (Table 2.5) or patented. These methods can be grouped into three main classes: those which prohibit discoloration by removing phenolic acids by pre-washing or diffusion of the dehulled

Table 2.3 Average composition of sunflower meal as compared with cottonseed and soybean meals (Salunkhe and Desai, 1986).

Constituent (% w/w)	Sunflower meal		Cottonseed meal		Soybean meal
	Expeller	Solvent extracted	Expeller	Solvent extracted	Solvent extracted
Moisture	7.0	7.0	7.0	9.0	11.0
Ash	6.8	7.7	6.1	6.5	5.8
Crude fiber	13.0	11.0	11.0	11.0	6.0
Ether extract	7.0	2.9	5.8	1.6	0.9
Protein (N x 6.25)	41.0	46.8	41.4	41.6	45.8

Table 2.4 Amino acid composition of defatted sunflower meal
(Sosulski and Fleming, 1977).

Amino acid	Content in defatted meal (g/16 g N)	Requirements of human adults *
Tryptophan	1.3	1.0
Lysine	3.1	5.4
Histidine	2.2	
Arginine	8.2	
Aspartic acid	8.6	
Threonine	3.2	4.0
Serine	3.8	
Glutamic acid	21.5	
Proline	3.8	
Glycine	5.2	
Alanine	3.9	
Methionine	2.1	
Half Cysteine	1.5	3.5
Valine	4.8	5.0
Isoleucine	3.9	4.0
Leucine	6.0	7.8
Tyrosine	2.0	
Phenylalanine	4.3	6.1
Ammonia	2.2	
Protein (% mass)	58.3	

* Source: Reference protein (FAO/WHO, 1973).

Table 2.5 Previous studies on preparations of colourless sunflower meals and isolates.

	Reference	Treatment
1.	Smith and Johnsen (1948)	Extraction of phenolic acids from defatted meal using 70 % aqueous ethanol (1:10 g:mL) at 60-70 °C for 3 hr.
2.	Gheyasuddin et al. (1970)	Protein extraction from defatted meal using aqueous solution (1:20 g:mL) at pH 10.5 and 0.1 % Na ₂ SO ₃ .
3.	Sosulski et al. (1972)	Diffusion of phenolic acids from dehulled seeds using 0.001M HCl at 80 °C for 1 hr. Seed to solution ratio of 1.5:100 g:g and 6 cycles.
4.	Fan et al. (1976)	i. Aqueous acid diffusion of dehulled seeds at 80 °C, pH 4.5, seed to solution ratio of 1:6 g:mL, and 5 stages of countercurrent extraction. ii. Washing of defatted meal using 70 % aqueous ethanol at 24 °C, pH 4.5, meal to solution ratio of 1:6 g:mL, and 5 stages of countercurrent extraction.
5.	Sodini and Canella (1977)	Washing of defatted meal using butanol/HCl solution (92:8 v/v), at pH 5, meal to solution ratio of 1:20 g:mL, and 8 cycles.
6.	Taha et al. (1981)	Protein extraction from defatted meal using aqueous solution at pH 10.5, 0.1 % Na ₂ SO ₃ , and meal to solution ratio of 1:20 g:mL. Countercurrent extraction.
7.	Lawhon et al. (1982)	Protein extraction from defatted meal at 60 °C, 24 in-Hg vacuum (no oxygen), pH 2-9, and meal to solution ratio of 1:20 g:mL.
8.	Bau et al. (1983)	Soaking of dehulled seeds in aqueous citric acid (0.2 %) at 100 °C for 20 min. Seed to solution ratio of 1:10 g:mL. Then the defatted meal is soaked in aqueous citric acid at 20 °C for 1 hr.
9.	Saeed and Cheryan (1988)	Washing of defatted meal using butanol/HCl solution (92:8 v/v), at pH 5, meal to solution ratio of 1:20 g:mL, and 8 cycles.
10.	Prasad (1990a)	Washing of defatted meal using aqueous acetone (H ₂ O:acetone = 1:9 v/v) or acidic aq. acetone (0.5M HCl:acetone = 1:9 v/v). Meal to solution ratio of 1:5 g:mL at 20 °C for 15 min.

seeds or defatted meal with organic solvents (methanol, ethanol, butanol, isopropanol, or acetone) or aqueous acidic solutions (O'Conoor, 1971; Pomenta and Burns, 1971; Sosulski et al., 1972; Fan et al., 1976; Sodini and Canella, 1977; Pearce, 1984; Saeed and Cheryan, 1988; Prasad, 1990a). The second method uses reducing agents such as sodium sulphite, sodium bisulphite, sodium hydrosulphite or citric acid to prevent the oxidation of phenolic acids (Gheyasuddin et al., 1970; Taha et al., 1981; Bau et al., 1983). The third method involves deactivation of the enzyme polyphenoloxidase (by heating) and exclusion of oxygen from the process. It is believed that the change in colour is due to the simultaneous presence of oxygen, enzyme polyphenoloxidase, and alkaline pH. Excluding any of the three items during processing will prohibit discolouration (Lawhon et al., 1982). The second method was used in this study. Rahma and Rao (1979); Sripad and Rao (1987); and Prasad (1990b) have reported that the nitrogen solubility and the recovered protein decreased depending on the type of solvent used to remove the phenolic acids. This is due to partial denaturation and solubilization of proteins caused by the solvent.

Figure 2.2 shows the approximate distribution of the sunflower proteins in the defatted meal. According to Kabirullah and Wills (1983), sunflower protein is composed of six to seven protein fractions with molar mass ranging from 10,000 to 450,000 kg/kmol. The major fraction has a molar mass of 125,000 kg/kmol. The average molar mass of sunflower protein is about 180,000 kg/kmol. In another study, Sabir et al. (1973) reported that the major fraction of salt-extracted protein has an average molar mass of 330,000 kg/kmol.

2.2 Recovery Process of Oilseed Proteins by Precipitation

Traditionally, precipitation processes are used to recover proteins from the solution. The aims of the protein precipitation are: to remove or inactivate enzymes for increasing storage time of protein (shelf life), to improve the flavour, colour, and texture of protein while retaining the nutritional value, and to remove toxic or undesirable compounds which are found together with proteins in the defatted meals. Proteins in the defatted meal are extracted (leaching) using aqueous alkaline solutions (pH 10). The ratio

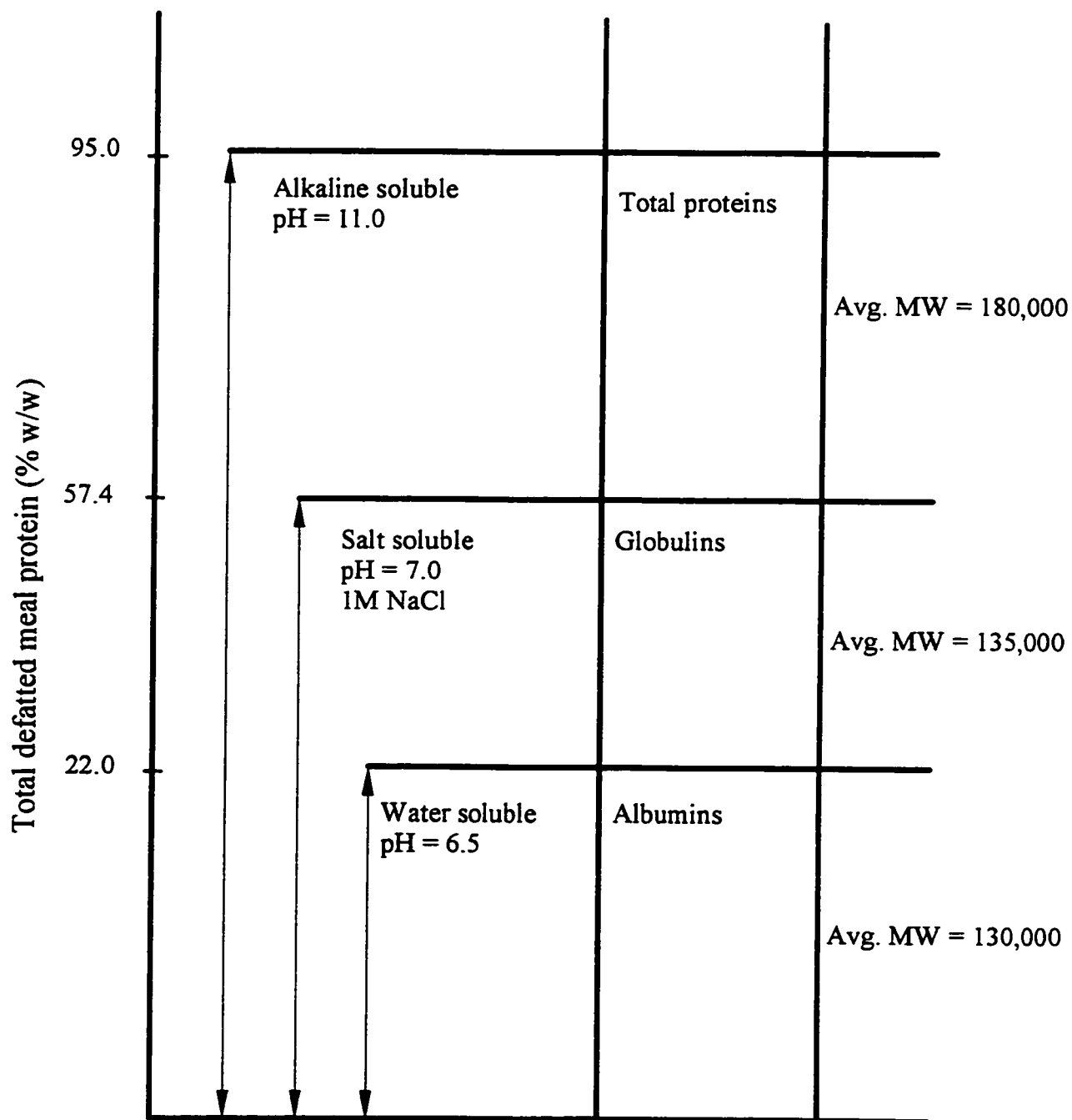


Figure 2.2 Approximate distribution of sunflower proteins in defatted meal (Kabirullah and Wills, 1983).

of solids (kg) to solvent (L) ranges from 1:10 to 1:20. For most oilseeds, over 90 %w/w of defatted meal proteins can be extracted within 1 hr. Prolonged extraction times leads to protein denaturation by alkaline solution. During extraction, there are other nitrogen-containing compounds (non-protein) which are also extracted, such as free amino acids and peptides. Figure 2.3 shows the general flowsheet for preparation of the protein solution from the defatted meal. The protein solution is separated from the spent defatted meal by sedimentation followed by filtration or centrifugation. Conversion of soluble proteins to solid proteins can be achieved by altering the solubility of protein molecules using various precipitating agents (Bell et al., 1983). The choice of the precipitant depends on the final use of the protein, denaturation effect, and the cost of the precipitant. During protein precipitation, a protein molecule is made insoluble by altering its structure (surface characteristic) or by changing the environment (solvent) (Table 2.6). This leads to high supersaturation which results in nucleation followed by aggregation. Solid proteins are subsequently recovered by unit operations processes such as settling, centrifugation, or filtration, followed by spray drying or freeze drying. Settling, centrifugation, and spray drying methods involve the settling velocity of particles (u_p) in the Stokes regime given by:

$$u_p = a_p d_p^2 \frac{(\rho_s - \rho)}{18\mu_L} \quad (2.2)$$

where a_p is the acceleration due to gravity or centrifugal force, d_p is the solid proteins mean particle size, ρ_s and ρ are the densities of the solid proteins and fluid, respectively. Protein particles have a density of about 1200 to 1300 kg/m³ (Bell et al., 1982; Singh, 1995) and the mother liquor has a density of about 1000-1200 kg/m³, depending on the type and the concentration of the precipitant used. Therefore, for effective solids-liquid separation and spray drying, it is imperative to have large particles with narrow particle size distribution. The simplified process flow sheet for oilseed protein recovery from defatted meals is shown in Figure 2.4.

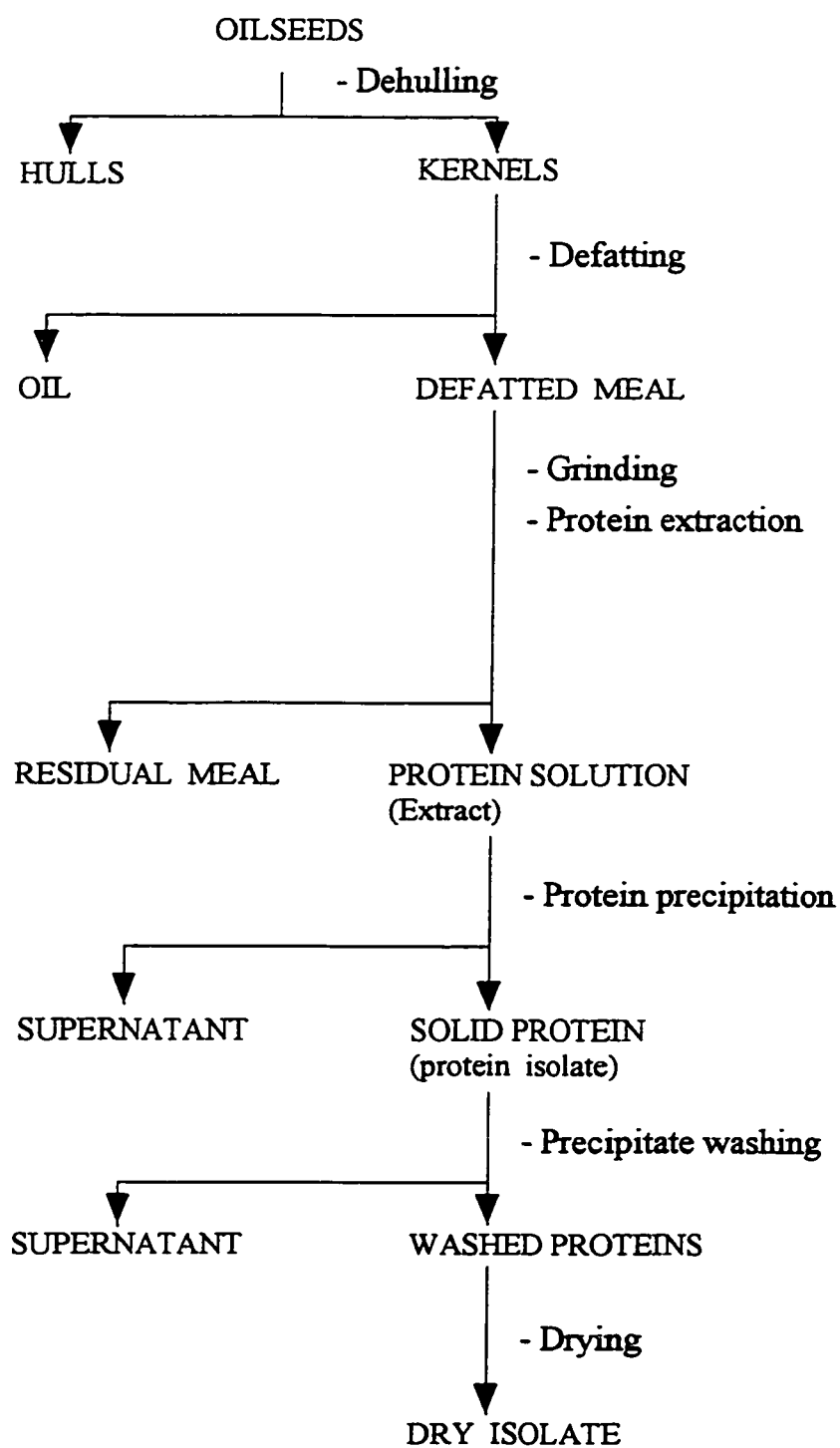


Figure 2.3 Flow diagram for preparation of dry protein isolate.

Table 2.6 Types of precipitants used in protein precipitation (Bell et al., 1983).

Precipitation mode	Precipitant	Examples
Changing of solvent environment	i. Heat	> 45 °C.
	ii. Neutral salts	NaCl, (NH ₄) ₂ SO ₄ , Na ₂ PO ₄ , Na ₂ SO ₄ , and K ₂ SO ₄ .
	iii. Organic solvents	ethanol, acetone, and ether.
	iv. Acids (pH adjustment)	HCl, H ₂ SO ₄ , and H ₂ PO ₄ .
	v. Non-ionic polymers	dextrans and PEG.
Direct interaction with protein molecules	i. Ionic polymers	CMC.
	ii. Polyelectrolytes	HMP.
	iii. Metal ions	Ca ²⁺ , Ba ²⁺ , and Zn ²⁺ .

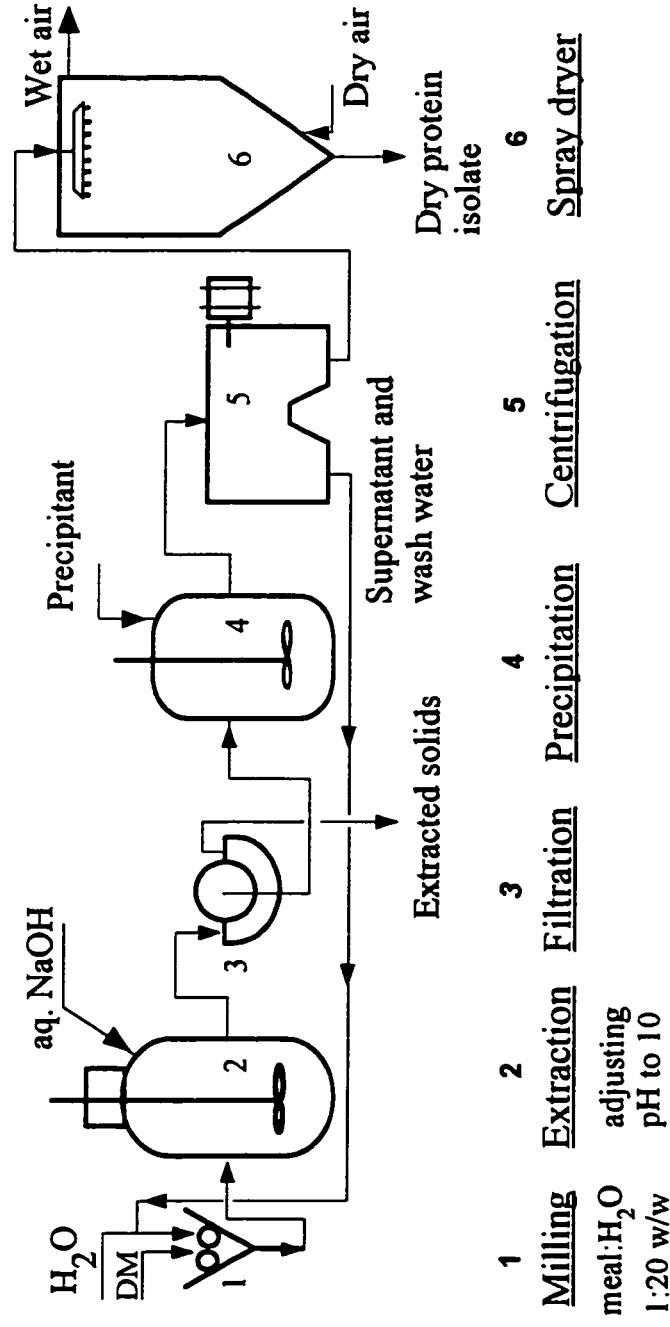


Figure 2.4 Process flowsheet for solid protein recovery from defatted oilseed meals.

2.3 Previous Studies on Oilseed Protein Precipitation

2.3.1 Precipitation Studies Using Batch Precipitators

Nelson and Glatz (1985) studied the formation of primary particles ($< 0.3 \mu\text{m}$) in a batch precipitator during isoelectric precipitation of soy protein. Effects of mixer speed, protein concentration, pH, ionic strength, and different precipitants on primary particle size were investigated. They reported that mixer speed, pH and ionic strength have no effect on primary particle size. Increasing the protein concentration increased the size of primary particles. This is because of increased degree of supersaturation. This agrees with Nielsen's model for homogeneous nucleation. It was also reported that the batch precipitator yields larger primary particles than the MSMPRP. This is due to the decrease in supersaturation caused by dilution in the MSMPRP. Also, they reported that the narrow PSD observed in an MSMPRP was due to the formation of a large number of new particles and not by the growth of the older particles. Due to short mean residence times, the aggregation of smaller particles with larger particles is not likely to occur. They also reported that the size of the primary particle is dependent on the type of the precipitant used ($\text{Ca}^{2+} < \text{H}_2\text{SO}_4 < \text{HCl}$).

Fisher et al. (1986) studied the effect of acid addition (rapid or slow) during isoelectric precipitation of soy protein. They reported that speed of acid addition has no effect on overall yield of solid proteins and protein composition. Rapid addition of acid produces a precipitate with larger primary particles, stronger aggregates, and a wider PSD due to high supersaturation and rapid aggregation. They suggested that rapid precipitation reduces the chances of particle attraction, depending on their surface charges and the opposite during slow acid additions resulting in a precipitate with multimodal PSD caused by particle-particle attractions (electrostatic bonds).

Chen and Rohani (1992) studied the precipitation of canola protein using several precipitants: HCl for the isoelectric method, CMC (carboxymethylcellulose) for the ionic polymer precipitation method, ammonium sulphate for the salting out method, and sodium hexametaphosphate (HMP) for the polyelectrolyte precipitation. They reported that the salting out method resulted in a higher yield (94 %w/w) and the presence of

HMP resulted in the largest mean particle size (32 μm). High yield by the salting out method shows that a large portion of extracted canola proteins were albumins, globulins, and glutelins which are readily soluble in aqueous solution (up to 90 %w/w of the soluble protein were extracted at pH 12). Using isoelectric precipitation, only 60 %w/w of soluble proteins were recovered, while 79 %w/w was obtained by HMP, and 61 %w/w by CMC. Lower yields by the isoelectric method is attributed to the existence of two isoelectric pH points at around pH 4 and 6.

2.3.2 Precipitation Studies Using Mixed-Stirred Precipitators

Grabenbauer and Glatz (1981) studied the precipitation of soy protein in a well-mixed vessel. They reported that aggregation is the dominant process in the formation of larger protein particles. The steady state PBE based on aggregate size with linear-size dependent aggregate growth rate, first order aggregate breakup term and birth rate was proposed. The authors used the least squares method to determine the model parameters from experimental data. From their study, they observed that: large protein particles were composed of primary particles of about 0.1 μm ; there was a sharp decline in the population of larger particles due to breakage resulting in higher populations of intermediate size. They proposed that stable aggregates are formed by collisions between primary particles and growing aggregates, and that there is a maximum stable size for aggregates determined by hydrodynamic forces. Increasing the protein concentration resulted in an increased solids concentration. Increasing the mixer speed increased the aggregate breakage rate.

Petenate and Glatz (1983a) studied the effects of operating parameters (pH, feed concentration, mean residence time, ionic strength, and speed of stirrer) on PSD of soy protein during isoelectric precipitation in an MSMPR precipitator. They reported that increasing the protein feed concentration shifts the PSD upwards (thus, no change in the mean particle sizes). Increasing the mixer speed increased the number of intermediate particle sizes, while the number of small particles and large particles decreased due to increased growth rate and breakage rate, respectively. Furthermore, they reported that increasing the mean residence time resulted in increased probability of particle-particle

collisions leading to the formation of larger aggregates.

Rohani and Chen (1993) studied the effects of the operating parameters: mean residence time (τ), precipitation temperature (T), apparent relative supersaturation (σ), stirrer speed (ω), and the ionic strength of the solution (IS) on isoelectric precipitation of canola proteins in an MSMRP. Using their experimental data they calculated the kinetic parameters of canola proteins. The kinetic parameters were obtained by a multiple regression method of the empirical correlations describing nucleation rate, growth rate and aggregation index. The three equations had a similar form as:

$$B^o = k_p \exp^{-E_p/RT} \sigma^{aa} (IS)^{ee} \omega^{cc} \tau^{dd} \quad (2.3)$$

They showed that increasing the relative supersaturation results in an increase of solids protein and the mean particle size. Increases in the relative supersaturation increased the kinetic rates (nucleation rate, growth rate and aggregation rate). They reported that the mean residence time had no effect on solids yields as the reaction was very fast and came to completion within a short time. But longer residence times resulted in larger mean size, probably due to formation of aggregates between small particles and large aggregates. They showed that the nucleation rate and growth rate increased with increase in mixer speed. Increasing the ionic strength increased the protein solubility, resulting in lower solid protein yields and decreases in the mean particle size. Also, they reported that high precipitation temperatures increased the protein solubility (lower solids yield) and the mean particle size, due to increased rate of nucleation resulting in a higher aggregation rate.

2.3.3 Precipitation Studies Using Tubular Precipitators

Virkar et al. (1982) studied the isoelectric precipitation of soy protein in a tubular precipitator under a turbulent flow regime. This was the first study published on the application of a tubular precipitator for recovery of proteins. In this study, 12-m and 23-m long tubular precipitators with inner diameters of 15 mm were used. The flow Reynolds number used was greater than 20,000 with the flow of protein solution being

much greater than that of the acid. They reported the following observations:

- (i) Precipitation process is a rapid formation of primary particles followed by collision-controlled aggregation as reported earlier by Grabenbauer and Glatz (1981).
- (ii) During isoelectric precipitation, solid protein comes out of the solution quickly and was complete within 1 s. Similar observations were also reported by Chan et al. (1986).
- (iii) Protein particle growth was mainly by aggregation mechanism.
- (iv) The rate of particle growth increased with increases in protein concentration and also with increases in the turbulence.
- (v) The mean particle size decreased with increases in the turbulence.
- (vi) The mean particle size increased with increases in protein concentration. This was attributed to increased rate of aggregation.
- (vii) The mean particle sizes were largest at the isoelectric pH.
- (viii) The mean particle size was independent of the precipitation temperature in the range 283-303 K.
- (ix) Longer mean residence time resulted in larger mean particle sizes, whereas the width of spread of particle size distribution (CV) decreased with increases in the mean residence time.

The authors modelled the growth of protein particles along the tubular precipitator using Smoluchowski's theory. They assumed that the particle growth is by orthokinetic aggregation of particles caused by particle-particle collision in the turbulent flow regime. That is, for two particles of radius r_i and r_j , the frequency of orthokinetic collision per unit volume in turbulent shear flow is:

$$F_{ij} = \frac{4}{3}(r_i + r_j)^3 N_i N_j \left(\frac{\eta}{\nu}\right)^{1/2} \left(1 - \frac{\delta}{2}\right) \quad (2.4)$$

where the energy dissipation per unit mass was defined as: $\eta = 2f_f \rho \nu_L^3 / d_t$. The rate of change of number density in the size range i was defined as:

$$\begin{aligned}
\frac{dN_i}{dt} = \frac{4}{3} \left(\frac{\eta}{\nu} \right)^{0.5} & \left[\sum_{j=i-5}^{i-3} (r_{i-1} + r_j)^3 N_{i-1} N_j \Lambda_{i-1,j} + 4r_{i-2}^3 N_{i-2}^2 \Lambda_{i-2,i-2} \right. \\
& - \sum_{\substack{j=i-4 \\ j \neq i}}^{i_{\max}} (r_i + r_j)^3 N_i N_j \Lambda_{i,j} - 4r_i^3 N_i^2 \Lambda_{i,i} \\
& \left. + (r_{i-2} + r_3)^3 N_{i-2} N_{i-3} \Lambda_{i-2,i-3} \right]
\end{aligned} \tag{2.5}$$

For effective collision leading to a lasting aggregation, the radius of a newly-formed aggregate was assumed to be less than r_{\max} (30 μm), otherwise the collision was ineffective. That is:

$$(r_i^3 + r_j^3)^{1/3} > r_{\max}, \quad \Lambda_{i,j} = 0 \quad \text{ineffective collision} \tag{2.6a}$$

$$(r_i^3 + r_j^3)^{1/3} \leq r_{\max}, \quad \Lambda_{i,j} = 1 \quad \text{effective collision} \tag{2.6b}$$

The fluid flow was assumed to be in plug flow regime and the particle growth time was assumed to be the same as the mean residence time of the fluid (particles have the same residence time as the fluid). The model results showed good predictions between the calculated and experimental mean particle sizes for the initial stages (at the start). As the mean residence times (growth time) increased, the calculated mean sizes were much larger than the experimental data. This was attributed to the lack of a proper model for the breakage of the larger aggregates (formed by the collisions that resulted in particles larger than r_{\max}) and due to the lack of the kinetics of precipitation.

Virkar and co-authors considered the tubular precipitator as an aggregator with limited particle breakage. Also, they considered that the dispersion along the tubular precipitator to be constant because of high flow Reynolds number (turbulent flow regime). The assumption that the precipitation process is a very fast reaction, almost complete within 1 s, neglects the molecular particle growth by diffusion which may continue beyond 1 s. This is because the diffusion process is a slow process and depends on the mixing of the suspension. Thus the particle growth may continue for some time

before the concentration gradient vanishes, although the contribution to the particle size change by the growth mechanism may be much smaller as compared to that caused by aggregation.

Chan et al. (1986) studied the kinetics of soy protein in a tubular precipitator using different precipitants. The tubular precipitator used in this study was 5.75 m in length and 4 mm in diameter. There were 10 sampling ports along the tubular precipitator. Experiments were carried out in the laminar flow regime ($Re = 500$ based on total feed flow rate). Their comparison experiments were set such that the final concentration of protein in the solution was the same (3 kg/m^3). In this case, the flow rate and concentration of protein were varied depending on the fixed concentration of the precipitant and the final protein concentration. They reported that changing both protein and precipitant concentration showed no significant effect on the mean particle size. Also, changing the mixing pressure showed no significant changes in the mean particle size. Since these experiments were performed to give a desired final concentration of protein in solution and at fixed total flow Reynolds number, this means that, if high concentration protein solution at high flow rate had to be used in order to keep the desired Reynolds number and the final protein concentration, the ratio of protein solution flow rate to acid flow rate would be large. However, the concentrations of acid used were too close, 0.022 and 0.036 mol/L, to significantly note the effects of volumetric feed ratio. Furthermore, they reported that, for high concentration protein solutions, the solid protein comes out of the solution within 1 s. The initial primary particles grow by aggregation and their final size depends on the growth and breakage rates controlled by shear forces and the type of the precipitant used.

In the present study, a full model incorporating primary nucleation, molecular particle growth, particle aggregation, particle breakage, and flow regimes along the tubular precipitator will be presented.

2.3.4 Precipitation Kinetics

Precipitation kinetics refers to the mathematical representations of the physical steps involved in precipitation or crystallization, that is, nucleation, particle growth (by

diffusion process at molecular level), particle aggregation, and particle breakage. Nucleation is the process by which new solid particles are formed. There are two types of nucleation: primary and secondary nucleation. Primary nucleation occurs when the degree of supersaturation is high and it is expressed theoretically as (Mullin, 1992):

$$\frac{dN}{dt} = k_n \exp\left(-\frac{k_m}{\log^2 S}\right) \quad (2.7)$$

where k_m and k_n are nucleation parameters; S is the supersaturation, C/C^* ; C and C^* are solution concentration and equilibrium saturated concentration, respectively. Primary nucleation can be homogeneous or heterogeneous. In the former, the formation of new solids is not influenced by the presence of solids, whereas, in the latter, the presence of solid phase enhances (catalyzes) the process. Nielson (1964) described the homogeneous nucleation using a power law equation as:

$$\frac{dN}{dt} = k(C - C^*)^{ab} \quad (2.8)$$

where k and ab are parameters. In this case, the nucleation rate is assumed to be a diffusion controlled process. In secondary nucleation the formation of new solids is initiated by the presence of solid particles. Secondary nucleation is normally expressed using empirical correlation (Jones, 1993) of the type:

$$\frac{dN}{dt} = k_s M_T^{js} \sigma^{bs} \quad (2.9)$$

where σ is the absolute supersaturation, $(S-1)$; M_T is total mass of solids; bs , js , and k_s are parameters. The exponent js determines the mode of erosion; $js = 1$ represents particle-vessel collisions, $js = 2$ for particle-particle collisions, and $js = 1$ to 2 for fluid shear. Protein precipitation from the solution by the isoelectric method is an instantaneous process, the solid protein comes out of the solution within 1 s (Grabenbauer and Glatz, 1981, Virkar et al., 1982; Raphael et al., 1985). Thus, homogenous nucleation process is used to represent the nucleation rate.

The growth of particles by aggregation has been modelled using diffusion-controlled theory (perikinetic) or shear-controlled theory (orthokinetic). The former theory is used for collisions of small particles, ca. 0.1 μm , and the latter is used for large particles. The perikinetic and orthokinetic aggregation rates are defined by (Hoare, 1982b) :

[The rate of change of number of particles of size L_k] = [The rate of formation of particles of size L_k by collision of smaller particles of size L_i and L_j] - [The rate of loss of particles of size L_k by collisions with particles of size L_i] + [Correction term for collision of like particles of size L_k]. That is, for the perikinetic aggregation:

$$\begin{aligned} \frac{dN_k}{dt} = & \left[\sum_{i=1}^{i=k-1} \pi(L_i+L_j)(D_i+D_j)N_iN_j \right] \\ & - N_k \left[\sum_{i=1}^{i=\infty} 2\pi(L_i+L_k)(D_i+D_k)N_i \right] \\ & + [4\pi L_k D_k N_k^2] \end{aligned} \quad (2.10)$$

and for the orthokinetic aggregation is given by:

$$\begin{aligned} \frac{dN_k}{dt} = & \frac{1}{16} \left[\sum_{i=1}^{i=k-1} \frac{4}{3} (L_i+L_j)^3 G_s N_i N_j \right] \\ & - \frac{N_k}{8} \left[\sum_{i=1}^{i=\infty} \frac{4}{3} (L_i+L_k)^3 G_s N_i \right] \\ & + \frac{1}{16} \left[\frac{32}{3} L_k^3 G_s N_k^2 \right] \end{aligned} \quad (2.11)$$

where particle sizes are related as $L_k^3 = L_i^3 + L_j^3$, D = particle diffusivity, G_s = average shear rate, and N is the number concentration of particles. The orthokinetic aggregation equation was used by Virkar and coauthors (1982) to model the growth of precipitate particles in a tubular precipitator.

Virkar et al. (1981) studied the effects of very high shear stress on globular

protein solutions. They measured the changes in enzyme activity and concentration of proteins in solution after shearing. They reported that no substantial damage of globular proteins was observed after about 1500 passes through several pumps.

Hoare (1982a) studied the aggregation of casein particles during precipitation by salting-out in a stirred precipitator. It was reported that increasing the mean residence or decreasing the stirrer speed resulted in an increase in the mean particle and vice versa. It was concluded that, during precipitation, there is a balance between particle growth by aggregation and particle breakage caused by shear. The author reported that the perikinetic theory can be used to model growth of particles during settling (ageing). Modelling of aggregate growth under shear was not successfully modelled using orthokinetic theory due to the presence of aggregate breakage.

Hoare et al. (1982) studied the effects of shear in couette flow and pumps on PSD of soy protein precipitate. They reported that peristaltic pumps cause no particle breakages. The gear pump caused the highest breakage, whereas centrifugal and moyno pumps caused less breakage. To minimize the production of fine particles, they recommended using flow by gravity or gas pressure.

Bell and Dunnill (1982) investigated the effects of aging and of exposure for short times (0.004 - 0.2 s) to high shear rates ($10^4 - 10^5 \text{ s}^{-1}$) on soy protein precipitates. Particle breakage is attributed to: deformation and rupture created by changes in pressure (internal and external), erosion of aggregates caused by particle-particle collisions and between particles and the vessel walls or mixer. The strength of the protein particles depends on the bonding type in the protein molecule and that holding the aggregate. Bell and Dunnill found that increasing the aging time increased the strength of the aggregates and the solid density, whereas the number of fine particles decreased. The strength of the aggregates was found to increase with increase in shear rate and that a continuous tubular precipitator with low-shear conditions would result in weaker aggregates.

Bell et al. (1982) measured the density of soy protein particles (3.4 - 6.5 μm) obtained by isoelectric precipitation. The proteins used in study were mostly of globulin nature (7S and 11S). The centrifugal sedimentation methods were used to determine the buoyant density of the protein aggregate. The average density was found to be 1296 kg/m^3 with hydration capacity of 0.2 kg water/kg protein. Their results were in

agreement with previous studies by Kinsella (1979). They reported that the protein aggregate density decreased with aggregate size ($\rho_a = 1004 + 246d^{-0.408}$), for larger aggregates the density become independent of aggregate size. Also the volume fraction of solid proteins in an aggregate was found to decrease with aggregate size. However, the aggregate density and void fraction in the aggregate depends on the strength of the aggregate. Strong aggregates had a higher density and a lower voidage.

Petenate and Glatz (1983b) presented the model describing the effects of turbulent collision and hydrodynamic forces on aggregate growth and breakage, respectively. It was assumed that stable (lasting) aggregates are formed as a result of collisions between the small aggregates and large aggregates (collectors). Furthermore, the nuclei particles were assumed to be formed by breakage of large particles and the rest of the PSD was divided into three regions: $< 2 \mu\text{m}$ as small particles, $2 - 6.5 \mu\text{m}$ as intermediate size, and $> 6.5 \mu\text{m}$ as large particles. The differential growth rate of aggregates was defined as a power-law in particle size as:

$$G_a = KL^g \quad (g < 1) \quad (2.12)$$

Breakage of the aggregates was considered to be the consequences of hydrodynamic forces, particle-particle collisions, erosion, and yield stress caused by the surrounding fluid. Taking into account all these effects, the breakage rate was defined as:

$$D_b = KpL^\gamma \quad (2.13)$$

The overall PBE for an MSMPR with aggregation was presented as:

$$\frac{\partial p}{\partial t} + \frac{\partial}{\partial L}(G_a p) + \frac{p}{\tau} + D_b = 0 \quad (L \geq L_o) \quad (2.14)$$

$$p(0, L) = p^o(L)$$

$$p(t, L_o) = p_o(t)$$

where L_0 is the aggregate nuclei diameter, $p^0(L)$ is the initial number density, and p_0 is the nuclei number density. The resulting PBE was solved analytically and kinetic parameters for D_a and G_a were obtained by fitting the experimental data using the least squares method.

Twineham et al. (1984) studied the effect of solid concentration on the shear-induced breakup of protein particles. It was reported that particle breakage is a consequence of particle-particle collisions. It follows a first order rate in particle size and it is concentration dependent for concentrations between 0.1 and 2.5 %w/v. Their study included solid concentrations from 0.001 %w/v to 5 %w/v and maximum breakage rate was observed at a solid concentration of 0.25 %w/v. In another study, Brown and Glatz (1987) reported that the breakage rate due to collisions was second order in particle concentration. Later, Fisher and Glatz (1988) modelled the collisional breakage of protein particles during polyelectrolyte precipitation. They reported that the data gave the best fit using a breakage model with second order in population density and a ninth order in particle size.

Glatz et al. (1986) evaluated the precipitation kinetics of aggregation of soy protein from isoelectric precipitation of protein in a CSTR. In this study they assumed that particle growth was by addition of smaller particle to the growing aggregate and aggregate breakage was related to the aggregate size by the power law. The steady state PBE with a linear growth rate for a MSMR in terms of aggregate size L was given as:

$$\frac{d(G_a p)}{dL} + \frac{p}{\tau} + D_b - B_b = 0 \quad (2.15)$$

where the growth rate (G_a), birth rate (B_b), and death rate (D_b) were defined as:

$$G_a(L) = K_g L \quad (2.16a)$$

$$D_b(L) = K_d L^b p(L) \quad (2.16b)$$

$$B_b(L) = f D_b(f^{1/3} L) \quad (2.16c)$$

In another study by Grabenbeuer and Glatz (1981), the growth rate was assumed to be size independent. The proposed model with linear aggregate growth rate showed a good fit of experimental data with bimodal distribution. They reported that the growth rate constant and the breakage rate constant were less dependent on choices of β and f . For high protein concentration (25 kg/m^3) β and f parameters were fixed at 1.5 and 3, respectively. At low protein concentration ($< 3 \text{ kg/m}^3$) β and f were set at 2.3 and 2, respectively. In this study, it was assumed that the final PSD was determined by shear-controlled breakage. Other factors like nucleation rate and molecular growth were not considered in the model. A similar method was employed by Raphael and Rohani (1995) to fit the model to the experimental data on precipitation of sunflower protein in an MSMPRP.

Fisher and Glatz (1988) reported that precipitation of proteins by polyelectrolyte (high molecular weight, 4×10^6) resulted in a precipitate which showed an increase in the mean size as the shear rate was increased. That is, increasing the mixer speed enhanced particle growth and not particle breakage as reported in acid precipitation systems. It was also observed that the mean particle size increased with an increase in mean residence time. All these were attributed to the presence of aggregation resulting in stronger aggregates than those observed with isoelectric precipitation. This was explained as due to the stronger bonds formed between the polyelectrolyte and the protein molecules and not a simple aggregation caused by electrostatic or hydrophobic bonds.

2.4 Other Related Studies on Crystallization and Precipitation

2.4.1 Studies on Particle Aggregation and Breakage

Determination of aggregation mechanism has been done by two methods: a determination of aggregation mechanism from steady state experimental data by assuming the mechanism then solving the PBE to obtain the parameters (inverse method) or by using an experimentally determined mechanism. The inverse method may sometimes result in multiple solutions (non-unique solution). There are two types of aggregation models: size-dependent and the size independent. The size independent

phenomena, if not checked, results in a narrower PSD and eventually results in a large single aggregate formed by the original particles.

Wright and Ramkrishna (1992) applied the method of inverse problem to determine the aggregation kernel from unsteady state PSD of purely aggregative system (no breakage or growth of particles) with "self-preserving" property.

Ilievski and White (1994) determined the aggregation mechanism of $\text{Al}(\text{OH})_3$ from experimental data using "inverse problem" method and "forward method". They found that the simple assumption, size-independent model, described the experimental data better. Several other systems have been modelled using this simple assumption successfully especially when the actual mechanism is not known.

Ilievski and Hounslow (1995) determined the aggregation kernel for the aggregation of $\text{Al}(\text{OH})_3$. The tracer method was used instead of the PSD data to identify the aggregation mechanism. In this case the tracer particles have to be the same as the seeding particles.

2.4.2 Studies on Precipitation in Batch Precipitators

Halfon and Kaliaguine (1976a) and (1976b) studied the crystallization of $\text{Al}(\text{OH})_3$ in a batch crystallizer with different seeding concentrations. Experimental data were used to determine nucleation and growth rate kinetics. They reported that aggregation increased with an increase in supersaturation and that aggregation rate was proportional to the fourth power of supersaturation.

Chen et al. (1990) simulated a batch precipitator with aggregation and aggregate breakage only at steady state. They reported that the time required for a precipitation system to attain steady state PSD is independent of the initial PSD for a given process. However, if the nucleation and growth rates are included in the simulation, the PSD simulation results in a multiple steady state.

Wachi and Jones (1992) modelled the precipitation of CaCO_3 in an unsteady state batch precipitator. They introduced a second co-ordinate in the PBE to account for the number of particles within an agglomerate. The purpose of this formulation was to distinguish between a single large particle and an agglomerated particle of equivalent

size. The solution of the PBE with homogeneous nucleation equation, size independent growth rate, particle aggregation with orthokinetic aggregation kernel and particle death (due to disruption) was solved using finite difference method. The calculated PSD showed a bimodal distribution, indicating the presence of large particles formed by aggregation rather than molecular growth.

Dash and Rohani (1993) used an iterative method to extract the kinetic parameter of KCl crystallization in a batch crystallizer. In their study the kinetic equations were given as :

$$B^o = k_b(G)^{aa}M_T^{bb} \quad (2.17a)$$

$$G = k_g(\Delta C/C^*) \quad (2.17b)$$

where $M_T = \rho k_v m_3(t)$, $\Delta C = C(t) - C^*(t)$, and aa , bb , k_b , and k_g are kinetic parameters to be determined. The governing PBE was solved using a two-step Lax-Wendorff finite difference method. The performance index (objective equation) to be optimized was defined as:

$$J = \sum_{i=1}^{nw} \sum_{j=1}^{nw} (\Delta W_{i,j})^2 \lambda_{i,j} \quad (2.18)$$

where $\Delta W_{i,j}$ is the difference between the measured and calculated weight of crystals and $\lambda_{i,j}$ is the weighting factor. However, the nucleation parameter bb could not be determined directly from the data and had to be fixed at 1. Also, due to instability and multiple minimum values, the search range of the parameter for global optimization was reduced. Sometimes this may result in a "ghost" optimum value if the search range is not properly selected.

2.4.3 Precipitation Studies in Mixed Suspension Mixed Product Removal Precipitators (MSMPRP)

Liao and Hulburt (1976) developed a model to determine kinetic parameters (nucleation rate, growth rate, and aggregation rate) from steady state PSD. A similar

method has been employed by Tavaré et al. (1985) to determine kinetic parameters for nickel ammonium sulphate, $\text{Ni}(\text{NH}_4)\text{SO}_4$, for an MSMPR Crystallizer.

Tavaré et al. (1985) studied the precipitation of nickel ammonium sulphate in an MSMPR crystallizer. The solution of the PBE with aggregation was solved analytically using the method of Liao and Hulburt (1976). The precipitation kinetics were obtained by an iterative method. They reported the following equations for the growth rate, $G(\mu\text{m/h})$, nucleation rate, $B^\circ(\text{no/L.h})$, and aggregation rate (A):

$$G = 3.68 \times 10^3 \Delta C^{0.71} \quad (2.19a)$$

$$B^\circ = 4.447 \times 10^{11} G^{-0.12} M_T^{0.025} NR^{-1.0} \quad (2.19b)$$

$$A = 9.45 \times 10^{-18} G^{0.52} B^{\circ 1.30} M_T^{-0.86} NR^{-0.22} \quad (2.19c)$$

where NR is the stirrer speed (rpm) and M_T is the total amount of solids.

Lamey and Ring (1986) studied the precipitation of TiO_2 in an MSMPR precipitator. They reported that aggregation is the dominant method of particle growth. To circumvent the difficulty posed by the aggregation equation (non-linear), they assumed that the aggregation was between the nuclei particles and large aggregates. Physically, this assumption is unrealistic if the total mass was to be conserved.

Delpech de Saint Guilhem and Ring (1987) presented the analytical solution for the continuous stirred tank crystallizer (CSTC) with aggregation. They assumed that when two particles aggregate the particle length is conserved that is:

$$B(L) = \int_0^L K p(L-x) p(x) dx \quad (2.20)$$

This assumption results in an unrealistic solution (Lui and Thompson, 1992, Hounslow, 1990b) when considering aggregation of particles with deformable mass. Furthermore, Lui and Thompson showed that the analytical solution developed by Delpech de Saint Guilhem and Ring did not predict the bimodal size distribution as claimed. Also,

Hounsflow showed that such an assumption lead to over estimation of CV for a given aggregation index. In another previous study, Lamey and Ring (1986) used the same definition for particle birth due to aggregation and made an assumption that the new aggregates are formed by collision between the nuclei and the large aggregates. Thus the birth equation reduces to:

$$B(L) = KLp^2(L) \quad (2.21)$$

This assumption was also unrealistic because the size of the nuclei particle was close to zero. Thus the collision of particles of size L with nuclei particles was not effective.

Shi et al. (1990) studied crystallization kinetics of α -lactose monohydrate in a cooling-type well mixed crystallizer. Nucleation rate and growth rate parameters were obtained from empirical correlation given as $B^o = K_B \exp(E_N/RT) M_T^{s_j} (S-1)^{s_i}$ and $G = K_G \exp(E_G/RT) (S-1)^{s_g}$, respectively. E_N and E_G are activation energies for nucleation and growth process, respectively, S = relative supersaturation ratio. The kinetic parameters were obtained by regression analysis. The resulting correlations were: B^o [no/mL min] = $1.99 \times 10^{18} \exp(-17.0/RT) M_T (S-1)^{1.9}$ and G [$\mu\text{m}/\text{min}$] = $6.1 \times 10^{15} \exp(-22.1/RT) (S-1)^{2.5}$. This shows that high E_G means the particle growth was not likely to be a diffusion mechanism. They suggested a surface integration mechanism similar to aggregation of smaller molecules by larger aggregates. Similarly, the unit exponent in M_T suggested that the first order secondary nucleation process was caused by particle-particle collisions.

Lee and Saleeby (1994) studied the behavior of CSD in an MSMPRC using different choices of parameters, CSD of seed particles, growth rate, and aggregation rate. The resulting PBE was solved using a Taylor series approximation (for the size dependent model) and a reversion method for the size independent model. They were able to show the combined effects of agglomeration and size dependent on CSD. They found that the calculated CSD for the size dependent model was always lower than that of the size independent model for $T = 2K\tau^2 G_o^o p_o > 0$, K = agglomeration factor, τ = mean residence time, G_o^o = initial growth rate, p_o = nuclei density and $\lambda = 2G_o^o a_g \tau \geq 1$ where a_g = is a growth parameter in $G(L) = (1 - a_g L)$. The trend reverses when $T > 0$ and $0 < \lambda < 1$.

Mersmann et al. (1994) presented experimental results on the effects of chemical reaction rate and mixing rate on mean particle size for Ba_2SO_4 , CaCO_3 , BaF_2 , and $\text{C}_6\text{H}_5\text{COOH}$ in an MSMRP. At low feed concentrations ($< 0.01 \text{ kmol/m}^3$) the mean particle size was found to be dependent on chemical reaction. At high feed concentration the mean particle size depended on the rate of mixing, and the particle size increased with increase in specific power input and with increase in mean residence time. They suggested that, for obtaining products with larger mean sizes, it is recommended to restrict maximum supersaturation (by dilution) by having a good macromixing of the entire vessel (high circulation rate) while keeping low micromixing of the feed stream. This was because high micromixing resulted in high local supersaturation leading to high nucleation rate resulting in smaller particles. The nucleation process was a spontaneous process, whereas particle growth rate was slow (diffusion controlled) and dependent on relative supersaturation. Also they recommended low feed concentrations.

Mydlarz and Jones (1994) assessed some published kinetic data obtained from an MSMPR crystallizer with size-dependent particle growth rate equations. They reported that, for larger particles, the growth rate becomes constant, independent of the particle size and the maximum growth rate could be estimated from the slope of the MSMPRC distribution equation.

Tai and Chen (1995) suggested simultaneous determination of nucleation rate and aggregation rate from steady state MSMPRP PSD. In this method the aggregation rate was assumed to be a function of relative supersaturation and solids concentrations.

2.4.4 Precipitation Studies in Plug Flow and Dispersed Flow Precipitators

Rivera and Randolph (1978) studied the continuous precipitation of pentaerythritol tetranitrate (TNT) in a short tubular precipitator. The precipitator was assumed to operate in the dispersed plug flow regime ($Pe = 51$) with the PBE given as:

$$D_z \frac{\delta^2 p}{\delta z^2} = u_z \frac{\delta p}{\delta z} + G \frac{\delta p}{\delta L} \quad (2.22)$$

This PBE was solved using the method of moments. In this study the nucleation rate and the growth rate along the tubular precipitator were assumed to be functions of the initial values, i.e., $B^o = B_o^o(1-z)^a$ and $G = G_o^o(1-z)^b$. A similar method was used by Raphael et al. (1995) for calculation of precipitation kinetic parameters for the sunflower protein from the tubular precipitator using the data in the dispersion region. In this study, the deconvolution of moments to generate the PSD using the matrix inversion method suggested by Randolph and Larson (1988) was not successful. Instead, a method suggested by Hulburt and Katz (1964) using weighted Laguerre polynomials was used.

2.5 Particle Size Distribution (PSD)

Particle size distribution represents a continuous model of the particle characteristic (number, length, volume, or weight) in a system at different size ranges. This distribution is described by two parameters, the mean particle size (d_m) and the coefficient of variation (CV). The CV shows the spread of the distribution about the mean, while the mean size represents a single linear dimension of particles in the system. The mean size can be expressed in terms of the length, or its surface, or its weight. In this study the mean particle size was based on the volume of particles as measured by a Coulter Counter. If Δv_i is the volume fraction of particles in the sampling channel i with the mean size L_i , then the mean particle size d_m is given by:

$$d_m = \sum_{i=1}^{nc} \Delta v_i L_i \quad (2.23)$$

Where nc is the total number of channels used in particle size measurement. The percent CV is given by:

$$CV(\%) = \frac{\left[\sum_{i=1}^{nc} [L_i - d_m]^2 \Delta v_i \right]^{1/2}}{d_m} 100 \quad (2.24)$$

The population density (n_i) of particles at channel size i is calculated by:

$$p_i = \frac{\Delta N_i}{\Delta L_i} \quad (2.25)$$

Where ΔN_i is the number of particles per unit volume in channel i and ΔL_i is the span of the i th channel defined as: $\Delta L_i = (L_{i+1} - L_{i-1})/2$. If the density of particles is assumed to be constant (independent of the particle size), then Equations (2.23) and (2.24) would also be valid for calculations of the mean particle size and CV based on weight.

2.6 Population Balance Equation (PBE) and Solution Methods

In order to determine the kinetic parameters for precipitation (from experimental data), it is necessary to represent the precipitation system using the population balance equation (PBE). The population balance equation represents a continuous distribution of the number of particles at different size ranges. The PBE conserves the rate of number density, that is:

$$\text{Rate of Input} - \text{rate of output} = \text{rate of accumulation} + \text{net rate of generation} \quad (2.26)$$

The population balance equations for crystallization and precipitation processes in the batch precipitator and mixed-stirred precipitators have been solved by several workers. The solution methods can be categorized into six main groups: analytical method, method of moments, method of weighted residue (MWR), method of classes, stochastic method, and finite difference method.

For a simple linearized PBE, Laplace transformation or inverse transformation

has been used to give an approximate solution. Saleeby and Lee (1994) solved analytically the PBE for an MSMPR crystallizer with agglomeration. The PBE solution was obtained by using the binomial and convolution theorems coupled with the reversion method. Two cases were solved, one with solid free feed and the other with exponential distribution in the feed. In this method the PBE was transformed using the Laplace transform, then the reversion method was applied to construct a series solution. For the very small population density region, up to 15 expansion coefficients were required for calculations. However, when non-linear terms (aggression or breakage) are included, the PBE solution by these analytical method became difficult.

Hurburt and Katz (1964) formulated the number density balance equation for continuous flow systems using a classical statistical mechanics method. They suggested the analytical method of moments for solving the balance equation, then gamma-weighted Laguerre polynomials were used to reconstruct the PSD from the moments. This deconvolution method has been reported to result in strong oscillations of the PBE (Randolph and Larson, 1988). Instead, Randolph and Larson proposed the matrix inversion method. In this method the moment equations are transformed into linear algebraic equations and solved numerically. However, this method resulted in positive and negative numbers of PSD (Raphael et al., 1995; Kim and Tarbell, 1991).

The method of moments developed by Randolph and Larson (1988) is widely used to solve PBE for the MSMPR precipitator. The method transforms the difficult-to-solve integro-differential equation into a set of ordinary differential equations by the moment method. In the absence of growth dispersion, aggregation, and particle breakage, the kinetic parameters are obtained from the slope and the intercept of the log-log plot of the population density versus particle size. The drawback of this method lies in the deconvolution of the moments to yield the PSD; sometimes convergence to the final solution is not achieved.

Frank et al. (1988) studied the kinetics of precipitation of salicylic acid in a batch and MSMPR precipitators. The resulting PBE were solved by the method of moments and the kinetic parameters were obtained by regression analysis from their experimental data.

MWR has found numerous applications in solving PDE and ODE in chemical

engineering (Finlayson, 1972). The method involves expanding the unknown solution using a combination of known trial functions and substituting into the original equation. The satisfying solution is obtained when the residual is zero or close to zero. This is achieved by orthogonalizing the residual with a set of weighting functions. These functions may be different from the trial solution. The difficult part of this method is in identifying the form of the trial function which represents the solution in the whole range. Orthogonal Collocation is a special form of MWR, in that the resulting residual is set at zero at fixed node points. In this case the collocation points are the roots of the trial function. The method is known to take shorter computation time. The method of weighed residue has been used to solve the difficult PBE. In this method the governing PBE was transformed into a set of ODE's using a set of orthogonal polynomials (Laguerre polynomial, shifted legendre polynomials, or problem specific polynomials).

Subramanian and Ramkrishna (1971) used the method of weighed residue to solve a PBE for cell growth in a batch and well stirred vessel. In this case the trial function and the weighing function were selected from the Laguerre polynomial, $L[0,\infty)$.

In another study, Singh and Ramkrishna (1975), used the problem specific polynomials (PSP) method to solve the PBE with particle coagulation. The trial solution was a generalized Laguerre polynomial. Then, orthogonal collocation and method of moments were used to solve for PBE. However, this method is simple to use for linear equations and it is almost impossible to construct a PSP when the governing PBE is non-linear.

Singh and Ramkrishna (1977) solved the PBE for a continuous MSMR crystallizer with binary particle breakage using MWR. They used the Gram-Schmidt (x^n) orthogonalization process to generate problem-specific polynomials as trial functions. Then the method of moments (Vorobyev's method) was used to generate a set of trial functions from the initial function. The method showed fast convergence and accurate results with less than four terms.

Chang and Wang (1984a) solved the PBE for a batch crystallizer using a shifted Legendre transformation method. The density function was expressed using a series of shifted Legendre functions to transform the PDE into a set of ODE. A similar method was used to solve the PBE for an MSMR crystallizer with particle breakage (Chang and

Wang, 1984b).

Sampson and Ramkrishna (1985) solved the integral-differential equation for a coagulating system using MWR with variable collocation points, especially near zero particle size range. The trial solution was developed using the PSP method.

Witkowski and Rawlings (1987) and Rawlings et al. (1992) applied the MWR; Galerkins method and orthogonal collocation method, respectively, to approximate the solution of the PBE. The integro-differential equation was transformed into a set of ODE by application of exponentially-weighted Laguerre polynomials as a trial solution. The choice of the Laguerre polynomial was based on the orthogonality range of these polynomials $[0, \infty)$. In another study, Lakatos et al. (1984) employed the orthogonal collocation method to simulate the solution of the PBE.

Bhatia and Chakraborty (1992) solved a PBE for a continuous agglomerative precipitation of $\text{Ni}(\text{NH}_4)\text{SO}_4$ and CaCO_3 to determine the kinetic parameters using the MWR and fraction moments. The approximating function was developed from the solutions of the simplified PBE (obtained from different truncations). Also a modified fraction moment method was used to satisfy the lower and upper ranges of the PSD.

The fourth method (method of classes) is based on the transformation of the PDE into a linear difference equation by discretization along the L direction. Machall et al. (1988) used the method of classes to solve the PBE for an unsteady system with size dependent growth rate, particle agglomeration or particle breakage. The partial differential equation describing the PBE is discretized in the L direction, then the resulting ODE is solved numerically together with the material balance equation.

Gupta and Dutta (1990) applied the stochastic analysis to predict the CSD from an MSMR crystallizer. Unlike the deterministic method, this method was based on random sampling of crystals. The CSD was calculated using data sampled randomly from the crystallizer (residence time, growth rate, shape factor, nucleation rate, particle size and weight of solids). The method was simple but showed larger oscillations in CSD when the sampling rate was increased. Furthermore, determination of the kinetic parameter is not possible from the given set of equation, since the growth rate and nucleation rate are also inputs to the equation.

Hounslow et al. (1988) developed a numerical method for solving the PBE for

a batch crystallizer using the discretization method. In this method, the continuous PSD, the PBE, and the moment equations were replaced by the approximate discrete equations. These transformed an integro-differential equation into a set of simple-to-solve ordinary differential equations. The method gave good agreement between predicted data and experimental data. A similar method was successfully used by Hounslow (1990a) to solve the PBE for an MSMPRC with an aggregation. Also, Hounslow (1990b) employed the discretization method to obtain the kinetic parameters (nucleation, growth, and aggregation rate) from steady state experimental data.

Lister et al. (1995) extended the discretized population method to accommodate variable sizes in particle size dimension. Unlike the original formulation by Hounslow et al. (1988), the discretization sizes were in geometric ratio of 2. The new scheme had the ratio $2^{1/q}$. The method gave comparable results for the PSD when q was made large ($q = 3$ or 4). Thus, a fine grid was required for accurate representation of the PSD.

Kim and Tarbell (1991) presented a numerical method scheme for solving a non-linear PBE for an MSMPRP and a semi-batch precipitator. In their scheme, they suggested solving the coupled ODE representing material balance and a moment equation. Then the PBE was solved using the finite difference method. In this way the non-linear terms in nucleation and growth rate are transformed into moments. The authors successfully applied the method in modelling of BaSO_4 precipitation in an MSMPR and semi-batch precipitators. This method cannot be applied in cases where the growth rate and nucleation rate equations cannot be expressed in moment forms and for rapid reactions where the concentration of solute drops sharply, very small time step sizes are required for integration.

Padia and Bhatia (1991) analysed the stability of the precipitation systems resulting from the coupling of the material balance equation, PBE, and kinetic equations for nucleation and growth rates. They stated that the solution of these coupled equations exhibited multiple steady states when certain ranges of kinetic parameters were used. Similar observations have been reported by Witkowski and Rawlings (1987) and Tavaré and Garside (1985).

CHAPTER 3

EXPERIMENTAL METHODS

3.1 Preliminary Experiments

3.1.1 Sunflower Protein Solubility and Solids Yield

Preliminary experiments with sunflower protein precipitation were performed to determine: the optimum pH for the extraction of proteins from defatted meals; minimum solubility pH for isoelectric precipitation; optimum NaCl concentration for protein extraction at natural pH 6.5; and calcium acetate concentration for optimum protein recovery from protein solutions. Calcium acetate was selected for precipitation of proteins at their natural pH because of its greater precipitating power for proteins in dilute solutions (Bell et al., 1983). Three types of defatted sunflower meals (DM) were used for this study. Two were laboratory defatted meals, while one was prepared from the oil-type seeds (CFT Foods., Altona, MB) and the other prepared from the confectionery-type seeds (Garden-land Packers, Altona, MB). The latter is readily dehulled and provides a higher meal yield than the oil-type. The third type was an industrially defatted meal obtained from Cargill Inc., West Fargo, ND. Dehulled sunflower seeds were ground using a food grinder to about 850 μm , then defatted with diethyl ether (40-60 °C) (BDH Inc., Toronto, ON) in a Goldfish extractor (LabConCo., Kansas City, MO) for 8 hr. The defatted meal (DM) was air-dried overnight, then ground and sieved through a 150 μm sieve. For determination of extraction curves (percentage protein extracted from defatted meal), sieved DM was mixed with distilled water at a ratio of 1 g of DM to 20 mL of distilled water. The pH of the slurry (measured using an Accumet pH meter 915, Fisher Scientific, Toronto, ON) was then adjusted to the

desired value (1 to 13) using 2 mol/L NaOH or 2 mol/L HCl. The amount of HCl or NaOH added was noted. The mixture was stirred for 2 hr at room temperature (22 ± 2 °C) using a magnetic stirrer while maintaining the pH constant. The residue (solid phase; solids leftover after extraction) and the supernatant (liquid phase; protein solution or extract) were separated by centrifugation (Beckman centrifuge model J2-21, Beckman Instruments Inc., Palo Alto, CA) at 6,000 rpm (5,520 xg) for 20 min. Nitrogen contents of the supernatant (protein solution) and the defatted meal were determined by the Kjeldahl method (Buchi digestion unit model 430 and distillation unit model 321, Buchi Lab. Technique Ltd., Flawil, Switzerland) following AOAC (1984) method. A factor of 5.7 was used to calculate protein content (Sosulski and Imafidon, 1990). The amount of protein in the solid residue after extraction was found by difference. The percentage of extracted protein was calculated as:

$$\text{Extracted protein (\% w/w)} = [V_p C_p / (M_s W_s)] \times 100 \quad (3.1)$$

where M_s is the weight of dry defatted meal, W_s is the protein content of the dry defatted meal (w/w), V_p is the total volume of liquid, C_p is the protein concentration in the solution (w/v), $M_s W_s$ is the total amount of protein in the dry defatted meal, and $V_p C_p$ is the total amount of extracted protein in the solution.

The protein solution (extract) for the determination of pH-solubility curves (amount of protein in the solution in equilibrium with the solid protein) was prepared by extracting protein from the defatted meal (1 g meal : 20 mL alkaline aqueous solution) at pH of 13. Extraction was done twice, each time for 1 hr. The two extracts were combined and diluted to 60 mL with aqueous solution (distilled water with adjusted pH at 13). During each precipitation run, 25 mL of the protein solution were adjusted to the desired pH value (1 to 10) by adding 2 mol/L HCl or 2 mol/L NaOH solution at room temperature. The amount of HCl or NaOH added was noted. The mixture was stirred continuously for 30 min while maintaining the pH constant. The precipitate (solid protein) and the supernatant (mother liquor) were separated by centrifuging twice at 10,000 rpm (15,300 xg) for 20 min, then filtered through a no. 42 Whatman filter paper. The initial protein solution (diluted extract) and the supernatant (mother liquor) were

then analyzed for the nitrogen content by the Kjeldahl method. The protein yield was calculated as:

$$\text{Protein yield (\% w/w)} = [(V_1 C_1 - V_2 C_2) / V_1 C_1] \times 100 \quad (3.2)$$

where V_1 (25 mL) and V_2 are the volumes and C_1 and C_2 are the protein concentrations of the extract and supernatant, respectively. The solubility of sunflower protein at that particular pH was given by C_2 .

For precipitation experiments using calcium acetate (at pH 6.5), extraction of proteins with aqueous NaOH was not used. This is because of low protein solubility at this pH. Therefore, washed and freeze dried protein isolate was used to prepare the aqueous protein solution. The aqueous solution of NaCl was used for protein dissolution at pH 6.5. Before this, experiments were performed to determine the concentration of NaCl which gave the maximum protein solubility at pH 6.5. It is known that, at low concentrations of NaCl, there is salting in (dissolution of protein) and at high concentrations of NaCl salting out (precipitation of protein) occurs. Protein solubility experiments were performed by suspending 2 g of dry protein isolate in 20 mL of aqueous solution at pH 6.5. The pH was adjusted using 0.01 mol/L acetic acid. Then a known amount of dry NaCl was added. The mixture was stirred for 30 min while maintaining the pH at 6.5, then centrifuged at 10,000 $\times g$ for 20 min. The supernatant was analysed (Kjeldahl method) for the dissolved protein (protein solubility). The experiment was repeated for graded concentrations of NaCl. Blank experiments (without NaCl) were used as controls. During precipitation experiments, increasing volumes (0.2 to 5.0 mL) of 1.0 mol/L calcium acetate solution with pH 6.5 (adjusted using 0.01 mol/L acetic acid) were mixed with 20 mL of protein solution (of known concentration) also at pH 6.5. The slurry was mixed for 30 min, then centrifuged and analysed for protein content as before.

In summary, these preliminary studies were used: firstly, to establish the optimum pH and maximum NaCl concentration for protein extraction from defatted meal (i.e., resulting in high protein extraction), and secondly, to determine the minimum solubility pH and optimum (high solids concentration and large particles) calcium acetate

concentration for protein precipitation from the solution (i.e., resulting in high yield).

3.1.2 Functional Properties of Sunflower Protein Isolates

In the formulation of food products, dry protein isolates are mixed with aqueous solutions to form a colloidal suspension. The physical, chemical, and organic properties of the suspension determine its functional properties. The most important functional properties include: water absorption capacity, dispersibility, blendability, fat absorption, foaming capability, emulsification, texturization, color and flavor. Some of these functional properties for sunflower proteins have been reported by Sosulski and Fleming (1977). In this study, the following tests on sunflower protein isolate were performed: whipability and foam stability (Lawhon, 1972), fat absorption (Inklaar and Fortunin, 1969), and water hydration capacity (Quinn and Paton, 1978). For comparison purpose, parallel experiments were performed using commercial soy protein isolate, Purina Protein, 500E, manufactured 1986.

3.1.3 Inhibition of Discoloration of Sunflower Protein Isolates

In this study; samples of dry defatted sunflower meal, spent meal after protein extraction, freeze dried sunflower protein isolates with and without Na_2SO_3 , protein solutions, and membrane separated protein solutions were analysed for the concentrations of chlorogenic acids (CA). Solid samples were washed with 70 % aqueous methanol, whereas for liquid samples, about 0.5 mL was diluted to 100 mL using 70 % aqueous methanol. The amount of CA dissolved in aqueous methanol solution was determined by measuring the optical density of the solution at 328 nm using a spectrophotometer (Milton Roy Spectronics, Rochester, NY.). The spectrophotometer was calibrated using prepared CA solutions with different concentrations.

3.1.4 Effects of HCl Concentration (Volumetric Ratio) and Precipitation Temperature on Protein Solubility

In this study, a constant-volume batch precipitator was used to study the effects of volumetric feed ratio (volume of aqueous HCl solution : volume of protein solution, v/v) and precipitation temperature, on the final concentration of the protein in the solution at isoelectric pH 4.0. Precipitation temperature was varied from 296 K to 318 K. Beyond this temperature, denaturation of protein by heat occurs. Volumetric feed ratio was varied from ca. 0.001 (using concentrated aq. HCl acid, 2.5 moles/L) to 12.5 v/v. That is, low volumetric ratio means the strength of HCl used high and vice versa for high volumetric ratio. Prior to mixing, the protein solution and the precipitant were brought to the required temperature, then mixed rapidly. The mixture was stirred continuously for 30 min while maintaining the pH and the temperature. Temperatures of the feed solutions and the slurry in the precipitator were maintained by a constant temperature water bath. The slurry was separated by centrifugation (10,000 xg) and the supernatant was analysed for the concentration of dissolved protein using the Kjeldahl method. Results from this study were used to correlate the dependence of protein concentration in the solution (in equilibrium with solid protein) to the precipitation temperature, and the volumetric feed ratio, using a simple equation defined as:

$$C^* = K_s \frac{C_o}{r+1} \quad (3.3a)$$

$$K_s = \frac{(rk_1+k_2)}{(r+1)^{k_3}} e^{-k_{ER}T} \quad (3.3b)$$

where C^* is the concentration of protein still in solution after precipitation; T is the precipitation temperature; r is the volumetric feed ratio; C_o is the initial protein concentration in the solution; K_s is a constant (function of r and T); and k_1 , k_2 , k_3 , and k_{ER} are all constants which were determined by the Least Squares method. Table 3.1 presents a series of experiments which were performed.

Table 3.1 Experiments performed in the batch precipitator to determine the effects of volumetric feed ratio and precipitation temperature on protein solubility.

Run no.	Protein feed concentration (mg N/mL)	Final protein concentration (mg N/mL)	Precipitation temperature (K)	Volumetric feed ratio ** (v/v)	Calculated $K_s(r,T)$ constant
1	4.2231	0.7663	296	0.002	0.1774
2	2.0317	0.3226	296	0.002	0.1774
3	0.5088	0.0831	296	0.002	0.1774
4	2.0317	0.3712	308	0.002	0.1833
5	2.0317	0.3801	318	0.002	0.1880
6	0.5266	0.0970	308	1.0	0.3396
7	2.0620	0.3333	308	1.0	0.3396
8	2.2206	0.3620	308	1.0	0.3396
9	0.5266	0.1005	318	1.0	0.3483
10	2.0610	0.3488	318	1.0	0.3483
11	2.2206	0.3811	318	1.0	0.3483
12	1.1675	0.1836	296	1.0	0.3287
13	2.0610	0.3277	296	1.0	0.3287
14	0.5266	0.0901	296	1.0	0.3287
15	8.3282	1.3450	296	1.0	0.3287
16	5.3627	0.8037	296	1.0	0.3287
17	3.9285	0.6731	296	1.0	0.3287
18	1.9677	0.3200	296	1.0	0.3287
19	1.3511	0.2310	296	1.0	0.3287
20	1.1432	0.1801	296	1.0	0.3287
21	0.7344	0.1663	296	1.0	0.3287
22	0.3880	0.1068	296	1.0	0.3287
23	0.2771	0.0797	296	1.0	0.3287
24	0.1975	0.0610	296	1.0	0.3287
25	2.0266	0.0606	296	5.0	0.1631
26	0.5075	0.0191	296	5.0	0.1631
27	4.2126	0.1247	296	5.0	0.1631
28	2.0266	0.0364	296	12.5	0.0791
29	0.5075	0.0130	296	12.5	0.0791
30	4.2126	0.0554	296	12.5	0.0791
31	4.2277	0.0924	296	8.3	0.1110
32	4.2126	0.1718	296	3.0	0.2246

** Feed ratio = volume of precipitant (aq. HCl)/ volume of protein solution

3.2 Isoelectric Precipitation of Sunflower Protein in a Tubular Precipitator

3.2.1 Description of the Experimental Set-up

A tubular precipitator (Figure 3.1) consisting of a horizontal 6-mm inner diameter (d) glass tube was used. Initially, the precipitator length was 10-m, then increased to 20 m. Eight 20 x 11 mm Kenics static mixers (Koch Engineering Co. Inc., Wichita, KA) were used at the entrance to mix the protein solution and the precipitant. Four (3-way Teflon valves with smooth internal surface, 6-mm bore diameter, and a sampling T-piece, 65-mm long) were used as sampling ports. For the 10-m long precipitator, the sampling ports were located at 0.4, 3.3, 6.5, and 9.7-m from the entrance point; and 0.4, 3.3, 9.5 and 20.0-m for the 20-m long precipitator. These 3-way valves were used to allow full flow either along the tubular precipitator or to the sampling ports, i.e., during sampling the flow was entirely diverted to the sampling bottle. Before starting precipitation experiments, the extent of dispersion in the tubular precipitator was determined by performing residence time distribution experiments.

Sunflower protein precipitation in the tubular precipitator was achieved by contacting the protein solution with the precipitant (aqueous HCl or aqueous calcium acetate) solution of known concentration. All acid precipitation runs in the tubular precipitator were performed at room temperature (22 ± 2 °C) using a protein feed solution at pH 10. Protein precipitation was carried out at pH 4. Ranges of protein concentration in the feed stream, flow Re number (based on feed flow rates), and volumetric feed ratio (HCl solution : protein solution) used in this study are presented in Table 3.2. For the given volumetric feed ratio and flow Re number, the concentration of the precipitant to be used was predetermined by titration. The feed solutions were pumped into the precipitator using peristaltic pumps through calibrated flow meters. The concentration of solid protein particles along the precipitator was measured using an on-line turbidimeter. The protein particle size analysis was determined from the collected samples of the flowing slurry. Samples were collected starting with the last port, no. 4, to avoid flow disturbances at other ports. Analysis of the mean particle size and particle size distribution was performed by a Coulter Counter, Model TA II (Coulter Electronics

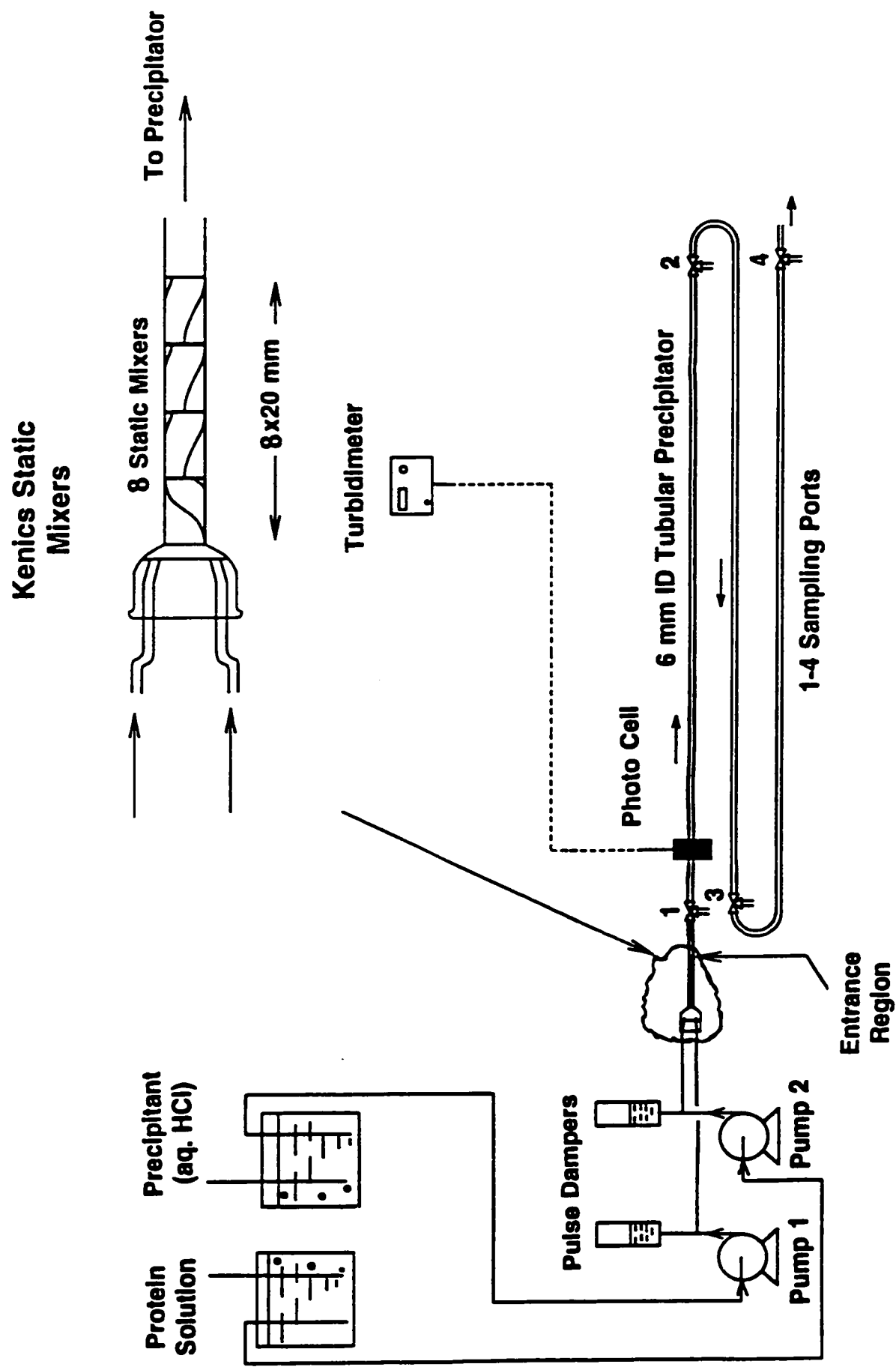


Figure 3.1 Experimental setup for the tubular precipitator

Table 3.2 List of precipitation experiments performed in the tubular precipitator at a fixed pH 4.0.

Run no.	Protein feed conc.		Flow Re no.	Feed ratio aq. HCl : protein sol. (v/v)	Precipitator length (m)
	(mg N/mL)	(kg/m ³)			
4	0.46	2.7	4800	2.6:1	10
11	0.45	2.6	778 (800)	1:1	10
12	0.45	2.6	4950 (5000)	1:1	10
13	0.39	2.2	5058 (5000)	12:1	10
14	2.01	11.4	778 (800)	1:1	10
15	2.01	11.4	4950 (5000)	1:1	10
16	2.01	11.4	5058 (5000)	12:1	10
17	0.49	2.8	778 (800)	1:1	10
18	0.49	2.8	4950 (5000)	1:1	10
19	0.49	2.8	5058 (5000)	12:1	10
20	2.04	11.6	778 (800)	1:1	10
21	2.04	11.6	4950 (5000)	1:1	10
22	2.04	11.6	5058 (5000)	12 :1	10
L1	2.06	11.7	778 (800)	1:1	20
L2	2.08	11.8	4950 (5000)	1:1	20
L3	2.08	11.8	778 (800)	1:1	20
L4	2.08	11.8	4950 (5000)	1:1	20
L5	2.08	11.8	778 (800)	1:1	20
L6	0.50	2.8	778 (800)	1:1	20
L7	0.50	2.8	4950 (5000)	1:1	20
I1	2.00	11.4	3000	1:1	20
I2	2.04	11.6	3000	1:1	20
I3	1.24	7.1	778 (800)	1:1	20
I4	1.24	7.1	4950 (5000)	1:1	20
M81	2.01	11.4	4950 (5000)	1:1	20
M42	2.01	11.4	778 (800)	1:1	20
M03	2.01	11.4	778 (800)	1:1	20
M84	2.01	11.4	778 (800)	1:1	20
M45	2.01	11.4	4950 (5000)	1:1	20
M06	2.01	11.4	4950 (5000)	1:1	20

Inc., Hialeah, FL) using a 70 or 200 μm aperture tube. The pH of the flowing slurry was checked by taking samples from the exit point. Readings were taken after steady state had been reached (constant readings of the turbidimeter).

3.2.2 Residence Time Distribution (RTD) Studies

In order to determine the extent of the dispersion in the tubular precipitator, RTD experiments were performed using a non-reactive tracer method. One mL of 1.0 mol/L KCl solution was injected at a point 20 cm before the mixing zone. The conductivity of the solution was measured at two locations, 67 cm and 572 cm from the injection point. The experimental response curves contain the contribution of a subsystem composed of dispersions from the injection needle, the static mixer, and the entrance to the precipitator (see Figure 3.1). In order to eliminate the mixing effects of this subsystem and investigate the dispersion in the tubular precipitator alone, the difference in variances of the exit age distribution curves at two locations was considered. Four increasing flow velocities (0.35, 0.48, 0.61, and 0.73 m/s) were used for this study.

3.2.3 Selection of Precipitation Conditions and Experimental Design

Factors affecting protein particle size distribution and yield during isoelectric precipitation in the tubular precipitator are:

- concentration of proteins in the feed solution,
- precipitation temperature,
- the volumetric ratio of the feed solutions,
- total feed rate in the precipitator, i.e. flow Re number, shear rate, and mean residence time,
- precipitation pH (maximum yield is obtained at isoelectric pH),
- precipitator length (mean residence time and flow dispersion), and
- premixing of the feed streams.

Results from the preliminary experiments showed that the solubility of protein increases with increasing pH. However, there was no substantial increase in solubility

beyond pH 10. Also, protein denaturation occurred at high pH. For this reason, the protein feed solutions were prepared at pH 10. To achieve maximum yield (solids recovery), precipitation was carried out at pH 4, isoelectric pH. This pH was determined experimentally (calculations gave approximate value at pH 3.6, APPENDIX A) as the pH corresponding to the minimum solubility of the proteins. Protein precipitation from highly concentrated protein solution results in high solid concentration. This causes solids deposition on the precipitator walls and on the static mixers. Also, the sensitivity and the accuracy of the turbidimeter (used for measurements of on-line solids concentration) is greatly reduced. To avoid this, two levels of volumetric feed ratio (volume flow rate of precipitant : volume flow rate of protein solution), 1 and 12 v/v, and three levels of protein feed concentration: 11.4 kg/m^3 (2.0 mg N/mL), 6.8 kg/m^3 (1.2 mg N/mL), and 3.0 kg/m^3 (0.5 mg N/mL) were selected. Preliminary results showed that, at high temperature, the protein solubility increases (lower yield). Therefore, $22 \pm 2 \text{ }^\circ\text{C}$ was selected as the working temperature. Selections of the flow velocities were based on achieving three flow regimes: a laminar flow regime ($Re < 2,100$), a flow transition regime, and a turbulent flow regime ($Re > 4,000$). For the laminar flow regime, $Re = 800$ was selected where $Re = 3,000$ was selected for the transition and $Re = 5,000$ for the turbulent flow regime. The corresponding mean residence times were 155 s, 40 s, and 24 s, respectively (based on a 20-m long precipitator from the entrance to exit points).

In order to study the effects of these parameters (mentioned above) on PSD and on protein yield, a factorial experimental design method was adopted. Since there are three main variables; concentration of protein in the feed solution, total feed rate (flow velocity), and volumetric feed ratio of the reactants, a factorial experiment design with a three level effect, high and low, was used. Each experiment was done with replication. The set of experiments which were performed is presented in Table 3.2.

3.2.4 Preparation of Sunflower Protein Feed Solutions

Protein feed solutions were prepared using defatted confectionery-type sunflower meal. Confectionery-type meal was selected because seeds are readily available in

dehulled form. Also, preliminary studies showed that protein solutions (aqueous extract from laboratory defatted meals) have similar solubility curves and protein yields. Defatted meal was mixed with distilled water in a ratio of 1 gm of DM to 20 mL of distilled water. The pH of the slurry was adjusted to 10 using 2.0 mol/L aqueous NaOH solution. Sodium sulphite (0.1 % w/w of the slurry) was added to prevent discolouration (Gheyasuddin et al., 1970). The mixture was stirred continuously for 2 hr while maintaining the pH constant. The solid residue (spent meal) and the supernatant (protein solution) were separated by centrifuging twice at 10,000 rpm (15,300 $\times g$) for 20 min, then filtered through a no. 42 Whatman filter paper. The desired protein concentration for the precipitation experiment was obtained by diluting with aqueous NaOH (clear filtered solution at pH 10 containing 0.1 % w/w Na_2SO_3).

3.2.5 Effect of Fluid-Induced Shear on Particle Size Distribution

To determine the effect of fluid-induced shear on protein particle size distribution (PSD), a protein slurry (fresh precipitate at pH 4 aged for about 2 hr) with a known PSD and solid concentration was fed to the tubular precipitator. Two flow velocities corresponding to $\text{Re} = 440$ and $\text{Re} = 5,000$ (low and high) were used in this study. A summary of the conditions used is presented in Table 3.3. Samples of the flowing slurry were drawn from the sampling ports and analyzed for the particle size distribution. Also, the solids concentration along the tube was measured using the on-line turbidimeter. The effect of fluid-induced shear on particle aggregation or breakage was distinguished from other factors like nucleation and particle growth by diffusion. No precipitation took place during these runs. Therefore, the fluid-induced shear was the main factor in the observed changes in the particle size distribution.

3.2.6 Effect of the Precipitator Length

In this study, the precipitator length was doubled, from 10-m to 20-m long. The effect of precipitator length on protein particle size distribution and solids concentration were studied. All other operating parameters (concentrations of protein and aqueous HCl

Table 3.3 List of experiments for studies of the effect of fluid-induced shear in the tubular precipitator.

Run no.	Flow Re no.	Solids conc. in the feed stream (g-solids/L of solid-free liquid)
1	5000	22.0
3	440	28.5
4	440	16.0
5	5000	17.5
6	5000	16.0
7	440	13.0
9	440	2.8
10	5000	1.7

in the feed solutions, flow rates, and precipitation pH) were kept constant.

3.2.7 Effect of Static Mixers

The effect of pre-mixing feed solutions in the static mixers on PSD and protein yield was studied. In this study, isoelectric precipitation experiments were performed at two different flow velocities ($Re = 400$ and $Re = 5,000$). The volumetric feed ratio used was 1 v/v. In one case there were no static mixers. In the second case there were four static mixers (20 mm x 11 mm each) and in the third case there were eight static mixers. In all cases the PSD and solids concentration along the tubular precipitator were measured.

3.3 Comparison With MSMPR and Batch Precipitators

3.3.1 Experimental Set-up for the MSMPR and the Batch Precipitators

An MSMPR precipitator (also used as a batch precipitator) was a stirred tank of 'Rushton' geometry with 77-mm inner diameter, 4 wall baffles, and a 25.4-mm three bladed propeller mixer (Figures 3.2 and 3.3). Feed inlets (protein solution and the precipitant) were positioned on the opposite sides of the impeller tip, whereas the withdrawal line was adjustable axially depending on the desired location. The speed of the agitator was kept constant at 600 rpm. The mean residence times for the MSMPR precipitator were 11.4, 25.3, 48.8, and 74.4 s (25.3 and 74.4 s matched the mean residence times of the 10-m long tubular precipitator). Before starting precipitation experiments, residence time distribution experiments were carried out to determine the extent of dispersion to ensure better mixing. For the batch precipitator, slurry samples were taken after 2, 10, 20, 40, and 90 min. The agitator speed was either 600 rpm or 900 rpm. The precipitation temperature was varied from 298 to 318 K (using a constant temperature water bath). List of experiments performed in the MSMPRP and the batch precipitator are presented in Tables 3.4 and 3.5, respectively.

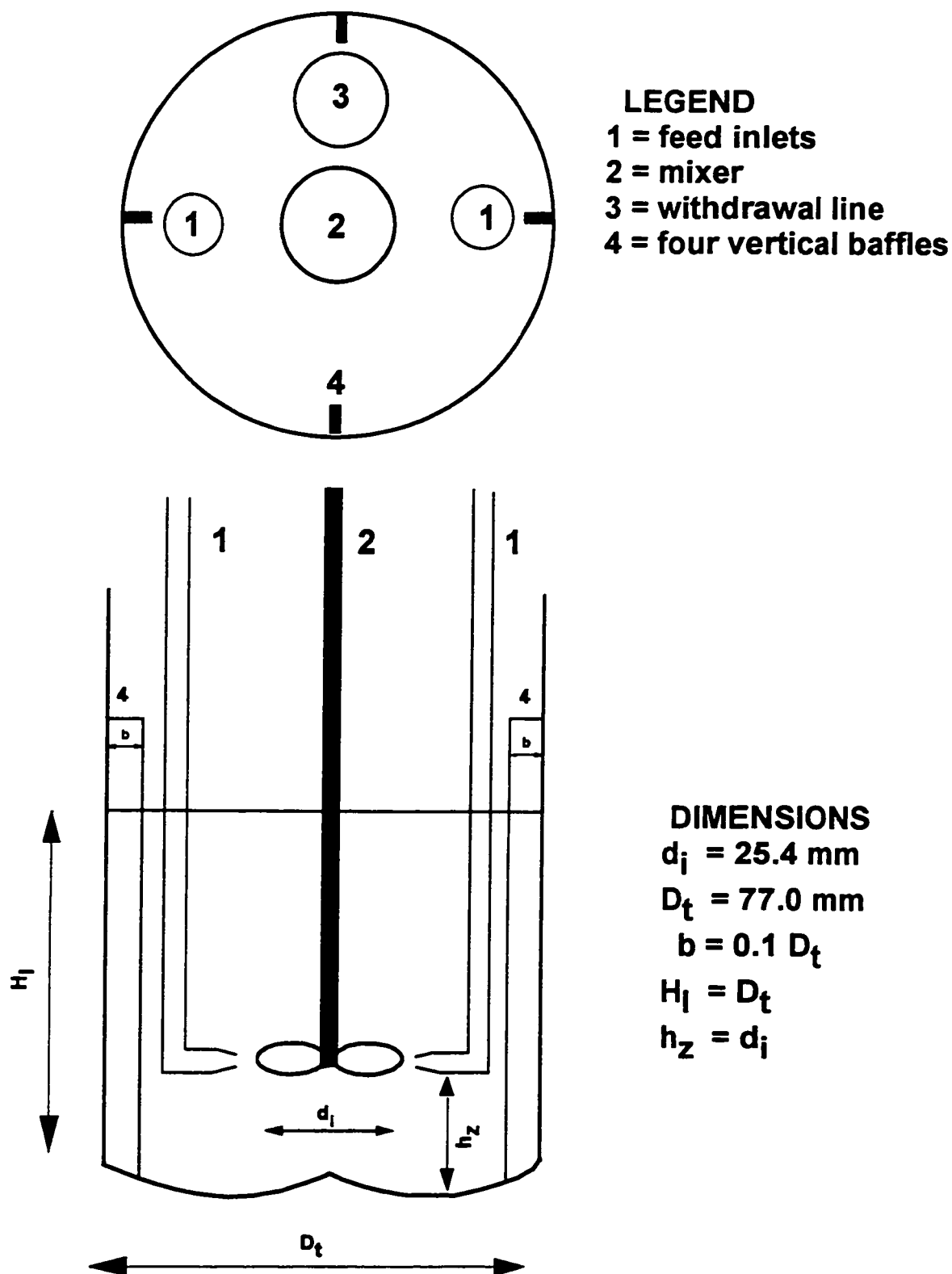


Figure 3.2 Geometrical configuration of an MSMPR precipitator (used also as a batch precipitator).

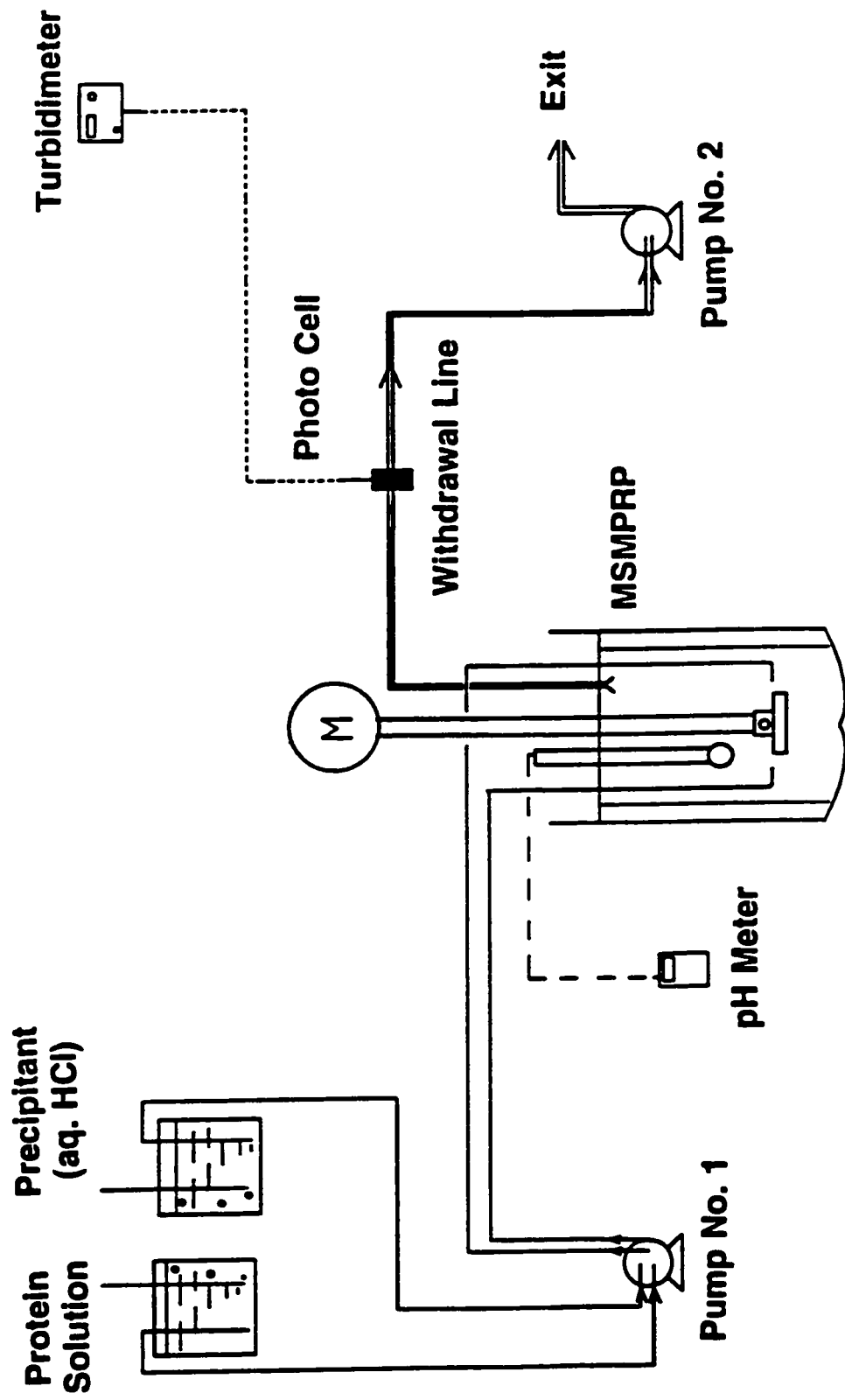


Figure 3.3 Experimental setup for an MSMRP precipitator.

Table 3.4 List of precipitation experiments performed in the MSMMPR precipitator at a fixed pH 4.0 and mixer speed at 600 rpm.

Run no.	Protein feed conc.		Time (s)	Volumetric feed ratio (v/v)
	(mg N/mL)	(kg/m ³)		
1	0.5	2.9	11.4, 25.3, 48.6, and 74.4	1:1
2	2.0	11.6	11.4, 25.3, 48.6, and 74.4	1:1
3	0.5	2.9	11.4, 25.3, 48.6, and 74.4	1:1
4	2.0	11.6	11.4, 25.3, 48.6, and 74.4	1:1

Table 3.5 List of isoelectric precipitation experiments performed in the batch precipitator at a fixed pH 4.0.

Run no.	Protein feed conc. (kg/m ³)	Precipitation temperature (K)	Mixer speed (rpm)
1	2.8	298	600 & 900
2	2.8	308	600
3	2.8	318	600
4	11.8	298	600 & 900
5	11.8	308	600
6	11.8	318	600

3.3.2 Residence Time Distribution (RTD) Studies

The extent of dispersions in the MSMPR precipitator at different flow velocities and mixer speed were determined using the RTD method. The RTD experiments were performed using PVC particles (150 μm) as a tracer. A single drop (ca 0.1 mL) of PVC aqueous slurry was injected into the precipitator. The concentrations of the solids in the precipitator as a function of time were measured using an on-line turbidimeter attached on the exit line. Four different flow rates (0.22, 0.34, 0.65, and 1.44 L/min) were used in this study.

3.4 Precipitation of Sunflower Protein Using Calcium Acetate

Unlike isoelectric precipitation, precipitation using aqueous calcium acetate was carried out at pH 6.5. This is the natural pH of sunflower protein and is near the neutral pH. Preliminary protein precipitation experiments were carried out in a batch precipitator at room temperature (22 ± 2 °C). These experiments were used to determine the concentration of calcium acetate which gives the maximum solids yield and a large mean particle size. The protein feed solution was prepared by extracting confectionery-type sunflower defatted meal with aqueous NaCl (1.0 mol/L) at pH 6.5. The pH was adjusted using 1.0 mol/L acetic acid or 1.0 mol/L NaOH solution. Slurry samples were withdrawn for determination of the protein particle size distribution and the solid protein yield (by filtration through a 0.2 μm micro-filter cartridge attached to a syringe). For precipitation in the tubular precipitator (comparison experiments), two runs (with replications) were performed. One run at flow $Re = 800$ and the other at flow $Re = 5,000$. The protein feed concentration was 12 kg/m^3 and volumetric feed ratio was 1 for both runs.

3.5 Experimental Measurements

3.5.1 Protein Concentration Measurement

The protein content of the supernatant (protein solution) and the defatted meal

were determined by the Kjeldahl method using AOAC (1984) procedure. A factor of 5.7 was used to calculate protein content (Sosulski and Imafidon, 1990) from the nitrogen content ($\% \text{ protein} = 5.7 \times \% \text{ nitrogen}$).

3.5.2 Solid Protein Concentration Measurement Using Turbidimeter

The turbidimeter consisting of a diode emitter and receiver was used to measure the solid protein concentration along the tube (Raphael and Rohani, 1996). The diode (emitter) transmits an infrared light beam through the glass walls of the tubular precipitator before being collected by the receiver on the opposite side of the tube. In the absence of solid particles (clear solution), transmission was set at 100 %. At total blockage the transmission was 0 %. The emitter and the receiver cells were embedded in a PVC ring which could be slid along the glass tube or snapped to different positions. The turbidimeter was calibrated by recirculating (using a peristaltic pump) a slurry with a known solid protein concentration (ranging from 0.00002 to 0.0533 g of solid/mL of liquid) through a horizontal short piece of glass tube. The initial slurry was prepared by adding 8 g of powder protein (moisture content = 1.8 % w/w) into 150 mL of filtered saturated protein solution (transmission = 100 %) at pH 4. Transmission data at other slurry concentrations were obtained by successive dilution of the slurry with filtered saturated protein solution at pH 4. The effects of flow velocity and change in the mean particle size (caused by pump shear) on transmission measurements were analyzed. The slurry was recirculated for 5 min at a pump speed of 100 rpm (ca. 120 mL/min) followed by 5 min at 600 rpm (ca. 1200 mL/min) and back to 100 rpm. At both speeds no changes in measured transmission were observed.

3.5.3 Protein Particle Size Distribution Measurement Using Coulter Counter

A Coulter Counter (Model TA II, Coulter Electronics Inc., Hialeah, FL) was used to measure the mean particle size and the particle size distribution of the samples. For measurements of the mean particle size below 10 μm , a 70 μm aperture tube was used, whereas for measurements of mean particle sizes above 10 μm , a 200 μm aperture tube

was used. The particle size analyzer was calibrated using standard samples: 9.72 and 42.49 μm polystyrene microspheres supplied by Coulter Electronics Inc. Sodium acetate buffer solution (pH = 4; concentration = 0.07 mol/L; filtered through a 1 μm membrane, Cole-Parmer Instruments Co., Chicago IL; background count of less than 1200 particles using a 70 μm aperture tube) was used as an electrolyte and for sample collection (dilution) to prevent further precipitation. For calcium acetate precipitation the electrolyte was at pH 6.5.

Samples for analysis were collected in 125 mL bottles containing buffer solution. The amount of sample collected was determined by weighing the bottles before and after sampling. The dilution ratio of the collected samples to the buffer solution was between 1:80 and 1:100 v/v. For analysis, 1 or 2 mL of the diluted samples were transferred into a round bottom beaker with 100 mL of clear electrolyte (buffer solution).

3.5.4 pH Measurement

The pH measurements were done using an Accumet pH meter 915 (Fisher Scientific, Toronto, ON) with standard pH electrode. The pH meter was calibrated using standard electrolytes with pH 7 and 10.

3.5.5 Measurements of Feed Flow Rate

Feed flow rates (precipitant and protein solution) into the tubular precipitator and the MSMRP were measured using pre-calibrated peristaltic pumps and on-line flow rotameters, both supplied by Cole-Parmer Instruments Co., Chicago IL. Pumps were calibrated at a range of speeds using a graduated cylinder and stop watch method by collecting the flowing liquid from the last sampling port. Distilled water at room temperature (22 ± 2 °C) was used as the calibrating fluid (densities of the HCl solution and protein solution are similar to water). The pump suction heads were maintained constant by using sealed feed tanks with vent tubes dipped into the solution. Air dampers were used to smoothen the liquid flow before entering the mixing zone of the tubular precipitator (see Figure 3.1). Linear calibration curves relating liquid flow rate versus

pump speed in rpm for the feed pumps were obtained.

3.5.6 Density of Solid Sunflower Protein

To determine the density of solid protein, 5.0 mL of slurry (washed twice with distilled water) at 22 °C were placed in a pre-weighed crucible. The weight of the crucible with the sample was also recorded. The free solvent was then evaporated in an oven at 110 °C for 4 hr. The weights of dry residue and free solvent were determined. The volume of solvent in the original slurry was calculated using the density (ca. water) obtained from steam tables (0.998 g/mL at 22 °C). Therefore, the solids volume was the difference between volume of the slurry and volume of the solvent. The experimentally determined solids mean density was 1.18 g/mL. In another method, dry samples of solid protein of known weight were submerged in distilled water (in a burette). The volume of the displaced liquid was recorded. The calculated average density of solids using this method was 1.253 g/mL. Therefore, the average density of solid protein used in this study was 1.21 g/mL. In the hydrated form, the solid protein density is slightly less than the calculated value due to the increase in volume caused by swelling.

3.5.7 Estimation of the Experimental Errors

In any experimental study, errors and uncertainties exist. They can be reduced by improving the experimental techniques and then estimated to establish the validity of the results. There are two types of errors: systematic errors and random errors. In this study, systematic errors were corrected frequently by checking the drift (from calibration) of the measuring instruments (Coulter Counter, flow meters, and pH meter) before starting the experiment. Random errors (fluctuation in observed results) were minimized by repeated experimentation (replication) and by refining the experimental methods. The estimation of the experimental error (SE) from the experiment with replications was calculated using a pooled estimate of variance (Se) (Box et al., 1978) defined as:

where m is the number of the experimental sets (conditions), $df_i = (nr_i - 1)$ is the degrees of freedom for the i th set performed with nr_i replications, and Se_i is the variance of the

$$Se = \sqrt{\frac{df_1 Se_1^2 + df_2 Se_2^2 + \dots + df_m Se_m^2}{df_1 + df_2 + \dots + df_m}} \quad (3.4)$$

ith set. For duplicate measurements ($nr_i = 2$) Se is simply given by:

$$Se = \sqrt{\frac{\sum_{i=1}^m (\Delta d_i)^2}{2m}} \quad (3.5)$$

where Δd_i is the difference of the duplicate measurements. The estimate of the standard error of the mean is given by:

$$SE = \frac{Se}{\sqrt{2m}} \quad (3.6)$$

CHAPTER 4

EXPERIMENTAL RESULTS AND DISCUSSION

4.1 Preliminary Experimental Results

4.1.1 Solubility of Sunflower Protein as a Function of pH

The purpose of this part of study was to determine the fraction of protein that can be extracted from different sunflower meals (defatted) under similar conditions. The fraction of inert material (non-nitrogenous material) had no effect on the results. The analysis was based on the total amount of protein present in the defatted meal and the total amount of protein that was extracted (in the solution). Table 4.1 shows the properties of the samples used in this study. The percentage of protein extracted was calculated using Equation (3.1). Results of protein extractability showed no significant difference between the two laboratory-prepared meals (Figure 4.1). The industrially defatted meal showed lower extractability of protein at all pH values. This suggests that the protein composition of the meals prepared from dehulled seeds (confectionery-type and oil-type) is similar. Whereas, the protein in the industrially defatted meal had undergone denaturation (during oil extraction the meal is heat treated before expelling the oil. Also, during solvent recovery defatted meal is stripped by steam). The decrease in protein solubility at all pH values implies that the denatured proteins are part of: albumins, globulins, and glutelins (see Table 2.2). That is, total protein (nitrogen) analysis of the defatted meal showed all proteins (natural and denatured) present in the meal, whereas in the solution only non-denatured proteins were dissolved. Extraction trends similar to Figure 4.1 had been reported by Sripad and Narasinga Rao (1987) and by Saeed and Cheryan (1988) while using laboratory defatted meals. The observed

Table 4.1 Properties of samples used in preparations of sunflower protein solution.

	Property	Confectionery- type seeds	Oil-type seeds	Industrially defatted meal *
1.	Hull content	no hulls	25.0 % w/w	10 - 15 % w/w
2.	Oil content (db)	58.69 % w/w	58.18 % w/w [¶]	< 1 % w/w
3.	Moisture content of defatted meal	8.95 % w/w	7.64 % w/w [¶]	11.52 % w/w
4.	Nitrogen content of defatted meal (db)	10.28 % w/w	10.18 % w/w [¶]	5.47 % w/w

* Obtained from Cargill Inc., West Fargo, ND. defatted meal contained hulls.

¶ Dehulled samples.

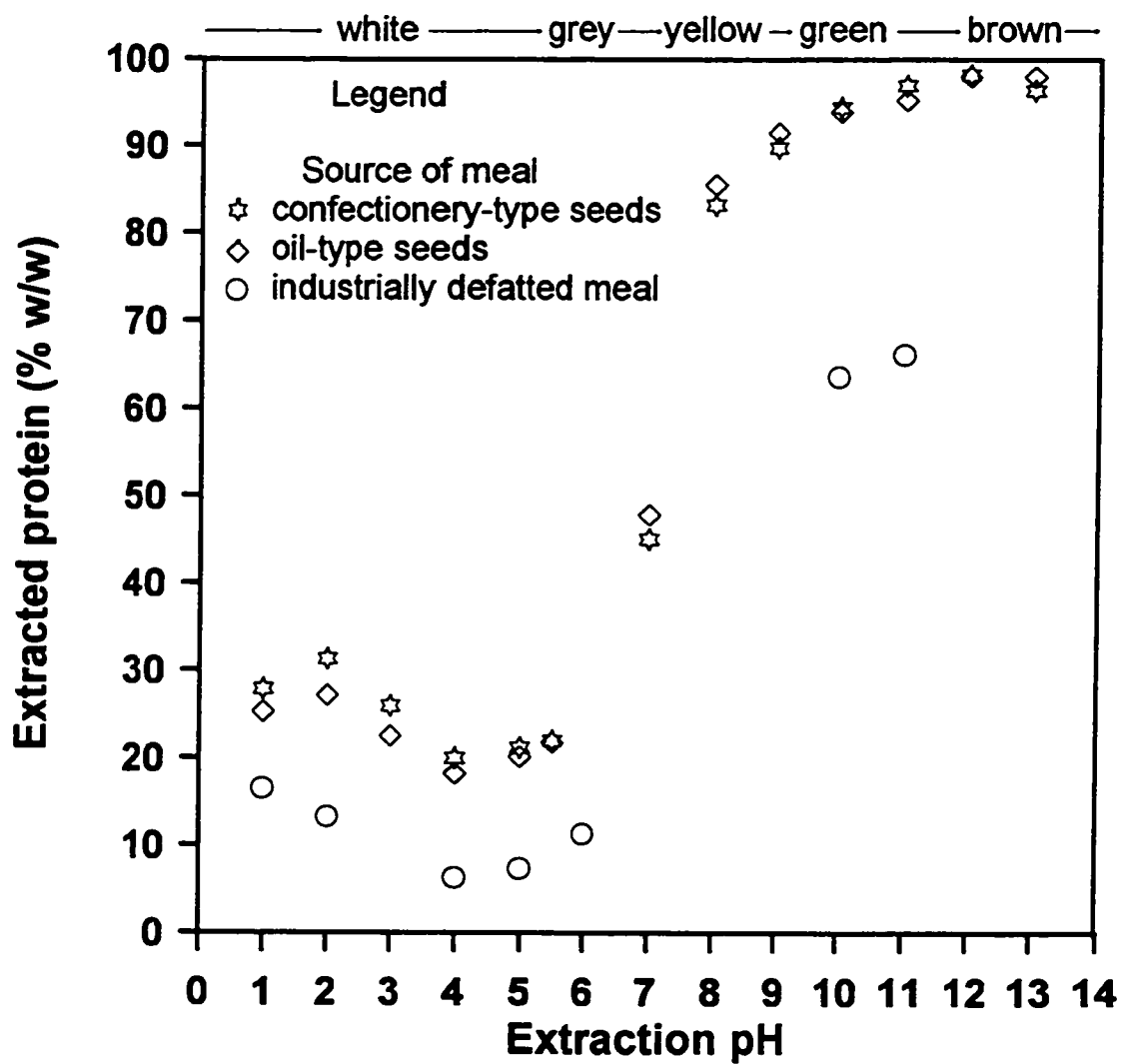


Figure 4.1 Effect of pH on protein extractability from laboratory and industrially defatted sunflower meals.

profile is attributed to the composition of the protein (the major portion being alkaline soluble protein).

Figure 4.2 shows the solubility of the sunflower protein in aqueous solutions at pH range from 1.0 to 10.0. Protein solubility was determined by suspending solid protein isolates in distilled water then adjusting the pH to the desired value. The solid protein was added until no more dissolution occurred. In another method, the saturated protein solution was prepared by lowering the pH of the protein solution (using aqueous HCl) until precipitation occurred. In both methods the protein solution was in equilibrium with the suspended solids. It was observed that the solubility of proteins is high (over 7 kg/m³ of solid free liquid) at pH values beyond 8.0 and then drops sharply in the pH range between 8.0 and 6.0. A small decrease in slope existed at an interval of pH range from 4.0 to 6.0. This minimum profile (minimum solubility) is due to the existence of several proteins with isoelectric points within this range. Using the overall amino acid composition of sunflower protein (Sosulski and Fleming, 1977), the estimated isoelectric pH was found to be approximately 3.6 (APPENDIX A), which is close to the experimentally observed isoelectric pH of 4.0. The reported extraction curves from other proteins, canola (Chen and Rohani, 1992) and soybean (Sosulski and Fleming, 1977) showed similar profiles with minimum solubilities at pH of around 4.0. This implies that sunflower protein has some similarities with other oilseed proteins. In the absence of the discoloration inhibitor (e.g., Na₂SO₃), the colour of the slurry (defatted meal with aqueous solution) changed with pH. At pH values less than 5.0 the slurry was white (milk-like), for pH between 5.0 and 7.0 the slurry was grey, at pH values between 7.0 and 8.0 the slurry was cream yellow, between 8.0 and 10.0 the slurry changed from yellow to dark green, and beyond pH value of 10.0 the slurry changed from dark green to dark brown. This colour band is shown in Figure 4.1. Sosulski and Fleming (1977) and Sosulski (1979b) suggested that the colour changes are caused by the oxidation of polyphenolic compounds (especially chlorogenic acid) at high pH values (alkaline conditions) which tend to bind with low molar mass proteins.

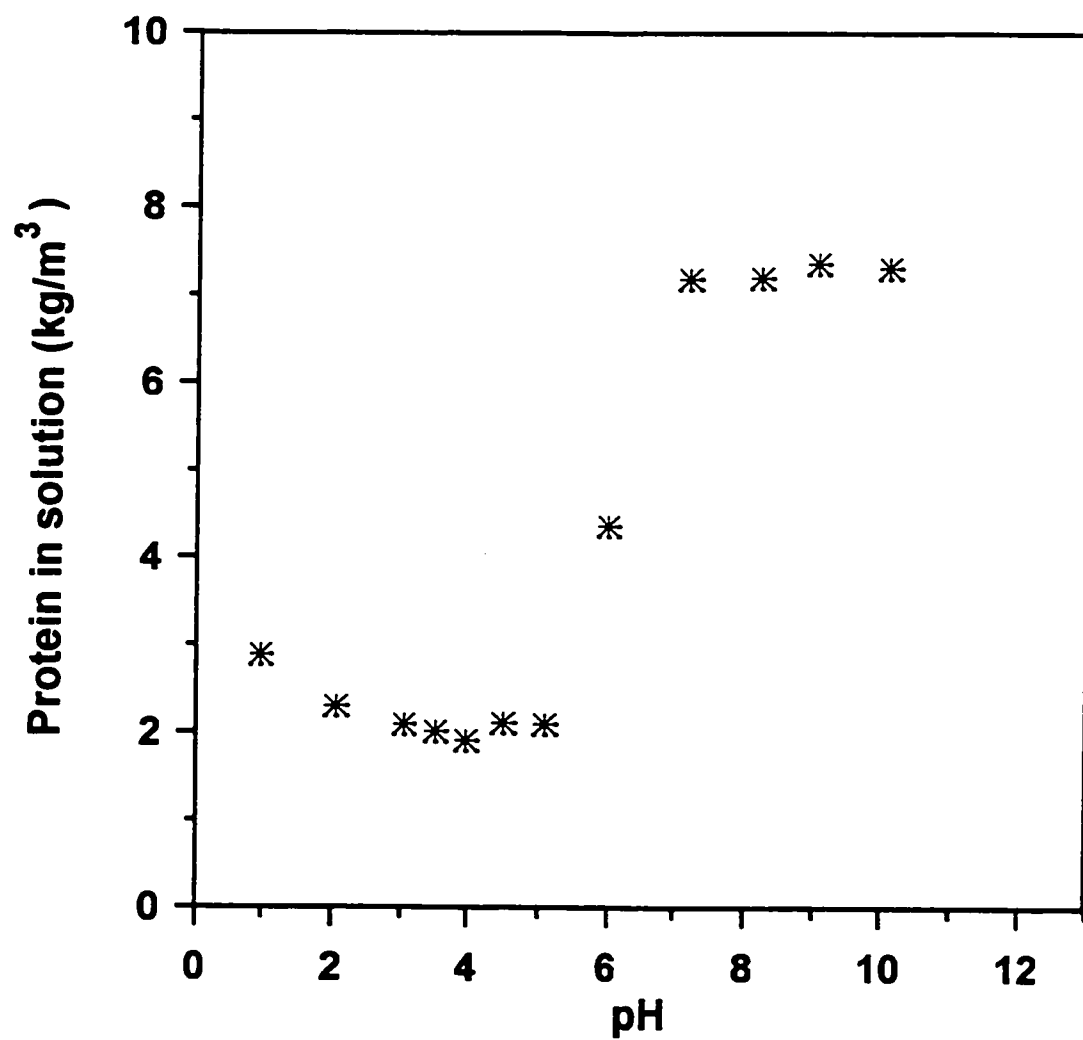


Figure 4.2 Solubility of sunflower proteins from confectionery-type seeds in aqueous solutions at pH 1.0 to 10.0.

4.1.2 Solubility of Sunflower Protein as a Function of NaCl Concentrations

As shown in Figure 4.2 the solubility of sunflower proteins in their natural pH 6.5 is very low, about 6 kg/m^3 of solid free liquid. Also, extraction using alkaline solution resulted in discolouration. Therefore, it was sought to extract and precipitate the proteins at their natural pH. The solubility of protein at pH 6.5 was increased by adding solid NaCl. Figure 4.3 shows the concentration of sunflower protein in the solution (in equilibrium with solid protein) at increasing concentrations of NaCl. The concentrations of dissolved protein increased with increases in NaCl concentration until the NaCl concentration was about 1 M. At this concentration of NaCl the protein concentration increased by almost three fold (about 16 kg/m^3). This is because of the salting-in process. At this pH and NaCl concentration, most of the soluble proteins were globulins. Beyond this concentration the solubility of the sunflower protein decreased (salting-out). High concentrations of NaCl reduced the interaction between H_2O -protein molecules resulting in reduced solubility. This concentration of NaCl (1 M) was later used for preparations of protein feed solutions for precipitation experiments at pH 6.5 using calcium acetate.

4.1.3 Precipitation Yields of Sunflower Protein by Aqueous HCl and Calcium Acetate

(a) Isoelectric Precipitation

Solid protein yields were studied by lowering the pH of the feed solution from 13.0 to the desired value (1.0 to 10.0) by adding aqueous HCl. The protein feed solution at pH 13.0 was under saturated. The percentage of protein recovered as solids at this range of pH values is shown in Figure 4.4. High yields (minimum solubility) were obtained at pH 4.0. High yields of sunflower protein (between 70 and 80 % w/w) as compared to other proteins like canola protein (53 % w/w obtained by Chen and Rohani, 1992) provide an economic incentive for the use of the former. Higher yields of sunflower protein is due to the single isoelectric point, unlike canola which has two isoelectric points between pH 4.0 and 6.0.

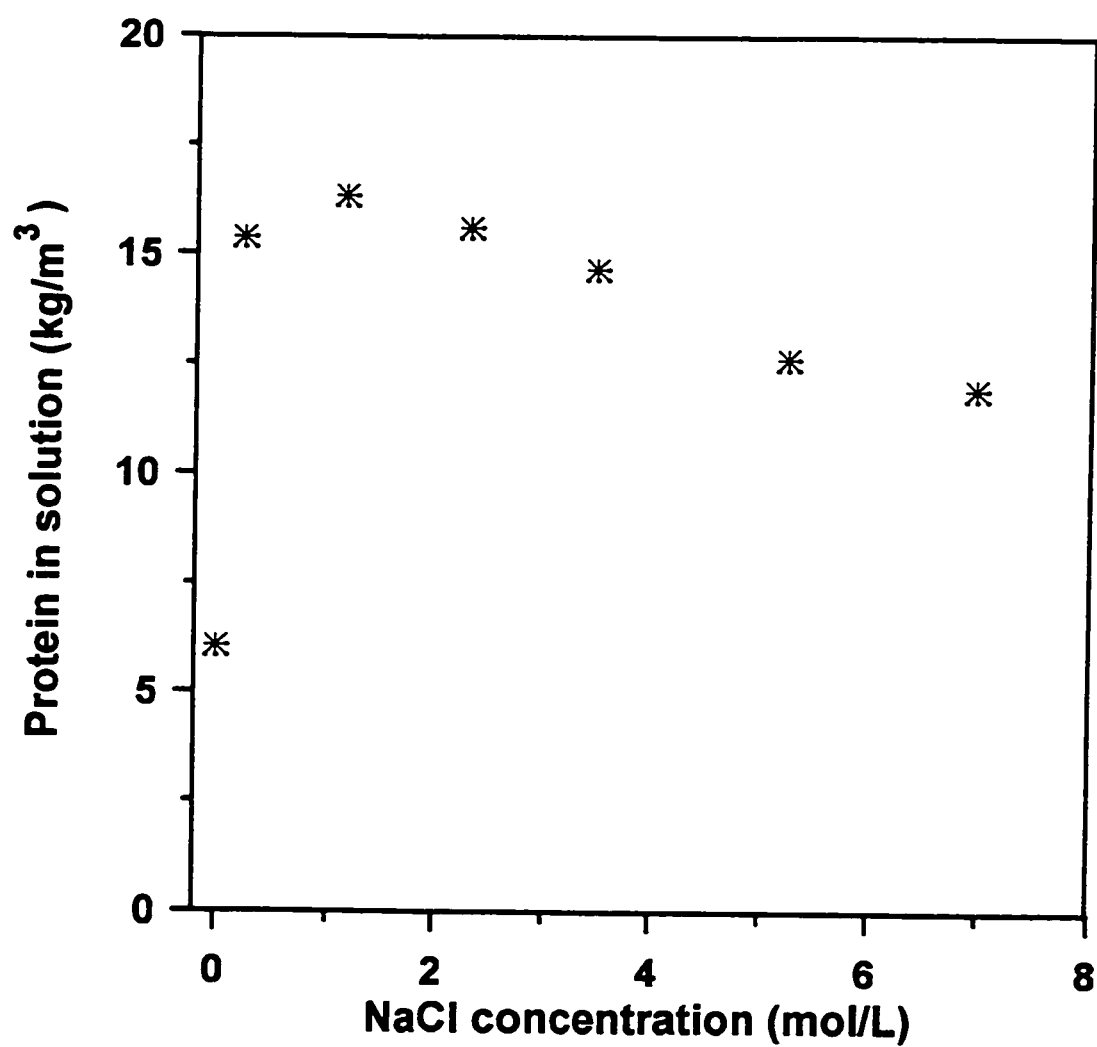


Figure 4.3 Solubility of sunflower proteins in increasing concentrations of aqueous NaCl solution at pH 6.5.

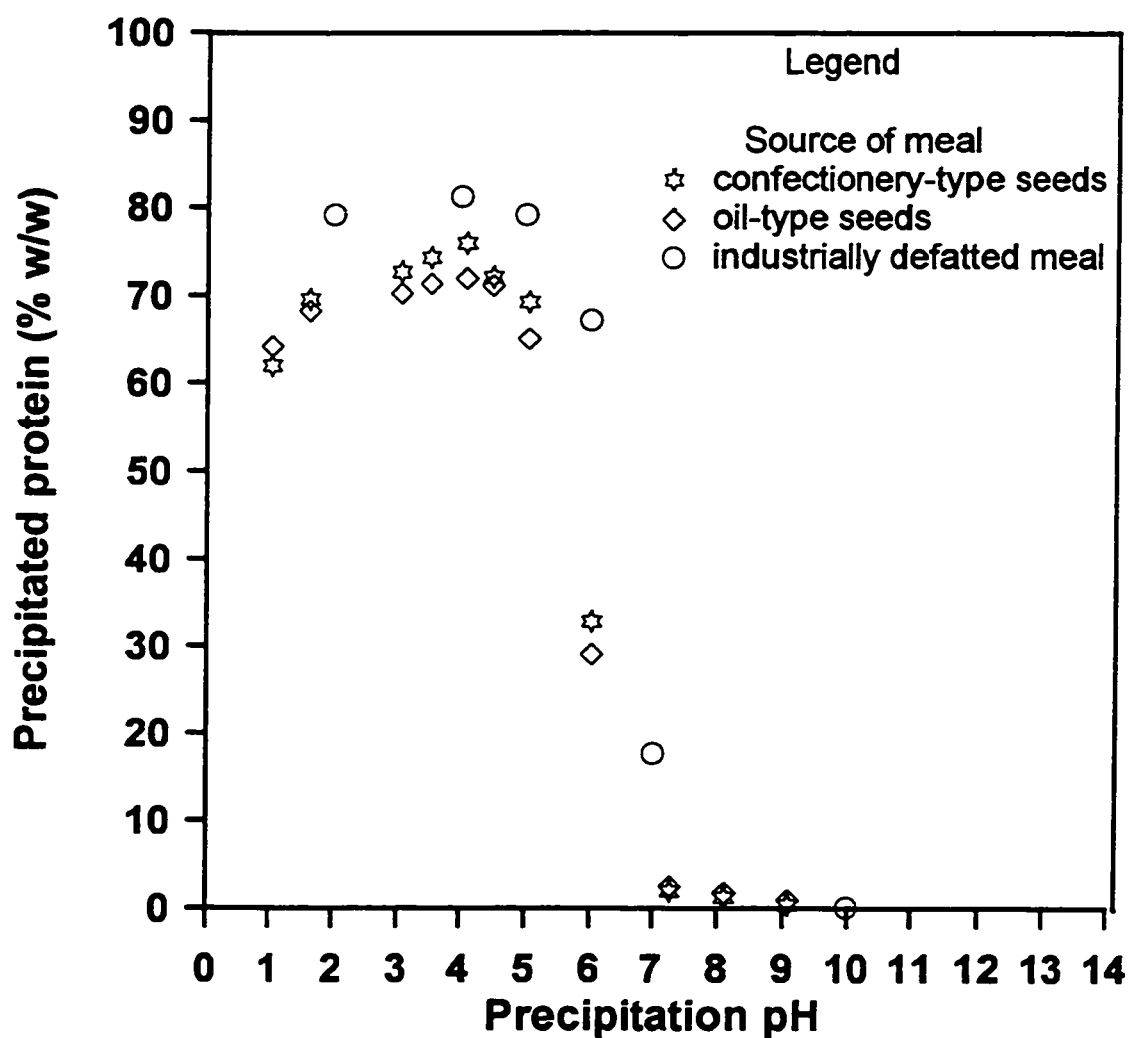


Figure 4.4 Effect of pH on precipitated protein yields for extracts from laboratory and industrially defatted sunflower meals.

The protein solution prepared from the industrially defatted meal showed slightly higher yields (Figure 4.4) than the laboratory prepared meals. This meant that the former had more precipitable proteins than the latter. The laboratory prepared meal contained proteins in their natural state, whereas the industrial meal had some of its proteins denatured during oil extraction process. It might be the presence of several proteins in the laboratory meal that causes interactions of the amino acid side groups, thus increasing their solubility (isoelectric point) as shown in APPENDIX A. Whereas, in the industrial meal the fraction of these proteins is reduced and hence reduced amino acids side groups interactions resulting in higher precipitation yields.

Further studies were done to investigate if two isoelectric points exist in the flat profile region (pH 4.0 to 6.0). Two pH points (4.0 and 6.0) were selected for the isoelectric precipitation. Solid proteins precipitated in this isoelectric range are called isolates. Protein solution for the preparation of protein precipitates (isolates) was prepared by single extraction of defatted meal (1 g : 20 mL alkaline solution) at pH of 10.0 for 2 hr at room temperature. Solid-liquid separation was carried out as before. The residues (leftover defatted meal after extraction) were freeze dried overnight and the supernatant (protein solution or extract) was ready for the preparation of isolates. The first isolate was prepared by adjusting the pH of the extract to 6.0 while mixing continuously at room temperature for 1 hr. The precipitate (first isolate) and the supernatant (mother liquor) were separated by centrifugation at 10,000 rpm (15,300 xg) for 20 min. The second isolate was prepared by adjusting the pH of the supernatant (mother liquor after precipitation at pH 6.0) to 4.0. The rest of the procedure was as for the first isolate. The isolates were then freeze dried overnight. Samples of the freeze dried residue and isolates, initial protein solution (extract), and supernatant were analyzed for nitrogen contents by Kjeldahl method. The protein yields at each stage were calculated using Equation (3.2).

The protein (nitrogen) balance for the two types of sunflower meals used are presented in Tables 4.2 and 4.3. For both samples, the first isolate (precipitate obtained at pH 6) had a higher protein content than the second isolate (92.2 % w/w as compared to 83.5 % w/w for confectionery-type and 93.8 % w/w against 86.3 % w/w for oil-type). The overall yield of isolates (first + second) based on the nitrogen (protein) contents of

Table 4.2 Nitrogen (protein) balance for precipitates (isolates) obtained at pH 4.0 and 6.0 from alkaline extracts of defatted confectionery-type sunflower meal.

Sample	Quantity 'as is'	Moisture content (% w/w)	Nitrogen content 'as is'	Protein content (% w/w)	Total mgN [**]
Defatted meal	20 g	8.95	9.38 %N w/w	53.47*	1876
extract ⁺ (pH=10.0)	395±5 mL		4.25 mgN/mL		1679 [89.5]
1st isolate ⁺⁺ (pH=6.0)	8.15 g	1.84	16.17 % w/w	92.16*	1318.5 [78.5]
filtrate 1 ⁺	352±5 mL		0.82 mgN/mL		289.2
2nd isolate ⁺⁺ (pH=4.0)	0.57 g	1.74	14.65 %N w/w	83.51*	84.1 [29.1]
filtrate 2 ⁺	325.5±5mL		0.39 mgN/mL		129.1
residue ⁺⁺	5.02 g	12.22	2.33 %N w/w	13.26*	116.8

* Protein content (% w/w) = 5.7 x % N (w/w).

⁺ 25 mL of sample were withdrawn for N content determination.

[**] Recovery of nitrogen (protein) based on the previous content (% w/w).

⁺⁺ After freeze drying.

There was a loss of protein of about 4.8 % w/w based on total protein in the defatted meal.

Table 4.3 Nitrogen (protein) balance for precipitates (isolates) obtained at pH 4.0 and 6.0 from alkaline extracts of defatted oil-type sunflower meal.

Sample	Quantity 'as is'	Moisture content (% w/w)	Nitrogen content 'as is'	Protein content (% w/w)	Total mgN [**]
Defatted meal	20 g	7.64	9.40 % N w/w	53.58*	1880
extract ⁺ (pH=10.0)	395±5 mL		4.3637 mgN/mL		1724 [91.7]
1st isolate ⁺⁺ (pH=6)	8.06 g	1.13	16.45 % N w/w	93.80*	1327.5 [77.0]
filtrate 1 ⁺	345±5 mL		0.91 mgN/mL		312.8
2nd isolate ⁺⁺ (pH=4)	0.89 g	1.93	15.14 % N w/w	86.32*	136.0 [43.5]
filtrate 2 ⁺	310±5 mL		0.29 mgN/mL		92.2
residue ⁺⁺	5.29 g	16.90	1.45 % N w/w	8.25*	76.7

* Protein content (% w/w) = $5.7 \times \% \text{ N (w/w)}$.

⁺ 25 mL of sample were withdrawn for N content determination.

[**] Recovery of nitrogen (protein) based on the previous content (% w/w).

⁺⁺ After freeze drying.

There was a loss of protein of about 10.7 % w/w based on total protein in the defatted meal.

the defatted meals was 74.8 % w/w for the confectionery-type and 75.5 % w/w for the oil-type. These yields are comparable to a single yield at pH 4.0 (see Figure 4.4). Furthermore, it shows that there is no substantial difference in protein yields between the two types of sunflower meals.

(b) Precipitation by Calcium Acetate

Figure 4.5 shows the percentage of protein which was precipitated at pH 6.5 using 0.01 to 3.5 mol/L concentrations of calcium acetate. Also, the mean particle size of the precipitates obtained at these concentrations of Ca^{2+} ions are shown. The amount of the precipitated protein increased with increases in calcium ion concentration. During precipitation, the Ca^{2+} neutralizes the charge by binding to the carboxylic acids (Bell et al., 1983). Therefore increases in the Ca^{2+} concentration increased the neutralization rate resulting in more protein to be precipitated. The precipitate formed had small mean particle size which varied little with Ca^{2+} concentration. Similarly, Nelson and Glatz (1985) reported that precipitation of soy protein with calcium acetate produced a precipitate with small particles compared to other precipitants. In industrial applications, Ca^{2+} is used in gelation processes together with heat to form a firm and expanded substance such as soybean tofu.

4.1.4 Effect of Temperature on the Mean Particle Size and Precipitation Yield

Figures 4.6 and 4.7 present the effect of precipitation temperature on the mean particle size and the solids concentration (yield). Experiments were performed in a batch precipitator immersed in a constant temperature water bath. Two concentrations of protein feed solution were used: low feed concentration 2.8 kg/m^3 and high feed concentration 11.8 kg/m^3 . In both cases the mean particle size of the precipitate increased with increase in the precipitation temperature. This might have been due to increased rate of particle aggregation. Increase in temperature reduced the fluid viscosity resulting in low drag friction acting on the particles and, therefore, more particle-particle collisions leading to lasting aggregation. At the same time, the increase in temperature

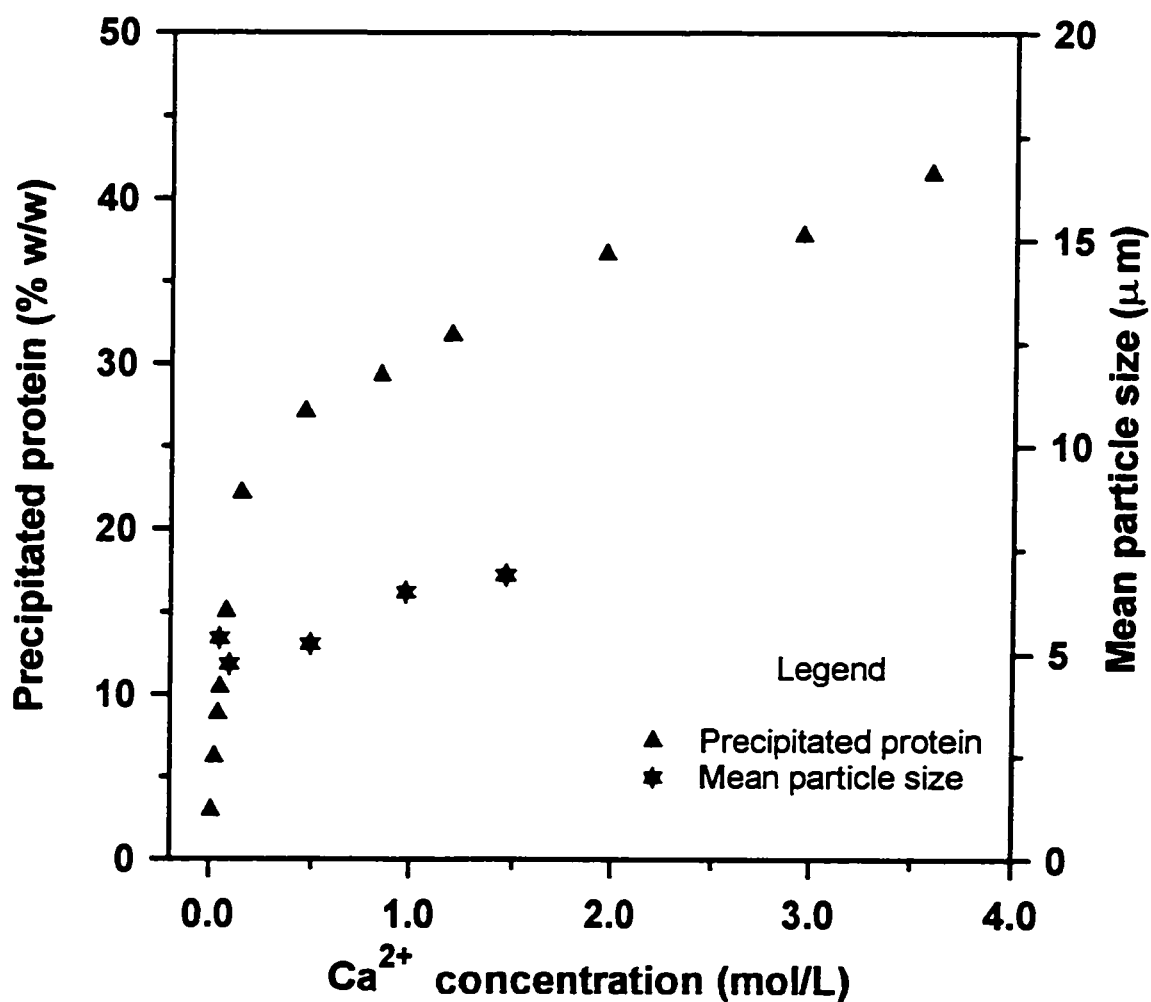


Figure 4.5 Effects of Ca^{2+} on precipitated protein and mean particle size at pH 6.5 using calcium acetate in a batch precipitator for protein conc. = 10.8 kg/m^3 with 1M NaCl and feed ratio = 1.0 v/v.

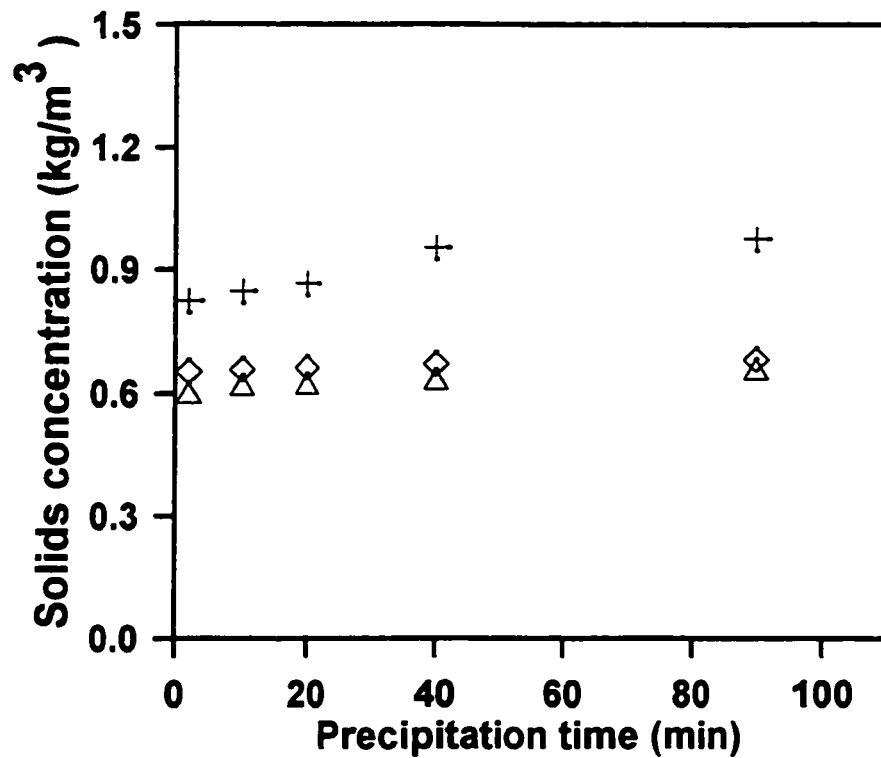
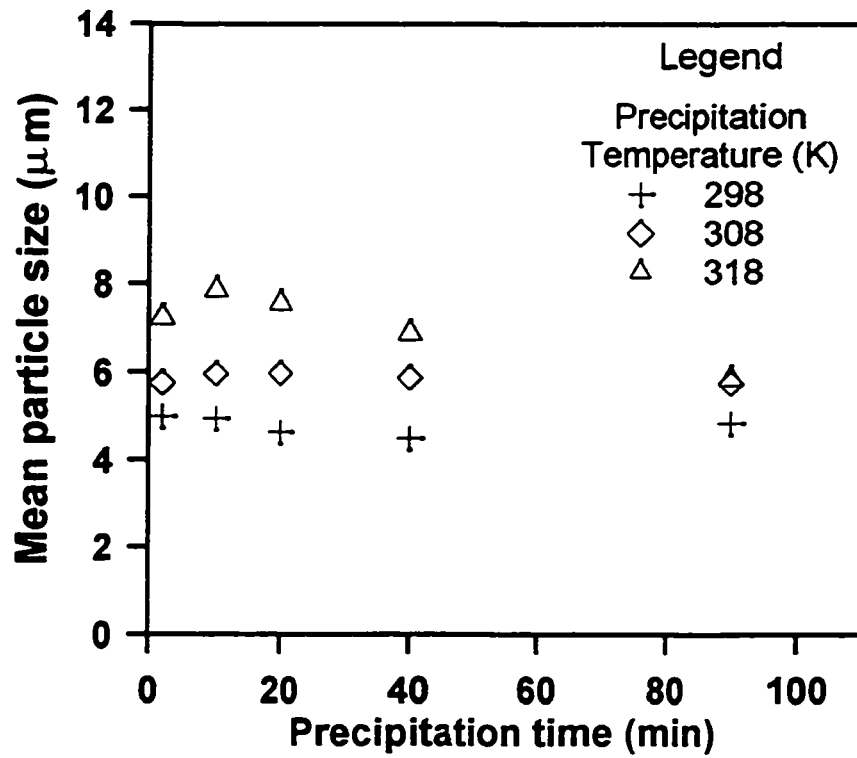


Figure 4.6 Effects of precipitation time and temperature on the mean particle size and solids concentration in a batch precipitator: mixer speed = 600 rpm and protein feed concentration = 2.8 kg/m³.

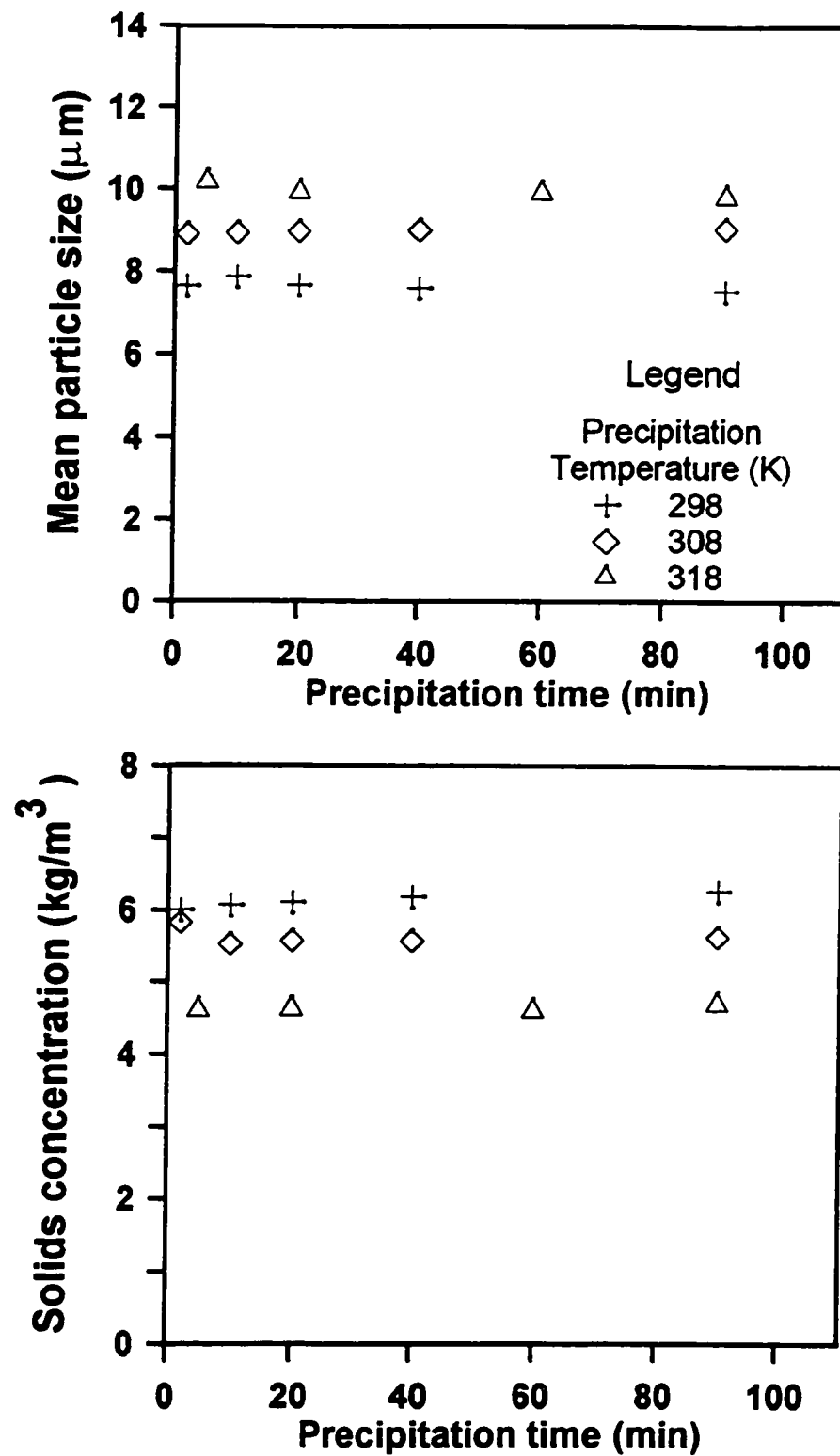


Figure 4.7 Effects of precipitation time and temperature on the mean particle size and solids concentration in a batch precipitator: mixer speed = 600 rpm and protein feed concentration = 11.8 kg/m^3 .

up to 318 K increased the protein solubility resulting in decreased solids concentration (yield). High temperature beyond 318 K results in protein precipitation by heat.

Prolonged precipitation times at constant temperature showed a slight decrease in the mean size. This could have been due to particle breakages caused by the mixer and the crystallizer vessel. The solids concentration showed no significant changes with precipitation time. This implies that no new solid protein was formed. This is because isoelectric precipitation process is a fast reaction and almost all precipitable proteins came out of the solution within the first minute.

4.1.5 Some Functional Properties of Sunflower Defatted Meal and Isolate

Table 4.4 shows some of the functional properties (water hydration capacity, fat absorption capacity, and foam stability test) for the sunflower defatted meal and isolate. Commercial soy isolate (Purina Protein, 500E, manufactured 1986) was used for comparison. Sunflower products showed low values of water hydration capacity compared to commercial soy isolate. This was because the commercial product was a very fine powder whereas the sunflower products were not size classified. The fineness of the soy isolate created a large surface area and voidage which meant a large wetting area. Sunflower products showed higher values of fat absorption capacity than commercial soy. During this experiment it was observed that the commercial product splits into two layers and the oil was trapped between the layers. This meant that some of the proteins in the commercial product were lighter than the oil used and they did not absorb oil. The foam stability of the sunflower isolate was inferior compared to the commercial product, but the defatted meal showed a very stable foam. Poor foam stability shown by the sunflower isolate was because of the absence of the stabilizing constituents removed during protein isolation.

4.1.6 Inhibition of Discoloration of Sunflower Protein Isolates

The application of sunflower protein as a food supplement is not extensive because of an unappetizing colour at pH near neutrality, although this colour is non-

Table 4.4 Some functional properties of sunflower defatted meal from confectionery
-type seeds and isolate obtained at pH 4.0.

Sample	WHC ¹ (mL/g)	% FAC ² (mL/g)	Foam volume (mL)				
			1 min	20 min	30 min	60 min	120 min
Defatted meal	1.05	322	730	670	622	570	472
Isolate	1.22	231	220	38	28	15	10
Soy isolate ³	5.17	133	260	190	175	170	165

¹ Water hydration capacity 'as is'.

² Fat absorption capacity 'as is'.

³ Commercial soy isolate (Purina Protein, 500E, manufactured 1986) with moisture content 5.41 % w/w.

toxic. Complete removal of phenolic acids by washing defatted meal or protein isolate with hot water or acidic solutions or organic solutions, requires large amounts of washing liquid which makes industrial scale applications uneconomical (handling of large amounts of solution with low concentration and disposal of effluent solution). The use of sodium sulphite at low concentration (0.05 to 0.1 % w/w) is known to prevent discolouration (Gheyasuddin et al., 1970) without significant effects on protein solubility and yield. Chlorogenic acids (CA) tests performed in this study showed that the chlorogenic acid content of the white isolate (prepared from protein solution containing 0.1 % w/w Na_2SO_3) was about 2.58 % w/w. Whereas that of the green coloured isolate (without Na_2SO_3) was 0.07 % w/w. This meant that the CA in the white isolate was easily washable with methanol solution. That is, the presence of Na_2SO_3 weakens the bond between the CA and the protein molecules. Washing the white isolate once with an aqueous solution at pH 4.0 reduced the CA content by 40 % w/w. Further washing with an aqueous solution turned the white isolate grey.

In another experiment, protein solutions (with 0.1 % w/w Na_2SO_3) were filtered through four types of membranes (AMICON Corporation, Lexington, MA) as shown in Table 4.5. The retention (cut-off) molecular weight of the membranes used was 1,000; 10,000; 30,000; and 300,000. It was intended to determine which fraction of protein is associated with CA. The CA and protein concentrations of the starting solution (feed), the collected filtrate, and the retained (residue) solution were all measured. The analysis showed that the filtrate obtained using the membrane type PM30 (retention MW = 30,000) had the highest ratio of the CA to protein (4.04 mg CA/mg N). This confirms the earlier studies that the majority of CA binds to low molecular weight proteins (see Section 2.1.3). However, the total removal of the CA was not achieved. Furthermore, the removal of these low molecular weight proteins would change the total composition and nutritional value of the sunflower protein.

4.1.7 Effects of HCl Concentration and Precipitation Temperature on Protein Solubility

The effect of the concentration of aqueous HCl during protein precipitation (in a batch precipitator at 298 K) on the final protein concentration is presented in Figure

Table 4.5 Efficiency of membrane filtration experiments to remove discolouring pigments in the sunflower protein (molecular weight of CA = 354.3 kg/kmol).

Type*	Retention MW	CA concentration (mg/ml)			Protein concentration (mg N/ml)			Ratio CA/protein (mg CA/mg N)		
		feed	filtrate	residue	feed	filtrate	residue	feed	filtrate	residue
UM2	1,000	0.96	0.04	1.08	2.68	0.0954	3.0853	0.36	0.42	0.35
UM10	10,000	1.68	0.09	1.96	2.68	0.1034	3.3557	0.63	0.87	0.58
PM30	30,000	1.24	0.90	1.37	2.68	0.2226	5.2404	0.46	4.04	0.26
XM300	300,000	1.56	1.47	1.40	2.68	0.7475	4.0237	0.58	1.97	0.35

* Membrane type Diaflo Ultrafilters manufactured by AMICON Corporation, Lexington, MA

4.8. Feed protein solutions at pH 10.0 with concentrations ranging from 0.4 to 8.3 mg N/mL (low to high) were contacted with aqueous HCl solution in a batch precipitator. Four volumetric feed ratios (ca. 0.01, 1.0, 5.0, and 12.5 v/v, i.e., volume of aqueous HCl : volume of protein feed solution) representing low to high ratios were used (predetermined by titration to give a desired volumetric ratio). In all runs the final pH of the slurry was 4.0. It was observed that as the concentration of aqueous HCl was increased the percentage yield of solids approached 84 % w/w. At very low volumes of aqueous HCl solution the solids yield is approximately given by $(C_o - C^*)/C_o$, where C_o and C^* are the initial and final concentrations of protein in the solution, respectively. This means that for highly concentrated protein solutions, multistage precipitation is required to recover most of the solids. Increasing the precipitation temperature increased the solubility of protein (see Table 3.1). From these experimental observations, the concentration of protein still in the solution (C^*) after precipitation was found to be related to the precipitation temperature (T in K), volumetric feed ratio (r), and the initial concentration of protein (C_o) by:

$$C^* = K_s \frac{C_o}{r+1} \quad (3.3a)$$

$$K_s = \frac{(rk_1 + k_2)}{(r+1)^{k_3}} e^{-k_{ER}T} \quad (3.3b)$$

Equations (3.3a) and (3.3b) were fitted to the experimental data using the Least Squares method in SAS. The optimized parameters obtained were: $k_1 = 2.63$, $k_2 = 0.405$, $k_3 = 2.0$, and $k_{ER} = 247.6$ K. Calculated values of K_s are also presented in Table 3.1. The above equations gave the best fit (deviations within ± 10 %) for low values of r (< 5). Therefore, the maximum yield of solid protein can be estimated from the given equations.

The developed equations, describing the final concentration of protein solution, were only valid for isoelectric precipitation of sunflower proteins by aqueous HCl. Also, these equations were not valid for protein solutions prepared by the salting-in method.

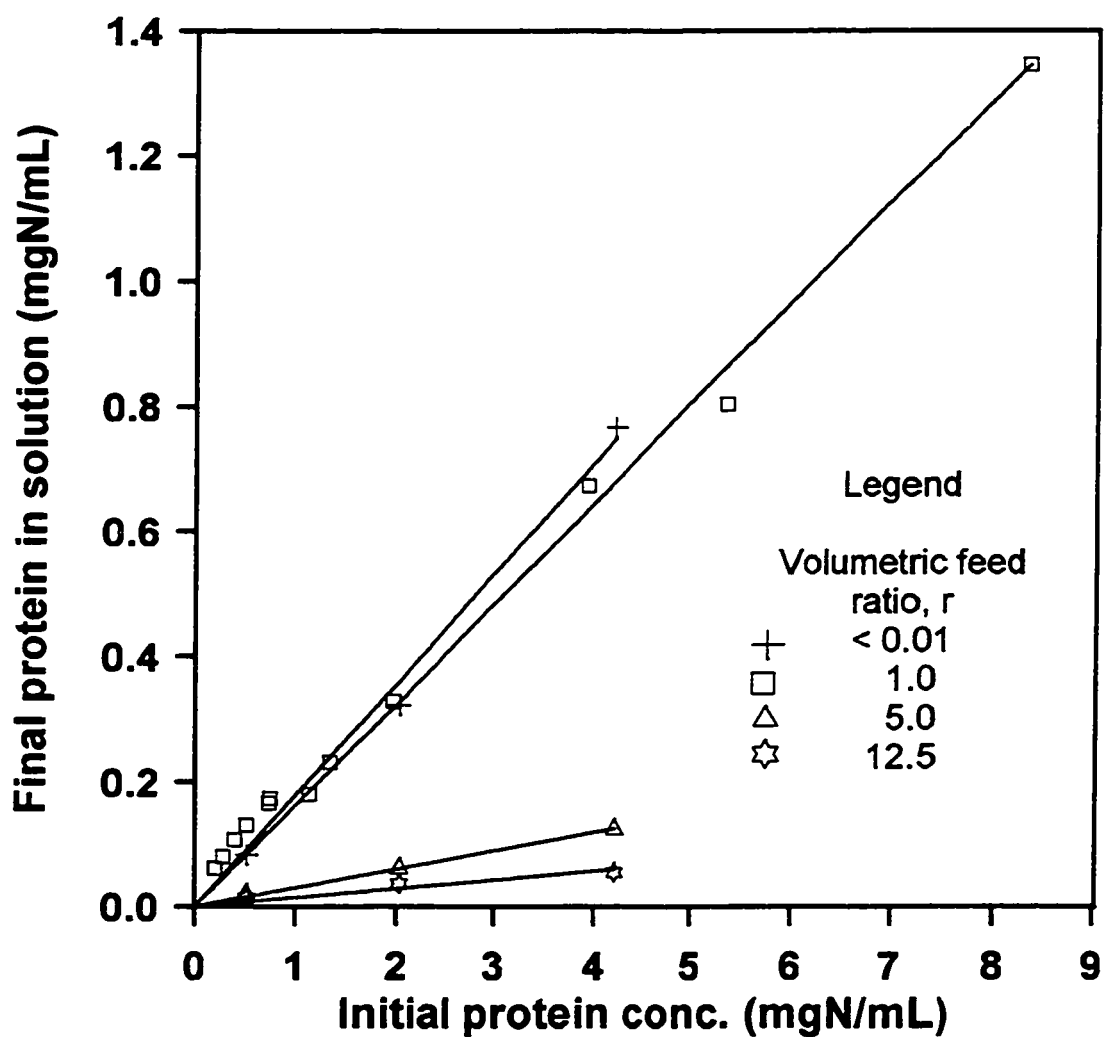


Figure 4.8 Effects of volumetric feed ratio and initial protein concentration on the final protein concentration in the solution during isoelectric precipitation (protein feed solution at pH 10.0 and final solution at pH 4.0).

4.1.8 Solids Concentration Measurement Using Turbidimetry Method

The turbidimeter used for on-line solids concentration measurements (for the tubular and MSMR precipitators) was calibrated as described in APPENDIX B. An extrapolated Beer-Lambert's equation was developed and used to fit the experimental data. A sixth order polynomial equation relating $\ln(\text{transmission})$ and $\ln(\text{concentration})$ was developed ($Y = -2.548 + 3.083X - 0.163X^2 - 0.442X^3 - 0.08852X^4 - 0.00677X^5 - 0.000184X^6$ with $R^2 = 0.998$; where Y is $\ln(Tr)$ and X is $\ln(Cs)$). For calculations of the solids concentration from the %Tr data, an iterative method was used. This polynomial equation gave an excellent fit of the measured transmission data over the entire range of solids concentration (0.00002 to 0.05 g of solid/mL of liquid).

4.2 Tubular Precipitator Results

4.2.1 Residence Time Distribution (RTD) Studies

The dispersion number along the tubular precipitator was determined in terms of the Peclet number ($Pe = zu/D_z$) using the pulse response data as described by Levenspiel (1972). The measured signal (voltage) was proportional to the tracer concentration. That is, when voltage (e_i) = 0.0, the concentration of KCl in the solution was 0.0 mol/L. The voltage-time data were discretized into time intervals, $\Delta t = 0.25$ min, to obtain e_i at corresponding t_i . The following parameters were calculated from the discretized pulse responses:

- a. the mean residence time between the two measuring points located at $(l_2 - l_1)$ apart:

$$t_{12} = (l_2 - l_1)/u \quad (4.1)$$

- b. the mean flow time to a measuring point (calculated from the response):

$$\Theta_{i0} = \sum(t_i e_i \Delta t) / \sum(e_i \Delta t) \quad (4.2)$$

c. the variance of the distributions:

$$\sigma_{ii}^2 = \sum(t_i^2 e_i \Delta t) / \sum(e_i \Delta t) - \Theta_{i0}^2 \quad (4.3)$$

d. the difference in variance between the two measuring points:

$$\sigma_{12}^2 = \sigma_{i2}^2 - \sigma_{i1}^2 \quad (4.4)$$

e. the dimensionless difference in variance:

$$\Delta\sigma_{\Theta}^2 = \sigma_{12}^2 / t_{12}^2 \quad (4.5)$$

f. and the dispersion number for the tubular precipitator was calculated as:

$$D_z / uz = \Delta\sigma_{\Theta}^2 / 2 = 1/Pe \quad (4.6)$$

Calculated results are shown in Table 4.6. These values show that there is intermediate amount of dispersion (range between 0.01 and 0.03, Levenspiel, 1972). At other flow velocities a linear regression was used to relate the $1/Pe$ and the flow velocity. The resulting best fit equation was given by $1/Pe = 0.0263 - 0.00015u(\text{cm/s})$ with $R^2 = 0.905$ (see Figure 4.9). For the flow velocities used in protein precipitation their dispersion numbers are presented in Table 4.7. The dispersion number was assumed to be constant along the tubular precipitator at a given flow velocity. These dispersion numbers were later used in the axial dispersion model for the tubular precipitator operating in the turbulent or laminar flow regime. According to Nauman and Buffham (1983), the axial dispersion model can be used to approximate the laminar flow systems even though the flow velocity profiles are not flat. In this case, the coefficient D_z combines the effects of laminar velocity profiles and the molecular diffusion (Taylor-Aris dispersion), this is valid for long tubes with small ratio of d_t/z_T .

4.2.2 Effect of the Static Mixers

The effect of premixing the feed solutions (aqueous HCl and protein solution) on

Table 4.6 Summary of RTD results for the tubular precipitator using KCl solution as a tracer.

Meas. pt. (i)	u (cm/s)	l_i (cm)	t_{12} (min)	Θ_{io} (min)	σ_u^2 (min ²)	$\Delta\sigma_{12}^2$ (min ²)	$\Delta\sigma_\Theta^2$ (--)	$0.5\Delta\sigma_\Theta^2$ = D/uz
1	34.8	67		0.0547	0.002801			
2	34.8	572	0.242	0.1211	0.005244	0.002442	0.0418	0.021
1	47.7	67		0.04	0.001256			
2	47.7	572	0.176	0.1501	0.002418	0.001162	0.0373	0.019
1	60.6	67		0.0321	0.000625			
2	60.6	572	0.139	0.1153	0.001332	0.000706	0.0366	0.018
1	73.5	67		0.027	0.00039			
2	73.5	572	0.115	0.0839	0.000771	0.000381	0.029	0.015

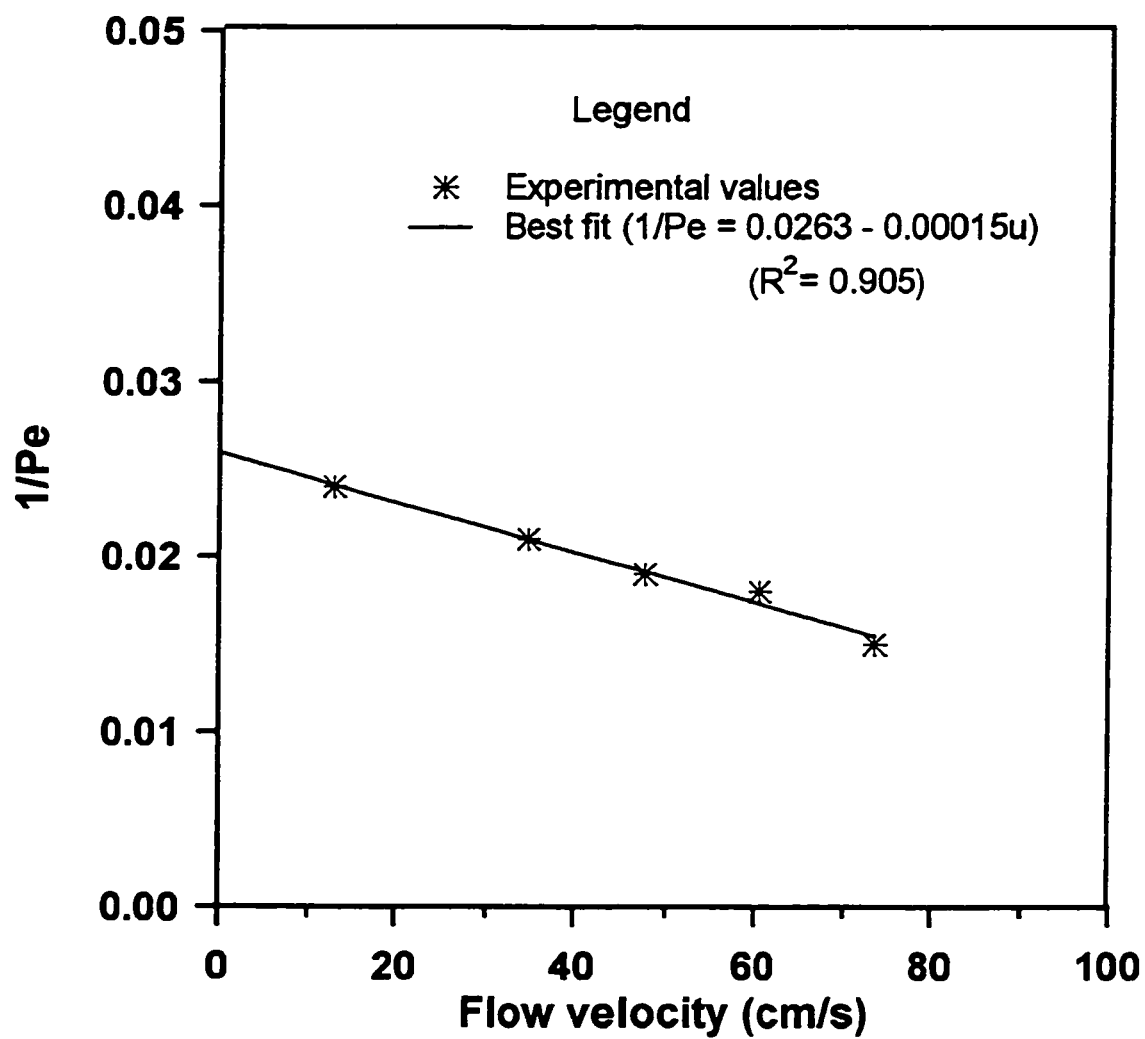


Figure 4.9 Linear fit for the experimental RTD data: $1/Pe$ versus flow velocity in the tubular precipitator.

Table 4.7 Calculated dispersion numbers for the tubular precipitator at increasing flow Re numbers used in this study.

Re no.	u (cm/s)	Calculated dispersion number, $1/Pe$
440	7.3	0.0252
778	13.0	0.0243
4800	80.0	0.0143
4950	82.5	0.0139
5058	84.3	0.0136

the mean particle size and the solids concentration is presented in Figures 4.10 and 4.11. In the absence of the static mixers and at low flow velocity (laminar flow regime, $Re = 800$), the mean particle size and the solids concentration were low (see Figure 4.10). Introducing the static mixers (4 or 8 pieces) increased the mean particle size and the solids concentration. However, no significant difference was observed when the number of static mixers was double from 4 to 8. In the turbulent flow regime ($Re = 5,000$) the differences between the three categories (no static mixers, 4 and 8 static mixers) were small (see Figure 4.11). This showed that proper premixing of the feed solutions is essential for initial nucleation of protein particle and high yields (solids concentration). Unlike the turbulent flow regime, the laminar flow regime is characterized by little fluid mixing in the radial direction. This results in packets of un-mixed reactants flowing down the precipitator.

4.2.3 Effect of the Precipitator Length

The effect of the precipitator length on the mean particle and the solids concentration is shown in Figures 4.12 and 4.13. Increasing the precipitator length from 10 m to 20 m showed similar profiles for the mean particle size. In the laminar flow regime (Figure 4.12A), the mean particle size increased with the precipitator length. This meant that the particle growth (by aggregation) was still taking place (similar results were observed with protein feed concentration of 11.8 kg/m^3). This was attributed to the presence of low fluid-induced shear in the laminar flow regime. In the turbulent flow regime, the fluid-induced shear does not favour particle-particle aggregation and this resulted in small particles with little variations in the mean size. As shown in both figures (Figure 4.12B and 4.13B), the solids concentrations at the exit ports were similar. This implies that most of the precipitable proteins comes out of the solution within the first 10-m of the precipitator. Beyond that, the particle growth is dependent on the shear forces surrounding the particles.

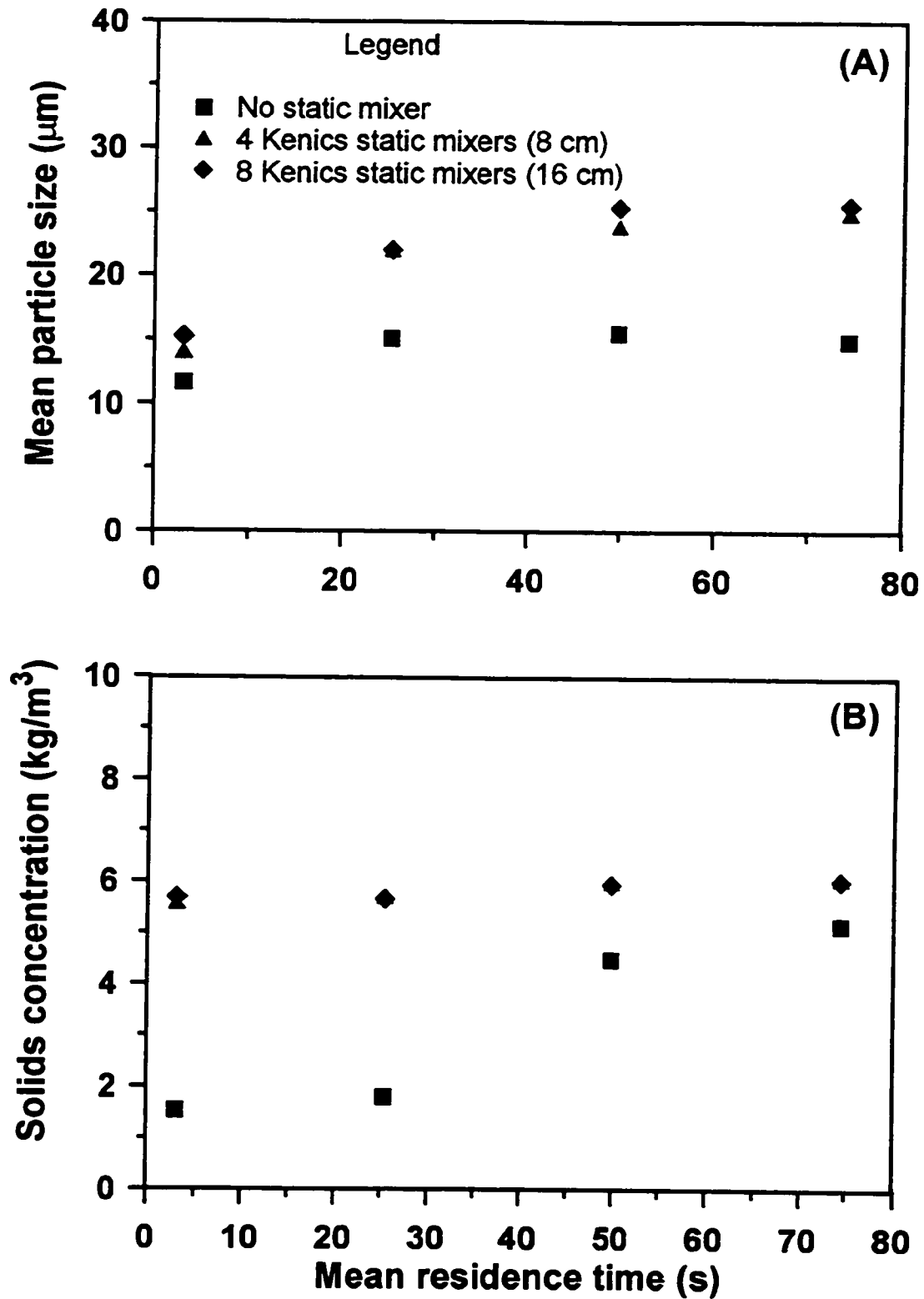


Figure 4.10 Effects of static mixer and mean residence time on the mean particle size and solids concentration in the tubular precipitator: protein feed conc. = $11.5 \text{ kg}/\text{m}^3$, flow Re no. = 800 and volumetric feed ratio = 1.0 v/v.

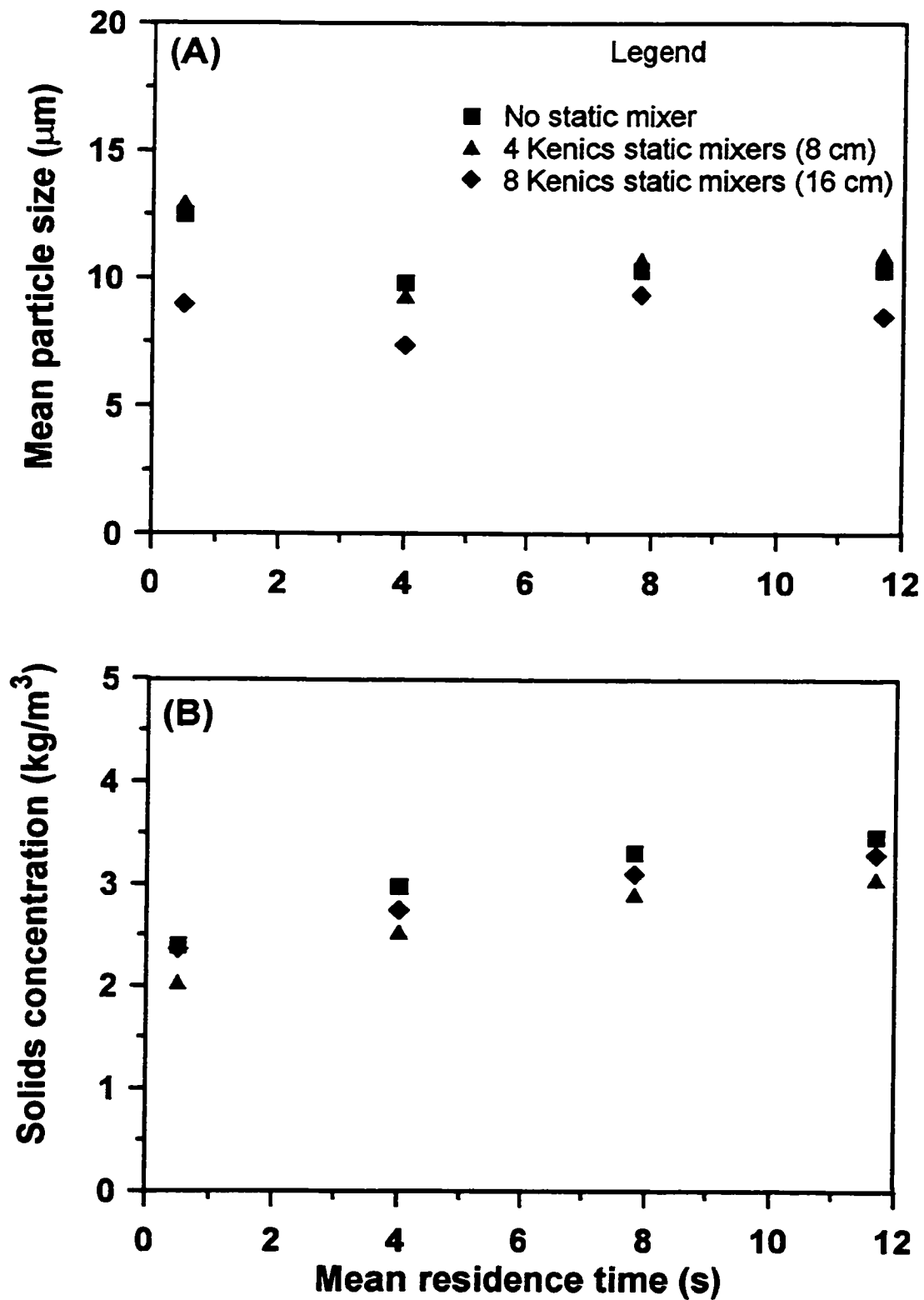


Figure 4.11 Effects of static mixer and mean residence time on the mean particle size and solids concentration in the tubular precipitator: protein feed conc. = $11.5 \text{ kg}/\text{m}^3$, flow Re no. = 5,000 and volumetric feed ratio = 1.0 v/v.

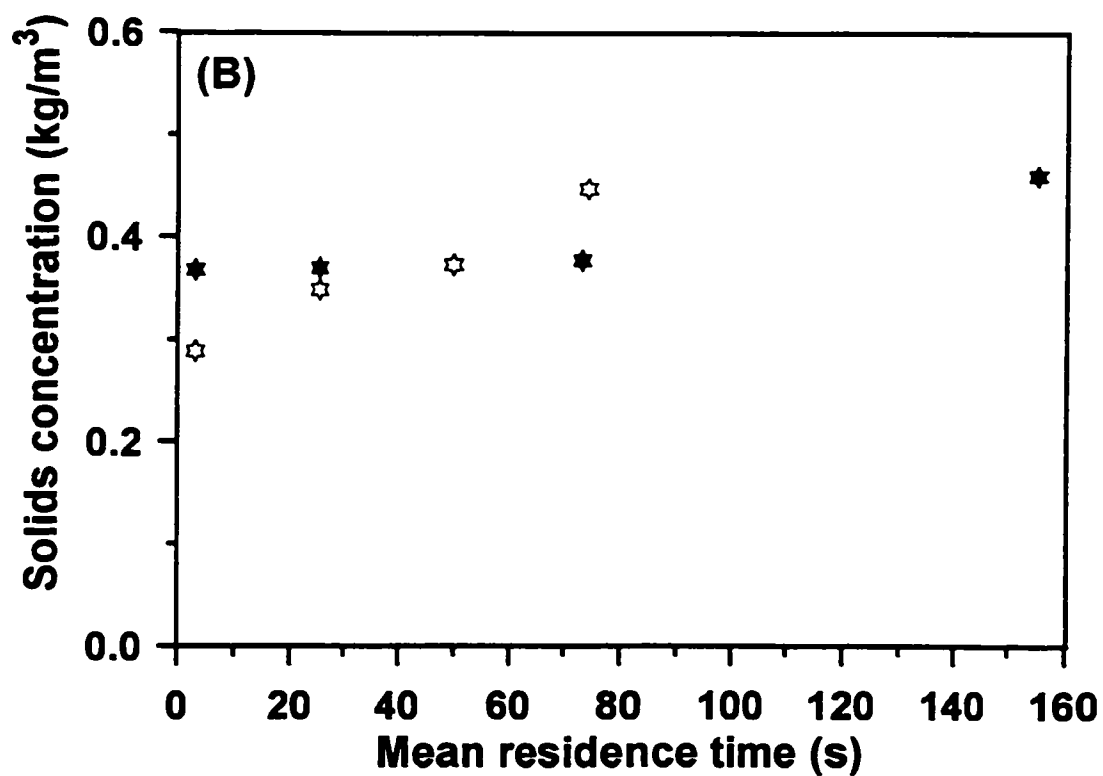
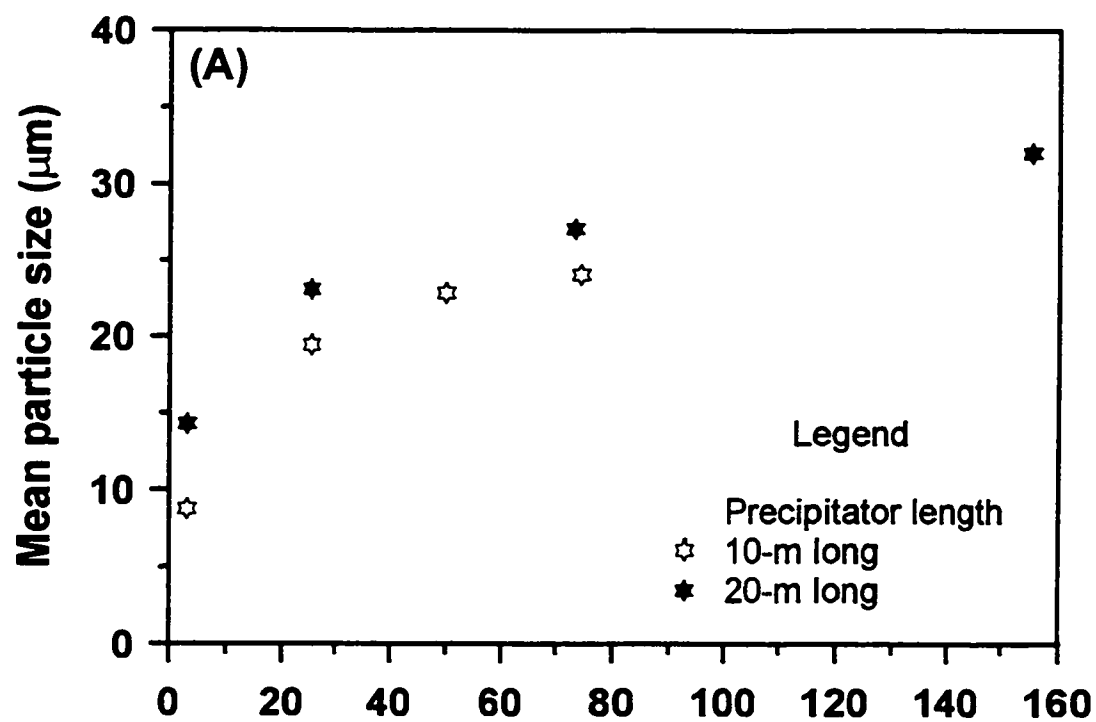


Figure 4.12 Effects of precipitator length and mean residence time on the mean particle size and solids concentration in the tubular precipitator: protein feed conc. = $2.8 \text{ kg}/\text{m}^3$, flow Re no. = 800 and volumetric feed ratio = 1.0 v/v.

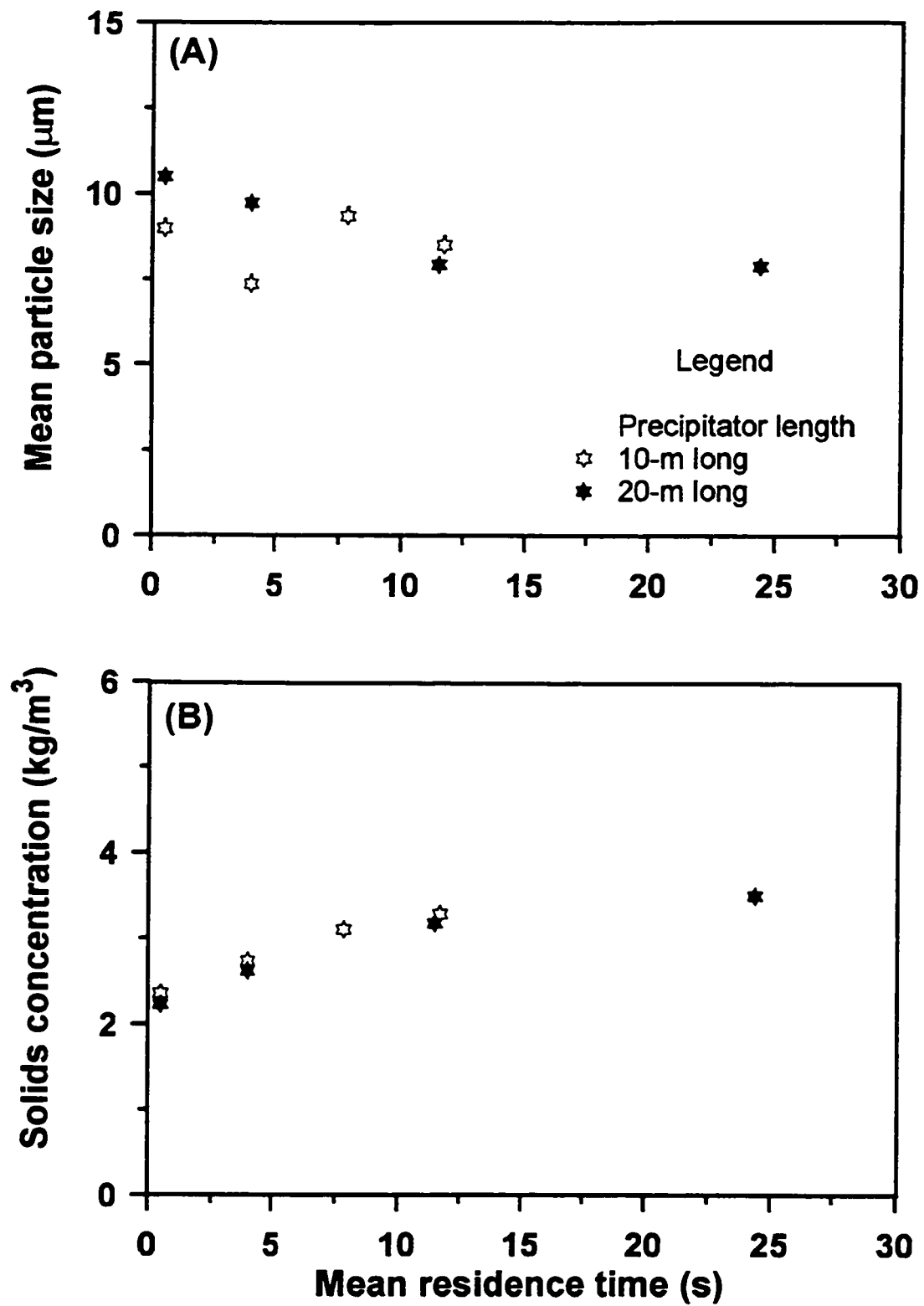


Figure 4.13 Effects of precipitator length and mean residence time on the mean particle size and solids concentration in the tubular precipitator: protein feed conc. = $11.8 \text{ kg}/\text{m}^3$, flow Re no. = 5,000 and volumetric feed ratio = 1.0 v/v.

4.2.4 Effect of the Protein Concentration in the Feed Stream

The effects of protein concentration in the feed stream on the mean particle size and the solid protein concentration (yield) are presented in Figures 4.14 and 4.15. It was observed that, in the laminar flow regime (Figure 4.14), the mean particle size and solids concentration increased with increases in the protein feed concentration. It is obvious that increases in the concentration of protein in the feed stream increased the nucleation rate, hence increased number of protein particles and solids concentration. In the turbulent flow regime (Figure 4.15) the mean particle size decreased with increases in the protein concentration in the feed stream. This might be due to increased rate of particle-particle collisions (under fluid-induced shear), resulting in particle breakages. However, profiles for the solids concentration were similar in both flow regimes which means that the yield (solids concentration) is dependent on the concentration of protein in the feed stream and less dependent on the flow regime.

The mean particle size, for runs with low protein feed concentration in the laminar flow regime, increased with mean residence time which indicated that particle growth by aggregation was significant. On the other hand, for runs with high protein feed concentration (Figures 4.14B and 4.15B), the solids concentration increased with mean residence time. This shows that longer mean residence times are required for the reactions to reach equilibrium or completion. Therefore, the observed increase in the mean particle size in the laminar flow regime for runs at high protein feed concentration was probably due to particle growth by diffusion and aggregation.

4.2.5 Effects of the Mean Residence time and Flow Velocity (Flow Regime)

The effects of the mean residence time (holding time = l/u) and flow velocity (flow regime) are presented in Figures 4.16 and 4.17. Each point in the figures is the average of two measurements. The tubular precipitator operating in the laminar flow regime ($Re = 800$) resulted in larger mean particle sizes which increased with increases in mean residence time (Figures 4.16A and 4.17A). The population density distribution (Figure 4.18a) showed a wide spread resulting in high coefficient of variation (CV)

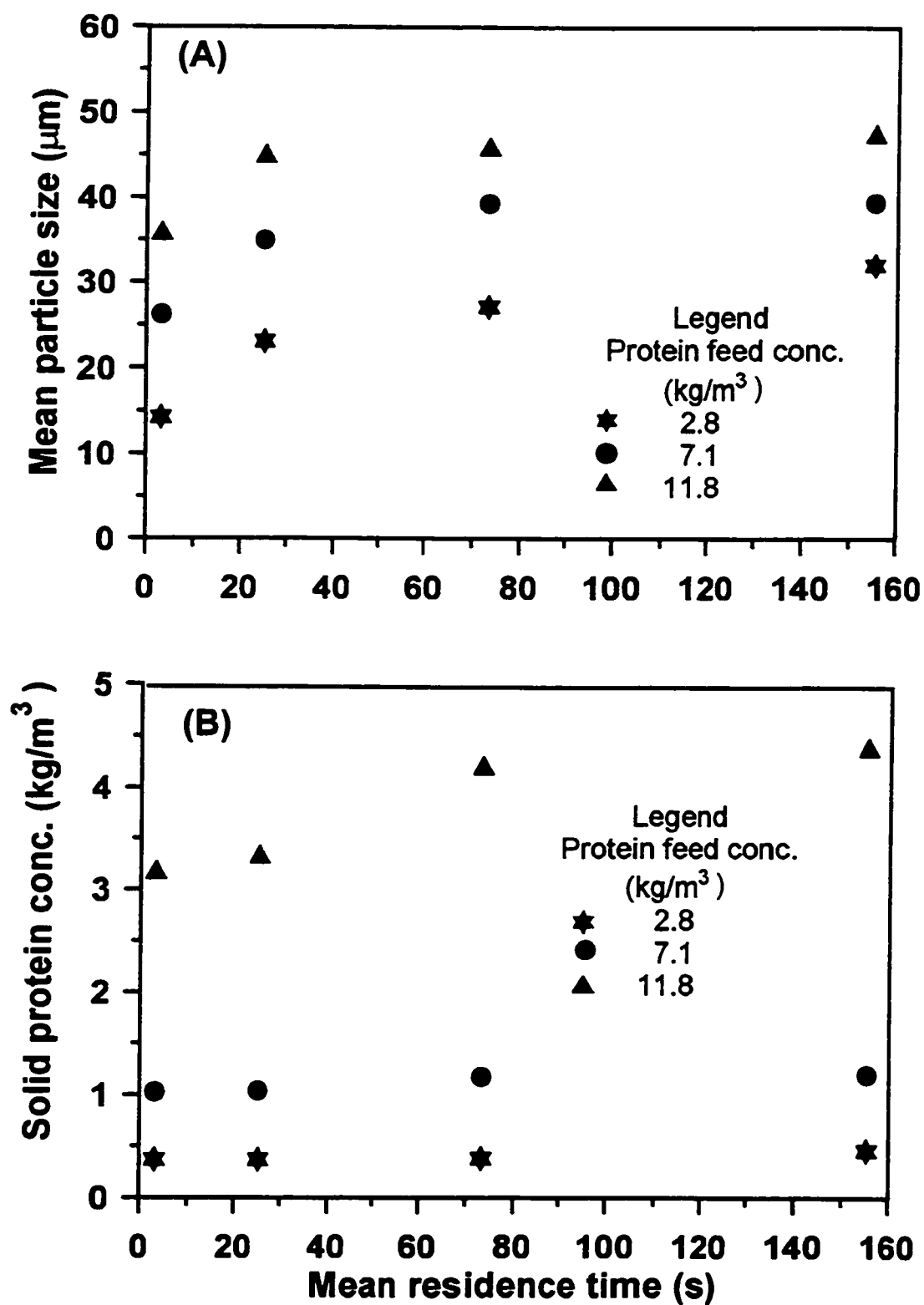


Figure 4.14 Effects of protein feed concentration and mean residence time on the mean particle size and solids protein concentration in the tubular precipitator: flow Re no. = 800 and volumetric feed ratio = 1.0 v/v.

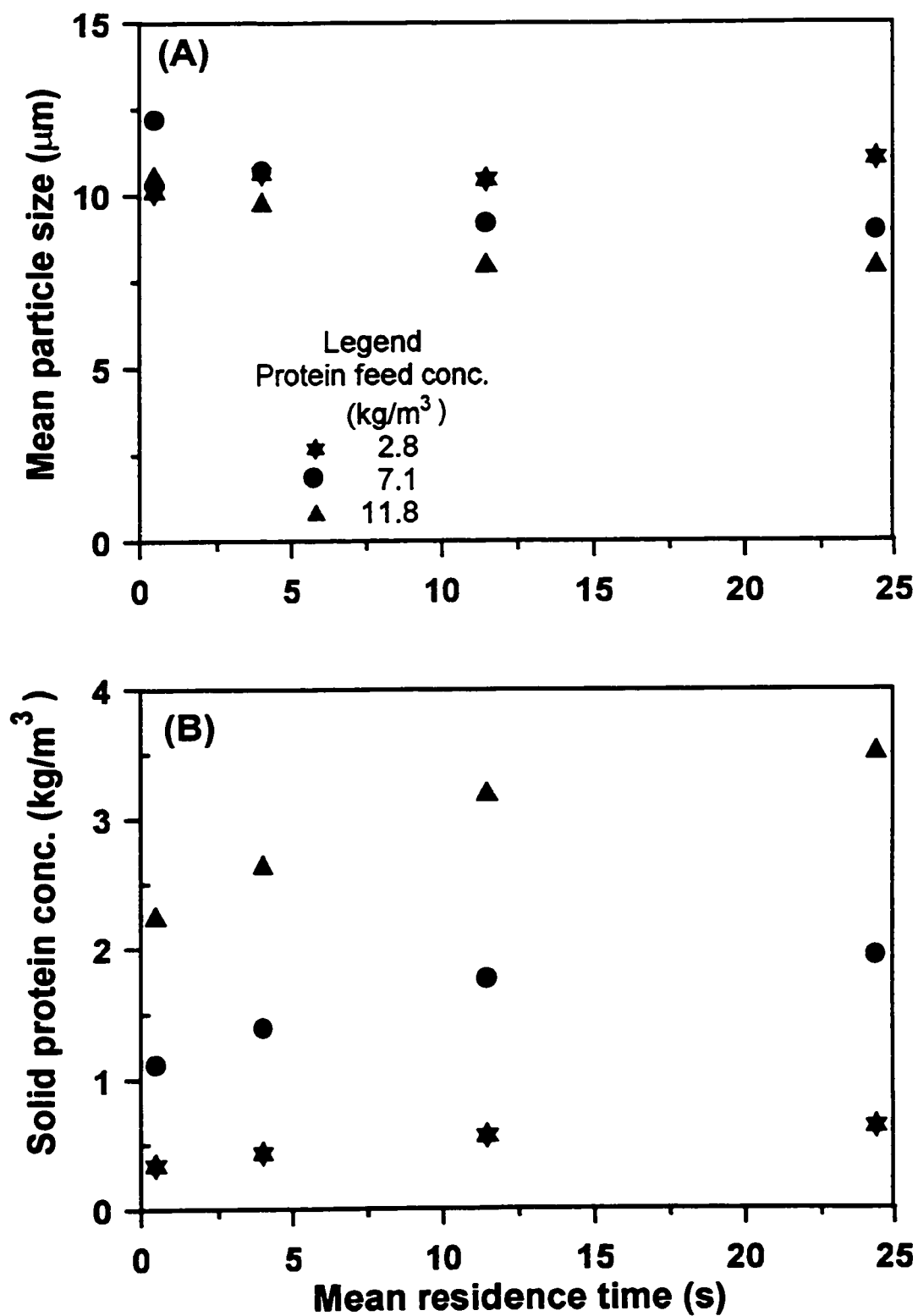


Figure 4.15 Effects of protein feed concentration and mean residence time on the mean particle size and solids protein concentration in the tubular precipitator: flow Re no. = 5,000 and volumetric feed ratio = 1.0 v/v.

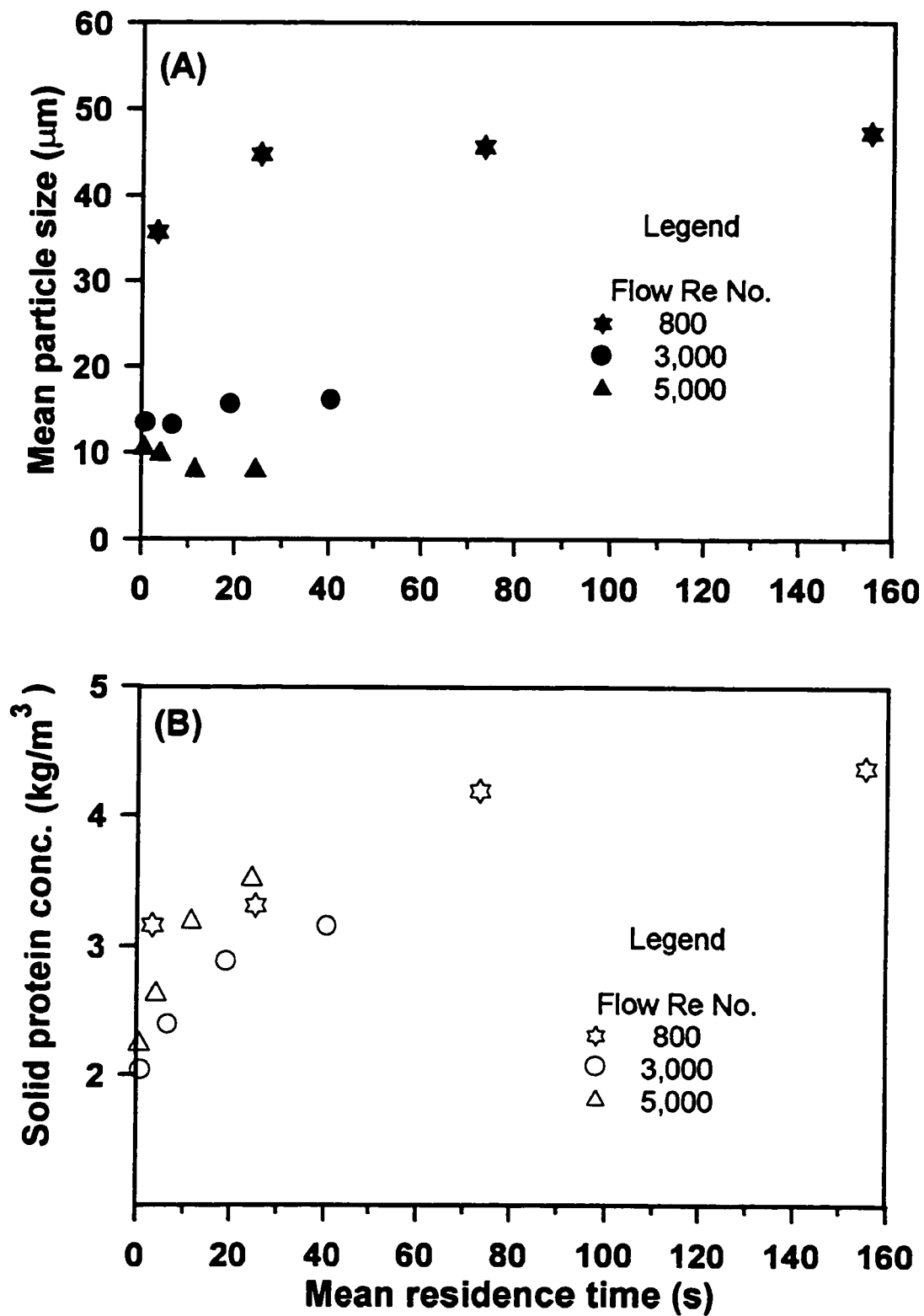


Figure 4.16 Effects of flow Re number and mean residence time on the mean particle size and solid protein concentration in the tubular precipitator: protein feed conc. = 11.8 kg/m³ and volumetric feed ratio = 1.0 v/v.

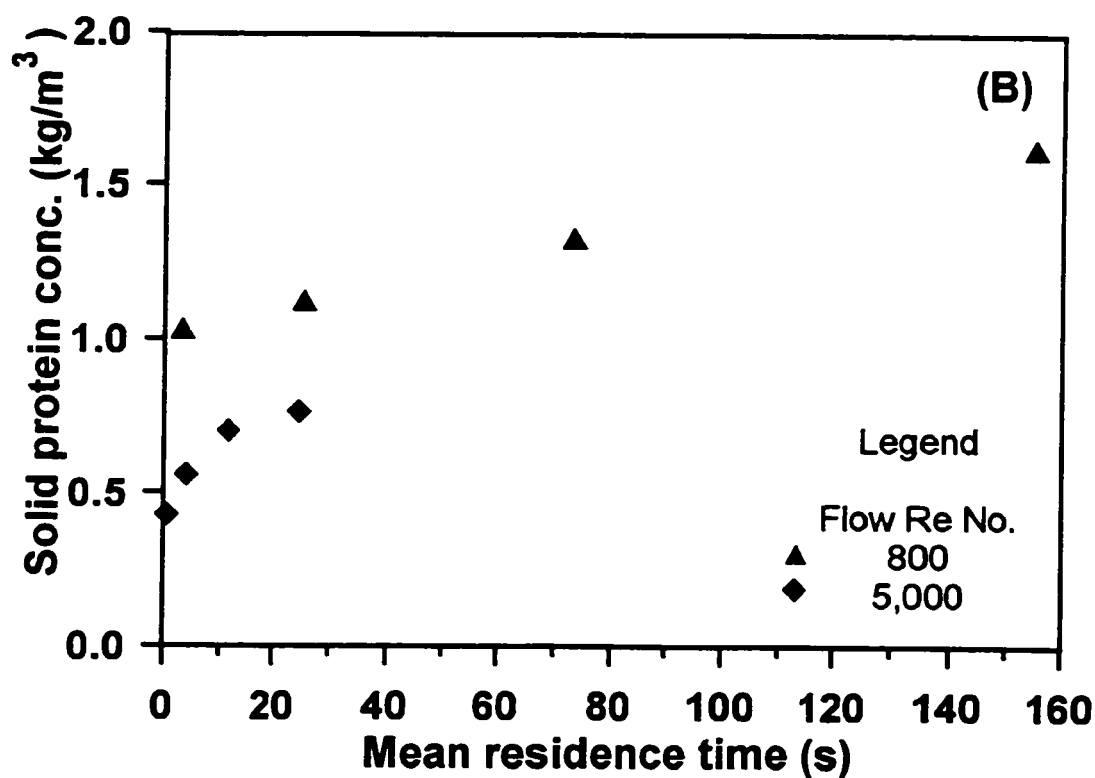
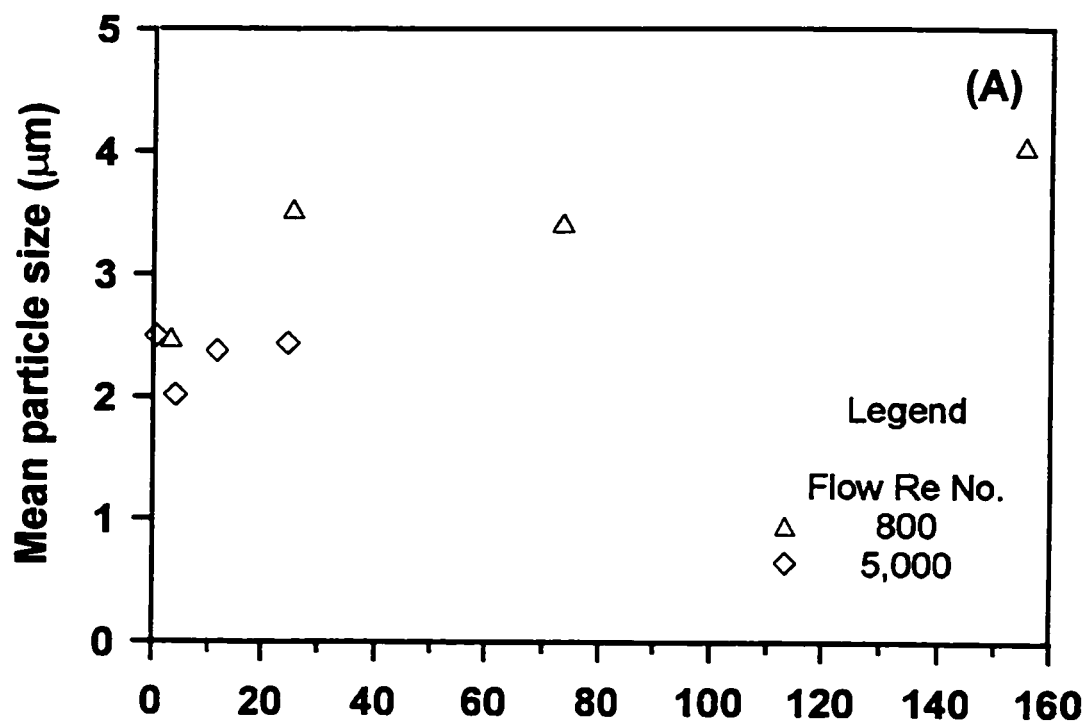


Figure 4.17 Effects of flow Re number and mean residence time on the mean particle size and solid protein concentration in the tubular precipitator using 0.05 M aq. calcium acetate as a precipitant: protein feed conc. = $12.0 \text{ kg}/\text{m}^3$ with 1.0M NaCl, feed ratio = 1.0 v/v, and precipitation pH 6.5.

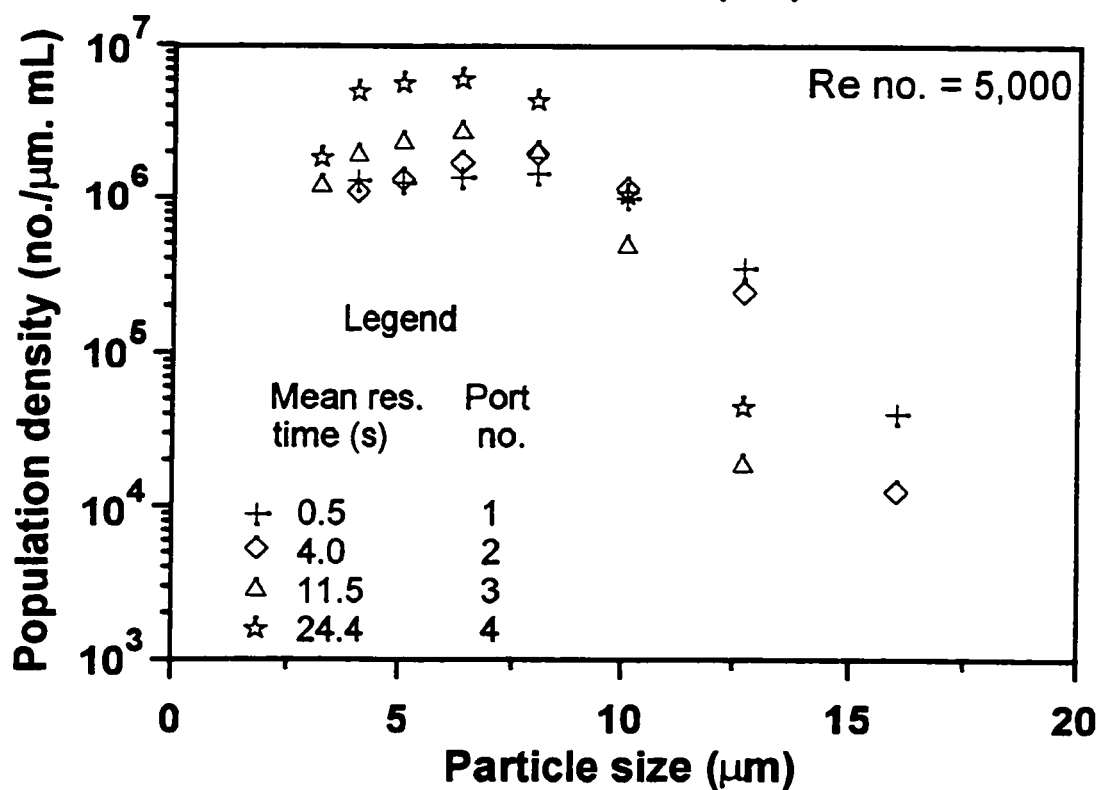
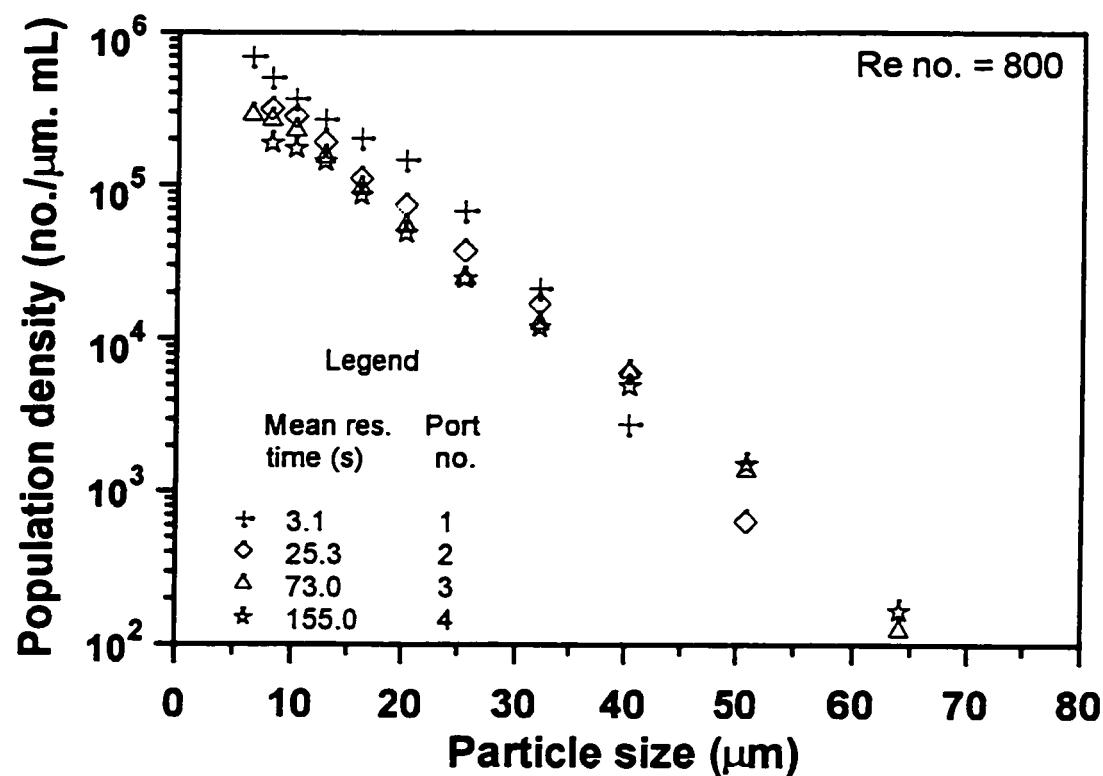


Figure 4.18 Effects of flow Re number and mean residence time on the population density of protein particles in the tubular precipitator: protein feed conc. = 11.8 kg/m^3 and volumetric feed ratio = 1.0 v/v.

values (Figure 4.19). This is due to continuous growth of smaller particles mainly by the aggregation process. Low fluid-induced shear rate in the laminar flow regime favours the formation of large and stable aggregates. In the turbulent flow regime ($Re = 5,000$), the mean particle sizes were small and decreased little with mean residence time (Figures 4.16A and 4.17A). The population density distribution showed a uni-modal distribution with a narrow spread (Figure 4.19). This suggests that fluid-induced shear determines the steady state PSD. Increasing the feed concentration under turbulent flow regime resulted in slightly smaller mean particle sizes due to increased solids concentration leading to increased aggregate breakage rate.

Precipitation using calcium acetate (0.05 M) at pH 6.5 showed similar trends as those observed from isoelectric precipitation (Figure 4.17). That is, a run in the laminar flow regime produced larger particles and higher solids concentrations than a run in the turbulent flow regime. However, calcium acetate resulted in the precipitate with smaller mean particle size and lower solids concentration compared to aqueous HCl as the precipitant. This might be due to a low degree of supersaturation in the case of calcium acetate precipitation or the presence of Ca^{2+} ions that hinder rapid particle aggregation.

4.2.6 Effect of Volumetric Flow Ratio of Feed Solutions

The effect of volumetric flow ratio of feed solutions (aqueous HCl solution : protein solution, v/v) on the mean particle size and solids concentration are presented in Figures 4.20 and 4.21, respectively. In this study, the total number of moles of HCl (conc. of HCl (M) x volume (L)) required for precipitation, i.e., lower the pH to 4, was constant. Therefore, if the volume of HCl to be used was large then its concentration had to be low. The mean particle size and the protein solids concentration decreased with increases in volumetric flow ratio. At a high volumetric feed ratio of 12:1, the solids concentration was low and varied little with mean residence time (Figures 4.21A and 4.21B). This was due to dilution (increase in the volume of liquid) and poor mixing at the molecular level (micromixing), which prevented HCl-protein molecules interactions. Decreasing the volumetric ratio to 1:1 improved the micromixing, hence an increase in protein yield and the mean particle size was observed (Figures 4.20A and 4.20B).

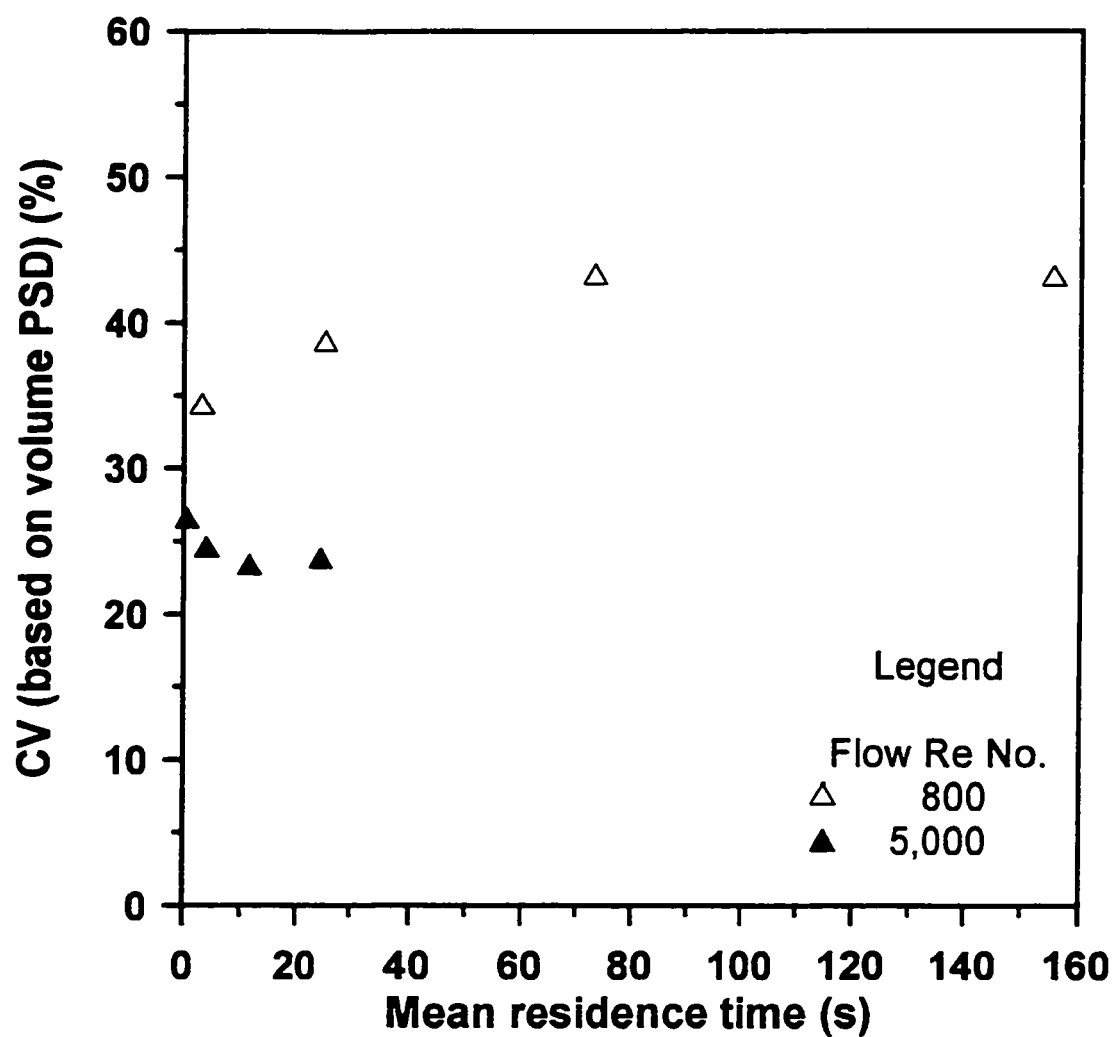


Figure 4.19 Effects of flow Re number and mean residence time on CV (based on volume distribution) for precipitates from the tubular precipitator: protein feed conc. = 11.8 kg/m^3 and volumetric feed ratio = 1.0 v/v.

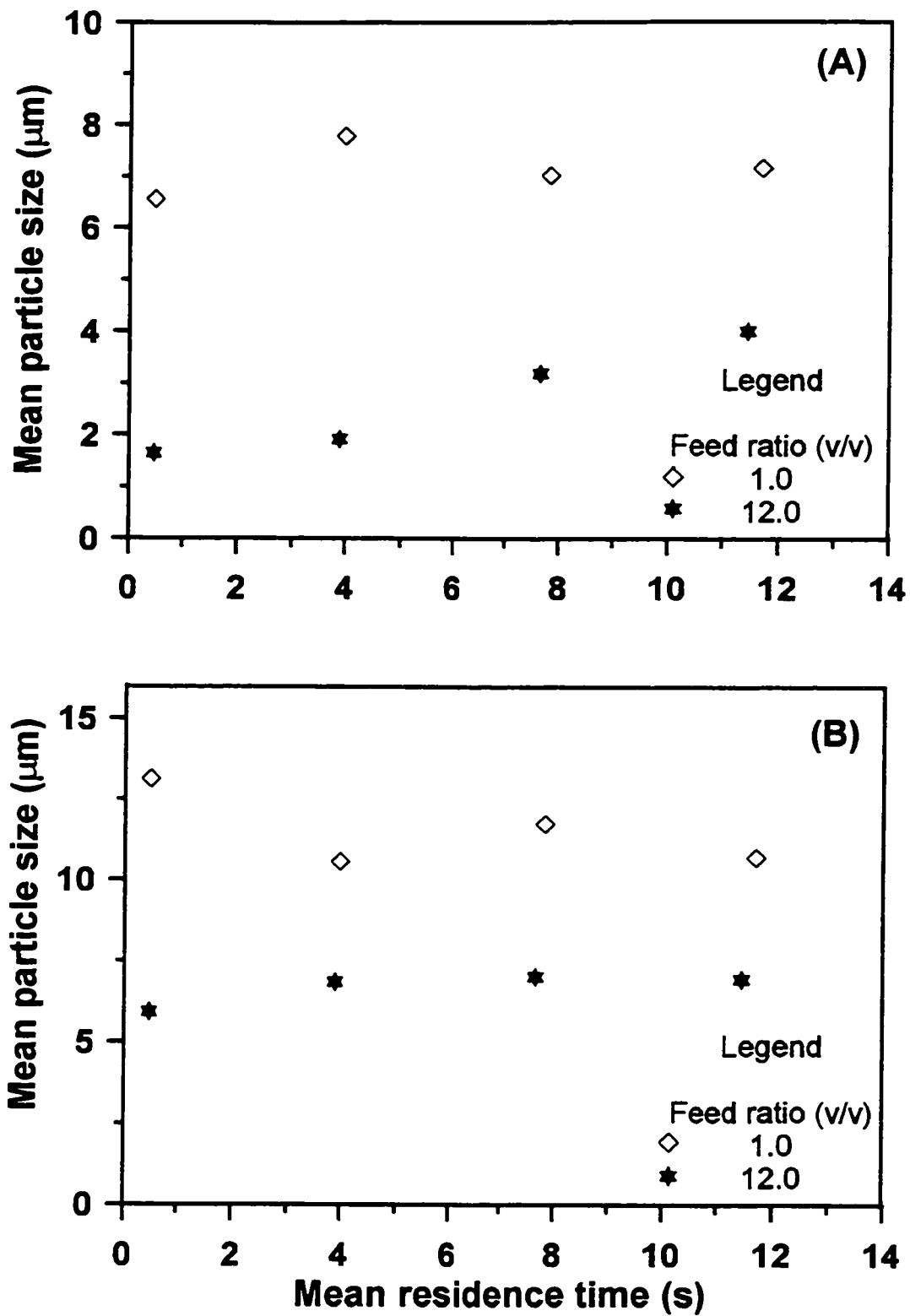


Figure 4.20 Effects of volumetric feed ratio and mean residence time on the mean particle size in the tubular precipitator with flow Re no. = 5,000:
 (A) protein feed conc. = 2.8 kg/m³ (B) protein feed conc. = 11.6 kg/m³.

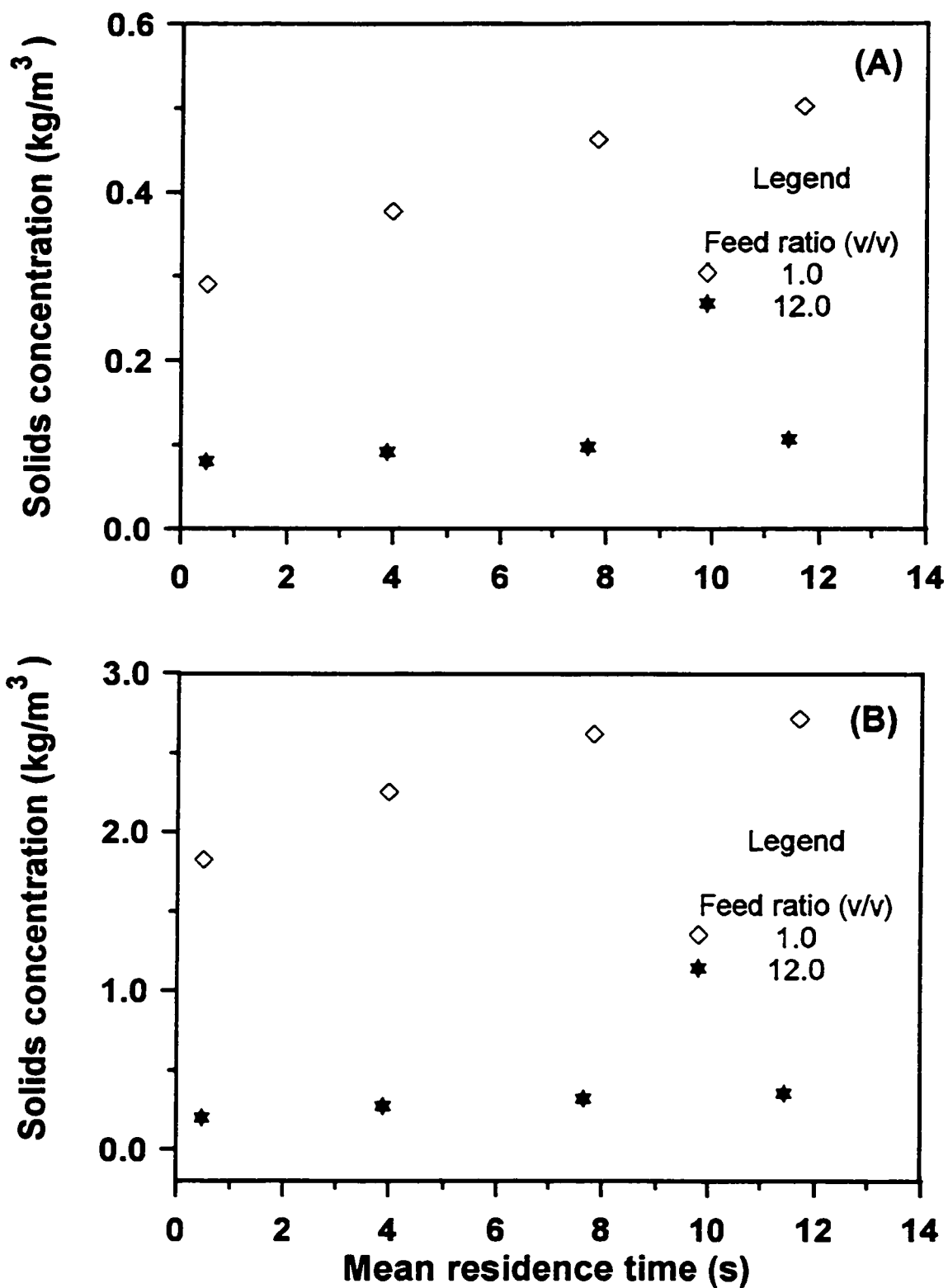


Figure 4.21 Effects of volumetric feed ratio and mean residence time on the protein solids concentration in the tubular precipitator with flow Re no. = 5,000: (A) protein feed conc. = 2.8 kg/m^3 (B) protein feed conc. = 11.6 kg/m^3 .

Furthermore, at high volumetric feed ratio the rate of aggregation was low because of low particle concentration. This lead to reduced particle-particle collisions. The opposite happened at low volumetric ratio.

4.2.7 Effect of Fluid-Induced Shear on Particle Size Distribution

The effect of fluid-induced shear on the mean particle size is presented in Figure 4.22. The mean particle size is expressed relative to the mean size of the particles measured at port number 1. At a low flow Re number of 440, the variations in the mean particle size with mean residence time were approximately $\pm 10\%$ relative to the mean size of particles at port number 1. At high solids concentration slurries (> 13 g/L), the mean particle size decreased with mean residence time up to the third sampling port followed by a slight increase in the mean size. At high flow Re number, 5000, the mean particle size showed a general decrease with mean residence time. The observed decrease in the mean particle size was approximately 7% relative to the mean size of particles at port number 1. Similar trends were observed for slurries with low and high solids concentrations. This means that, at high flow velocities, the effect of fluid-induced shear on the mean particle size was significant. In summary, at low flow velocity, particle-particle interactions leading to agglomeration are prevalent. Whereas, at high flow velocity approaching plug flow regime, the flow is segregated and particle-particle interactions are less frequent due to less dispersion.

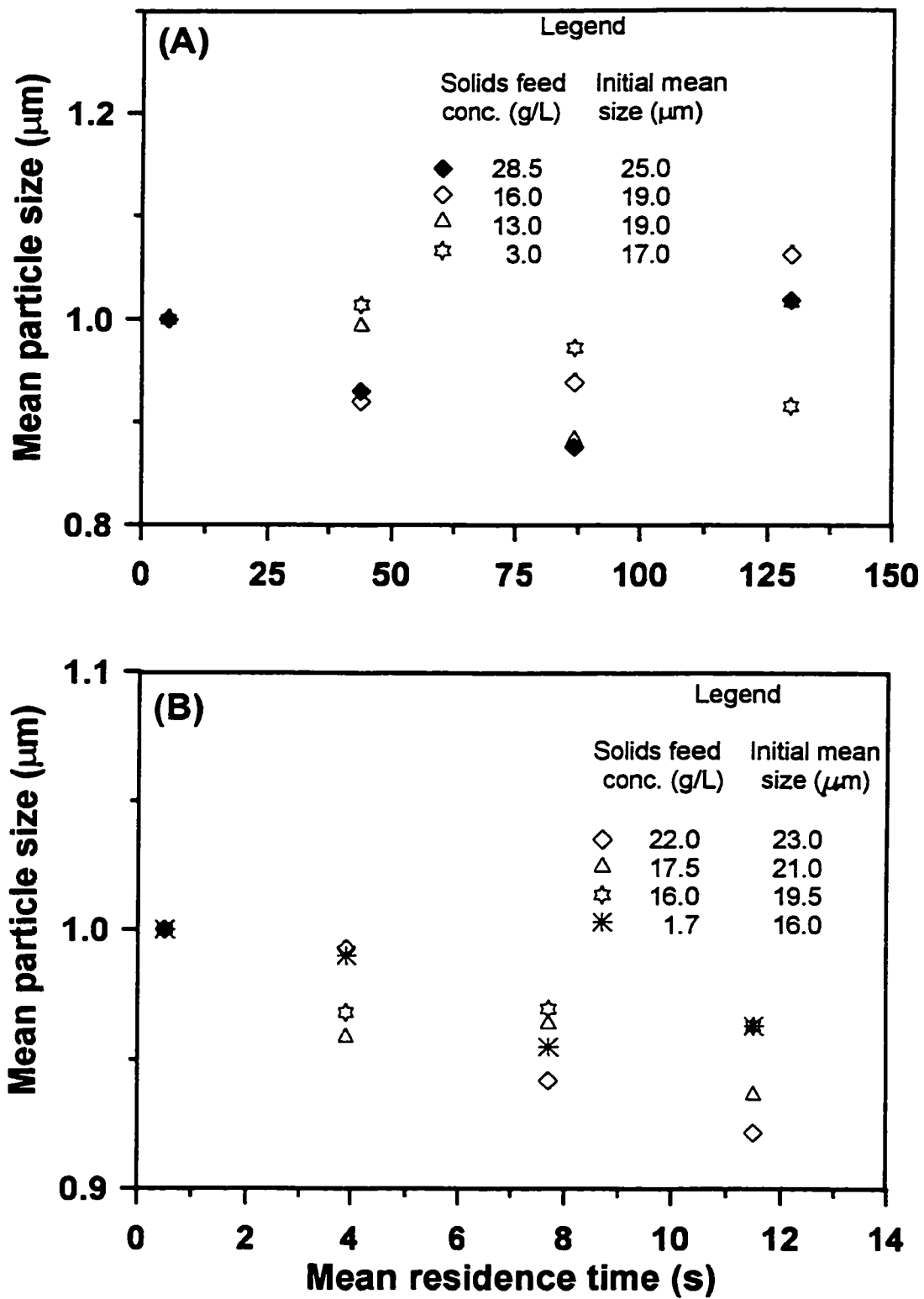


Figure 4.22 Effects of the flow regime (fluid-induced shear) and mean residence time on the mean particle size: (A) laminar flow regime Re no. = 440 (B) turbulent flow regime Re no. = 5,000.

4.3 Comparison Studies of the Tubular Precipitator With the MSMPR and the Batch Precipitators

4.3.1 Residence Time Distributions Studies for the MSMPR Precipitator

In order to determine the extent of mixing (bypass, dead volumes, and hold-ups) in the MSMPR precipitator, the areas under the tracer response graphs were calculated as described in Section 4.2.1. Also, it was determined that a mixer speed of 600 rpm produced adequate mixing. Higher speeds (> 600 rpm) resulted in the formation of foam which affected the turbidimeter readings and loss of proteins in the foam. The experimental and calculated mean residence times are presented in Table 4.8. The calculated values were higher than the experimental values ($< 20\%$). This implied that the particles stayed longer in the vessel than the liquid. This might have been due to the presence of dead zones near the wall-baffles and in the small layer of foam formed on the top surface. However the deviation of 20% is also because of the approximation method used in calculating the areas under the graph.

4.3.2 Comparison Between the Tubular and the MSMPR Precipitators: Effects of the Mean Residence Time and the Protein Feed Concentration on the Mean Particle Size and the Solids Concentration

In the following discussions involving the batch, MSMPR, and the tubular precipitator, it is important to clarify the difference between the mean residence time and the precipitation time. In this study, the mean residence time ($= V/Q$) applies to the MSMPRP and the tubular precipitator (flow types). Precipitation time applies to the batch precipitator (non-flow type) to indicate the reaction time elapsed. For the MSMPR and the batch precipitator analysis, samples were taken near the top and at the bottom of the precipitator. In most cases similar results were obtained. The experimental data presented in this study represent the average of these two measurements.

For the tubular precipitator protein nucleation occurs in the mixing zone (static mixers) where the protein supersaturation is high. Beyond this zone, the protein

Table 4.8 Comparison between the calculated and the experimental mean residence times for the MSMR precipitator using PVC particles as a tracer.

Total feed rate = Q (L/min)	Mean residence time $\tau = V/Q$ (s)	Calculated mean residence time (s)	Deviation (%)
0.22	74.4	78.6	7
0.34	48.6	57.8	19
0.65	25.2	29.1	16
1.44	11.4	12.3	8

supersaturation is almost depleted. Therefore, secondary nucleation and molecular growth of particles by solute deposition are not significant. For the MSMPR precipitator, protein supersaturation is always constant. Primary nucleation, secondary nucleation, and molecular growth occur side by side, thus influencing the PSD of the precipitate.

The effects of mean residence time and protein feed concentration on the mean particle size and solids concentration for the MSMPRP are presented in Table 4.9. High protein concentration in the feed stream resulted in larger mean particle sizes compared to the low protein concentration at all mean residence times. This is due to the increased number of primary particles available for aggregation. For both feed concentrations, increasing the mean residence time resulted in a precipitate with a smaller mean particle size and lower coefficient of variation (CV) of volume distribution (CV shows how wide is the spread of the PSD). However, the feed solution with high protein concentration showed a larger decrease in mean particle size than the low protein concentration (from 23.7 μm to 13.0 μm as compared to 9.0 μm to 8.6 μm , respectively). The decrease in mean size with mean residence time is attributed to aggregate breakage by shear forces (caused by the mixer and the fluid shear) and by aggregate-aggregate collisions. At low protein feed concentrations there were fewer primary particles to cause a significant aggregate growth. The mean particle size at low protein feed concentration seemed to vary little with the mean residence time, but the CV values decreased from 54.3 % to 23.7 % showing that there was a shift from a wider spread PSD to a narrower PSD. This shows that the shear forces are responsible in determining the maximum stable size of the aggregates.

Aggregation and the presence of newly formed particles together with aged particles may cause a bimodal PSD as shown in Figures 4.23 and 4.24. The PSD shows the disappearance of primary particles ($L < 10 \mu\text{m}$) by aggregation to larger size. The larger aggregates grow by addition of primary particles. Increasing the protein feed concentration (and consequently the solids concentration) and the mean residence time results in a uni-modal PSD (Figure 4.24). This transition from bimodal PSD to uni-modal PSD is not observed for runs with low protein concentration in the feed stream (low solids concentration) as shown in Figure 4.23. This indicates that at increased solids concentration, particle-particle collisions are more frequent and effective in forming a stable aggregate.

Table 4.9 Experimental results from the MSMPPR: Effects of the mean residence time and the protein feed concentration on the mean particle size, solids concentration, and the coefficient of variation (protein feed concentrations: Runs MS2_series = 11.6 kg/m³ and Runs MS3_series = 2.9 kg/m³).

Run no.	Q (mL/min)	τ (s)	Solids conc. (kg/m ³)	d_m^\dagger (μ m)	CV [§] (%)
MS2_1	220	74.4	2.76	13.0	22.5
MS2_2	336	48.8	2.75	14.0	22.8
MS2_3	647	25.3	2.75	19.0	25.0
MS2_4	1437	11.4	2.31	23.7	27.0
MS3_1	220	74.4	0.39	8.6	23.7
MS3_2	336	48.8	0.36	9.5	28.8
MS3_3	647	25.3	0.31	9.6	36.9
MS3_4	1437	11.4	0.30	9.0	54.3

$$^\dagger d_m = \sum(L_i v_i); i = 1 \text{ to } nc$$

$$^\S CV = [\sum(L_i - d_m)^2 v_i]^{1/2} / d_m$$

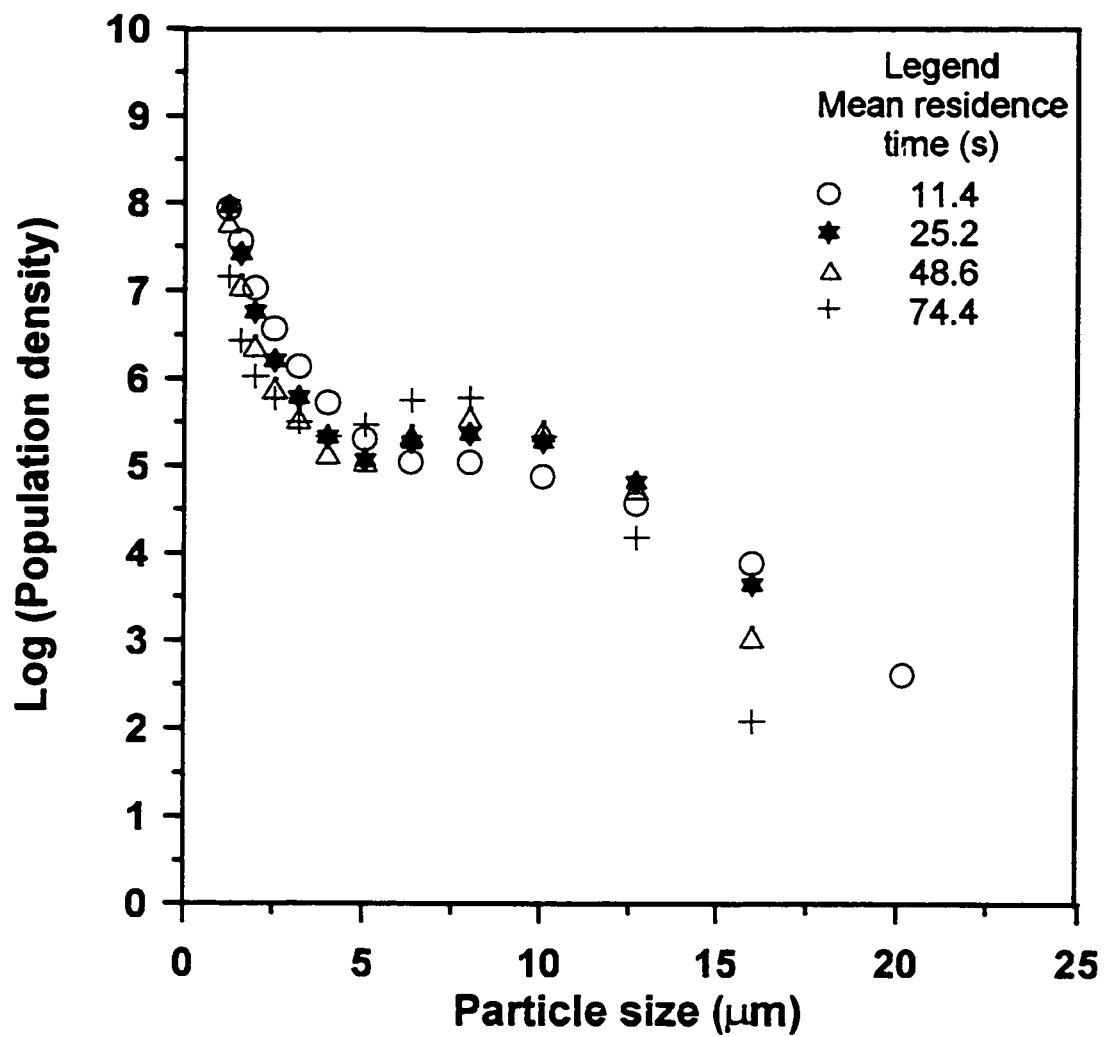


Figure 4.23 Population density of sunflower protein aggregates in an MSMPR precipitator as a function of mean residence time: protein feed concentration = 2.9 kg/m^3 and volume feed ratio = 1.0 v/v.

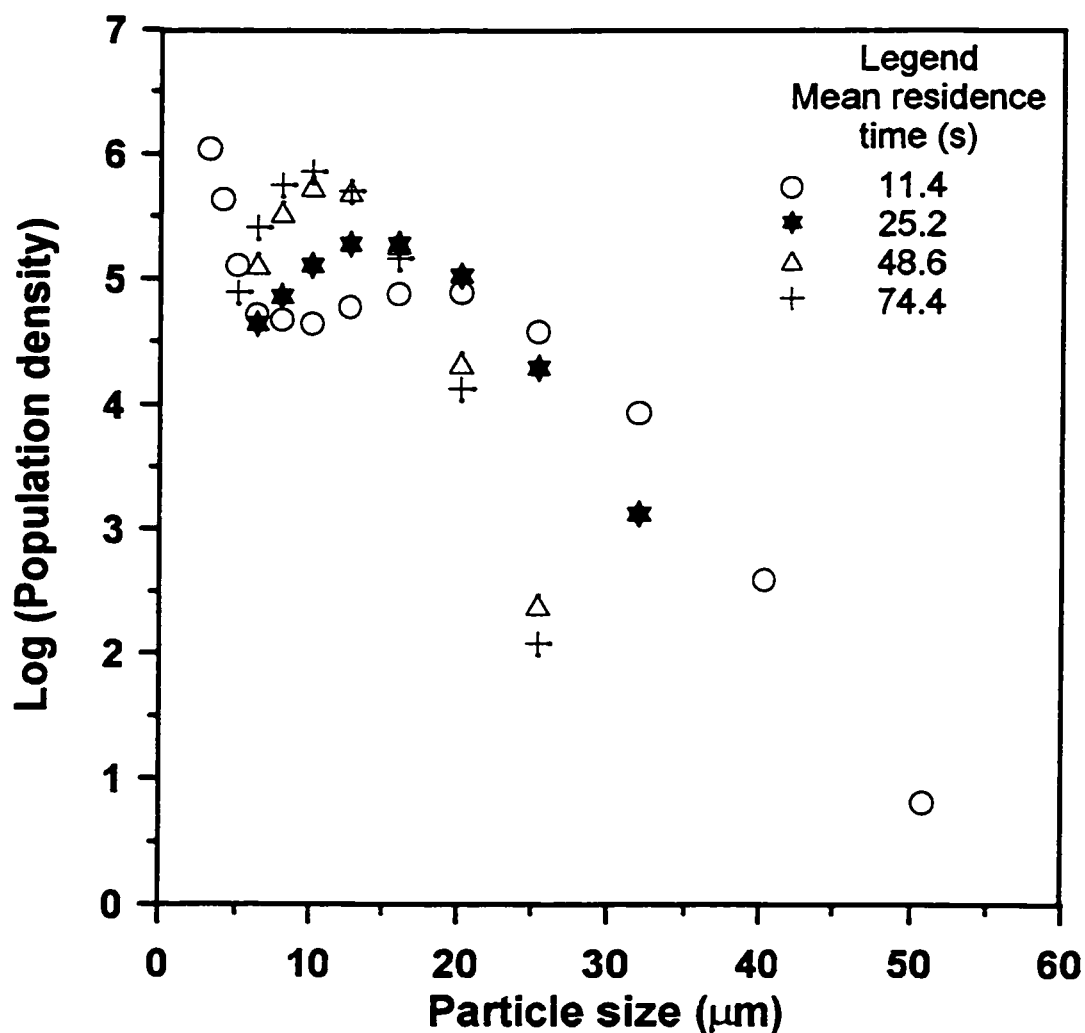


Figure 4.24 Population density of sunflower protein aggregates in an MSMPR precipitator as a function of mean residence time: protein feed concentration = 11.6 kg/m^3 and volume feed ratio = 1.0 v/v.

4.3.3 Comparison Between the Tubular and the Batch Precipitators: Effects of the Precipitation Time and Protein Feed Concentration on the Mean Particle Size and the Solids Concentration

The protein supersaturation for the batch and the tubular precipitators are similar. For both precipitators the degree of supersaturation is highest at the start and then drops to zero. Thus secondary nucleation and molecular growths may not contribute significantly in the PSD of the precipitates after the depletion of the protein supersaturation.

The batch precipitator resulted in precipitates with small mean particle sizes compared to flow-type precipitators (MSMPR and the tubular precipitators). Similar trends were observed at both high and low protein concentrations in the feed streams (Figures 4.25 and 4.26). The population density distribution of the protein particles showed a uni-modal distribution at both high and low protein feed concentrations as shown in Figures 4.27 and 4.28, together with those from the MSMPR and the tubular precipitators. This resulted in low values of the coefficient of variation (CV based on volume distribution) (Figure 4.29). For the precipitates from the batch precipitator, the mean particle size, the CV, and the solids concentration (Figure 4.30) varied little with precipitation time. This was because of the rapid reactions (completed in less than 1s, Virkar et al., 1982) which resulted in high nucleation rates. Due to high mixing intensity, breakage rates of aggregates by shear forces, by particle-particle collisions, and by collisions between particles and the mixer or precipitator walls were high. This resulted in smaller particles with a narrower PSD. The steady state PSD was dependent on the hydrodynamics of the surrounding fluid. Increasing the impeller speed, from 600 rpm to 900 rpm, resulted in a decrease in the mean particle size due to an increase in the shear rate (Figure 4.25 and 4.26).

The solids concentrations (yield) from the three types of the precipitators are shown in Figure 4.30. The tubular precipitator operating in the laminar flow regime and the batch precipitator (long reaction times) produced the highest yields (ca. 50 % of the protein in the feed solution). This means that a slower process of protein depletion from the solution (particle growth by aggregation and diffusion) follows an initial rapid nucleation process. Figure 4.30 shows that about 2 min were required for the tubular precipitator to give similar yields as the batch precipitator.

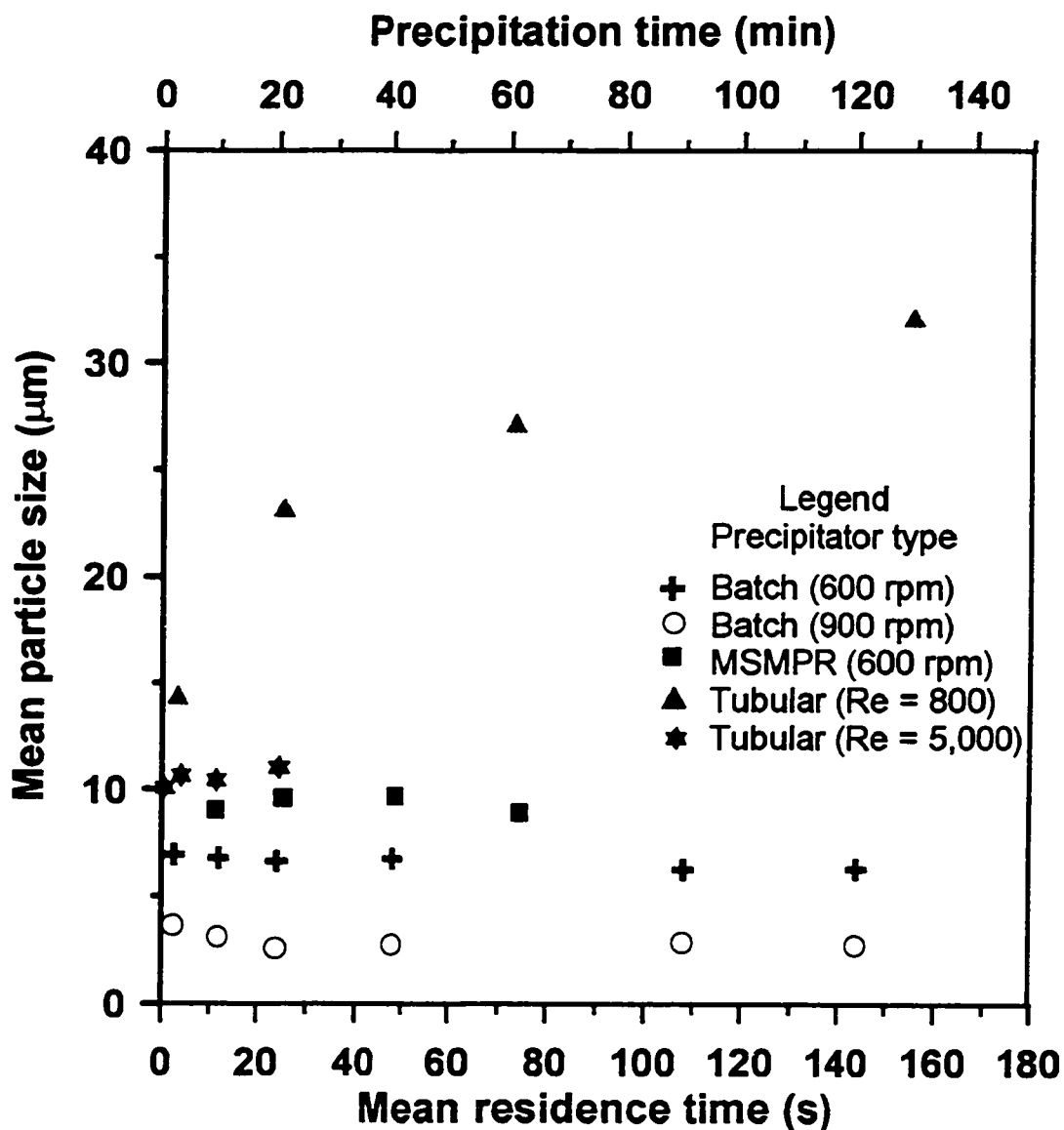


Figure 4.25 Effects of precipitation time (for the batch precipitator) and mean residence time (for the MSMPR and the tubular precipitators) on the mean particle sizes of precipitates for protein feed conc. = 2.8 kg/m³ and volume feed ratio = 1.0 v/v.

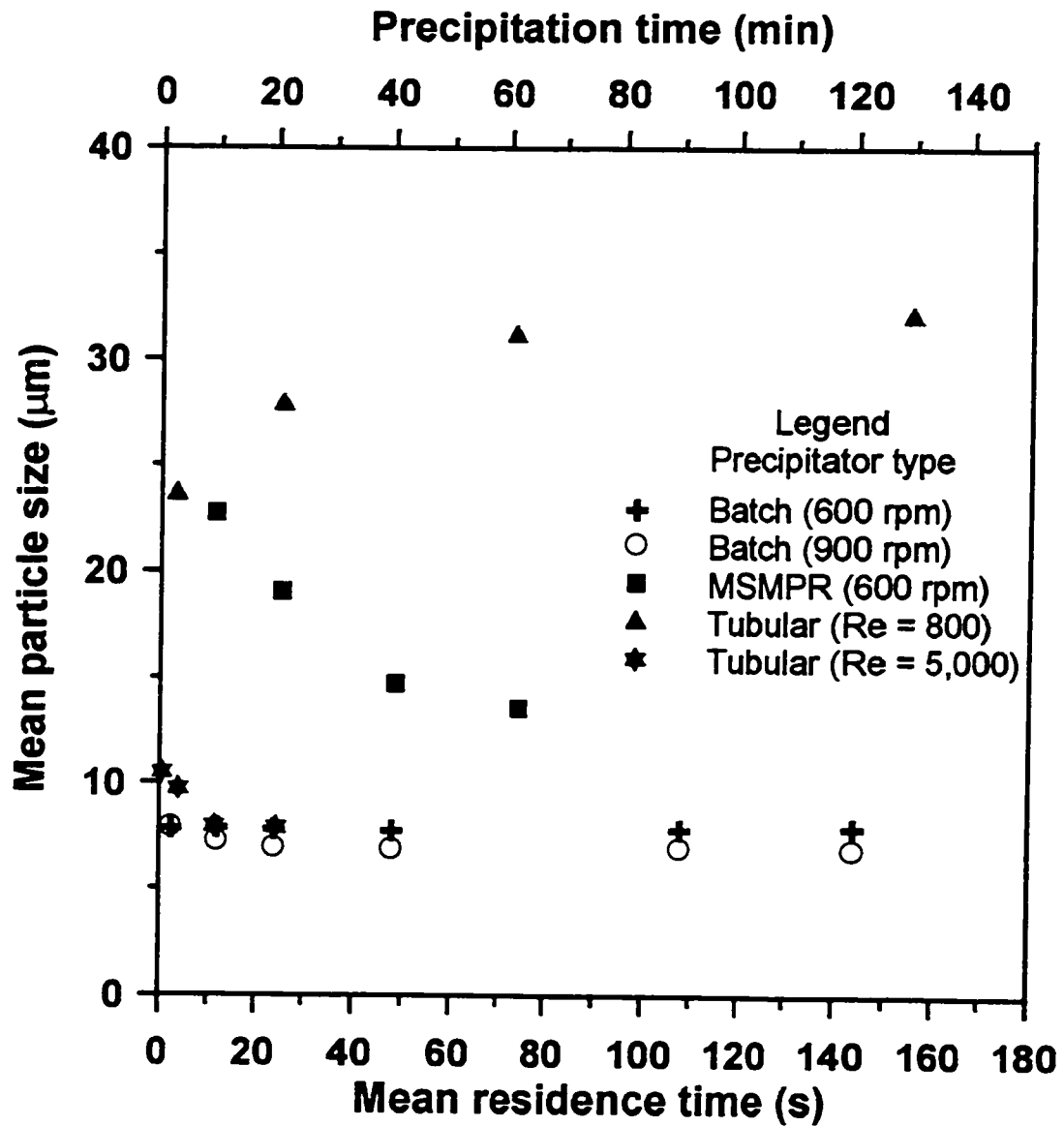


Figure 4.26 Effects of precipitation time (for the batch precipitator) and mean residence time (for the MSMPR and the tubular precipitators) on the mean particle sizes of precipitates for protein feed conc. = 11.8 kg/m³ and volume feed ratio = 1.0 v/v.

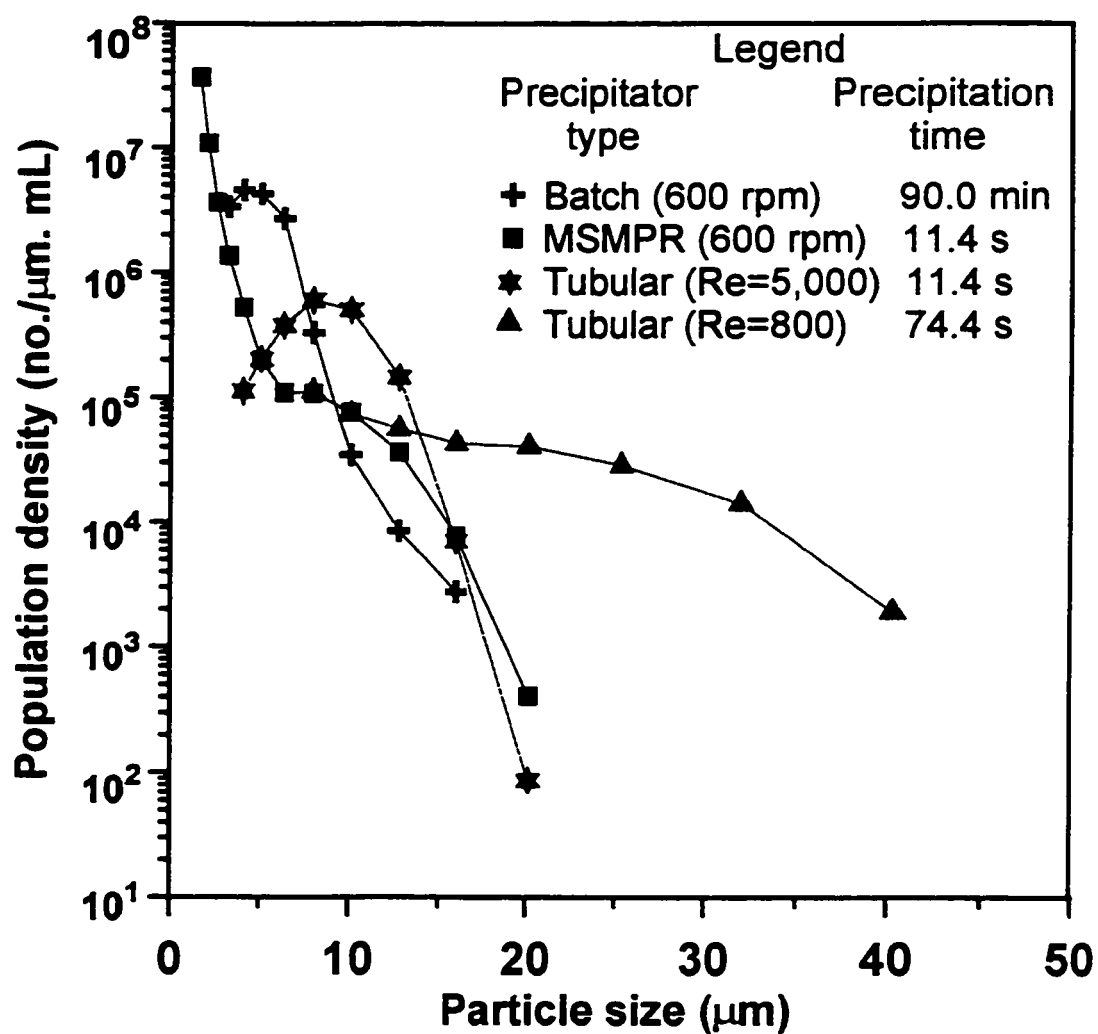


Figure 4.27 Comparison of the population densities of precipitates from the batch, MSMPR, and the tubular precipitators for protein feed concentration = 2.8 kg/m³ and volume feed ratio = 1.0 v/v.

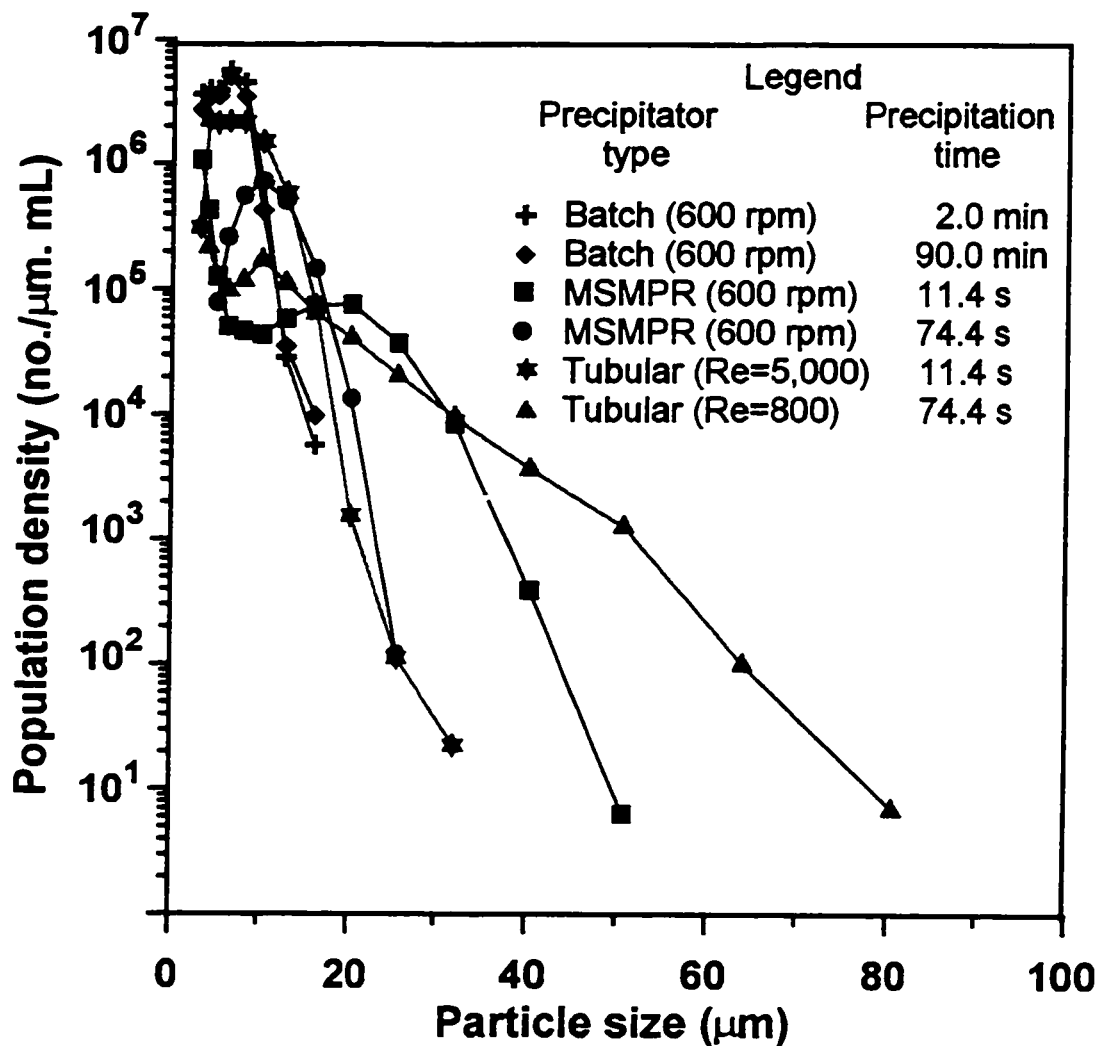


Figure 4.28 Comparison of the population densities of precipitates from the batch, MSMPR, and the tubular precipitators for protein feed concentration = 11.8 kg/m^3 and volume feed ratio = 1.0 v/v.

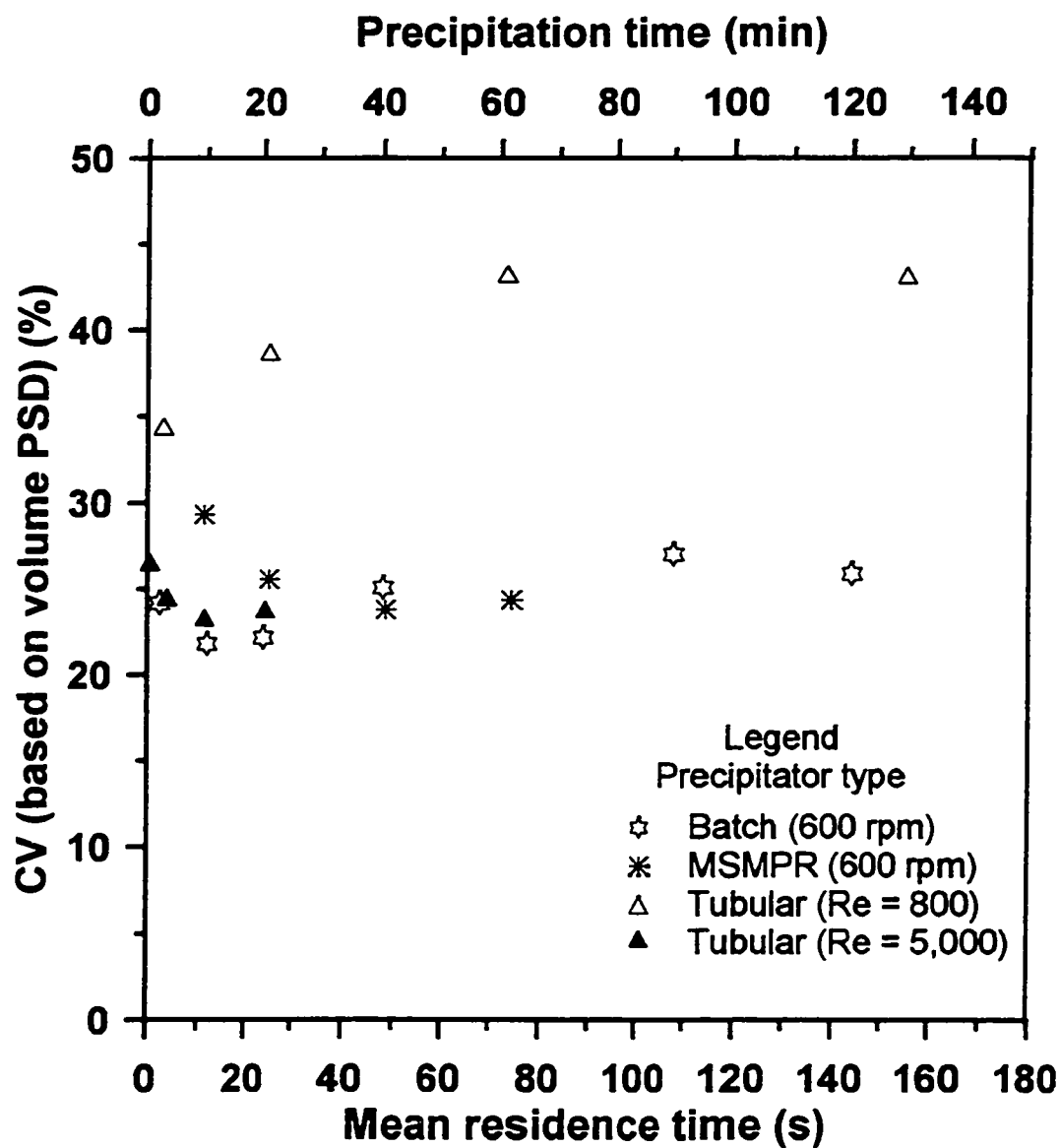


Figure 4.29 Effects of precipitation time (for the batch precipitator) and mean residence time (for the MSMPR and the tubular precipitators) on on the coefficient of variation (CV) for protein feed concentration = 11.8 kg/m^3 and volume feed ratio = 1.0 v/v.

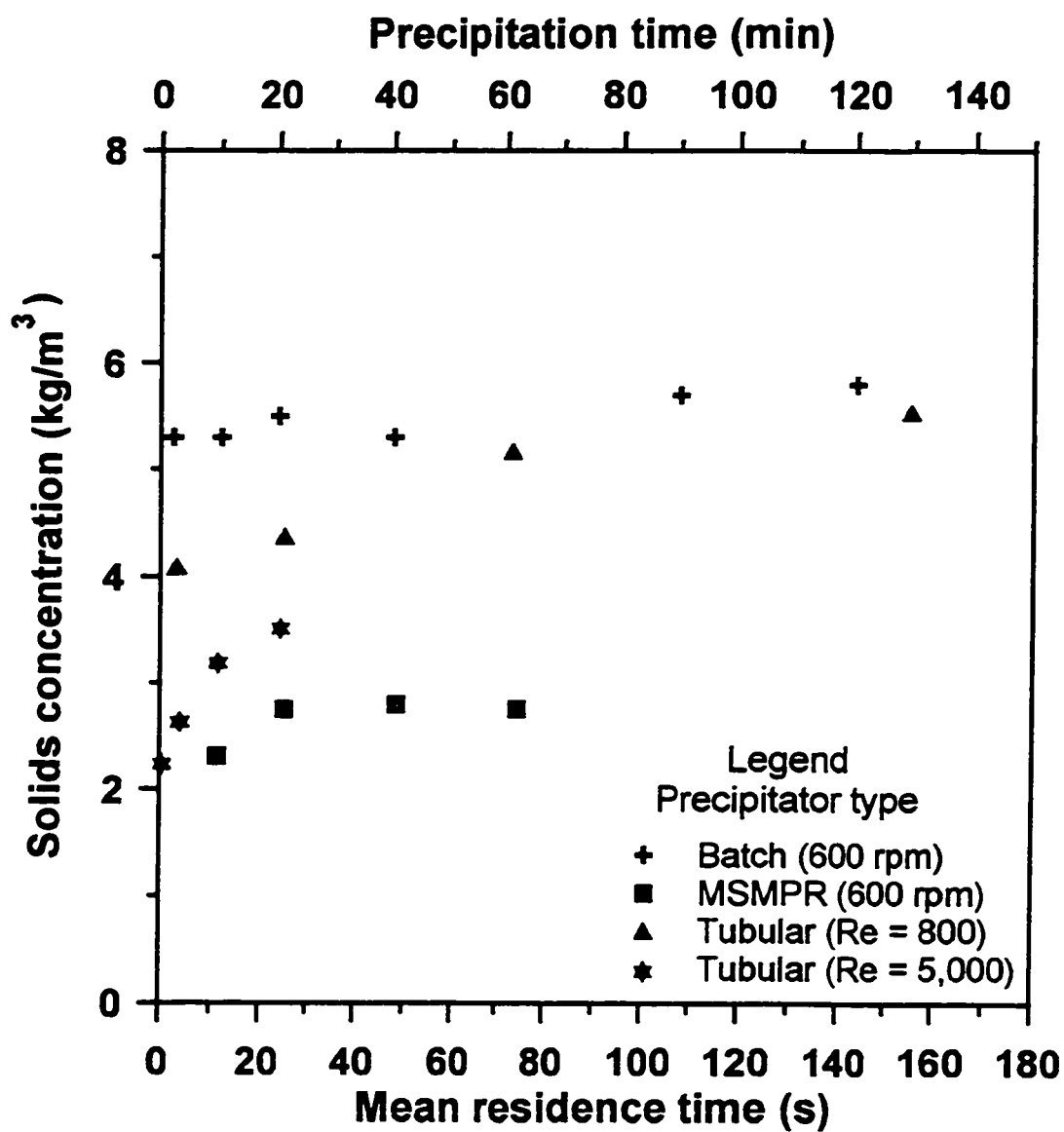


Figure 4.30 Effects of precipitation time (for the batch precipitator) and mean residence time (for the MSMPR and the tubular precipitators) on the solids concentration (yield) for protein feed concentration = 11.8 kg/m^3 and volume feed ratio = 1.0 v/v.

4.3.4 Scanning Electron Micrographs of the Precipitates

Figures 4.31 and 4.32 show the scanning electron micrographs (SEM) of sunflower proteins obtained by isoelectric precipitations from the batch, MSMPR, and the tubular precipitators. It can be seen that all precipitates are composed of primary particles (spherical particles). Aggregation of these primary particles leads to the formation of larger particles. The maximum size of the aggregate depends on its strength to withstand the shear forces induced by the mixer and the surrounding fluid. The tubular precipitator operating in the laminar flow regime produced large primary particles (ca. $1.0\ \mu\text{m}$) (see Figure 4.31a). The turbulent flow regime and the high shear rates in the batch and MSMPR precipitators produced small primary particles (ca. $0.2\ \mu\text{m}$) see Figures 4.31b and 4.32.

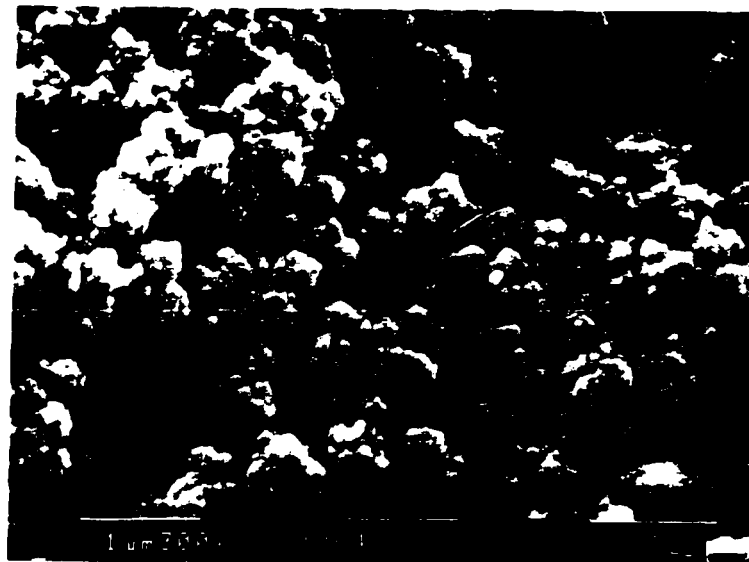
4.4 Estimation of the Experimental Errors

Standard errors of the experimental measured mean values (mean particle size and solid concentrations) were estimated as described in Section 3.5.7 (Equation 3.5). Table 4.10 shows the mean particle sizes and solids concentrations obtained from the four sampling ports in the tubular precipitator. Each data point represented the average of two measurements. Experimental data were divided into two groups, those obtained from the 10-m long precipitator and those obtained from the 20-m long precipitator. This division was necessary because the two set-ups had different locations of sampling ports. Table 4.11 presents the estimated standard error of the means for the shorter set-up. Six runs were done with duplication: runs 11, 12, 13, 14, 15, and 16 and their corresponding duplicate runs were: runs 17, 18, 19, 20, 21, and 22. For the longer set-up, three runs were done with duplication: runs L2, L5, and M81 and their corresponding duplicates were L4, L3, and M45, respectively.

The estimated standard errors showed high uncertainties for mean particle sizes from ports no. 1 and no. 4 and low values for the interior ports. This implied that there were fluctuations in the measured values. Aggregation process and particle breakage (shear forces) results in the presence of large and small aggregates. However, the

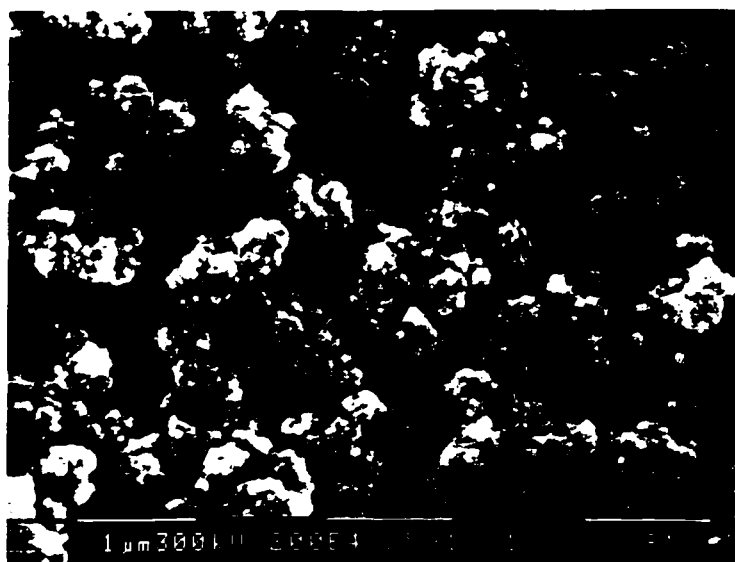


A

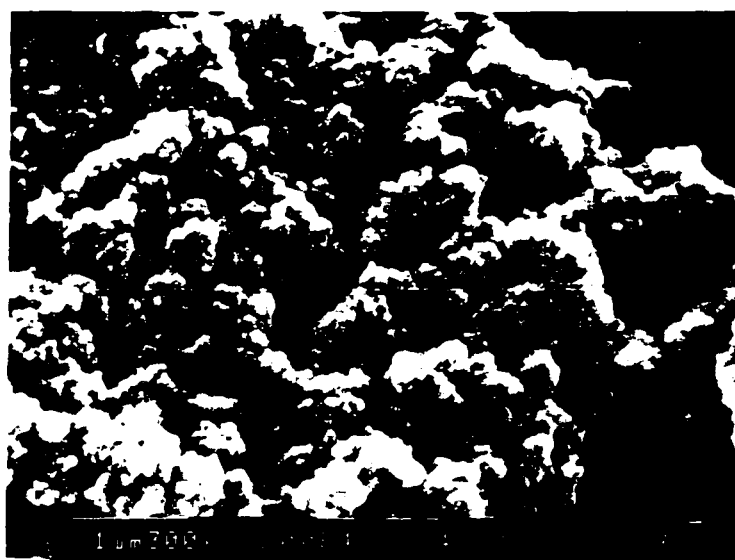


B

Figure 4.31 SEM of washed precipitates from the tubular precipitator for protein feed conc. = 11.8 kg/m^3 and volume feed ratio = 1.0: v/v (A) laminar flow regime (B) turbulent flow regime.



A



B

Figure 4.32 SEM of washed precipitates (A) from the batch precipitator (B) from the MSMR precipitator: protein feed conc. = 11.6 kg/m^3 and volume feed ratio = 1.0 v/v.

Table 4.10 Experimental results of isoelectric precipitation of sunflower protein in a tubular precipitator at pH 4.0: Effects of protein feed concentration, flow Re number, and feed ratio on the mean particle size and solids concentration.

Run no.	Protein feed conc. (kg/m ³)	Flow Re no.	Feed ratio (v/v)	Mean particle size (µm)				Solids concentration (kg/m ³)			
				Port no. 1	Port no. 2	Port no. 3	Port no. 4	Port no. 1	Port no. 2	Port no. 3	Port no. 4
4	2.6	4800	2.6	4.9	10.1	10.6	10.9	0.094	0.112	0.124	0.122
11	2.6	800	1.0	9.9	22.5	29.3	33.8	0.273	0.331	0.345	0.326
12	2.6	5000	1.0	6.3	9.3	11.2	12.2	0.142	0.206	0.254	0.279
13	2.2	5000	12.0	2.8	2.2	2.3	1.9	0.073	0.075	0.075	0.076
14	11.4	800	1.0	25.6	31.6	34.5	38.1	2.357	2.650	2.723	3.012
15	11.4	5000	1.0	13.3	12.6	12.6	13.1	1.289	1.641	1.889	2.011
16	11.4	5000	12.0	6.0	7.1	8.4	7.8	0.193	0.262	0.313	0.339
17	2.8	800	1.0	8.8	19.4	22.9	24.1	0.289	0.348	0.372	0.446
18	2.8	5000	1.0	6.6	7.8	7.0	7.2	0.290	0.377	0.462	0.501
19	2.8	5000	12.0	1.7	1.9	3.2	4.0	0.080	0.092	0.098	0.107
20	11.6	800	1.0	20.2	28.1	29.0	31.9	2.750	2.979	3.307	3.631
21	11.6	5000	1.0	13.1	10.6	11.7	10.7	1.819	2.252	2.620	2.713
22	11.6	5000	12.0	5.9	6.9	7.0	7.0	0.199	0.271	0.320	0.352
L1	11.8	800	1.0	23.6	27.8	31.1	32.1	4.066	4.351	5.146	5.520
L2	11.8	5000	1.0	10.5	9.7	7.9	7.9	2.233	2.624	3.183	3.508

Table 4.10 continued

L3	11.8	800	1.0	33.2	46.9	55.4	56.0	3.108	3.131	3.306	3.323
L4	11.8	5000	1.0	19.1	15.6	11.7	15.2	2.355	2.805	3.391	3.675
L5	11.8	800	1.0	35.7	44.7	45.6	47.2	3.155	3.307	4.188	4.370
L6	2.8	800	1.0	14.3	23.1	27.1	32.0	0.367	0.369	0.377	0.459
L7	2.8	5000	1.0	10.1	10.6	10.4	11.0	0.336	0.429	0.559	0.633
I1	11.4	3000	1.0	11.2	9.6	12.0	11.2	2.114	2.350	2.730	2.902
I2	11.6	3000	1.0	13.5	13.2	15.6	16.2	2.035	2.394	2.883	3.154
I3	7.1	800	1.0	26.2	34.9	39.3	39.4	1.020	1.023	1.163	1.188
I4	7.1	5000	1.0	12.2	10.7	9.2	8.9	1.110	1.389	1.765	1.946
M81	11.4	5000	1.0	9.0	7.4	9.3	8.5	2.357	2.742	3.105	3.293
M42	11.4	800	1.0	13.8	21.9	23.7	24.8	5.530	5.657	5.942	6.030
M03	11.4	800	1.0	11.6	15.1	15.5	15.0	1.527	1.795	4.482	5.169
M84	11.4	800	1.0	15.2	22.0	25.4	25.5	5.677	5.657	5.942	6.030
M45	11.4	5000	1.0	12.8	9.2	10.6	10.8	2.006	2.501	2.878	3.033
M06	11.4	5000	1.0	12.5	9.8	10.3	10.3	2.390	2.975	3.307	3.465

Table 4.11 Estimations of the experimental errors for mean particle size and the solids concentration for the runs performed in the tubular precipitator.

Calculations	Mean particle size (μm)				Solids concentration (kg/m^3)			
	Port no. 1	Port no. 2	Port no. 3	Port no. 4	Port no. 1	Port no. 2	Port no. 3	Port no. 4
<u>10-m long precipitator:</u>								
Total: $\sum [(\Delta d_i)^2/2]$; $i = 1 \text{ to } 6$	15.921	13.913	45.917	85.054	0.228700	0.255953	0.460126	0.470485
Est. of variance: $\text{Se}^2 = \{\sum [(\Delta d_i)^2/2]\}/6$	2.654	2.319	7.653	14.176	0.038117	0.042659	0.076688	0.078414
Se	1.629	1.523	2.766	3.765	0.195235	0.206540	0.276925	0.280025
Est. std error of the mean: $\text{SE} = \text{Se}/[2 \times 6]^{1/2}$	0.5	0.4	0.8	1.1	0.056	0.060	0.080	0.081
<u>20-m long precipitator</u>								
Total: $\sum [(\Delta d_i)^2/2]$; $i = 1 \text{ to } 3$	47.605	21.070	55.333	67.589	0.070	0.061	0.436	0.596
Est. of variance: $\text{Se}^2 = \{\sum [(\Delta d_i)^2/2]\}/3$	15.868	7.023	18.444	22.530	0.023	0.020	0.145	0.199
Se	3.984	2.650	4.295	4.747	0.153	0.142	0.381	0.446
Est. std error of the mean: $\text{SE} = \text{Se}/[2 \times 3]^{1/2}$	1.6	1.1	1.7	1.9	0.062	0.058	0.156	0.182

estimated standard errors were less than 25 % for all mean particles sizes greater than 5.0 μm . Part of this error for small sizes was because of the limitations of the measuring method using the Coulter Counter. The smallest size measured by this method was 1.0 μm while using a 70 μm aperture tube. Similarly the measured solids concentrations using the turbidimetry method showed increasing standard errors as the solids concentrations increased. This was because of the increased particle sizes and the solids concentrations. At very high solids concentrations, the % transmission approached 0 % and for very dilute solids concentrations, the % transmission approached 100 %. At these extreme ranges, the sensitivity of the measuring instruments decreased. However, for solids concentrations above 0.2 kg/m^3 , the calculated standard error of the mean was less than 25 %, which is considered acceptable.

CHAPTER 5

MATHEMATICAL MODELLING

5.1 MSMPR Precipitator

5.1.1 Fitting of the Aggregation-Breakage Model to the Experimental Data

Protein particle growth by turbulent collision mechanism and breakage by shear mechanism was modelled using an approach similar to Glatz et al. (1986). The presence of large aggregates together with smaller aggregates and primary particles resulted in a bimodal PSD. In such a system, determination of kinetic parameters is difficult because the number of primary particles changes rapidly due to aggregation, and large particles cannot be distinguished from aggregates.

Precipitation of proteins by the isoelectric method is a very fast process. Experimental studies have shown that the precipitation reactions go to completion almost instantaneously. The effective size enlargement process is by aggregation of the primary particles with the growing aggregates as shown in scanning electron micrographs of protein precipitate. Tiny particles (primary particles) can be seen on the surfaces of spherical protein particles. The growth of these primary particles is by a diffusion-controlled mechanism.

Grabenbauer and Glatz (1981), Petenate and Glatz (1983), and Glatz et al. (1986) studied aggregate growth of protein particles by turbulent collision mechanism and breakage by hydrodynamic shear mechanism. Based on their experimental data and previous studies on protein precipitation, they developed a model for protein precipitation. The model assumes that solid protein comes out of the solution instantly after the precipitant is added. This results in the formation of a large number of primary

particles. Growth of aggregates is by collision of primary particles with smaller aggregates. The effectiveness of collisions between primary particles and smaller aggregates is independent of their size. Collisions between larger aggregates, however, is assumed to be ineffective in forming a lasting aggregate. Larger aggregates break up to form smaller aggregates. The daughter aggregates are assumed to be of equal size and their number is greater when a large aggregate breaks. Thus, in this model the growth of aggregates (G_a) is viewed as a continuous process of adding primary particles to a growing aggregate due to turbulent collisions. The primary particles are considered as growth entities and larger aggregates as collectors. Shear-induced forces by the surrounding fluid or aggregate-precipitator and aggregate-aggregate collisions result in the breakage of the growing aggregates. The population balance equation written in terms of the aggregate size L is given as:

$$\frac{d(G_a p)}{dL} + \frac{p}{\tau} = B_b - D_b \quad (2.15)$$

where G_a is the growth rate of aggregate by additions of primary particles. Petenate and Glatz (1983) proposed the following expressions for each term:

$$G_a(L) = k_G L^s \quad (2.16a)$$

$$D_b = k_D L^b p(L) \quad (2.16b)$$

$$B_b = f D_b (f^{1/3} L) \quad (2.16c)$$

Equation (2.16c) represents the birth of particles of size L due to the death of particles of size $f^{1/3}L$ given in Equation (2.16b). f is the number of equal-size daughter fragments. This means that the total particle volume during aggregate breakage is conserved. Substituting Equations (2.16a) to (2.16c) in Equation (2.15) yields:

$$\frac{dp}{dL} = \frac{k_D}{k_G} L^{\beta-1} [f^{\beta/3} p(f^{1/3} L) - p] - p \left[\frac{g}{L} + \frac{1}{\tau k_G L^g} \right] \quad (5.1)$$

with the boundary condition that the calculated total volume of aggregates equals the measured aggregate volume.

In the previous study by Glatz et al. (1986), the values of β and f were fixed at reasonable values, 2.3 and 2 for low protein concentrations (0.15 and 3 kg/m³) and 1.5 and 3 at high protein concentrations (25 kg/m³), respectively, and g was assumed to be 1 (linear growth rate). In this study, all five parameters, namely, k_G , g , k_D , β , and f , were determined by optimizing a cost function given by:

$$HM(L_i) = \left[1 - \frac{\left(\frac{dp}{dL} \right)_{cal}}{\left(\frac{dp}{dL} \right)_{exp}} \right]_{L_i}^2 \quad (5.2)$$

The best value of $S(L_i)$ is zero at all particle sizes (L_i). $(dp/dL)_{exp}$ was calculated from the experimental data as:

$$p(L_i) = \frac{\Delta N(L_i)}{\Delta L_i} \quad (5.3)$$

where $\Delta N(L_i)$ is the number of particles/mL (as measured by the Coulter Counter) between two consecutive channels and $\Delta(L_i)$ is the channel size difference. In order to evaluate dp/dL and $p(f^{1/3}L)$ at different values of $f^{1/3}L$, it was necessary to fit the experimental data from each independent run with some analytical expression. This was achieved by first fitting the experimental population density, $p(L)$ versus L , using a fourth order smooth cubic spline algorithm (IMSL routine DCSAKM). Precautions were taken not to extrapolate beyond the experimental range. Then the derivatives of this cubic spline function were calculated numerically (IMSL routine DCSDER) at selected sizes (L_i) which matched the size increments measured experimentally. The set of non-linear algebraic equations resulting from Equation (5.1) (one equation for each size) was

solved to determine the minimum sum of $HM(L_i)$ using a Least Squares method (IMSL routine DUNLSF) or the Simplex method (IMSL routine DUMPOL). During each iteration the value of f (number of daughter particles) was varied from 1 to 10. The set of parameters resulting in the minimum $HM(L_i)$ was used to solve Equation (5.1). The resulting ODE was solved using a sixth-order Runge-Kutta-Verner method (IMSL routine DIVPRK) to obtain the size distribution $p(L)$. It was necessary to set the initial condition for $p(L)$ at the smallest experimentally observed particle size. The overall calculation algorithm is presented in Figure 5.1.

5.1.2 Model Fitting Results

Iterations resulted in a minimum value of S when $f = 2$ in all runs. This means the number of daughter fragments, f , formed by breakage of larger aggregates was 2. This value is in agreement with that used by Glatz et al. (1986). Larger values of f resulted in an increase in HM and lower values of predicted $p(L)$ at the maximum size. At $f = 1$ the predicted values of $p(L)$ were larger than the experimental values at all sizes. The optimum model parameters are presented in Table 5.1 for each independent run. The growth rate exponent, g , showed that at high solids concentrations, the particle growth rate was linear with respect to particle size (see Table 5.1, the exponent g is ca. 1). At low solids concentration the growth rate exponent increased with the mean residence time showing that the growth rate was dominant.

Figures 5.2 and 5.3 represent the experimental data and model fitting for low and high protein feed concentration runs, respectively. For both cases, it was found that the death rate constant, k_D , and the growth rate constant, k_G , decreased with increase in the mean residence time. Comparing the breakage (death) and growth rate constants (Figure 5.4) showed that, at high protein feed concentrations, the death process is dominant, hence resulting in smaller particles with uni-modal distribution after longer mean residence times. At low protein feed concentrations the growth process is dominant, resulting in the bimodal distribution even at longer mean residence times. This is due to the low number of collisions caused by low number of primary particles. Hence it takes a longer time for the aggregates to reach the maximum stable size before they break.

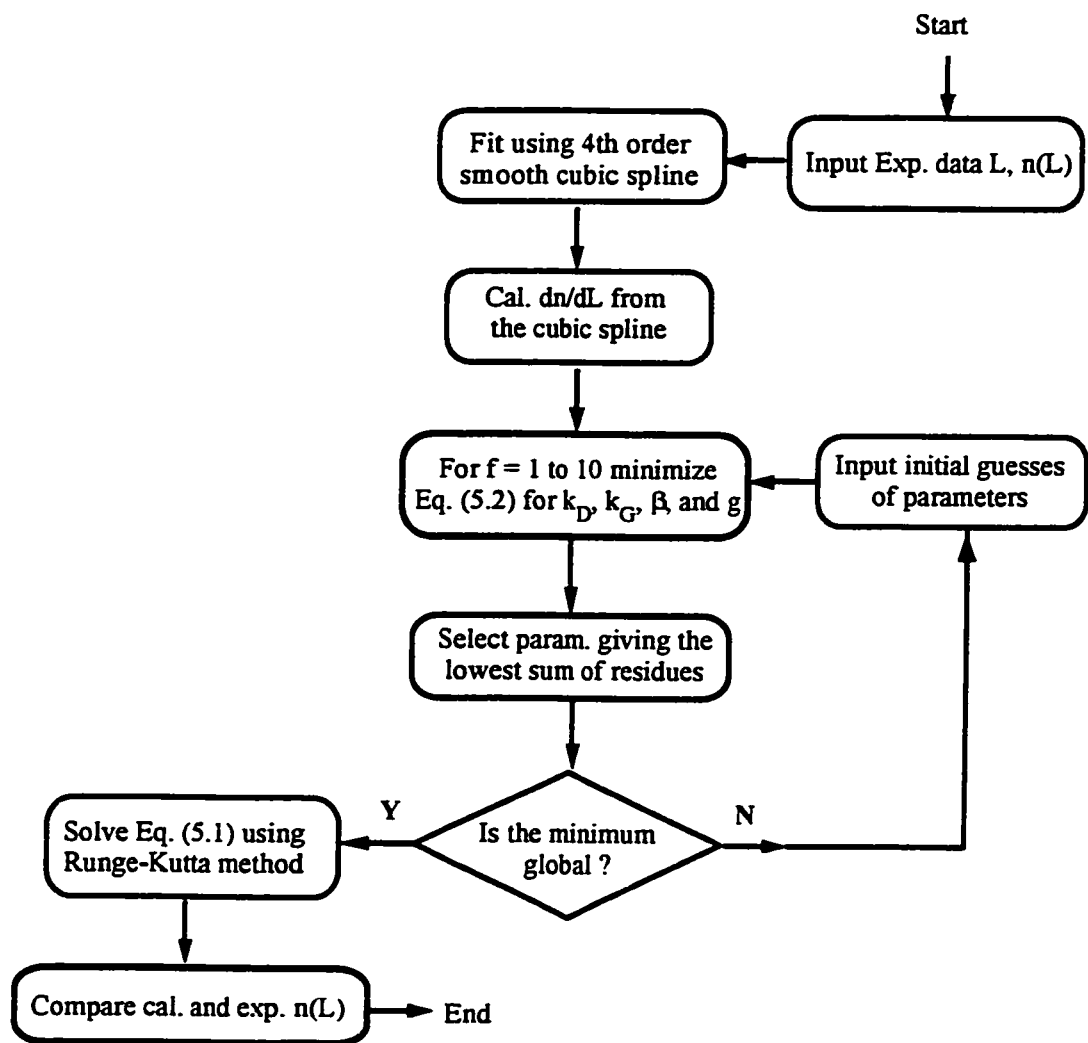


Figure 5.1 The algorithm for calculating the aggregation and breakage rates parameters from the MSMPR precipitator experimental data.

Table 5.1 Calculated parameters for the MSMMPR precipitator model with protein particles aggregation and breakage (protein feed concentrations: runs MS2_series = 11.6 kg/m³ and runs MS3_series = 2.9 kg/m³).

Run No.	τ (s)	Calculated model parameters					R^2
		k_D	k_G	β	g	f	
MS2_1	74.4	0.0356	0.0179	0.0143	1.06	2.0	0.999
MS2_2	48.8	0.0500	0.0299	0.0016	0.97	2.0	0.998
MS2_3	25.3	0.1754	0.1144	0.0137	1.05	2.0	0.973
MS2_4	11.4	0.3604	0.2591	0.1280	1.16	2.0	0.998
MS3_1	74.4	0.0200	0.0361	0.0084	0.45	2.0	0.981
MS3_2	48.8	0.0341	0.0523	0.0475	0.61	2.0	0.996
MS3_3	25.3	0.1146	0.1466	0.0230	0.80	2.0	0.988
MS3_4	11.4	0.2976	0.2400	0.0007	0.97	2.0	0.997

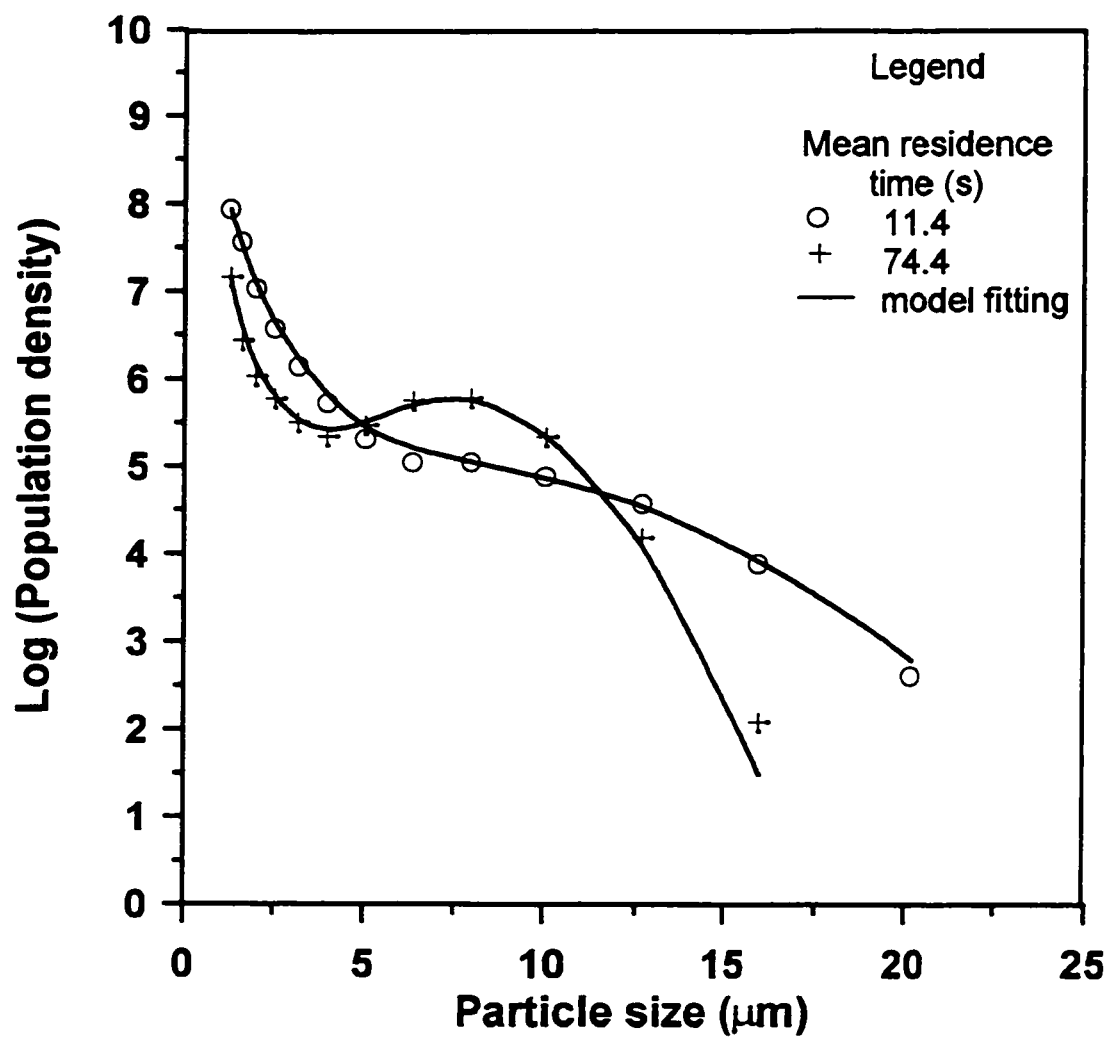


Figure 5.2 Population density of sunflower protein aggregates in an MSMR precipitator: comparison of the experimental data with the model fitting for protein feed concentration = 2.9 kg/m^3

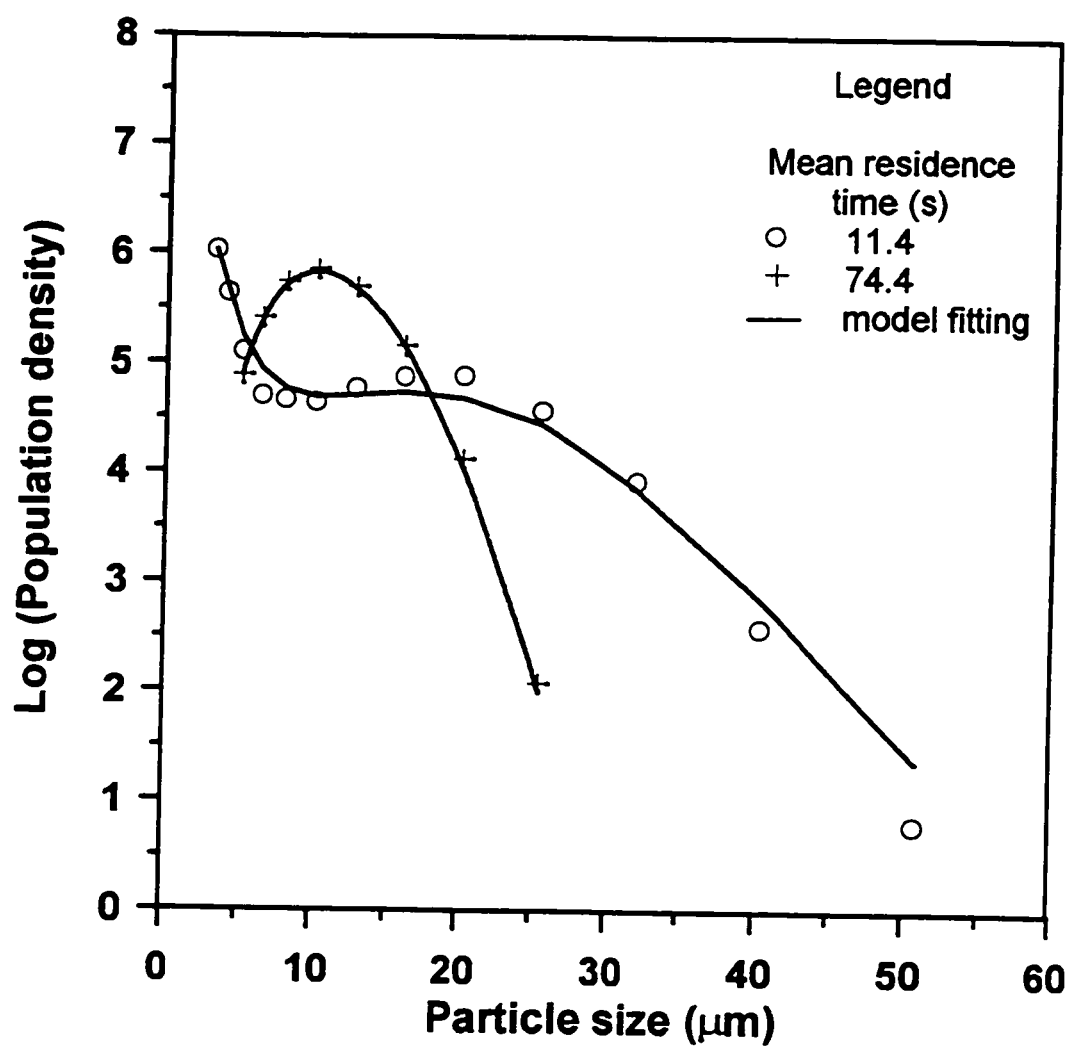


Figure 5.3 Population density of sunflower protein aggregates in an MSMR precipitator: comparison of the experimental data with the model fitting for protein feed concentration = 11.6 kg/m^3 .

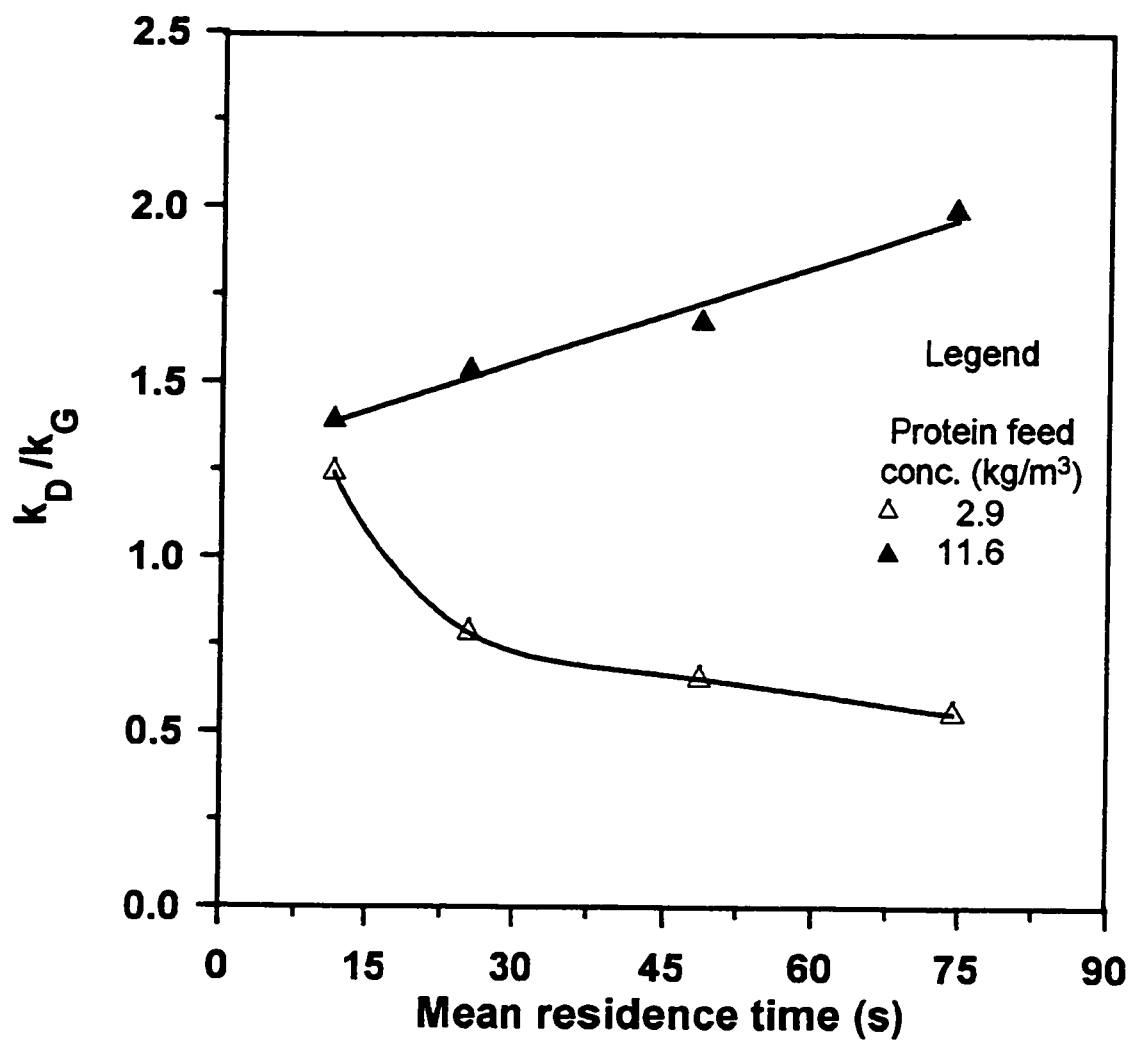


Figure 5.4 Ratio of the breakage and the growth rate constants as a function of protein feed concentration and mean residence time in an MSMR precipitator.

5.2 Modelling of a Tubular Precipitator With Particle Aggregation and Breakage

5.2.1 Population Balance Equation for the Tubular Precipitator

At steady state the population balance equation for the tubular precipitator with particle aggregation and breakage is given by:

$$D_z \frac{\delta^2 p}{\delta z^2} - u_z \frac{\delta p}{\delta z} - \frac{\delta G p}{\delta L} + (B_a - D_a) + (B_b - D_b) + \beta_o^\circ \delta(L - L_o) = 0 \quad (5.4)$$

where p (the population density) is a function of particle size L and position (z) along the tubular precipitator. D_z is the axial dispersion coefficient, u_z is mean flow velocity, G is the molecular particle growth rate, $(B_a - D_a)$ is the net rate of particle aggregation, $(B_b - D_b)$ is the net rate of particle breakage, and β_o° is the secondary nucleation rate of particles of size L_o . Equation (5.4) assumes no radial dispersion and has initial condition; $p(0, z) = B^\circ/G$ as $L \rightarrow 0$ (B° is the nucleation rate) and boundary conditions; $u_z p(L, 0) - D_z dp(L, 0)/dz = 0$ that is, no seeding or solids at the entrance. At the exit, $dp/dz = 0$. The radial dispersion was neglected because the ratio of the tube diameter to the length was very small (3×10^{-4}).

(a) Dimensionless Parameters

Introducing the dimensionless parameters defined as:

$$\zeta = z/z_T, \quad x = L/L_c, \quad \text{and} \quad y(x, \zeta) = p(x, \zeta)/N_s = L_c p(L, \zeta)/N_s \quad (5.5)$$

where ζ is the dimensionless distance along the tubular precipitator, z_T is the total length of the tubular precipitator, x is dimensionless particle size, and L_c is the maximum measurable particle size divided by the largest root of the Laguerre polynomial. L_c ($= 3.528 \mu\text{m}$) is used to scale down the experimental particle size range to be within the

range of the zeros of the Laguerre polynomial. $y(x, \zeta)$ is the dimensionless population density. N_s is a constant value (number density) used to reduce the magnitude of population density. In this study N_s was set at 10^5 . Substituting dimensionless parameters in Equation (5.4) and assuming negligible secondary nucleation and particle growth rate is independent of particle size, Equation (5.4) becomes:

$$\frac{\partial^2 y}{\partial \zeta^2} - Pe \frac{\partial y}{\partial \zeta} - Pe \tau_m \frac{G}{L_c} \frac{\partial y}{\partial x} + Pe \tau_m \frac{L_c}{N_s} [(B_a - D_a) + (B_b - D_b)] = 0 \quad (5.6)$$

where Pe is the Peclet Number ($u_z z_T / D_z$). As $Pe \rightarrow 0$, the flow approaches the mixed flow regime and as $Pe \rightarrow \infty$, the flow approaches the plug flow regime. In dimensionless variables the initial and boundary conditions are:

$$y(x, \zeta) \big|_{x=0} = \frac{B^0 / N_s}{G / L_c} ; \quad x = 0 \quad (0 \leq \zeta \leq 1) \quad (5.7a)$$

$$y(x, 0) - \frac{1}{Pe} \frac{dy(x, 0)}{d\zeta} = 0 ; \quad \zeta = 0 \quad (x > 0) \quad (5.7b)$$

$$\frac{dy(x, 1)}{d\zeta} = 0 ; \quad \zeta = 1 \quad (x > 0) \quad (5.7c)$$

(b) Nucleation Rate (B^0)

The formation of new particles is assumed to be a continuous process which occurs throughout the precipitator. However, the rate of nucleation rate decreases as the fluid moves downstream. The nucleation rate along the tubular precipitator is expressed as a function of the initial nucleation rate (B_0^0), that is, the nucleation rate at $\zeta = 0$. At the entrance there is a high degree of supersaturation leading to high nucleation rate. As the degree of supersaturation decreases along the tubular precipitator, so does the nucleation rate. The nucleation rate is expressed as:

$$B^o = B_o^o (1 - k_B \zeta)^a \quad (5.8a)$$

where the initial nucleation rate is determined using the homogeneous nucleation theory for fast reactions (Mullin, 1972) as:

$$B_o^o = k_{Bo} \exp \left[-\frac{k_m}{(\ln S_o)^2} \right] \quad (5.8b)$$

where the supersaturation ratio, $S_o = C_o/C^*$, k_m and k_{Bo} are constants. C_o and C^* are the protein feed concentration and the equilibrium protein concentration, respectively. Equation (5.8b) predicts a rapid increase in nucleation rate with increases in the degree of supersaturation (S_o). Then Equation (5.8a) becomes:

$$B^o(\zeta) = k_{Bo} \exp \left[-\frac{k_m}{(\ln S_o)^2} \right] (1 - k_B \zeta)^a \quad (5.8c)$$

(c) Growth Rate (G)

Molecular growth rate of particles due to deposition of protein from the solution on the particle surface is modelled using a similar argument as for the nucleation rate. The growth rate by molecular mechanism increases with an increase in concentration gradient. Near the entrance the growth rate is high and decreases as the concentration gradient decreases along the tubular precipitator. Therefore the growth rate is expressed as function of initial growth rate (G_o^o), that is, the growth rate at $\zeta = 0$, maximum growth rate. This is written as:

$$G(\zeta) = G_o^o (1 - k_G \zeta)^b \quad (5.9a)$$

Where G_o° is defined as:

$$G_o^\circ = k_{Go} \sigma_o^g \quad (5.9b)$$

The relative supersaturation at $\zeta = 0$ is given by; $\sigma_o = (C_o - C^*)/C^*$. The parameter g determines the mechanism governing particle growth. When $g = 1$, the particle growth is diffusion controlled, $1 < g < 2$ implies screw dislocation mechanism controls the particle growth, and $g > 2$ means the polynuclear mechanism controls the particle growth. Substituting Equation (5.9b) into Equation (5.9a) yields:

$$G(\zeta) = k_{Go} \sigma_o^g (1 - k_g \zeta)^b \quad (5.9c)$$

(d) Protein Concentration Balance

The rate of depletion of protein from the solution at any location along the tubular precipitator must equal the rate at which the mass is gained by the solid phase. At any location (ζ) along the tubular precipitator, the protein balance is given by:

$$QC_o - QC(\zeta) = QM_T(\zeta) \quad (5.10)$$

where Q is the volumetric flow rate of protein free liquid, M_T is solid protein concentration per volume of protein free liquid, whereas C_o and $C(\zeta)$ are concentrations of protein (based on protein free liquid) at the precipitator entrance and at location ζ , respectively. The total rate of particle growth on the surface of the particles at any location is given by (Randolph and Larson, 1988):

$$QM_T(\zeta) = \frac{1}{2} \int_0^\zeta A_T V G(\zeta) d\zeta \quad (5.11)$$

A factor of 1/2 is because G is a growth rate of particle based on diameter. V is the total volume and A_T is the total surface area defined as: $A_T = \int_0^\infty k_p L^2 dL$, all defined at a location ζ . Therefore the protein concentration at any location along the tubular precipitator is given by:

$$C(\zeta) = C_0 - \frac{\rho_s}{2} \int_0^\zeta \left[\int_0^\infty k_p L^2 dL \right] \zeta \tau(\zeta) G(\zeta) d\zeta \quad (5.12)$$

where $\tau(\zeta) = \zeta t_m$ is the mean residence time at location ζ . Introducing the dimensionless variables, Equation (5.12) becomes:

$$W(\zeta) = 1 - \frac{\rho_s}{2C_0} k_d N_s L_c^2 t_m \int_0^\zeta \left[\int_0^\infty y(x, \zeta) x^2 dx \right] \zeta^2 G(\zeta) d\zeta \quad (5.13)$$

where $W(\zeta) = C(\zeta)/C_0$. Equation (5.13) gives the protein concentration profile along the tubular precipitator. The values of $G(\zeta)$ and $y(x, \zeta)$ are obtained from the population balance equation. In this study, material balance equation was not used in simulation. Numerical solution of the coupled PBE with material balance equation is known to be very unstable resulting in multiple steady states (see last paragraph Section 2.6).

(e) Particle Breakage Rate

The particle breakage rate term, $B = (B_b - D_b)$, is assumed to be a two body-equal volume breakage (Glatz et al., 1986). That is, a breaking particle (death) results in a birth of two particles of equal volume. This simple model is given as:

$$D_b(L) = k_d L^3 p(L, z) \quad (5.14)$$

$$B_b(L) = 2D_b(2^{1/3}L, z) \quad (5.15)$$

Then the net rate of particle breakage, B is given as:

$$B = k_d L^\beta [(2^{\beta/3+1} p(1.26L, z) - p(L, z))] \quad (5.16)$$

Introducing the dimensionless variables into Equation (5.16), results in:

$$B(\zeta) = k_d \frac{N_s}{L_c} (x L_c)^\beta [(2^{\beta/3+1} y(1.26x, \zeta) - y(x, \zeta))] \quad (5.17)$$

(f) Particle Aggregation Rate

The particle aggregation rate is modelled using the formulation of Hulburt and Katz (1964). The death and birth of particles due to aggregation is given by:

$$A = (B_a - D_a) = \frac{L^2}{2} \int_0^L K(L_1, L_2) \frac{p(L_1, z) p(L_2, z) dL_1}{L_2^2} - p(L, z) \int_0^\infty K(L_1, L_2) p(L_1, z) dL_1 \quad (5.18)$$

where $L_2^3 = L^3 - L_1^3$. Because of the limited knowledge of aggregation kernel, $K(L_1, L_2)$, it is assumed to be constant, β_0 , and independent of the particle size. Introducing the dimensionless variables into Equation (5.18) yields:

$$A(\zeta) = P_A \frac{x^2}{2} \int_0^x \frac{y[(x^3 - \epsilon^3)^{1/3}, \zeta] y(\epsilon, \zeta)}{(x^3 - \epsilon^3)^{2/3}} d\epsilon - P_A y(x, \zeta) \int_0^\infty y(\epsilon, \zeta) d\epsilon \quad (5.19)$$

where $P_A = \beta_0 N_s^2 / L_c$ and $\epsilon = L_1 / L_c$ is the size of particles less than size x .

5.2.2 The Solution of the Population Balance Equation

The resulting population balance equation (PBE), after introducing the aggregation and breakage terms, is a non-linear integro-differential equation with initial

and boundary conditions. In this study, the solution of the PBE is obtained using orthogonal collocation-multiple shooting method. The non-linear multiple shooting method (MSM) of Ascher et al. (1988) is used to solve the PBE in the ζ direction (precipitator length), whereas the orthogonal collocation method (OCM) is used to solve the problem in the x direction (particle size).

The collocation method allows the use of uneven mesh in the x direction while the MSM is applied on the even grid mesh (Figure 5.5). The procedure is to assume a Lagrange polynomial as a solution of the PBE. This trial solution is selected from a set of functions defined in the domain $[0, \infty)$. For this reason, the Laguerre functions were selected. The trial solution is defined as:

$$y_n(x, \zeta) = \sum_{i=1}^n \alpha_i(\zeta) \Phi_{i-1}(x) \quad (5.20)$$

where $\alpha(\zeta)$ is function of ζ and $\Phi(x)$ is a function of x . In Equation (5.20), y_n is a $(n-1)$ th polynomial in x . The function $\Phi(x)$ is defined as:

$$\Phi_i(x) = e^{-x} \psi_i(x) \quad (5.21)$$

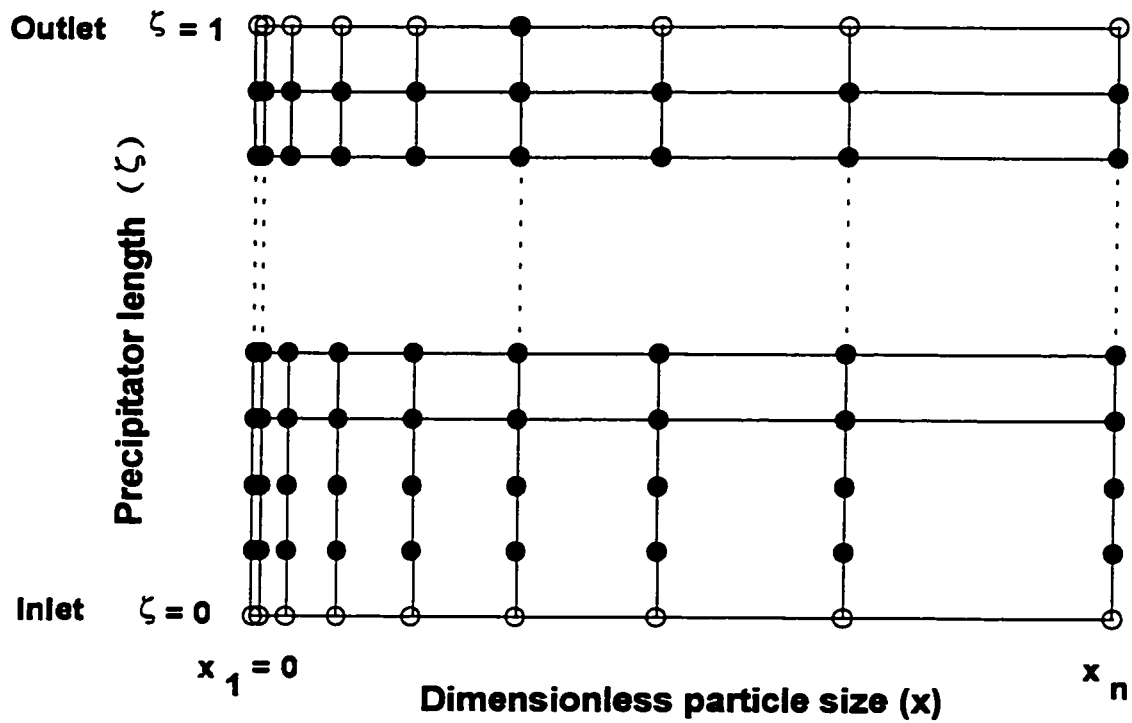
where $\psi_i(x)$ are the Laguerre polynomials. The n th Laguerre polynomial (Courant and Hilbert, 1966) is defined as:

$$\psi_n(x) = \sum_{j=0}^n \frac{(-1)^j (n!)^2 x^j}{j! (n-j)!} \quad (5.22)$$

with $\psi_0(x) = 1$, $\psi_1(x) = -x+1$, and $\psi_2(x) = x^2-4x+2$. The recurrence formula for $n \geq 2$ is given by:

$$\psi_n(x) = (2n-x-1)\psi_{n-1}(x) - (n-1)^2\psi_{n-2}(x) \quad (5.23)$$

These polynomials are orthogonal with respect to the exponential weighting in the range $[0, \infty)$. This means that:



- b.c. are applied at these points
- collocation points (residue = 0.0)

Figure 5.5 Node points scheme for orthogonal collocation-multiple shooting method for solving the population balance equation for the tubular precipitator.

$$\int_0^{\infty} e^{-x} \psi_n(x) \psi_m(x) dx = \begin{cases} 0 & m \neq n \\ 1 & m = n \end{cases} \quad n, m = 0, 1, 2, \dots \quad (5.24)$$

The recurrence formula for the derivative of the Laguerre polynomial is given by:

$$\psi'_n(x) = n[\psi'_{n-1}(x) - \psi_{n-1}(x)] \quad n \geq 2 \quad (5.25)$$

The solution procedure is to substitute Equation (5.20) in the PBE. Since the expansion solution is an approximation, a non-zero residual, $R(x, \zeta)$, will result after this substitution. The basis of the orthogonal collocation method is to set this residual to zero at all collocation points, x_i . This is done by determining the coefficients $\alpha_i(\zeta)$ ($i = 0, 1, 2, \dots, n-1$) so that $R_i(x_i, \zeta) = 0$. For "exact" solution when using the orthogonal collocation method, it is required that the collocation points x_i to be the roots (zeros) of the n th order Laguerre polynomial (Villadsen and Michelsen, 1978).

In this study, the approximating function Equation (5.20) is used to approximate both the interior and initial condition points. This method is called the mixed method. Equation (5.20) has a total of n adjustable parameters, $\alpha_i(\zeta)$. One for the initial condition ($x_1 = 0$) and $(n-1)$ for the interior points. Equation (5.20) can be written in matrix form as:

$$\bar{Y} = \bar{\Phi} \bar{\alpha} \quad (5.26)$$

where

$$\bar{Y} = [y(x_1, \zeta) \ y(x_2, \zeta) \ y(x_3, \zeta) \ \dots \ y(x_n, \zeta)]^T \quad (5.27)$$

$$\bar{\alpha} = [\alpha_0(\zeta) \ \alpha_1(\zeta) \ \alpha_2(\zeta) \ \dots \ \alpha_{n-1}(\zeta)]^T \quad (5.28)$$

and

$$\overline{\overline{\Phi}} = \begin{bmatrix} \phi_{1,0} & \phi_{1,1} & \phi_{1,2} & \cdot & \cdot & \cdot & \phi_{1,n-1} \\ \phi_{2,0} & \phi_{2,1} & \phi_{2,2} & \cdot & \cdot & \cdot & \phi_{2,n-1} \\ \phi_{3,0} & \phi_{3,1} & \phi_{3,2} & \cdot & \cdot & \cdot & \phi_{3,n-1} \\ & & & \cdot & & & \\ & & & \cdot & & & \\ & & & \cdot & & & \\ \phi_{n,0} & \phi_{n,1} & \phi_{n,2} & \cdot & \cdot & \cdot & \phi_{n,n-1} \end{bmatrix} \quad (5.29)$$

where $\phi_{i,k} = e^{-x} \psi_k(x)$ for $x = x_i$, $i = 1, 2, 3, \dots, n$ and $k = 0, 1, 2, 3, \dots, n-1$. Similarly, the derivatives are given by:

$$\frac{d\overline{Y}}{dx} = \sum_{i=1}^n \alpha_i(\zeta) \frac{d(e^{-x} \psi_{i-1}(x))}{dx} = \overline{\overline{T}} \overline{\alpha} \quad (5.30a)$$

$$\frac{d\overline{Y}}{d\zeta} = \overline{\overline{\Phi}} \overline{\alpha'} \quad (5.30b)$$

$$\frac{d^2\overline{Y}}{d\zeta^2} = \overline{\overline{\Phi}} \overline{\alpha''} \quad (5.30c)$$

where

$$\overline{\alpha'} = [\alpha'_0(\zeta) \ \alpha'_1(\zeta) \ \alpha'_2(\zeta) \ \cdot \cdot \cdot \ \alpha'_n(\zeta)]^T \quad (5.31a)$$

$$\overline{\alpha''} = [\alpha''_0(\zeta) \ \alpha''_1(\zeta) \ \alpha''_2(\zeta) \ \cdot \cdot \cdot \ \alpha''_n(\zeta)]^T \quad (5.31b)$$

and

$$\bar{\bar{T}} = \begin{bmatrix} \gamma_{1,0} & \gamma_{1,1} & \gamma_{1,2} & \cdots & \gamma_{1,n-1} \\ \gamma_{2,0} & \gamma_{2,1} & \gamma_{2,2} & \cdots & \gamma_{2,n-1} \\ \gamma_{3,0} & \gamma_{3,1} & \gamma_{3,2} & \cdots & \gamma_{3,n-1} \\ & & \cdot & & \\ & & \cdot & & \\ & & \cdot & & \\ \gamma_{n,0} & \gamma_{n,1} & \gamma_{n,2} & \cdots & \gamma_{n,n-1} \end{bmatrix} \quad (5.32)$$

where $\gamma_{i,k} = e^{-x} [k\psi'_{k-1}(x) - k\psi_{k-1}(x) - \psi_k(x)]$ for a given $x = x_i$ ($i = 1, 2, 3, \dots, n$) also $\psi'_0 = 0$ and $\psi_1 = -1$. x_i are the n roots of the Laguerre polynomial.

(a) Particle Aggregation

The integrals in the aggregation equation, Equation (5.19), were solved using Gaussian-Laguerre quadrature defined as:

$$\int_0^\infty h(x) dx = \sum_{i=1}^n w_i e^{x_i} h(x_i) \quad (5.33)$$

where x_i are the n zeros of the Laguerre polynomial and w_i are the corresponding weighting factors. Equation (5.19) can be written in matrix form as:

$$\bar{A} = P_A \left[\frac{x_k^2}{2} \bar{L}_k - I_n \bar{Y} \right] \quad (5.34a)$$

where

$$\bar{A} = [A(x_1, \zeta) \ A(x_2, \zeta) \ A(x_3, \zeta) \ . \ . \ . \ A(x_n, \zeta)]^T \quad (5.34b)$$

$$\bar{Lx}_k = [Lx_1 \ Lx_2 \ Lx_3 \ . \ . \ . \ Lx_n]^T \quad (5.34c)$$

and

$$Lx_k = \int_0^{x_k} f(\epsilon, \zeta) \ d\epsilon = \sum_{i=1}^k w_i e^{\epsilon_i} f(\epsilon_i, \zeta) \quad (5.35)$$

$$f(\epsilon_i, \zeta) = \frac{y(q_k, \zeta) \ y(\epsilon_i, \zeta)}{q_k^2}; \quad q_k = (x_k^3 - \epsilon_i^3)^{1/3} \quad (5.36a)$$

$$y(q_k, \zeta) = \sum_{i=1}^n \alpha_i e^{-q_k \psi_{i-1}(q_k)} \quad (5.36b)$$

therefore

$$\begin{aligned} Lx_1 &= w_1 e^{\epsilon_1} f(\epsilon_1, \zeta) \\ Lx_2 &= Lx_1 + w_2 e^{\epsilon_2} f(\epsilon_2, \zeta) \\ Lx_3 &= Lx_2 + w_3 e^{\epsilon_3} f(\epsilon_3, \zeta) \\ &\vdots \\ &\vdots \\ Lx_n &= Lx_{n-1} + w_n e^{\epsilon_n} f(\epsilon_n, \zeta) \end{aligned} \quad (5.37)$$

The term I_∞ is given by:

$$I_\infty = \int_0^\infty y(\epsilon, \zeta) \ d\epsilon = \sum_{i=1}^n w_i e^{\epsilon_i} y(\epsilon_i, \zeta) \quad (5.38)$$

Since ε_i are values of $x \leq x_n$, then in Equation (5.38) ε_i are replaced by x_i .

(b) Breakage Rate

The breakage rate, Equation (5.17), can be represented in matrix form as:

$$\bar{B} = B_{\text{con}} [\bar{Y}_1 - \bar{Y}_2] \quad (5.39)$$

where $B_{\text{con}} = k_d N_s (L_c^{\beta-1})$ and

$$\begin{aligned} \bar{B} &= [B(x_1, \zeta) \ B(x_2, \zeta) \ B(x_3, \zeta) \ \dots \ B(x_n, \zeta)]^T \\ \bar{Y}_1 &= 2^{\beta\beta+1} [x_1^\beta y(1.26x_1, \zeta) \ x_2^\beta y(1.26x_2, \zeta) \ x_3^\beta y(1.26x_3, \zeta) \ \dots \ x_n^\beta y(1.26x_n, \zeta)]^T \\ \bar{Y}_2 &= [x_1^\beta y(x_1, \zeta) \ x_2^\beta y(x_2, \zeta) \ x_3^\beta y(x_3, \zeta) \ \dots \ x_n^\beta y(x_n, \zeta)]^T \end{aligned} \quad (5.40)$$

Substituting the approximate solution into the PBE and introducing the matrix notation results in:

$$\frac{d\bar{\alpha}^2}{d\zeta^2} - Pe \frac{d\bar{\alpha}}{d\zeta} - Pe \frac{Gt_m}{L_c} (\bar{\Phi}^{-1} \bar{T}) \bar{\alpha} + Pe \frac{L_c t_m}{N_s} \bar{\Phi}^{-1} [\bar{A} + \bar{B}] = \bar{\Phi}^{-1} \bar{R}(x, \zeta) \quad (5.41)$$

where the matrix $\bar{R}(x, \zeta)$ is the residue. Therefore, the PBE has been transformed into a set of second order ordinary differential equations (boundary value problem). The corresponding boundary conditions in matrix form are:

$$\overline{\overline{\Phi}}\alpha(\zeta)|_{x=0} = \frac{B^0/N_s}{G/L_c}; \quad x \rightarrow 0 \quad (0 \leq \zeta \leq 1) \quad (5.42a)$$

$$Pe \bar{\alpha} - \frac{d\bar{\alpha}}{d\zeta} = 0; \quad \zeta = 0 \quad (x > 0) \quad (5.42b)$$

$$\overline{\overline{\Phi}} \frac{d\bar{\alpha}}{d\zeta} = 0; \quad \zeta = 1 \quad (x > 0) \quad (5.42c)$$

5.2.3 Node by Node Calculations

The node points values of $\alpha_i(\zeta_j)$ at x_i ; $i = 1, 2, \dots, n$ and ζ_j ; $j = 1, 2, \dots, m$ are represented Equation (5.41). The second order ordinary differential equations can be transformed into a set of first order ordinary differential equations as:

$$\bar{f} = \frac{d\bar{\alpha}}{d\zeta} \quad (5.43a)$$

$$\bar{f}' = \frac{d^2\bar{\alpha}}{d\zeta^2} \quad (5.43b)$$

Therefore Equation (5.41) becomes:

$$\frac{d\bar{\alpha}}{d\zeta} = \bar{f} \quad (5.44a)$$

$$\frac{d\bar{f}}{d\zeta} - Pe \bar{f} - Pe \frac{Gt_m}{L_c} (\overline{\overline{\Phi}}^{-1} \overline{\overline{T}}) \bar{\alpha} + Pe \frac{L_c t_m}{N_s} \overline{\overline{\Phi}}^{-1} [\bar{A} + \bar{B}] = \overline{\overline{\Phi}}^{-1} \bar{R}(x, \zeta) \quad (5.44b)$$

Using 8 interior node points along x and one node point (x_1) as the initial condition Equations (5.44a) and (5.44b) can be written in matrix form as:

$$\begin{bmatrix} \alpha'_1 \\ \alpha'_2 \\ \alpha'_3 \\ . \\ . \\ . \\ . \\ \alpha'_9 \end{bmatrix} = \begin{bmatrix} IC \\ f_1 \\ f_2 \\ . \\ . \\ . \\ . \\ f_8 \end{bmatrix}$$

(5.45)

$$\begin{bmatrix} f'_1 \\ f'_2 \\ f'_3 \\ . \\ . \\ . \\ . \\ f'_8 \end{bmatrix} = Pe \begin{bmatrix} f_1 \\ f_2 \\ f_3 \\ . \\ . \\ . \\ . \\ f_8 \end{bmatrix} + Pe \frac{Gt_m(\overline{\Phi}^{-1} \overline{T})}{L_c} \begin{bmatrix} \alpha_2 \\ \alpha_3 \\ \alpha_4 \\ . \\ . \\ . \\ . \\ \alpha_9 \end{bmatrix} - Pe \frac{L_c J_m \overline{\Phi}^{-1} [\overline{A} + \overline{B}]}{N_s}$$

Therefore a total of 17 first order ODE are to be solved (16 equations represent the interior nodes and 1 equation represents the initial condition). However, in order to solve Equation (5.45), equation defined by α'_1 which is given by the IC (initial condition) was defined. This was necessary to form a closed set of equations (17 equations and 17 unknowns; 8 f's and 9 α' s). Substituting the approximate solution into the initial condition equation, Equation (5.42a), and taking the limit as the size $x_k \rightarrow 0$ gives:

$$\sum_{i=1}^n \alpha_i(\zeta) \psi_{i-1}(x_k) \Big|_{x_k \rightarrow 0} - \frac{B^o/N_s}{G/L_c} = R_k(0, \zeta) ; x \rightarrow 0 (0 \leq \zeta \leq 1) \quad (5.46)$$

Differentiating once Equation (5.46) with respect to ζ gives:

$$\alpha'_1\psi_0(0)+\alpha'_2\psi_1(0)+\alpha'_3\psi_2(0)+\dots+\alpha'_9\psi_8(0)-\frac{d}{d\zeta}\left(\frac{B^o/N_s}{G/L_c}\right)\Big|_{\zeta=0}=0 \quad (5.47)$$

where

$$\frac{d}{d\zeta}\left(\frac{B^o/N_s}{G/L_c}\right)\Big|_{\zeta=0}=\frac{B_o^o L_c(1-k_{Bo}\zeta)^a}{G_o^o N_s(1-k_G\zeta)^b}\left[\frac{bk_g}{1-k_g\zeta}-\frac{ak_{Bo}}{1-k_{Bo}\zeta}\right] \quad (5.48)$$

solving for α'_1 and substituting for f results in:

$$\alpha'_1=\frac{1}{\psi_0(0)}\left(\frac{B_o^o L_c(1-k_{Bo}\zeta)^a}{G_o^o N_s(1-k_G\zeta)^b}\left[\frac{bk_g}{1-k_g\zeta}-\frac{ak_{Bo}}{1-k_{Bo}\zeta}\right]-[+f_1\psi_1(0)+f_2\psi_2(0)+\dots+f_8\psi_8(0)]\right) \quad (5.49)$$

where $\psi_0(0) = 1$. This is now a closed system of equations. This set of 17 equations is solved at different values of ζ . In this study, the number of node points along the ζ direction was 101. This means a total of 101 x 17 first order ODE are solved each time. The corresponding boundary condition at the entrance, $\zeta = 0$, $1/Pe \rightarrow \infty$ (approaches mixed flow). Therefore the boundary condition at the entrance can be simplified as:

$$\bar{\alpha} = 0 ; \quad \zeta = 0 \quad (x > 0) \quad (5.50a)$$

or if at any other starting location, then the boundary condition corresponds to the PSD at that location. The boundary condition at the exit $\zeta = 1$ is given by:

$$\bar{f} = 0 ; \quad \zeta = 1 \quad (x > 0) \quad (5.50b)$$

which means α_i 's are constant at the exit. For known PSD at the exit, $Y(x,1)$, Equation (5.42c) can be integrated once to give:

$$\bar{\alpha} = \bar{L}^{-1} \bar{Y} ; \quad \zeta = 1 \quad (x > 0) \quad (5.50c)$$

This form of boundary condition was used during determination of kinetic parameters from the experimental data. In that case the values of $Y(x,\zeta)$ at the four sampling ports (different ζ) are known.

5.2.4 Simulation of the Model Solution

For simulation purposes, to observe the flexibility and the efficiency of the proposed numerical scheme, the effects of different parameters on the PSD profiles were simulated. The model parameters and the boundary PSD (dimensionless) were selected arbitrarily, but within the parameter search range used in optimization. The dimensionless PSD at the port near the entrance, $\zeta = 0.02$, and at some other point, $\zeta = 0.5$, (exit) were assumed to be continuous and represented by simple distribution equations. At the entrance the PSD was defined as:

$$y(x, \zeta_o) = \frac{K_o}{\mu_o} \exp\left[-\frac{(x-x_o)}{\mu_o}\right] \quad (5.51)$$

where x_o is assumed to be the dimensionless nuclei size (very small number = 0.001), $\mu_o = 1$ and $K_o = 10$ and at the exit the density function distribution was assumed as:

$$y(x, \zeta_e) = \frac{K_e}{\mu_e} \exp\left[-\frac{(x-x_e)^2}{\mu_e^2}\right] \quad (5.52)$$

where x_e is assumed to be the dimensionless exit mean particle size ($= 11$), $\mu_e = 1.41x_e CV_e$, $K_e = 14\pi^{-1/2}$, and $CV_e = 0.45$. The two PSDs are shown in Figure 5.6. The entrance (port 1) PSD shows the existence of many small particles due to homogeneous nucleation. Then it is assumed that, after some time, the slurry will have moved a distance ζ_e ($= 0.5$) along the tubular precipitator. During this time, nucleation, particle growth, particle aggregation, and particle breakage take place. Using the two PSD as boundary conditions and assumed values of parameters, see Table 5.2 (not optimized), the PBE was solved using OCMSM to generate the intermediate PSD profiles based on various parameters (no intermediate constraints). When the breakage rate is increased, by increasing the constant k_d or the parameter β , the PSD shifts towards the small particle size range (see Figure 5.7), indicating that the population density of fine particles has increased. Increasing the rate of depletion of the initial nuclei by increasing parameter α or k_B , leads to a fast depletion of the supersaturation. This results in a low population of the small particles along the tubular precipitator due to the absence of the nucleation process (Figure 5.8). Whereas, if the value of k_B is made equal $= 0$ (slow depletion of supersaturation), the nucleation process becomes very slow and takes place throughout the tubular length. This, together with particle breakage, results in high values of fine particles (Figure 5.9).

Figure 5.10 shows the PSD profiles generated by varying the growth rate exponent. Growth rate is associated to the molecular growth of the small particles and primary particles before they join with larger aggregates. Increasing the growth rate exponent (g) results in multi-modal PSD. This shows the presence of mixed sizes of particles, the aggregates and large particles formed by molecular growth. Larger values of the growth exponent (g) leads to multiple solutions of the PBE solution.

Increasing the flow velocity (high Reynolds number) shows that the PSD does not form a multi-modal distribution (Figure 5.11). This might be due to high shear rate

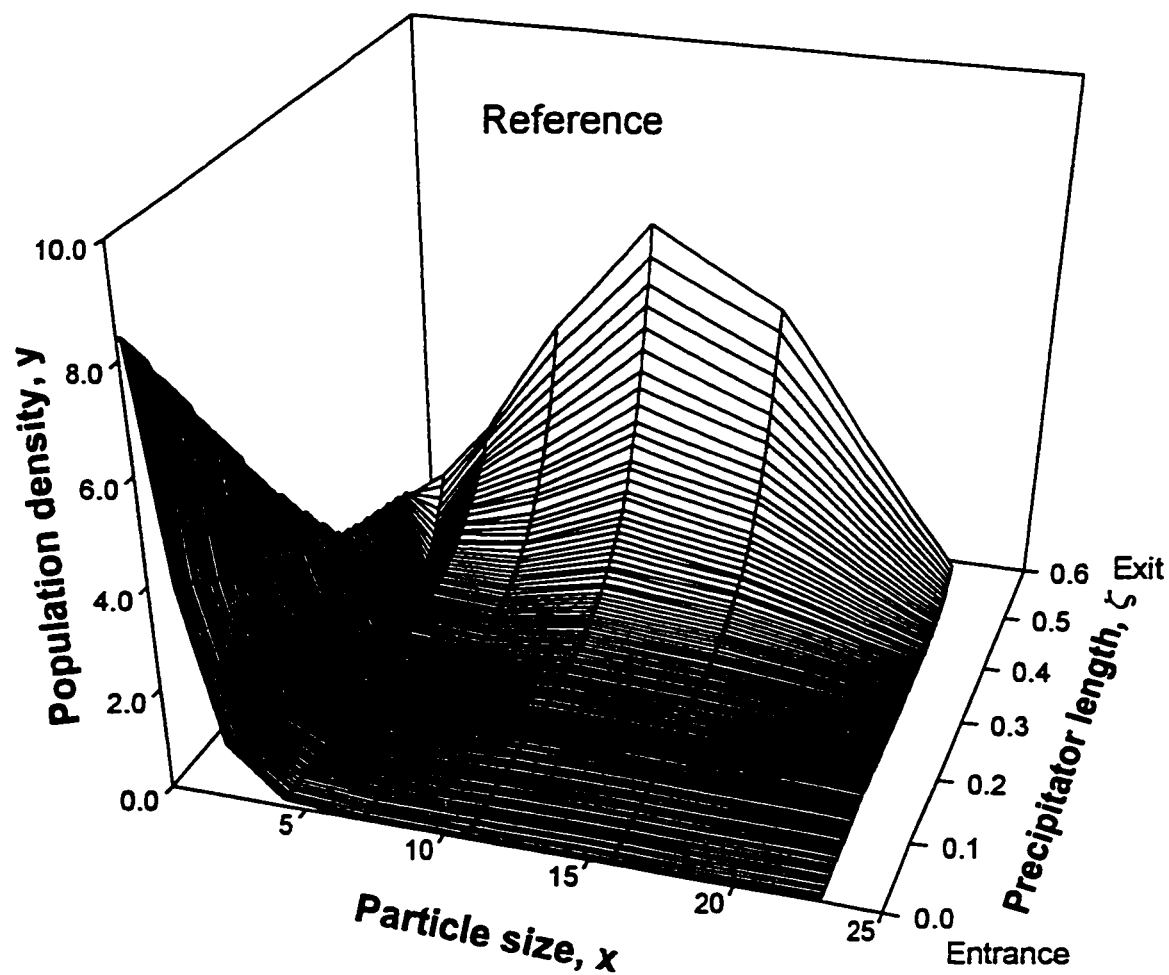


Figure 5.6 Simulated reference PSD along the tubular precipitator using parameters shown in Table 5.2.

Table 5.2 Values of parameters used in the simulation of the model (reference data).

Nucleation rate:	$a = 3.5$	$k_B = 0.5$	$k_{Bo} = 1 \times 10^8 \text{ no./mL s}$	$k_m = 40.0$
Growth rate:	$b = 2.0$	$k_G = 0.30$	$k_{Go} = 4 \times 10^{-5} \mu\text{m/s}$	$g = 2.0$
Breakage rate:	$\beta = 0.2$	$k_d = 5 \times 10^{-6}$		
Aggregation rate:	$\beta_o = 1 \times 10^{-15} \mu\text{m}^4\text{mL s/no.}$			
Protein conc.:	$C_o = 12.0 \text{ kg/m}^3$	$C^* = 2.0 \text{ kg/m}^3$		
Flow velocity:	$u_z = 0.13 \text{ m/s}$			

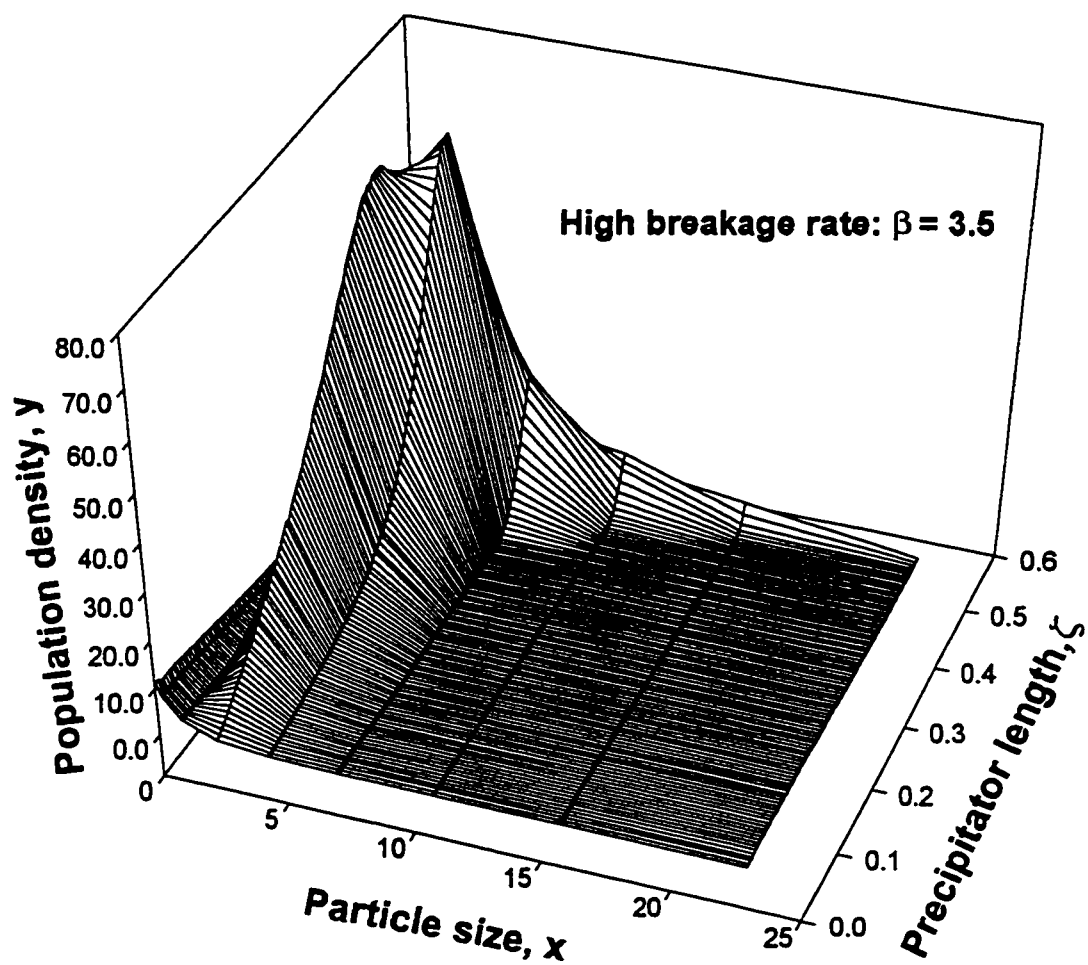


Figure 5.7 Simulated PSD along the tubular precipitator with a high breakage rate parameter, $\beta = 3.5$.

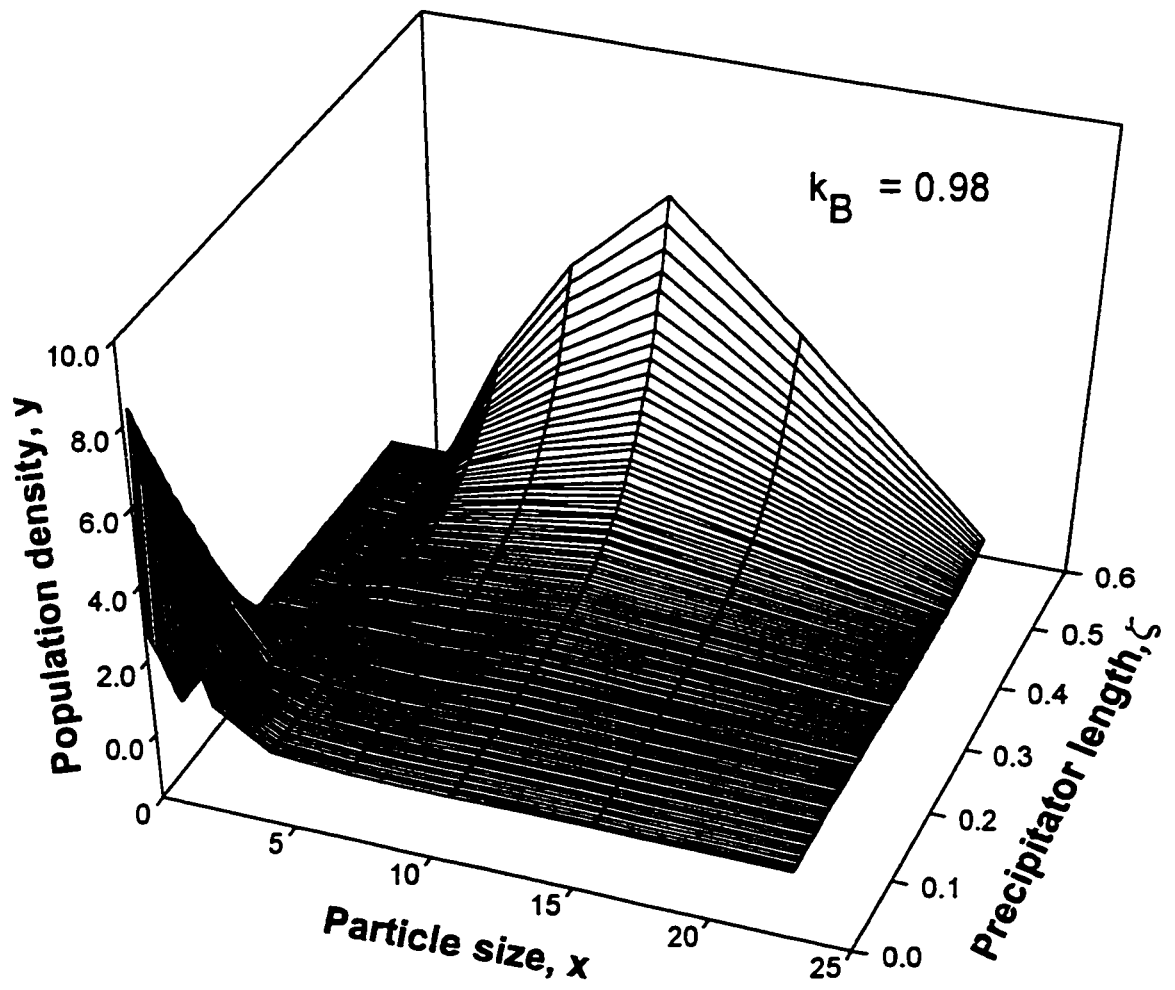


Figure 5.8 Simulated PSD along the tubular precipitator for high nucleation rate constant ($k_B = 0.98$).

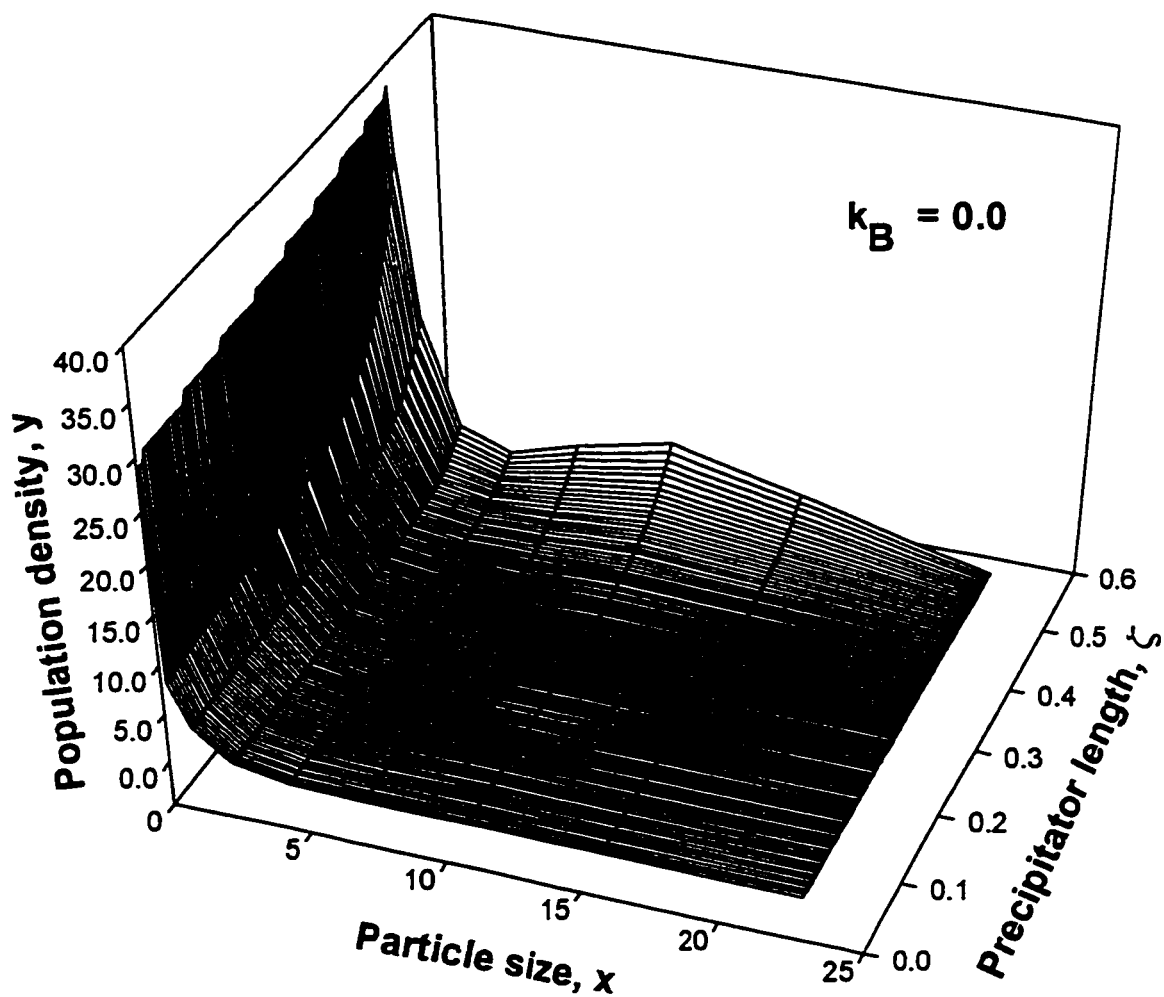


Figure 5.9 Simulated PSD along the tubular precipitator for a low nucleation rate constant ($k_B = 0.0$).

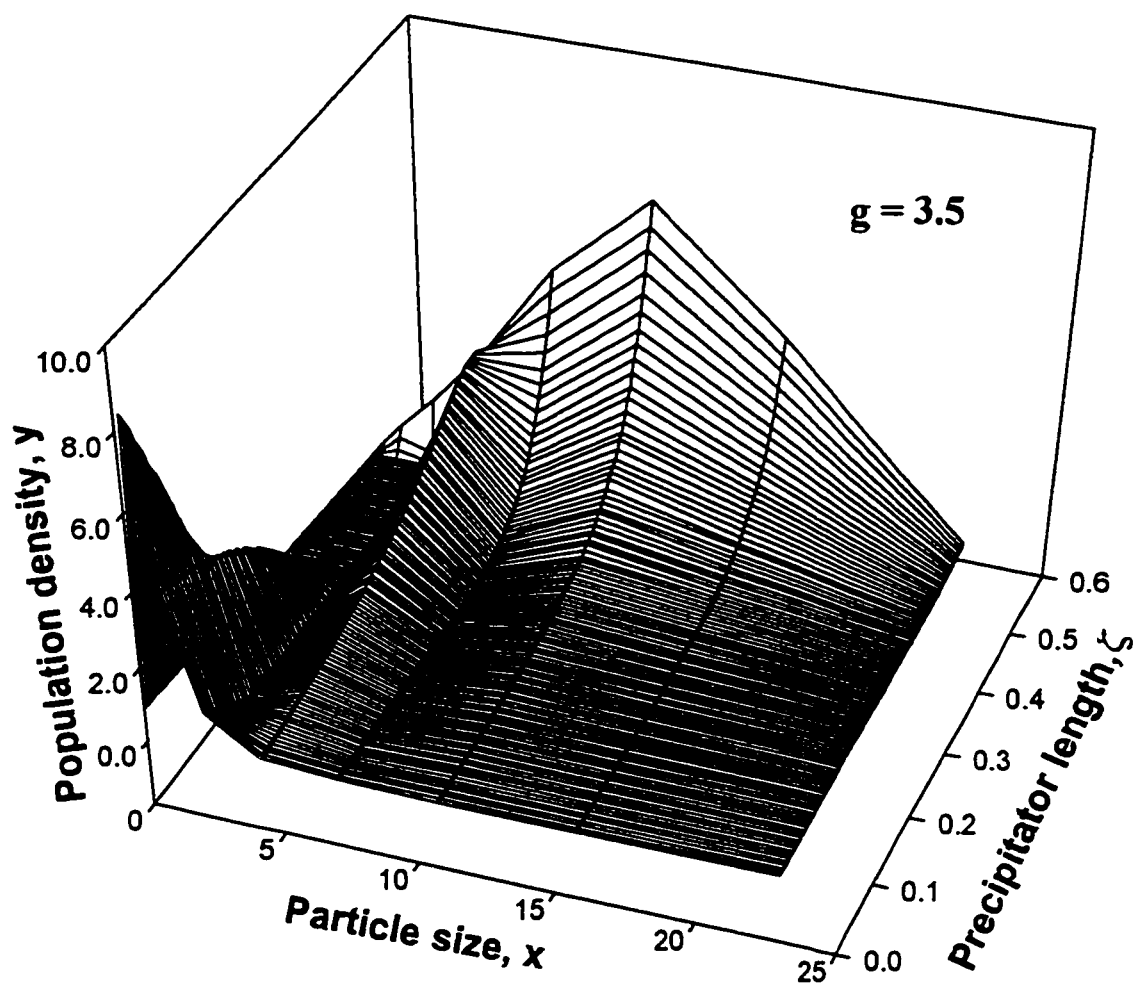


Figure 5.10 Simulated PSD along the tubular precipitator for high growth rate exponent ($g = 3.5$).

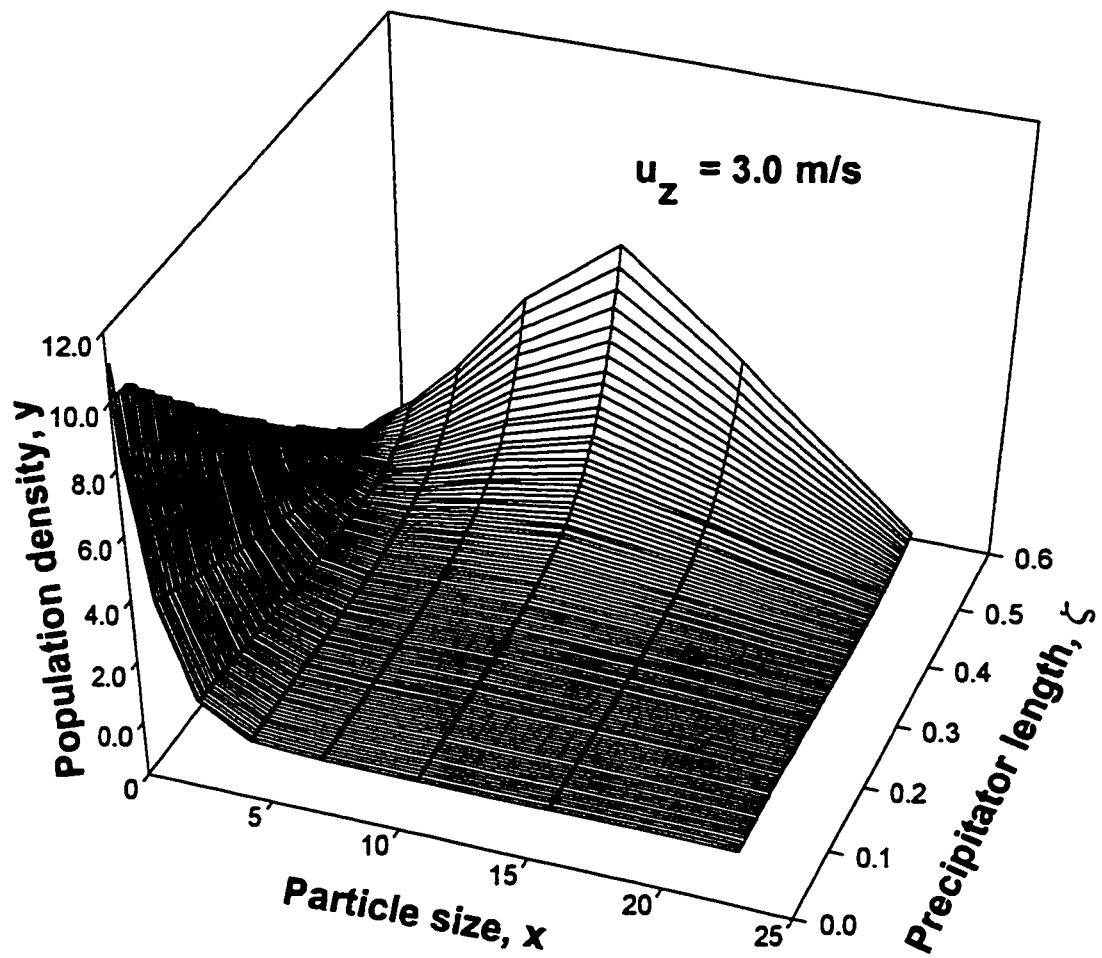


Figure 5.11 Simulated PSD along the tubular precipitator for high flow velocity ($u_z = 3.0 \text{ m/s}$).

caused by turbulent flow, resulting in breakage of the intermediate sized aggregates, or that the particle-particle collisions are not effective in forming a lasting aggregate.

These example illustrations shows that the numerical scheme is flexible enough to generate the PSD profiles to match the experimentally obtained PSD (boundary conditions). A similar scheme was used during parameter optimization where four different data sets (each with 2 inner constraints) were used to determine the best set of parameters resulting in the minimum residue.

5.2.5 Determination of Precipitation Kinetic Parameters From Experimental Data

A total of 11 parameters from model equations (nucleation rate equation parameters: a , k_B , k_{Bo} , and k_m ; growth rate equation parameters: b , k_G , k_{Go} , and g ; breakage rate equation parameters; β , and k_d ; and aggregation rate equation parameter: β_o) were determined by optimization method. The estimated parameters were then substituted into the respective equation for solving the population density equation along the tubular precipitator. The calculated population density data were used to determine the local mean particle size and the coefficient of variation (corresponding to experimental sampling ports). Parameter optimization was done, using Simulated Annealing Method (SAM by Goffe et al. 1994), for determination of the global parameters. The method is slow, but sure. The Multiple Shooting Method (MSM) was used to obtain the PSD profiles between the two boundary conditions, the entrance port and the exit port, using the iterative method. During each calculation pass, the boundary conditions were satisfied. The PSD for the interior ports (2 and 3) were represented using the mean particle size and the coefficient of variation. These interior data were used as constraints for the optimization equation, that is, the optimum parameters should satisfy the two boundary conditions profiles and the interior distributions at ports 2 and 3. Four sets of experimental data were used for this optimization (Table 5.3). The objective equation to be optimized was given as:

Table 5.3 Summary of the runs in the tubular precipitator used in the determination of precipitation kinetic parameters: experimental conditions and measured mean particle size and CV of samples from ports 2 and 3.

Run no.	Co (kg/m ³)	C* (kg/m ³)	u _z (m/s)	d _{i2} [§] (μm)	d _{i3} [§] (μm)	CV _{i2} (%)	CV _{i3} (%)
L1	11.8	1.9	0.13 (800)†	27.8±1.1	30.7±1.7	38.5	43.1
L2	11.8	1.9	0.83 (5000)†	8.6±1.1	7.9±1.7	24.3	23.1
L6	2.8	0.47	0.13 (800)†	22.8±1.1	27.6±1.7	35.5	28.6
L7	2.8	0.47	0.83 (5000)†	10.2±1.1	9.5±1.7	22.1	21.8

† Total flow Re number in the tubular precipitator.

§ Recalculated mean particle size using particle size ranges corresponding to the first 8 zeros of the Laguerre polynomial.

$$\min_P H = \sum_{i=1}^{j-3} \left[\left(\frac{dm_{i,j}}{d_{i,j}} - 1 \right)^2 + \left(\frac{CVm_{i,j}}{CV_{i,j}} - 1 \right)^2 \right] \quad (5.53)$$

where P is a matrix of parameters, $[a \ k_B \ k_{Bo} \ k_m \ b \ k_G \ k_{Go} \ g \ \beta \ k_d \ \beta_o]$, $dm_{i,j}$ and $CVm_{i,j}$ are the calculated values of the mean particle size and the coefficient of variation for run i at port j, respectively. and $d_{i,j}$ and $CV_{i,j}$ are the corresponding experimental values. $dm_{i,j}$ and $CVm_{i,j}$ were calculated as:

$$d_{m_{ij}} = \frac{\sum_{j=1}^{nc} L_j^4 p_j \Delta L_j}{\sum_{j=1}^{nc} L_j^3 p_j \Delta L_j} \quad (5.54)$$

$$CVm_{ij} = \frac{\sqrt{\frac{\sum_{j=1}^{nc} L_j^3 (L_j - d_{m_{ij}})^2 p_j \Delta L_j}{\sum_{j=1}^{nc} L_j^3 p_j \Delta L_j}}}{d_{m_{ij}}} \quad (5.55)$$

Table 5.4 shows the list of the initial estimates and the search range used for optimization. Some of these data were based on the knowledge from previous studies (Raphael et al., 1995; Raphael and Rohani, 1996a).

The algorithm (Figure 5.12) starts by entering the scaled down PSD for the boundary conditions at selected node points (the roots of the trial function). This was achieved by fitting the experimental PSD data using a cubic spline polynomial then interpolated at the desired nodes. The interpolated data were checked for accuracy by recalculating the mean particle size and the CV which was then compared with the original data. In all interpolated data used in this parameter estimation, the accuracy was

Table 5.4 Initial estimates of kinetic parameters, the search range used in optimization, and the final optimum values.

Equation	Parameter	Min. value	Max. value	Initial value	Optimum value
Nucleation rate:	a	0.5	10.0	1.0	= 2.567
	k_B	0.001	0.98	0.5	= 0.353
	k_{Bo} (no./mL s)	1.0	10^{14}	10^6	= 2.385×10^{10}
	k_m	1.0	10^2	50.0	= 61.420
Growth rate:	b	0.0	5.0	1.0	= 1.842
	k_G	0.001	0.98	0.5	= 0.199
	k_{Go} ($\mu\text{m/s}$)	0.0	1.0	0.1	= 1.107×10^{-4}
	g	0.0	5.0	1.0	= 1.512
Breakage rate:	β	0.1	5.0	1.0	= 0.784
	k_d	0.0	5.0	0.1	= 2.744×10^{-6}
Aggregation rate:	β_o ($\mu\text{m}^4\text{mL s/no.}$)	0.0	10^{-9}	10^{-12}	= 9.549×10^{-16}

Final value of H = 0.577

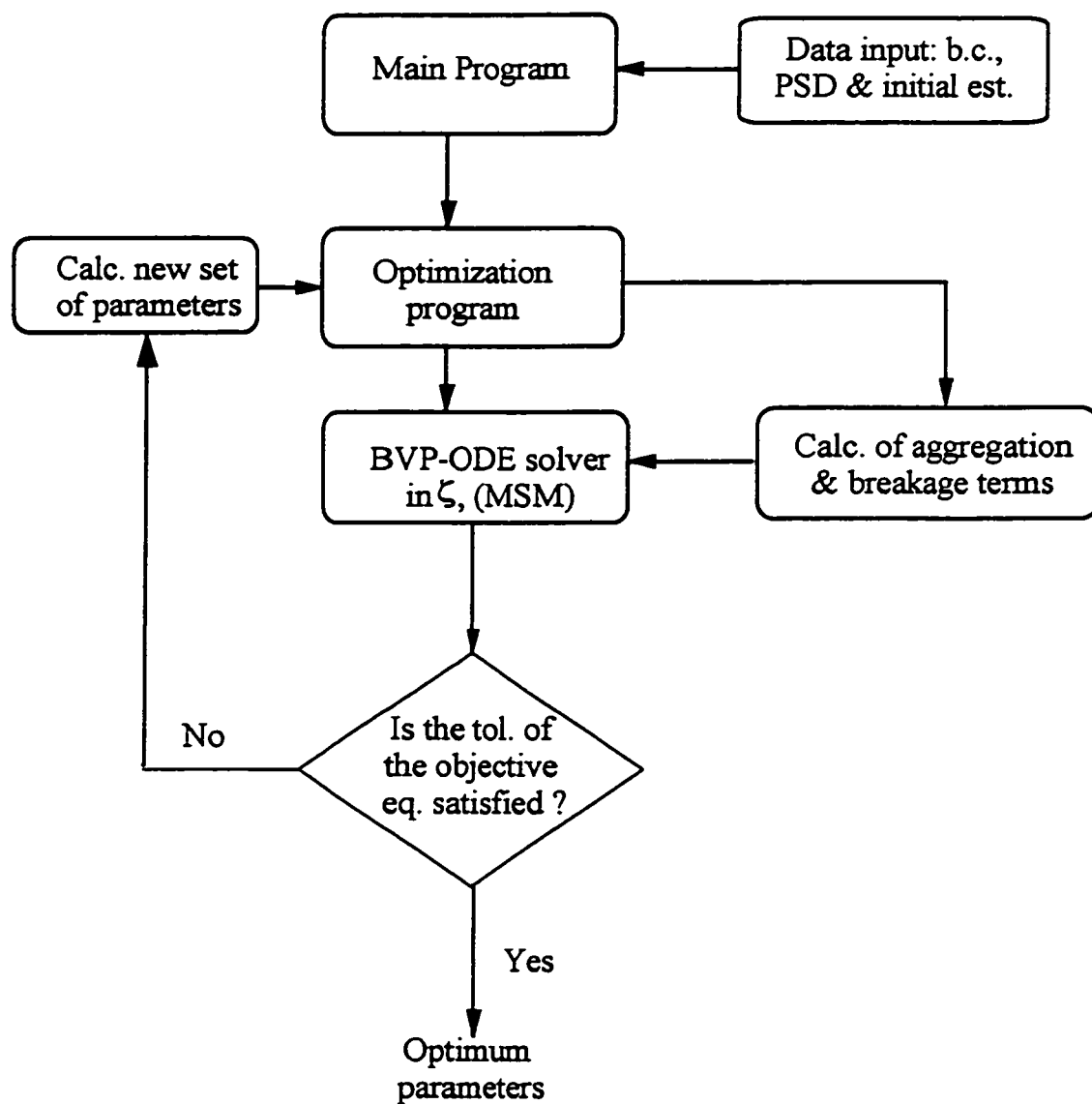


Figure 5.12 Calculation algorithm for determination of the optimum kinetic parameters from the tubular precipitator experimental data.

within $\pm 8 \%$ for the mean particle sizes less than $10 \mu\text{m}$ and within $\pm 5 \%$ for the mean particle sizes larger than $10 \mu\text{m}$. Interpolated CV data showed discrepancies of up to $\pm 50 \%$ because the roots of the Laguerre polynomial do not match the experimental measuring sizes (many roots are in the lower end and sparsely distributed in the higher end). Then the initial guesses of parameters for the optimization routine were entered. The optimization program (Simulated Annealing Method) solved the objective function value by calling the BVP-ODE solver with 101-equally spaced node points in ζ direction (along the tubular precipitator). The BVP-ODE solver (Non-linear Multiple Shooting Method (MSM) by Ascher et al. (1988)) called the other subroutines which calculated the net aggregation and net breakage terms. The integrals in the aggregation term were estimated using a Gaussian-Laguerre quadrature with 9 terms. After the integration, the MSM generated the calculated PSD profiles (between the the boundary conditions, inclusive) for all four data sets used. The optimization routine extracted the estimated mean particle sizes and the CVs representing the interior ports (2 and 3) for substitution into the objective function. The method is repeated until the objective function is satisfied and the consecutive values of the calculated parameters satisfy the set tolerance (10^{-4}). The set of the optimum parameters obtained from this study are presented in Table 5.4. Table 5.5 shows the model fit of the experimental data used in the optimization.

5.2.6 Model Predictions of the Experimental Results

The kinetic parameters obtained from the experimental data were used to predict the PSD from four different experiments (Table 5.6). This time, instead of solving the PBE as a boundary value problem, it was solved as an IVP (initial value problem) using the LSODE package (Hindmarsh, 1980). In order to start the integration, it was necessary to supply the initial PSD. It was hoped that, by supplying the feed concentration and the total flow velocity, the program would be able to generate the entire PSD profile for the tubular precipitator (starting from initial nucleation at $\zeta = 0$). It turned out that the problem was very stiff and, at reduced tolerances, the predicted values showed a large discrepancy from the experimental values. To circumvent this

Table 5.5 Deviations between the model calculated (fit using optimum parameters) mean particle sizes and the experimental mean particle sizes from runs used in optimization.

Run no.	Port no.	Model fit mean size (μm)	Experimental [§] mean size (μm)	% Difference from mean
L1	1	23.9	23.9 ± 1.6	0.0*
	2	23.9	27.8 ± 1.1	-14.0
	3	24.0	30.7 ± 1.7	-21.8
	4	32.1	32.1 ± 1.9	0.0*
L2	1	10.5	10.5 ± 1.6	0.0*
	2	10.4	8.6 ± 1.1	20.9
	3	10.5	7.9 ± 1.7	32.9
	4	7.9	7.9 ± 1.9	0.0*
L6	1	14.4	14.4 ± 1.6	0.0*
	2	18.5	22.8 ± 1.1	-19.0
	3	26.6	27.6 ± 1.7	-3.6
	4	32.0	32.0 ± 1.9	0.0*
L7	1	9.0	9.0 ± 1.6	0.0*
	2	8.9	10.2 ± 1.1	-12.7
	3	9.0	9.5 ± 1.7	-5.3
	4	11.1	11.1 ± 1.9	0.0*

* PSD data at these ports were used as boundary conditions.

§ Recalculated mean particle size using particle size ranges corresponding to the first 8 zeros of the Laguerre polynomial.

Table 5.6 Comparison between the model predicted (using optimum parameters) mean particle sizes and the experimental mean particle sizes.

Run no.	Co (kg/m ³)	C* (kg/m ³)	u _z (m/s)	Port no.	Pred. mean size (μm)	Exp. mean [§] size (μm)	% Difference
L5	11.8	1.9	0.13 (800)†	1	34.9	34.9 ± 1.6	0.0*
				2	36.6	44.7 ± 1.1	-18.1
				3	39.6	45.1 ± 1.7	-12.2
				4	41.2	47.4 ± 1.9	-13.1
I1	11.4	1.8	0.5 (3000)†	1	11.5	11.5 ± 1.6	0.0*
				2	11.5	8.3 ± 1.1	38.5
				3	11.5	12.6 ± 1.7	-8.7
				4	11.6	11.6 ± 1.9	0.0
I2	11.6	1.9	0.5 (3000)†	1	13.4	13.4 ± 1.6	0.0*
				2	13.4	13.3 ± 1.1	0.8
				3	13.4	15.5 ± 1.7	-13.5
				4	13.6	16.3 ± 1.9	-16.6
I4	7.1	1.1	0.83(5000)†	1	12.6	12.6 ± 1.6	0.0*
				2	12.6	10.9 ± 1.1	15.6
				3	12.6	8.0 ± 1.7	57.5
				4	12.7	8.0 ± 1.9	58.8

* PSD data at these ports were used as initial conditions.

† Total flow Re number in the tubular precipitator.

§ Recalculated mean particle size using particle size ranges corresponding to the first 8 zeros of the Laguerre polynomial.

stiffness, the experimental data from the first port ($\zeta = 0.02$, close to the precipitator entrance) were used as the initial condition. Predicted results and the experimental data are compared in Table 5.6. For precipitates with small mean particle sizes, the predicted results showed a wider deviation from the experimental results. When the experimental errors are taken into account, the discrepancies are within the experimental errors.

CHAPTER 6

CONCLUSIONS AND RECOMMENDATIONS

The primary objectives of this research, as mentioned in Section 1.2, were achieved. Original contributions from this research include: experimental data on isoelectric precipitations of sunflower proteins in the MSMPR and the tubular precipitators, on-line measurements of solids concentration using the turbidimeter (beyond Beer Lambert's law), the solution of the PBE with particle aggregations and breakages in the tubular precipitator, and the kinetic parameters of isoelectric precipitation of sunflower proteins.

6.1 Conclusions and Recommendations on the Three Types of Precipitators and Precipitants Used in This Study for Protein Recovery

For optimum recovery of solids protein from the solution, it is required to have a precipitate with large particles and a narrow PSD. Also, to ensure maximum yields it is essential to allow particle aggregation and growth by diffusion to take place (additional time after initial nucleation). As shown experimentally in this study, it is difficult to have a precipitate with both large particles and a small CV. The tubular and the batch precipitators, operating at high yields, produce solids with a wide PSD or small mean particle size, respectively. An MSMPR precipitator performed worse than the batch or the tubular precipitator. The yield was low, the mean particle size was always small, and the PSD showed a bi-modal distribution when the protein feed concentration was high. It is suggested that a batch precipitator operating initially at a high impeller speed (during nucleation), followed by particle settling at low mixing speed (reduced shear rates), may result in a precipitate with large particles and a narrow PSD. A narrow

tubular precipitator operating in the laminar flow regime (with flow velocity greater than the settling velocity of the desired mean particle size) would result in low shear rates. The narrow tube reduces the rate of backmixing, hence the aggregation of particles will be in the radial direction. Thus, the maximum size of the aggregate will depend on the mean residence time and the diameter of the tube. The diameter of the tubular precipitator can be varied to produce aggregates with different mean particle sizes.

Isoelectric precipitation of proteins from alkaline extracts produced higher yields than precipitation of proteins by Ca^{2+} from NaCl extracts. This is because the alkaline extract contained several proteins (albumins, glutelins, and globulins) while the salt extract contained mostly globulins. Also, the mean particle size of Ca^{2+} precipitates were smaller as compared to isoelectric precipitates because of low aggregation rate caused by low number of primary particles.

Complete removal of CA from the sunflower products results in a loss of low molecular weight proteins associated with CA. It is recommended to use reducing agents to prohibit discolouration.

6.2 Conclusions on Precipitation Kinetic Parameters Obtained From the MSMPR Precipitator Data

The model by Petenate and Glatz (1983) with a modified computational algorithm was found to adequately represent the aggregation of sunflower protein in an MSMPR precipitator. Analysis of the experimental data showed that a uni-modal PSD can be obtained in an MSMPR precipitator operating at high solids concentration and longer residence time. At high solids concentration, the PSD can be modelled by assuming a linear growth rate of the protein aggregates. The maximum size of the aggregate is determined by the hydrodynamics of the precipitator and the mean residence time of the particles in the precipitator. Results of this aggregation-breakage model were used in determination of the precipitation kinetic parameters from the tubular precipitator data.

6.3 Conclusions and Recommendations on the Results of the Tubular Precipitator Modelling

In this study, kinetics parameters of the sunflower protein precipitation in the tubular precipitator by isoelectric method (aqueous HCL) were determined. The solution of the non-linear PBE for the tubular precipitator, including the particle aggregation and breakage, was solved using the orthogonal-collocation and multiple shooting methods. The numerical algorithm converged when various values (combinations) of the model parameters in the search range were used. This facilitated the determination of the precipitation kinetic parameters by global optimization. Calculated parameters predicted the PSD along the tubular precipitator within the experimental errors. Using these kinetic parameters, the length of the tubular precipitator required to give the desired mean particle size of the precipitate can be calculated.

Instead of using the PSD from port number 1 as the lower boundary condition or as the initial condition, it is recommended to determine the solution of the model equation using boundary conditions very close to the mixing zone. In this region, the model equation is a stiff differential equation due to a large number of particles (nuclei) with very small size and it requires a lot of computer time.

REFERENCES

- Anfinsen, C. B. and H. A. Scheraga, "Experimental and Theoretical Aspects of Protein Folding", *Advan. Protein Chem.* **29**, 205-300 (1975).
- AOAC., "Official Method of Analysis of the Association of Official Analytical Chemists", 14th ed., Association of Official Analytical Chemists, Arlington, VA, (1984).
- Ascher, U., R. Mattheij, and R. D. Russel, "Numerical Solution of Boundary Value Problem for Ordinary Differential Equation", Prentice-Hall Inc., pg. 157 (1988).
- Bau, H. M., D. J. Mohtadi-nia, L. Mejean, and G. Debry, "Preparation of Colorless Sunflower Protein Products: Effect of Processing on Physicochemical and Nutritional Properties", *J. Amer. Oil Chem. Soc.* **60**, 1143-1148 (1983).
- Bell, D. J., D. Heywood-Waddington, M. Hoare, and P. Dunnill, "The Density of Protein Precipitation and its Effects on Centrifugal Sedimentation", *Biotechnol. Bioeng.* **24**, 127-141 (1982).
- Bell, D. J. and P. Dunnill, "Shear disruption of Soy Protein Precipitate Particles and Effect of Aging in a Stirred Tank", *Biotechnol. Bioeng.* **24**, 1271-1285 (1982).
- Bell, D. J., M. Hoare, and P. Dunnill., "The Formation of Protein Precipitates and Their Centrifugal Recovery", *Adv. Biochem. Eng. Biotechnol.* **26**, 1-72 (1983).
- Bhatia, S. K. and D. Chakraborty, "Modified MWR Approach: Application to Agglomerative Precipitation", *AIChE J.* **38**, 868-878 (1992).
- Brown, D. L. and C. E. Glatz, "Aggregate Breakage in Protein Precipitation," *Chem. Engng. Sci.* **42**, 1831-1839 (1987).
- Box, E. P. G., W. G. Hunter, and J. S. Hunter, "Statistics for Experimenters," John Wiley & Sons, NY (1978).
- Cater, C. M., S. Gheyasuddin, and K. F. Mattil, "Effect of Chlorogenic, Quinic and Caffeic Acids on the Solubility and Colour of Protein Isolates, Especially From Sunflower Seed", *Cereal Chem.* **49**, 508-514 (1972).
- Chan, M. Y., M. Hoare, and P. Dunnill, "The Kinetics of Protein Precipitation by

- Different Reagents", *Biotechnol. Bioeng.* **28**, 387-393 (1986).
- Chang, R. and M. Wang, "Modelling the Batch Crystallization Process via Shifted Legendre Polynomials", *Ind. Eng.. Chem. Process Des. Dev.* **23**, 463-468 (1984a).
- Chang, R. and M. Wang, "Shifted Legendre Function Approximation of Differential Equations: Application to Crystallization Process", *Comp. and Chem. Engineering* **8**, 117-125 (1984b).
- Chen, W., R. R. Fisher, J. C. Berg, "Simulation of Particle Size Distribution in an Aggregation-Breakup Process", *Chem. Engng. Sci.* **45**, 3003-3006 (1990).
- Chen, M. and S. Rohani, "Recovery of Canola Meal Protein by Precipitation", *Biotechnol. Bioeng.* **40**, 63-68 (1992).
- Clandinin, D. R., "Sunflower Seed Oil Meal", in "Processed Plant Protein Foodstuffs", edited by Altschul, A.M., Academic Press Inc., NY, 556 (1958).
- Courant, R. and D. Hilbert, "Methods of Mathematical Physics", Vol. 1, Wiley Interscience, NY (1961).
- Dabrowski, K. J. and F. W. Sosulski, "Composition of Free and Hydrolyzable Phenolic Acids in Defatted Flours of Ten Oilseeds", *J. Agric. Food Chem.* **32**, 128-130 (1984).
- Dash, S. R. and S. Rohani, "Iterative Parameter Estimation for Extraction of Crystallization Kinetics of Potassium Chloride From Batch Experiments", *Can. Chem. Eng.* **71**, 539-548 (1993).
- Delpech de Saint Guilhem, X. and T. A. Ring, "Exact Solution for the Population in a Continuous Stirred Tank Crystallizer With Agglomeration", *Chem. Engng. Sci.* **42**, 1247-1249 (1987).
- FAO/WHO, "World Health Organization Energy and Protein Requirements", Techn. Rep. Series No. 522, Food and Agric. Organ. and World Health Organ., Geneva, (1973).
- Fan T. Y., F. W. Sosulski, and N. W. Hamon, "New Techniques for Preparation of Improved Sunflower Protein Concentrate", *Cereal Chem.* **53**, 118-125 (1976).
- Finlayson, B. A., "The Method of Weighted Residuals and Variational Principles", Academic Press, NY (1972).
- Fisher R. R., C. E. Glatz, and P. A. Murphy, "Effects of Mixing During Acid Addition on Fractionally Precipitated Protein", *Biotechnol. Bioeng.* **28**, 1056-1063 (1986).
- Fisher, R. R. and C. E. Glatz, "Polyelectrolyte Precipitation of Proteins: I. The Effects of Reactor Conditions", *Biotechnol. Bioeng.* **32**, 777-785 (1988).

- Frank, P., R. David, J. Villermaux, and J. Klein, "Crystallization and Precipitation Engineering II. A Chemical reaction Engineering Approach to Salicylic Acid Precipitation: Modelling of Batch Kinetics and Application to Continuous Operation", *Chem. Engng. Sci.* **43**, 69-77 (1988).
- Gheyasuddin, S., C. M. Cater, and K. F. Mattil, "Preparation of Colorless Sunflower Protein Isolate", *Food Technol.* **24**, 242-243 (1970).
- Glatz, C. E., M. Hoare, and J. Landa-Vertiz, "The Formation and Growth of Protein Precipitates in a Continuous Stirred Tank Reactor", *AIChE J.* **32**, 1196-1204 (1986).
- Grabenbauer, G. C. and C. E. Glatz, "Protein Precipitation-Analysis of Particle Size Distribution and Kinetics", *Chem. Eng. Commun.* **12**, 203-219 (1981).
- Goffe, B., G. D. Ferrier, and J. Rogers, "Global Optimization of Statistical Functions With Simulated Annealing", *J. Econometrics* **60**, 65-99 (1994).
- Gupta, B. S. and T. K. Dutta, "Monte Carlo Simulation of Transient CSD in a Continuous Crystallizer", *Chem. Eng. Technology* **13**, 392-397 (1990).
- Halfon A. and S. Kaliaguine, "Alumina Trihydrate Crystallization Part 1. Secondary Nucleation and Growth Rate Kinetics", *Can. Chem. Eng.* **54**, 160-167 (1976a).
- Halfon A. and S. Kaliaguine, "Alumina Trihydrate Crystallization Part 2. A Model of Agglomeration", *Can. Chem. Eng.* **54**, 168-172 (1976b).
- Hindmarsh, A. C., "LSODE and LSODI, Two New Initial Value Ordinary Differential Equation Solvers", *ACM SIGNUM newsletter* Dec. (1980).
- Hoare, M., "Protein Precipitation and Precipitate Ageing Part I: Salting-Out and Ageing of Casein Precipitates", *Trans. Inst. Chem. Eng.* **60**, 79-87 (1982a).
- Hoare, M., "Protein Precipitation and Precipitate Ageing Part II: Growth of Protein Precipitates During Hindered Settling or Exposure to Shear", *Trans. Inst. Chem. Eng.* **60**, 157-163 (1982b).
- Hoare, M., T. J. Narendranathan, J. R. Flint, D. Heywood-Waddington, D. J. Bell, and P. Dunnill, "Disruption of Protein Precipitate During Shear in Couette Flow and in Pumps", *Ind. Eng. Chem. Fundam.* **21**, 402-406 (1982).
- Hounslow, M. J., R. L. Ryall, and V. R. Marshall, "A Discretized Population Balance for nucleation, Growth, and Aggregation", *AIChE J.* **34**, 1821-1832 (1988).
- Hounslow, M. J., "A Discretized Population Balance for a Continuous System at Steady State", *AIChE J.* **36**, 106-116 (1990a).

- Hounslow, M. J., "Nucleation, Growth, and Aggregation Rates From Steady State Experimental Data", *AIChE J.* **36**, 1748-1752 (1990b).
- Hulburt, H. M. and S. Katz, "Some Problems in Particle Technology: A Statistical Mechanical Formulation", *Chem. Engng. Sci.* **19**, 555-574 (1964).
- Ilievski, D. and E. T. White, "Agglomeration During Precipitation: Agglomeration Mechanism Identification for $\text{Al}(\text{OH})_3$ Crystals in Stirred Caustic Aluminate Solutions", *Chem. Engng. Sci.* **49**, 3227-3239 (1994).
- Ilievski, D. and M. J. Hounslow, "Agglomeration During Precipitation: II. Mechanism Deduction From Tracer Data," *AIChE J.* **41**, 525-536 (1995).
- IMSL, "International Mathematics and Statistics Libraries Inc.", Houston, TX (1991).
- Inkelaar, P. A. and I. Fortuin, "Determining the Emulsifying and Emulsion Stabilizing Capacity of Protein Meal Additives", *Food Technology* **23**, 103-107 (1969).
- Jones, A. G., "Particle Formation and Separation in Suspension Crystallization Processes", in "Processing of Solid-Liquid", edited by Shamlou, P. A., Butterworth Heinemann, London, 93-117 (1993).
- Kabirullah, M. and R. B. H. Wills, "Characterization of Sunflower Protein", *J. Agric. Food Chem.* **31**, 953-956 (1983).
- Kim, W. -S. and J. M. Tarbell, "Numerical Technique for Solving Population Balances in Precipitation Processes", *Chem. Eng. Comm.* **101**, 115-129 (1991).
- Kinsella, J. E., "Functional Properties of Soy Proteins", *JAOCs* **56**, 242-258 (1979).
- Lah, L. C. and M. Cheryan, "Protein Solubility Characteristics of an Ultrafiltered Full-fat Soybean Product", *J. Agric. Food Chem.* **28**, 911-916 (1980).
- Lakatos, B., E. Varga, S. Halasz, and T. Blickle, "Simulation of Batch Crystallizers", in "Industrial Crystallization", 84, edited by Jancic, S. J. and E. J. de Jong, Elsevier Science Publishers B.V. Amsterdam, 185-190 (1984).
- Lamey, M. D. and T. A. Ring, "The Effects of Agglomeration in a Continuous Stirred Tank Crystallizer", *Chem. Engng. Sci.* **41**, 1213 -1219 (1986).
- Lawhon, J. T., C. M. Cater, and K. F. Mattil, "Comparative Study of the Whipping Potential of an Extract From Several Oilseeds", *Cereal Science Today* **17**, 241-244 (1972).
- Lawhon, J. T., R. W. Glass, L. J. Manak, and E. W. Lusas, "White-Colored Protein Isolate From Sunflower: Processes and Products", *Food Technology* **36**, 76-87 (1982).

- Lee, H. W. and E. G. Saleeby, "Mathematical Behavior of the Population Balance of a MSMPRC With Agglomeration, Feed and Size-Dependent Growth Rate", *Comp. Chem. Engng.* **18**, 899-907 (1994).
- Lehninger, A. L., "Principles of Biochemistry", Worth Publishers, Inc., NY (1982).
- Levenspiel, O., "Chemical Reaction Engineering", 2nd ed., Wiley, NY (1972).
- Liao P. F. and H. W. Hulburt, "Agglomeration Process in Suspension Crystallization", AIChE Meeting, Chicago, Dec., 1976.
- Lister, J. D., D. J. Smit, and M. J. Hounslow, "Adjustable Discretized Population Balance for Growth and Aggregation", *AIChE J.* **41**, 591-603 (1995).
- Lui, Y. -M. R. and R. W. Thompson, "Analysis of a Continuous Crystallizer With Agglomeration", *Chem. Engng. Sci.* **47**, 1897-1901 (1992).
- Lusas, E. W., "Sunflower Seed Proteins", in "New Protein Food", vol. 5, edited by Altschul, A. M. and H. L. Wilcke, Academic Press, NY, 393-433 (1985).
- Machall, P., R. David, J. P. Klein, and J. Villiermaux, "Crystallization and Precipitation Engineering I. An Efficient Method for Solving Population Balance in Crystallization With Agglomeration", *Chem. Engng. Sci.* **43**, 59-67 (1988).
- Mersmann, A., M. Angerhofer, and J. Franke, "Controlled Precipitation", *Chem. Eng. Technol.* **17**, 1-9 (1994).
- Mullin, J. W., "Crystallization", 3rd ed., Butterworth, London (1992).
- Mydlarz, J. and A. G. Jones, "An Assessment of MSMPR Crystallization Kinetics Data Modelled by Size-Dependant Crystal Growth Rate Functions", *The Chem. Eng. Journal* **55**, 69 - 80 (1994).
- Nauman, E. B. and B. A. Buffham, "Mixing in Continuous Flow Systems", Wiley, NY (1983).
- Nelson, C. D. and C. E. Glatz, "Primary Particle Formation in Protein Precipitation", *Biotechnol. Bioeng.* **27**, 1434-1444 (1985).
- Nielson, A. E., "Kinetics of Precipitation", Pergamon Press, NY (1964).
- O'Conoor, D. E., "Light-Coloured Protein From Sunflower-Meal", US Pat. 3,586,662 (1971).
- Padia, B. K. and S. K. Bhatia, "Multiplicity and Stability Analysis of Agglomeration Controlled Precipitation", *Chem. Engng. Commun.* **104**, 227-244 (1991).

- Pearce, R. J., "Preparation of Protein Isolate From Sunflower Seed", US Pat. 4,435,319 (1984).
- Petenate, A. M. and C. E. Glatz, "Isoelectric Precipitation of Soy Protein, I. Factor Affecting Particle Size Distribution", *Biotechnol. Bioeng.* **25**, 3049-3058 (1983a).
- Petenate, A. M. and C. E. Glatz, "Isoelectric Precipitation of Soy Protein, II. Kinetics of Protein Aggregate Growth and Breakage", *Biotechnol. Bioeng.* **25**, 3059-3078 (1983b).
- Pomenta, J. V. and E. E. Burns, "Factors Affecting Chlorogenic, Quinic and Caffeic Acid Levels in Sunflower Kernels", *J. Food Sci.* **36**, 490-492 (1971).
- Powrie, W. D. and S. Nakai, "Processing effects on Protein Systems", in "Utilization of Protein Resources", edited by Stanley, D. W., E. D. Murray, and D. H. Lees, Food and Nutrition Press Inc., Westport, CT, 73-109, 1981.
- Prasad, D. T., "Proteins of the Phenolic Extracted Sunflower Meal: 1. Simple Method for Removal of Polyphenolic Components and Characteristics of Salt Soluble Proteins", *Leben.-Wiss. u. Technol.* **23**, 229-235 (1990a).
- Prasad, D. T., "Proteins of the Phenolic Extracted Sunflower Meal: 2. Solubility Fractionation and Characterization of Major Protein Fractions", *Leben.-Wiss. u. Technol.* **23**, 236-241 (1990b).
- Quinn, J. R. and D. Paton, "A Practical Measurement of Water Hydration Capacity of Protein Materials", *Cereal Chem.* **56**, 38 (1978).
- Rahma, E. H. and M. S. Narasinga Rao, "Characterization of Sunflower Proteins", *J. Food Sci.* **44**, 579-582 (1979).
- Randolph, A. D. and M. A. Larson, "Theory of Particulate Processes", 2nd ed., Academic Press, NY (1988).
- Raphael, M., S. Rohani, and F. Sosulski, "Isoelectric Precipitation of Sunflower Protein in a Tubular Precipitator", *Can. J. Chem. Engng.* **73**, 470-483 (1995).
- Raphael, M. and S. Rohani, "Isoelectric Precipitation of Sunflower Protein in an MSMPR Precipitator: Modelling of PSD With Aggregation", *Chem. Engng. Sci.* **51**, 4379-4384 (1996a).
- Raphael, M. and S. Rohani, "On-line Estimation of Solids Concentrations and Mean Particle Size Using a Turbidimetry Method", *Powder Technology* **89**, 157-163 (1996b).
- Rawlings, J. B., W. R. Witkowski, and J. W. Eaton, "Modelling and Control of Crystallizers", *Powder Technology* **69**, 3-9 (1992).

- Rivera, T. and A. D. Randolph, "Model for the Precipitation of Pentaerythritol Tetranitrate", *Ind. Eng. Chem. Process Des. Dev.* **17**, 182-188 (1978).
- Rohani, S. and M. Chen, "Aggregation and Precipitation Kinetics of Canola Protein by Isoelectric Precipitation", *Can. J. Chem. Eng.* **71**, 689-698 (1993).
- "SAS User's Guide: Statistics", SAS Institute Inc., 5th ed., Cary, NC (1985).
- Sabir, M. A., F. W. Sosulski, and S. L. Mackenzie, "Gel Chromatography of Sunflower Protein", *J. Agric. Food Chem.* **21**, 988-993 (1973).
- Sabir, M. A., F. W. Sosulski, and J. A. Kernan, "Phenolic Constituents in Sunflower Flour", *J. Agric. Food Chem.* **22**, 572-575 (1974).
- Saeed, M. and M. Cheryan, "Sunflower Protein Concentrates and Isolates Low in Polyphenols and Phytate", *J. Food Sci.* **53**, 1127- 1131 (1988).
- Saleeby, E. G. and H. W. Lee, "Solution and Analysis for Crystallization With Agglomeration", *Chem. Engng. Sci.* **49**, 1879-1884 (1994).
- Salunkhe, D. K. and B. B. Dace, "Postharvest Biotechnology of Oilseeds", CRC Press, FL, 57-69 (1986).
- Sampson, K. J. and D. Ramkrishna, "A New Solution to the Brownian Coagulation Equation Through the Use of Root Shifted Problem-Specific Polynomials", *J. Colloid Interface Sci.* **103**, 245-254 (1985).
- Schmidt, R. H., "Gelation and Coagulation", in "Protein Functionality in Foods", ACS Symposium Series, **147**, edited by Cherry, J. P., 131-147 (1981).
- Shen, J. "Solubility and Viscosity", in "Protein Functionality in Foods", ACS Symposium Series, **147**, edited by Cherry, J. P., 89-109 (1981).
- Shi, Y., B. Liang, and R. W. Hartel, "Crystallization Kinetics of Alpha-Lactose Monohydrate in a Continuous Cooling Crystallizer", *J. Food Sci.* **3**, 817-820 (1990).
- Singh, P. N. and D. Ramkrishna, "Transient Solution of Brownian Coagulation Equation by Problem-Specific Polynomials", *J. Colloid Interface Sci.* **53**, 214-223 (1975).
- Singh P. N and D. Ramkrishna, "Solution of Population Balance Equation by MWR", *Comp. Chem. Engng.* **1**, 23-31 (1977).
- Singh, R. K., "Precipitation of Biomolecules", in "Bioseparation Processes in Foods", edited by Singh, R. K. and S. S. H. Rizvi, Marcel Dekker Inc., 139-173 (1995).
- Smith, A. K. and V. L. Johnsen, "Sunflower Seed Protein", *Cereal Chem.* **25**, 399-406

(1948).

Sodini, G. and M. Canella, "Acidic Butanol Removal of Color-Forming Phenols From Sunflower Meal", *J. Agric. Food Chem.* **25**, 822-825 (1977).

Sosulski, F. W. and A. Bakal, "Isolated Proteins From Rapeseed, Flax and Sunflower Meals", *Can. Inst. Food Technol. J.* **2**, 28-32 (1969).

Sosulski, F. W., C. W. McCleary, and F. S. Soliman, "Diffusion Extraction of Chlorogenic Acid From Sunflower Kernels", *J. Food Sci.* **37**, 253-256 (1972).

Sosulski, F. W., M. A. Sabir, and S. E. Fleming, "Continuous Diffusion of Chlorogenic Acid From Sunflower Kernels", *J. Food Sci.* **38**, 468-470 (1973).

Sosulski, F. W. and S. E. Fleming, "Chemical, Functional, and Nutritional Properties of Sunflower Products", *J. Amer. Oil Chem. Soc.* **54**, 100a-104a (1977).

Sosulski, F. W., "Food Uses of Sunflower Proteins", *J. Amer. Oil Chem. Soc.* **56**, 438-442 (1979a).

Sosulski, F. W., "Organoleptic and Nutritional Effects of Phenolic Compounds on Oilseed Protein Products: A Review", *J. Amer. Oil Chem. Soc.* **56**, 711-716 (1979b).

Sosulski, F. W. and G. I. Imafidon, "Amino Acid Composition and Nitrogen-to-Protein Conversion Factors for Animal and Plant Foods", *J. Agric. Food Chem.* **38**, 1351-1356 (1990).

Sripad, G. and M. S. Narasinga Rao, "Effect of Methods to Remove Polyphenols From Sunflower Meal on the Physicochemical Properties of the Proteins", *J. Agric. Food Chem.* **35**, 962-967 (1987).

Stroud, A. H. and D. Secrest, "Gaussian Quadrature Formulas", Prentice-Hall, Englewood Cliffs, N.J. (1966).

Subramanian, G. and D. Ramkrishna, "On the Solution of Statistical Models of Cell Populations", *Mathematical Biosciences* **10**, 1-23 (1971).

Taha, F. S., M. Abbasy, A. S. El-Nockrashy, and Z. E. Shueb, "Countercurrent Extraction-Isoelectric Precipitation of Sunflower Seed Protein Isolates", *J. Sci. Food Agric.* **32**, 166-174 (1981).

Tai, C. Y. and P. Chen, "Nucleation, Agglomeration and Crystal Morphology of Calcium Carbonate", *AIChE J.* **41**, 68-77 (1995).

Tavare, N. S., M. B. Shah, and J. Garside, "Crystallization and Agglomeration Kinetics of Nickel Ammonium Sulphate in an MSMR Crystallizer", *J. Powder Technology* **44**,

13-18 (1985).

Tavare, N. S. and J. Garside, "Multiplicity in Continuous MSMMPR Crystallizers in an Isothermal Crystallizer", *AIChE J.* **31**, 1121 (1985).

Twineham, M., M. Hoare, D. J. Bell, "The Effects of Protein Concentration on the Breakup of Protein Precipitate by Exposure to Shear", *Chem. Eng. Sci.* **39**, 509-513 (1984).

Uzzan, A., "Vegetable Protein Products From Seeds: Technology and Uses in the Food Industry", in "Developments in Food Proteins-6", edited by Hudson, B. J., Elsevier Applied Science, 73-118 (1988).

Valentas, K. J., L. Levine, and J. P. Clark, "Food Processing Operations and Scale-Up", Marcel Dekker, Inc., 59-73 (1991).

Villadsen, J. and M. L. Michelsen, "Solutions of Differential Equation Models by Polynomial Approximation", Prentice Hall, Englewood Cliffs, NJ (1978).

Virkar P. D., T. J. Narendranathan, M. Hoare, and P. Dunnill, "Studies of the Effects of Shear on Globular Proteins: Extension to High Shear Fields and to Pumps", *Biotechnol. Bioeng.* **23**, 425-429 (1981).

Virkar, P. D., M. Hoare, M. Y. Y. Chan, and P. Dunnill, "Kinetics of the Acid Precipitation of Soya Protein in a Continuous-Flow Tubular Reactor", *Biotechnol. Bioeng.* **24**, 871-887 (1982).

Viroben, G. and D. Bertrand, In "Proteins Vegetables", edited by Godon, B., Techniques et Documentation Paris, 523 (1985).

Wachi, S. and A. G. Jones, "Dynamics Modelling of Particle Size Distribution and Degree of Agglomeration During Precipitation", *Chem. Engng. Sci.* **47**, 3145-3148 (1992).

Wall, J. S. and F. R. Huebner, "Adhesion and Cohesion", in "Protein Functionality in Foods", ACS Symposium Series, **147**, edited by Cherry, J. P., ACS, 111-130 (1981).

Whitaker, J. R., "Denaturation and Renaturation of Proteins", in "Food Proteins", edited by Whitaker, J. R. and S. R. Tannenbaum, Avi Publishing Co., Inc., 14-49 (1977).

Witkowski, W. R. and J. B. Rawlings, "Modelling and Control of Crystallizers", *Proc. 1987, American Control Conf.*, Minneapolis, MN, 1400-1405, June 1987.

Wright, H. and D. Ramkrishna, "Solutions of Inverse Problems in Population Balances I. Aggregation Kinetics", *Comp. Chem. Engng.* **16**, 1019-1038 (1992).

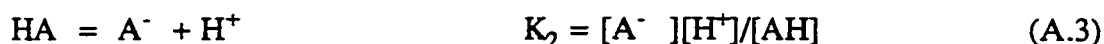
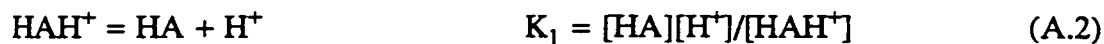
APPENDIX A

ESTIMATION OF THE ISOELECTRIC POINT OF SUNFLOWER PROTEIN

The amino acids can be arranged into groups according to their ionizable groups found in the side chains. Each ionizing group has a charge after a loss of proton and a dissociation constant K_R ($pK_R = -\log K_R$). The amino acid composition of sunflower protein (Sosulski and Fleming, 1977) were converted into mole fractions and then grouped accordingly. At isoelectric point the net charge is zero. The net charge is calculated as:

$$Net\ charge = \sum M_i(+1) \left[1 - \frac{10^{pH-pK_R}}{1+10^{pH-pK_R}} \right] + \sum M_i(-1) \left[\frac{10^{pH-pK_R}}{1+10^{pH-pK_R}} \right] \quad (A.1)$$

Where M_i is the mole fraction of amino acid group. Equation (A.1) is derived by considering a two-step deprotonation equation of a simple amino acid as follows:



using the definitions of $pK_1 = -\log K_1$, $pK_2 = -\log K_2$, and $pH = -\log H^+$, then the above equations can be written as:

$$pH = pK_1 + \log([HA]/[HAH^+]) \quad (A.4)$$

$$pH = pK_2 + \log([A^-]/[HA]) \quad (A.5)$$

At isoelectric point, (pI), $[A^-] = [HAH^+]$, that is the net charge is 0. Therefore, from

Equations (A.4) and (A.5):

$$\begin{aligned} 2\text{pH} &= \text{pK}_1 + \text{pK}_2 + \log\left(\frac{[\text{HA}][\text{A}^-]}{[\text{HAH}^+][\text{HA}]}\right) \\ &= \text{pK}_1 + \text{pK}_2 \end{aligned} \quad (\text{A.6})$$

Thus, $\text{pI} = \text{pH} = (\text{pK}_1 + \text{pK}_2)/2$. This is the pH of neutral solution of pure amino acid. With known values of pK_R 's (available from Lehninger, 1982) the fraction ff_R of any species that has deprotonated can be calculated as:

$$\text{pH} = \text{pK}_R + \log (\text{ff}_R/(1 - \text{ff}_R)) \quad (\text{A.7})$$

solving for ff_R yields:

$$\text{ff}_R = \frac{10^{\text{pH}-\text{pK}_R}}{[1 + 10^{\text{pH}-\text{pK}_R}]} \quad (\text{A.8})$$

Therefore, the net charge (Z) of ionizable amino acid mixture can be computed as:

$$\text{Z} = \sum(+1)(1-\text{ff}_1) + \sum(-1) (\text{ff}_2) \quad (\text{A.9})$$

that is:

$$\begin{array}{ccc} \text{Net charge} = & \text{sum of positive charges} & + \text{sum of negative charges} \\ & \text{before deprotonation} & \text{after deprotonation} \end{array}$$

which is the same as Equation (A.1) at isoelectric point net charge = 0. Therefore, with known values of pK_R 's and the fraction ff_R (amino acids composition of the protein), the value of pH at the isoelectric point can be calculated by the iterative method. The pK_R 's of amino acids bonded inside a protein change dramatically. The values of pK_R 's and charges of these bonded amino acids (grouped) can be found in the literature (Lehninger, 1982) as listed in Table A.1.

Table A.1 Values of pK_R and charges of ionizable amino acid groups
(Lehninger, 1982).

Amino acid group	Charge after loss of proton	pK_R	Mole fraction
α -COOH (Glycine, Serine, and Threonine)	-	3.75	0.160
Non- α -COOH (Aspartate and Glutamate)	-	4.6	0.414
Imidazolium (Histidine)	0	7.0	0.016
Non- α - NH_2 (Lysine)	0	10.2	0.026
Phenolic (Tyrosine)	-	9.6	0.014
Guanidinium (Arginine)	0	12.5	0.057
Sulfhydryl (Cysteine)	-	8.3	0.030

Using an iterative method, the isoelectric pH for sunflower protein was found to be 3.6.

APPENDIX B

CALIBRATION OF THE TURBIDIMETER FOR ON-LINE MEASUREMENTS OF SOLIDS CONCENTRATION

Measurement of solids concentration by filtration followed by drying is not only time consuming, but also susceptible to errors due to contamination and loss of material during transfer and washing. Measurements of light transmission through a suspension of known solids concentration provides a practical method for determination of the mean particle size. The method is simple and data can be analysed rapidly for process control purposes. The transmission (Tr) of light through a dilute monodisperse suspension is given by Beer-Lambert's law as:

$$Tr = \frac{I}{I_0} = \exp(-\epsilon Cs l) \quad (B.1)$$

where I_0 is the intensity of the light source of wavelength λ_0 , I is the intensity of the emerging beam, l is the travel path, Cs is the solids concentration per unit volume, and ϵ is the absorbance coefficient. The Beer-Lambert's law can be used only if ϵ is known and a linear relationship exists between the $\ln(Tr)$, the solids concentration (Cs) and the travel path (l). For suspensions with high solids concentration and larger particles, the reduction in light intensity (I) as it traverses the sample (of thickness χ) due to the scattering process is measured by turbidity (Υ) which is defined as:

$$\begin{aligned} \frac{dI}{d\chi} &= -\Upsilon I \\ Tr &= \frac{I}{I_0} = \exp(-\Upsilon l) \end{aligned} \quad (B.2)$$

Calibration Experiments

White sunflower protein particles ($< 50 \mu\text{m}$) and two photo cell sensors were used in this study. The experimental setup is shown in Figure B.1. The photo cell sensors were constructed using infrared light emitting diodes (OP 133 IRED) and receiver (OP 804) manufactured by Texas Instruments, Carrollton, TX. The wavelength of the emitted light was 900 nm. These diodes (emitter and receiver) were embedded, facing each other, in a dark PVC ring which was clamped on the glass tube fixed on the line. The signals from the diodes were sent to the analyzer and displayed as % transmission ($Tr = I/I_0$). For clear solutions (solid free), the % Tr was set at 100 %. This was checked each time a different photo cell sensor or liquid medium was used. The travel paths for the photo cell sensors were 1.86 and 2.66 cm. The travel path was measured from the emitting source to the receiving point inside the diodes. Protein particles were suspended in a clear and saturated aqueous sunflower protein solution at pH 4 (minimum solubility pH for sunflower protein). The mean particle size of the protein particles was determined using a Coulter Counter model TAPI (Coulter Electronics, Inc., Hialeah, FL).

During the experiment the suspension was prepared by adding known amount of solids in a known volume of clear filtered liquid. Sometimes the dilute suspension was made by adding clear liquid to the existing suspension. The solids were kept in suspension by a magnetic stirrer which swept the entire base of the 500 mL beaker to create a homogeneous suspension. For transmission measurements, the suspension was recirculated at a flow rate of about 1 L/min (using a peristaltic pump) through a short glass tube with a turbidimeter attached onto it (see Figure B.1) The speeds of the pump and the magnetic stirrer were monitored to avoid suction of the air bubbles in the flow lines. Readings were taken after the % Tr was steady (normally after 5-10 min). At high solids concentration the steady value was reached faster than in the dilute suspensions. In the absence of air bubbles or foam, the pump speed had no effect on % Tr readings.

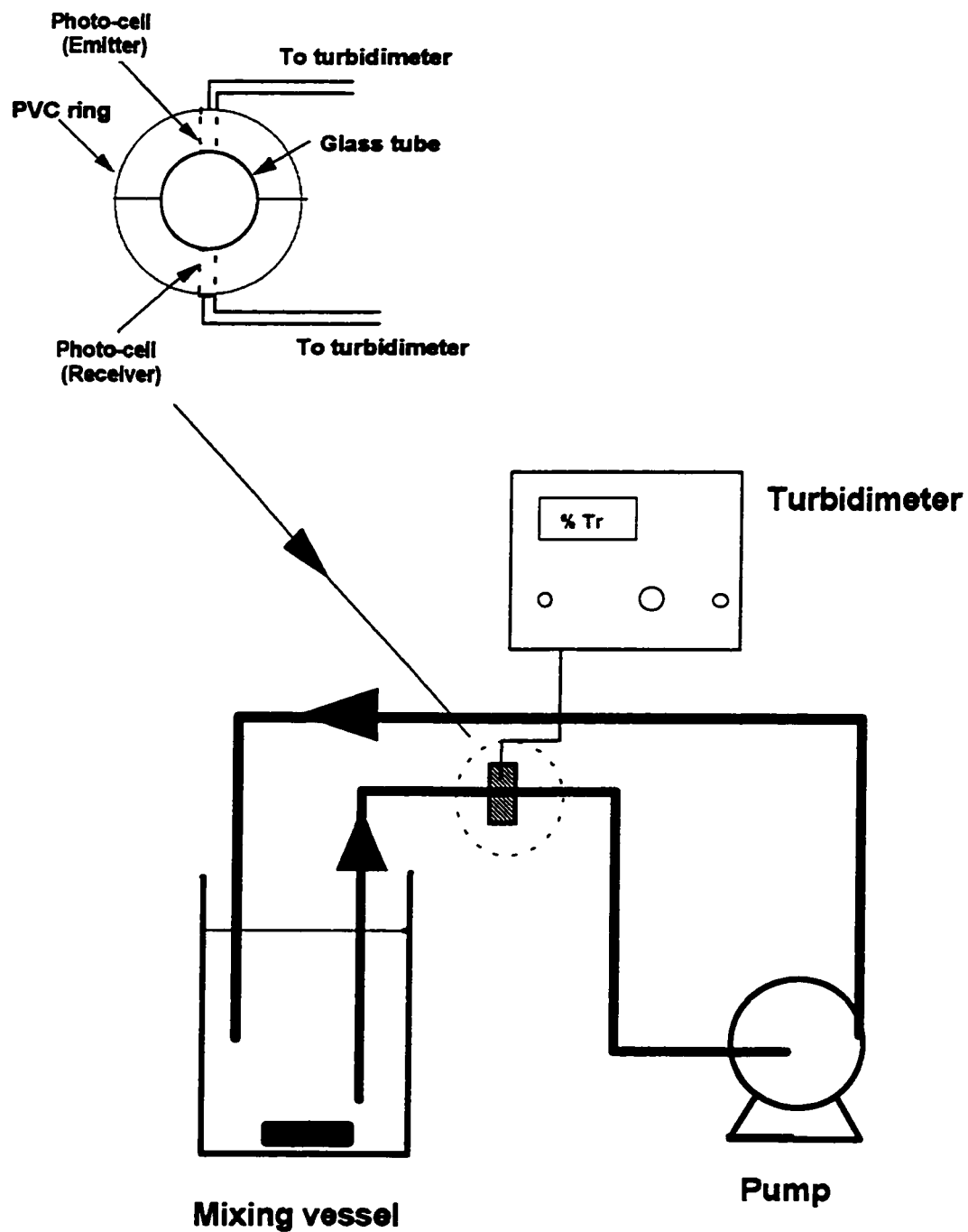


Figure B.1 Experimental setup for the calibration of the turbidimeter

Experimental Results

For all test samples used in this study, the plots of $\ln(Tr)$ as a function of solids concentration showed a similar trend as shown in Figure B.2. Samples with small particles (protein suspensions) obeyed the Beer-Lambert's law up to solids concentrations of about 1 % w/w (ca. 0.01 g/mL). Whereas samples with large particles (> 50 μm), the range was up to about 10 % w/w (ca. 0.1 g/mL) and the slopes of the lines decreased with increases in the mean particle size (Further studies using different types of materials can be found in Raphael and Rohani, 1996b). In other words, the Beer-Lambert's law is violated as the number of particles per unit volume increases. At low and high solids concentrations, the %Tr data from all photo cell sensors approached 100 % and 0%, respectively. For a dilute suspension composed of small uniform particles and a measuring photo cell with a fixed travel path (l) and fixed absorption coefficient, ϵ , the transmission is related to concentration (Beer-Lambert's law) by:

$$\ln(Tr) = -\kappa Cs \quad (\text{B.3})$$

where κ is a constant. This equation can be extrapolated to include the high solids concentration range using the Taylor series expansion as:

$$\begin{aligned} \ln(Tr) &= -\kappa Cs = -\kappa e^{(\ln Cs)} \\ \ln(Tr) &= A_0 + A_1 \ln Cs + A_2 (\ln Cs)^2 + A_3 (\ln Cs)^3 + \dots + A_n (\ln Cs)^n \end{aligned} \quad (\text{B.4})$$

where A_i 's are the coefficients of the approximating polynomial. The parameters A_i 's in Eq. (B.4) were obtained from experimental data by regression analysis. For the range of solids concentration used in this study, the highest order was 6 for the protein suspension. Regression analysis was used to determine the unknown coefficients. Figure B.3 shows the best fitting equation for the protein suspension ($Y = -2.548 + 3.083X - 0.163X^2 - 0.442X^3 - 0.08852X^4 - 0.00677X^5 - 0.000184X^6$ with $R^2 = 0.998$; where Y is $\ln(Tr)$ and X is $\ln(Cs)$). This equation was obtained specifically for the 6-mm tube using a photo-cell with $l = 2.66$ cm, and it provided good reproducibility of on-line solids concentration measurements of sunflower protein from the measured %Tr data.

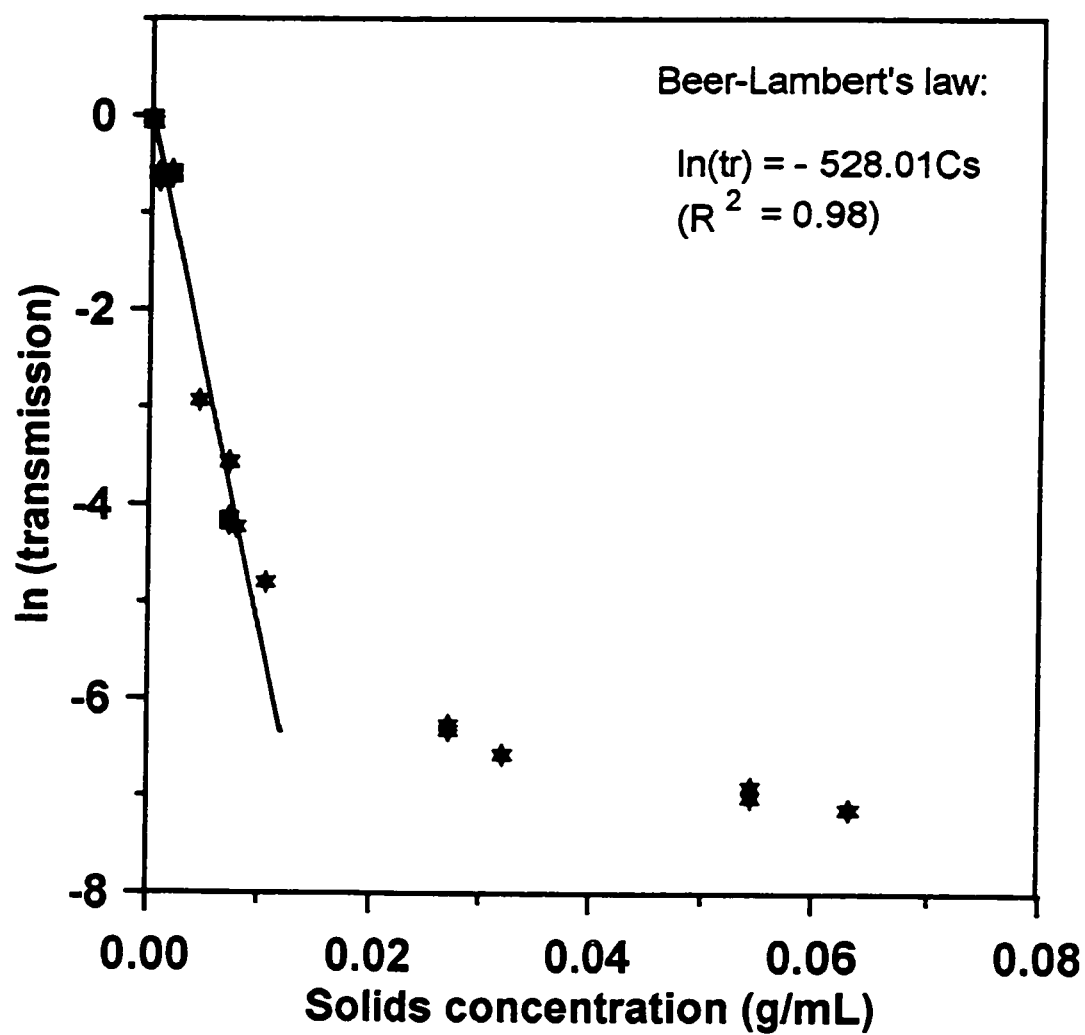


Figure B.2 Fit of Beer-Lambert's law to experimental data: $\ln(\text{Tr})$ as a function of protein solids concentration for a photo-cell with $l = 2.66$ cm.

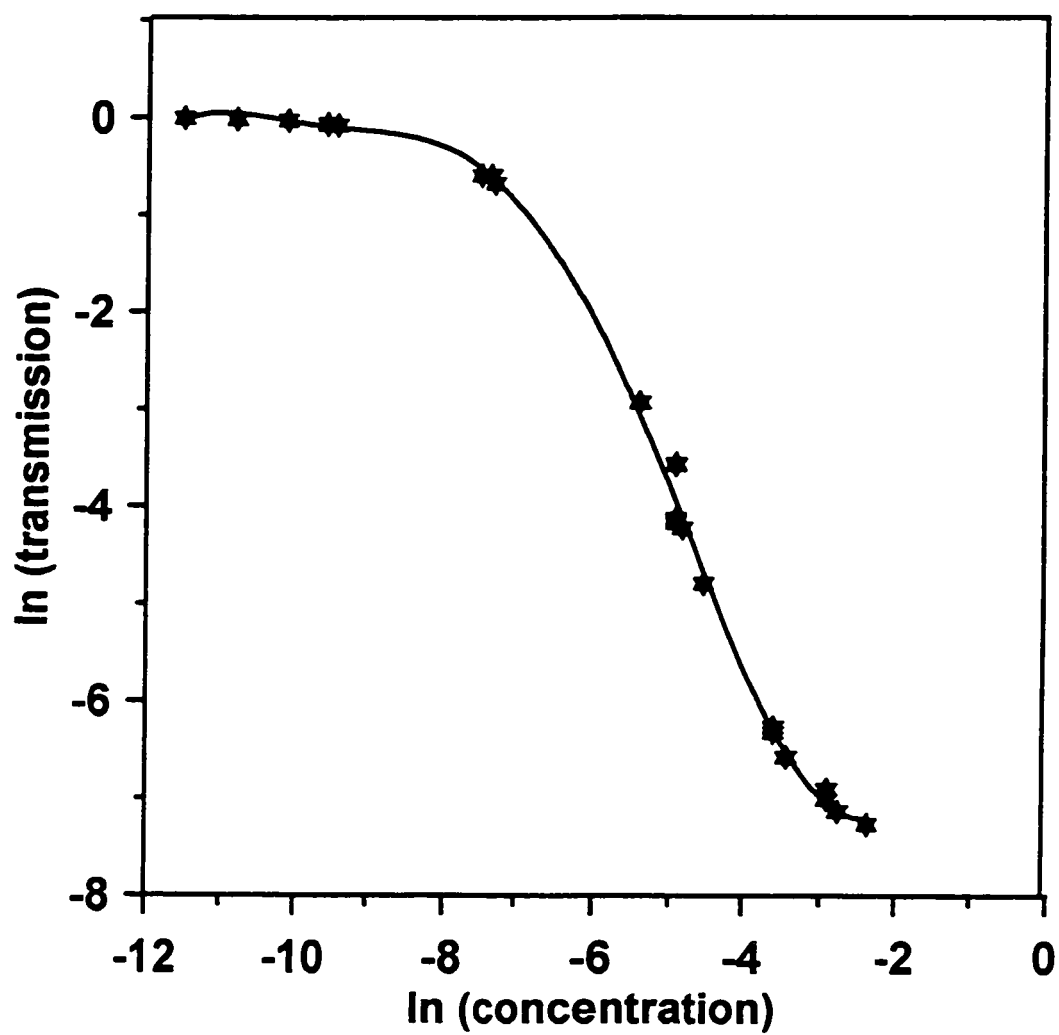


Figure B.3 Polynomial fit ($\ln(\text{Tr})$ as a function of $\ln(\text{Cs})$) for protein particles suspension.

APPENDIX C

MEASUREMENTS OF PSD USING COULTER COUNTER

C.1 Determination of the Number of Particles in the Sample (Number Count)

The number of particles in the sampled volume was determined by dilutions method. Experimental data were entered in a spreadsheet similar the one shown in Table C.1. First, the actual volumes of the dilution electrolyte (cell F,6) and the collected slurry (cell F,9) were determined by weight difference method. Volumes of the samples were calculated by dividing the weights with the density. Densities of the electrolyte and the slurry were very close to the density of water. Second, known volume of the diluted slurry (cell K,3 in Table C.1) was added into a known volume of electrolyte (I,2) in a Coulter Counter (CC) beaker. Using the Coulter Counter, a known volume of the sample was sampled (K,4) and the time used to collect the sample was recorded (J,2). This sampling procedure was repeated 3 times and the average count of particles in the sampled volume was recorded (K,5). Thirdly, the total number of particles and particle concentration in the original slurry from the precipitator (F,9) were calculated, (K,9) and (K,10), respectively. These results were then used for calculations of the population density.

C.2 Calculations of the Mean Particle Size and the Coefficient of Variation From the Coulter Counter Data

Sixteen Coulter Counter channels (nc) were used for particle size measurements. The size range (smallest size to the largest size) of the channels used depended on the tube size used (H,2). The normalized differential volume fractions (Δv_i) for each channel

size (L_i) were entered in column 3, below DIF. Equation (2.23) was used to calculate the mean particle size (\bar{d}_m), shown in (M,4) as a sum of ($L_i \cdot \Delta v_i$) for all 16 channels. The CV was calculated using Equation (2.24). Calculated values were entered in (Q,5).

C.3 Calculations of the Population Density From the Coulter Counter Data

Coulter Counter channels are configured in a geometrical ratio. Two consecutive channels have a volume ratio of 2 that is:

$$V_{ci} = 2V_{ci-1} \text{ or } L_i = L_{i-1} \cdot [2^{1/3}] \quad (C.1)$$

The number of particle count for each channel (ΔN_i) was given by the Coulter Counter or calculated from the volume fractions as follows (Coulter Counter users' manual):

$$\Delta N_i = K_{fi} R_i \Delta v_i \quad (C.2)$$

where K_{fi} is the conversion factor for the particle concentration and is given by:

$$K_{fi} = \frac{NT}{\sum_{i=1}^{i=nc} R_i \Delta v_i} \quad (C.3)$$

where NT is the particle concentration in the undiluted suspension (K,10). R_i is the relative number. This is the equivalent number of particles in the i th channel with the total volume as the volume of a single particle in the largest channel ($nc=16$). That is, 1 particle in channel nc is equivalent to 2 particles in channel ($nc-1$) or 4 particles in channel ($nc-2$) or in general, for the i th channel it is $R_i = 2^{(nc-i)}$.

The size of the channel (L_i) represents the mid value of that channel. The span of the i th channel (ΔL_i) was given by the average of two channels adjacent to it as: $(L_{i+1} - L_{i-1})/2$. The population density (p_i) was calculated using Equation (2.25) given

as:

$$p_i = \frac{\Delta N_i}{\frac{(L_{i+1} - L_{i-1})}{2}} \quad (C.4)$$

where ΔN_i represents the measured particle concentration in the i th channel. the calculated values were entered in column 10, below p_i .

Table C.1 Sample data sheet for calculations of the PSD (particle count, mean particle size, CV, and the population density) from the experimentally measured data using Coulter Counter.

1	2	3	4	5	6	7	8	9	10
A. Run no./Port no.	L1/4								
B. Temp. (C)	23.0								
C. Feed ratio (v/v)	1.0	Sample collection from the precipitator for Coulter Counter analysis							
D. Material	Protein	Sampling bottle wt. (g)	Bottle + electrolyte (g)	Wt. of electrolyte (g)	Vol. of electrolyte (mL)	Bottle + electrolyte + sample (g)	Sample wt. (g)	Sample vol. (mL)	Total slurry vol (mL)
E. % Tr	1.15								
F. Solids conc. (g/mL)	0.00552	23.6870	101.1690	77.4820	77.6373	105.0353	3.8663	3.8740	81.5113
G. Coulter Counter Analysis	Particle count using Coulter Counter								
H. Tube size (µm)	200	Vol. of sample added (mL)	CC sampled vol. (mL)	Avg. count (no.)	Particle conc. (no./mL)	Total particles in CC beaker (no.)	Sample conc. (no./ml)	Total particle count (no.)	Original conc., NT (no./mL)
I. Vol. of elect. (mL)	100.0								
J. Sampling time (s)	12.5								
K. Particle count (no.)	7397	4.00	2.0	7397	3699	384644	96161	7838210	2.023E+06
L. Determination of PSD using Coulter Counter									
ch. size L_i (µm)	V_{ci} (µm ³)	nc	Δv_i DIF (avg)	$L_i^* \Delta v_i$	$(d_i - d_m)^2 \Delta v_i$	R_i	$\Delta v_i^* R_i$	$\Delta N_i = K_{ff} \Delta v_i^* R_i$	$P_i = \frac{\Delta N_i}{\Delta L_i}$
2.52	8.377	1	0.000	0.000	0.0000	32768	0.000	0.0	0.0
3.18	16.75	2	0.000	0.000	0.0000	16384	0.000	0.0	0.0

Table C.1 Continued

4.00	33.51	3	0.000	0.000	0.000	0.0000	8192	0.000	0.0	0.0
5.04	67.02	4	0.000	0.000	0.000	0.0000	4096	0.000	0.0	0.0
6.35	134.0	5	0.000	0.000	0.000	0.0000	2048	0.000	0.0	0.0
8.00	268.1	6	0.011	0.090	0.090	6.4974	1024	11.463	348273.9	186711
10.08	536.2	7	0.026	0.263	0.263	12.6559	512	13.374	406319.6	172891
12.7	1072	8	0.054	0.688	0.688	20.3612	256	13.862	421155.9	142234
16.0	2145	9	0.082	1.314	1.314	21.2523	128	10.508	319251.1	85576
20.2	4289	10	0.118	2.369	2.369	16.7234	64	7.520	228473.5	48608
25.4	8578	11	0.149	3.793	3.793	6.6798	32	4.777	145141.2	24509
32.0	17160	12	0.181	5.792	5.792	0.0013	16	2.895	87968.7	11790
40.3	34310	13	0.190	7.680	7.680	12.9104	8	1.524	46289.0	4924
50.8	68630	14	0.147	7.484	7.484	51.5929	4	0.589	17900.7	1511
64.0	13730	15	0.041	2.620	2.620	41.7126	2	0.082	2487.4	167
80.7	27450	16	0.000	0.000	0.000	0.0000	1	0.000	0.0	0.0
M. Sum for all channels			1.00	32.09	190.39			66.59	2023261	
N. Mean particle size, dm (μm):				32.1						
O. VAR				190.4	$K_{\Pi} = NT/\Sigma(R_i \cdot v_i)$			30381.6		
P. STD = $\sqrt{\text{VAR}}$				13.8						
Q. CV % = STD/dm *100				43.0						

APPENDIX D

COMPUTER ALGORITHMS FOR SOLVING THE TUBULAR PRECIPITATOR MODEL

The population balance equation for the tubular precipitator was solved using the Orthogonal Collocation-Multiple Shooting Method. The model equation was an IVBVP (initial-value-boundary-value problem) ordinary differential equation. The initial value problem was solved using the collocation method and the boundary problem was solved using the non-linear multiple shooting method (MUSN package). The optimum parameters for the model were determined from the experimental data using the global optimization method, Simulated Annealing Method (SIMANN package). For predictions of the experimental results from the model, the initial value problem was solved using Gears method (LSODE package for stiff and non-stiff problems). Standard Fortran 77 source codes were written and linked with packages (MUSN, SIMANN, and LSODE) obtained from the NETLIB (database for numerical and scientific computing software, WWW.NETLIB.ORG). Figures D.1 and D.2 shows the flow sheets of the programs used in the determination of the optimum model parameters from the experimental data and model predictions of the experimental data, respectively.

D.1 Determination of the Optimum Model Parameters From the Experimental Data (Figure D.1)

TUBE_MOD.FOR: This is the main program. The experimental data to be used in the optimization routine were read from the data file TUBEN8.DAT. These included the initial estimates of parameters (Table 5.4), operating conditions (feed flow rate, protein feed concentration, volume feed ratio, precipitator length, and sampling ports distances),

number of the experimental runs, and the population densities of samples from the two sampling ports (boundary conditions) for each run. These parameters were changed into respective dimensionless forms using Equation (5.5)

TUBE_OPT.FOR: This is the optimization calling program. It was the first program to be called by the main program. The parameters for the optimization routine, **SIMANN.FOR**, were entered here. Initial estimates of the parameters were transferred from the main program to this subroutine. The search range and the tolerance of the **SIMANN.FOR** were entered here. Also the set of the equations used in the objective equation (Equation 5.53) were calculated in this program in the subroutine **FCN** using Equations 5.54 and 5.55. This subroutine **FCN** sent out the model parameters optimized by the **SIMANN.FOR** and the boundary condition data to the subroutine **TUBEN8.FOR** for the calculations of the population balance equation. **TUBEN8.FOR** returned the calculated population densities at selected ports (2 and 3) for comparison with the experimental data. Once the objective equation was satisfied the program stopped and printed out the results. Otherwise new parameters were calculated by **SIMANN.FOR** for another iteration.

SIMANN.FOR: This is the optimization program called by the **TUBE_OPT.FOR**. It is a standard program available at NETLIB.

TUBEN8.FOR: This is a calling program for the ODE solver program (**MUSN.FOR**). It was called by the subroutine **FCN** in the **TUBE_OPT.FOR** each time the PBE was to be solved using a new set of the model parameters. At the end of each pass the program was reset to its original values. This program solved 17 first order ODEs. Sixteen equations represented the interior node (collocation nodes) points (Equation 5.45) and 1 equation for the initial condition Equation 5.49. A total of 101 node points were used to solve the set of ODEs between the two boundaries using the program **MUSN.FOR**.

MUSN.FOR: This is a boundary value ODE solver in the ζ direction. It was called by the **TUBEN8.FOR** which supplied the initial guesses for this program via the subroutine

YOT, the set of the ODEs to be solved via the subroutine FDIF, and the Jacobians of the boundary conditions via the subroutine G.

FDIF: This is a subroutine in the TUBEN8.FOR which inputs the set of the ODEs to be solved by the MUSN.FOR. FDIF called the program SCOEFF.FOR to get the zeros and the integration weights of the Laguerre polynomial of order 8, matrices Y (Equation 5.26), Φ (Equation 5.29), T (Equation 5.32), Φ^{-1} , and the matrix product $\Phi^{-1}.T$. Then it called the program AGGBRK.FOR for the values of the aggregation and breakage terms I_{x_k} and I_{∞} as presented in Equations 5.34a and 5.39, respectively.

AGGBRK.FOR: This is the program for solving the aggregation and breakage terms I_{x_k} and I_{∞} in Equations 5.34a and 5.39. The program called the SMATRIX.FOR for the values of the Laguerre zeros, Gaussian-Laguerre quadrature weights, and the matrix Φ . The integration was done using the quadrature method as presented in Equation (5.33).

SCOEFF.FOR: This is the program for calculating the matrices Y , T , Φ (also Φ^{-1}) as given by Equations 5.26, 5.32, and 5.29, respectively. The program called LAGUERS.FOR for the zeros and integration weights of the Laguerre polynomial, SMATRIX.FOR for calculating Φ and T matrices, and SCALC.FOR for the calculation of the Φ^{-1} matrix. SCOEFF.FOR sent out x , w_i , and matrices T , Φ , and the product of $\Phi^{-1}.T$ to the subroutine FDIF.

LAGUERS.FOR: This is the program for calculating the zeros and the integration weights of the 8th order Laguerre polynomial. The Laguerre polynomial was approximated using the Gamma function (Stroud and Secrest, 1966) and the zeros were determined using an iterative method, Newton Raphson method.

D.2 Model Predictions of the Experimental Data (Figure D.2)

PSD_PRD.FOR: This is the main program for solving the model equation as an initial value problem. The program read the input data from the data file, PSD_PRD.DAT.

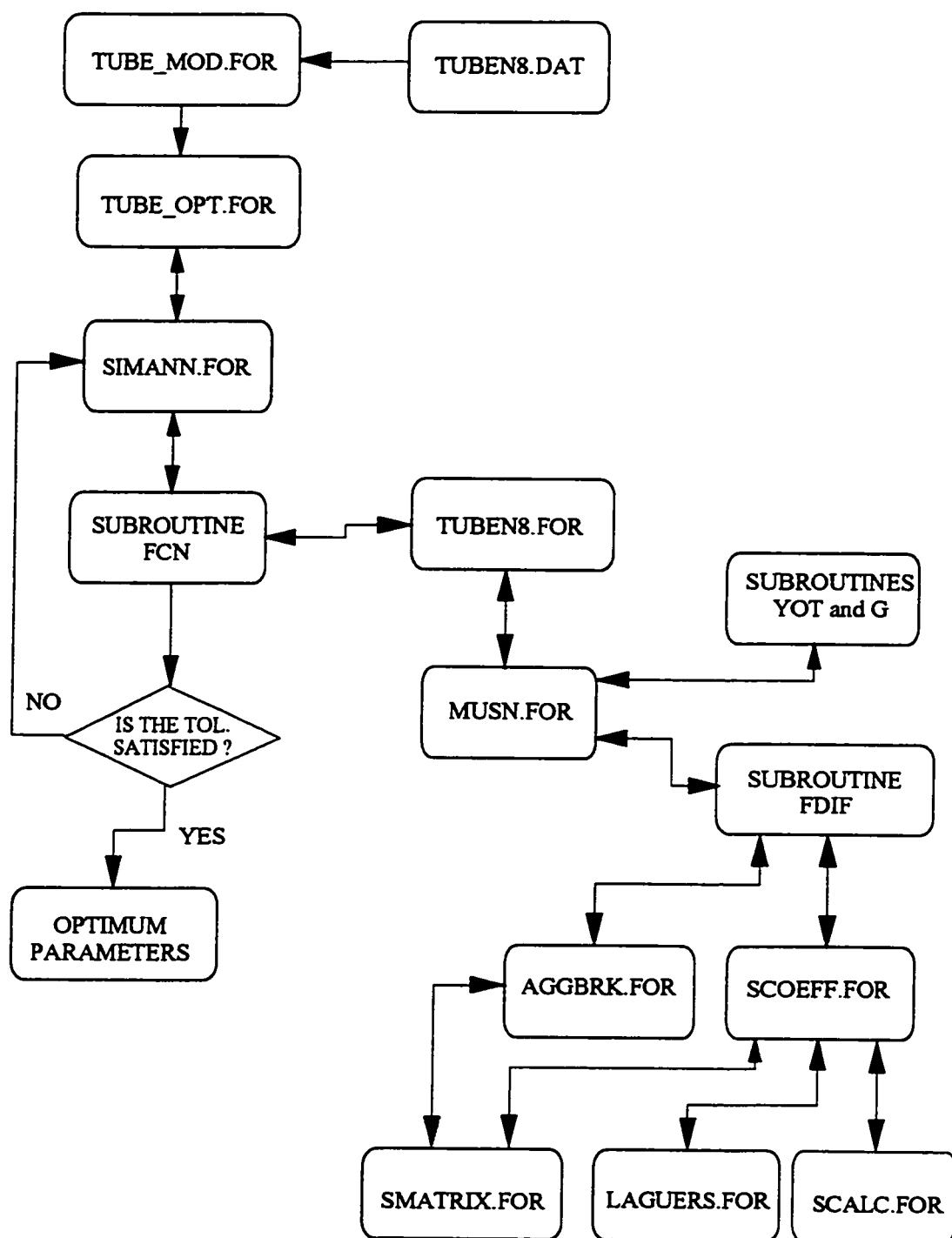


Figure D.1 The flow sheet of the computer programs used in the calculation of the optimum model parameters from the experimental data.

Input data included the optimum model parameters, tubular precipitator operating condition (feed flow rate, protein feed concentration, volume feed ratio, precipitator length, and sampling port distance), population density of the precipitate obtained from the sampling port, and the desired exit port (or distance) along the tubular precipitator. The solution of the model equations was generated as a population density profile starting from the sampling port to the exit port using 101 node points. Zeros of the Laguerre polynomial were used for characterization of the particle size distribution. Equations 5.54 and 5.55 were used to calculate the predicted mean particle size and the coefficient of variations from the calculated population densities. This was done in the program PSD_PORT.FOR. Advancement of the solution in the ζ direction for the 9 node points (8 interior and 1 for initial condition) was done using Gears methods (LSODE package). A total of 17 first order ODEs representing the collocation points and the IC were solved at all 101 node points.

LSODE.FOR: This is the initial value ODE solver. It implements Gears method for solving the stiff and non-stiff ODEs. This program package is available at NETLIB. The set of the ODE to be solved were entered in the subroutine FCN. The aggregation and breakage terms and the matrices (Y , T , Φ , and Φ^{-1}) were calculated as before using the programs AGGBRK.FOR and SCOEFF.FOR. The model parameters were transferred to this subroutine using a common block.

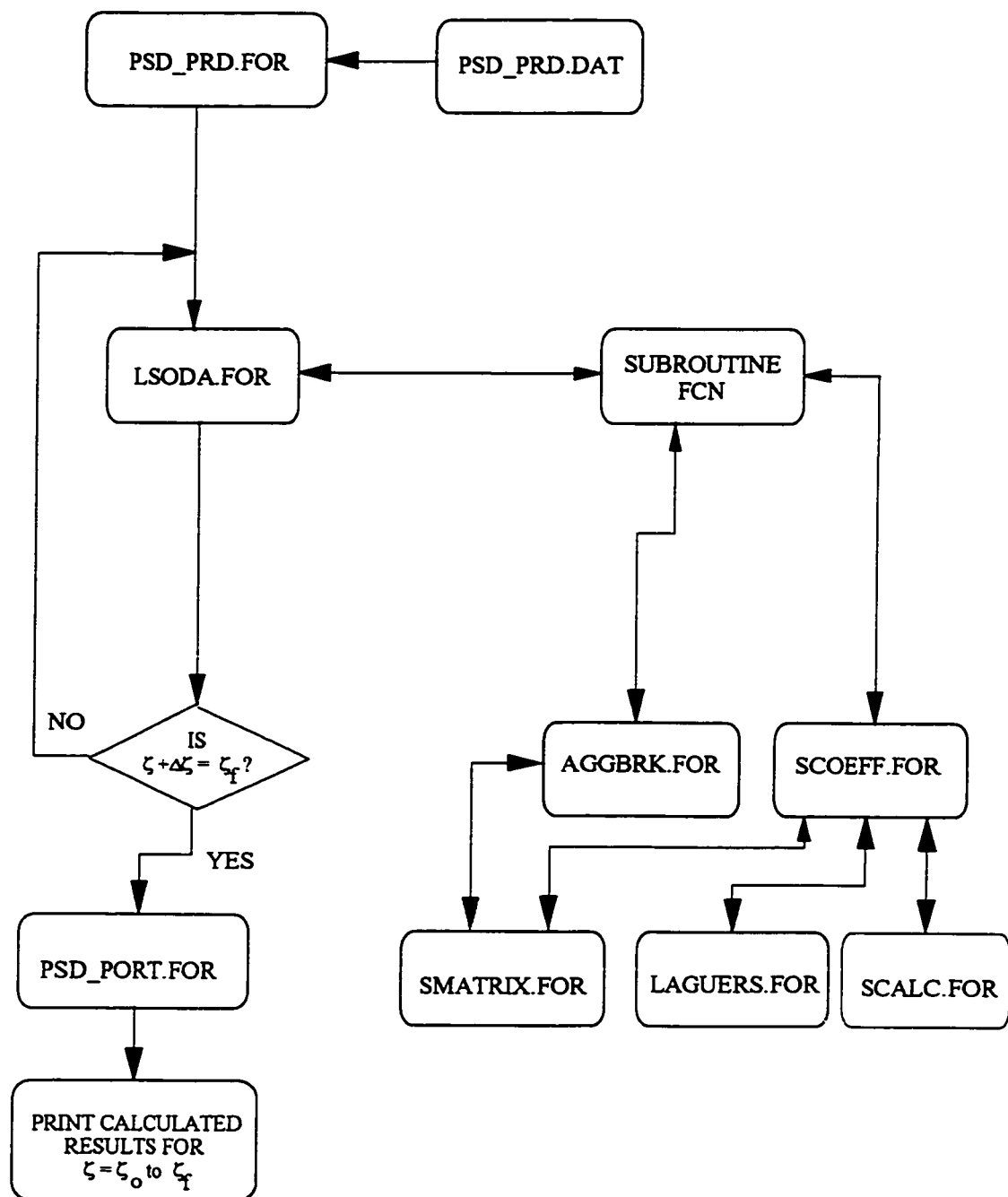


Figure D.2 The flow sheet of the computer programs used in the predictions of the experimental data from the model.

VITA

Name: Matheo Lue Raphael

Date of Birth: February 11th 1960, Singida, Tanzania

Permanent Address: University of Dar-Es-Salaam
Chemical and Process Engineering Department
P. O. Box 35131
Dar-es-Salaam, Tanzania.

September, 1984 B.Sc. 1st class, Hon, (Chemical Engineering) 1980-1984, Univ. of Dar-es-Salaam, Tanzania.

May, 1988 M.Sc. (Chemical Engineering) 1986-1988, Texas A & M Univ., College Station, TX, U.S.A.

October, 1991 Industrial Training: 1990-1991, BP Chemicals International, Baglan Bay, Wales, U.K.

Publications

1. Bukur, D. B., S. A. Patel, and M. Raphael, "Hydrodynamic Studies in Fischer-Tropsch Derived Waxes in Bubble Column", Eng. Commun. Fund. 60, 63-78 (1987).
2. Bukur, D. B., S. A. Patel, J. G. Daly, M. Raphael, and G. B. Tatterson, "Hydrodynamics of Fischer-Tropsch Synthesis in Slurry Bubble Column Reactors", Report to the DOE for Contract No. DE-AC22-84PC0027 (1987c).
3. Raphael, M., "Undergraduate Laboratory Manual ", CPE Dept. (1991).
4. Raphael, M., S. Rohani, and F. Sosulski, "Isoelectric Precipitation of Sunflower Protein in a Tubular Precipitator", Can. J. Chem. Eng. 73, 470-483 (1995).
5. Raphael, M. and S. Rohani, "On-Line Estimation of Solids Concentration and Mean Particle Size Using Turbidity Method", J. Powder Technology 89, 157-163 (1996).

6. Raphael, M. and S. Rohani, "Isoelectric Precipitation of Sunflower Protein in an MSMRP: Modelling of PSD With Aggregation", Chem. Eng. Sci. 51, 4379-4384 (1996).
7. Raphael, M., S. Rohani, and F. Sosulski, "Recent Studies on Recovery of Oilseed Protein by Precipitation", in "Separation and Purification by Crystallization", edited by Botsaris, G. D. and K. Toyokura, ACS Symposium Series 667, 188-209 (1997).

Conferences

1. Bukur, D. B., S. A. Patel, J. G. Daly, and M. Raphael, "Bubble Size and Gas-Liquid Interfacial Area Measurement Using Molten Paraffin Waxes in Bubble Columns", Proceedings of the AIChE Annual Meeting, New York, NY, Nov. 15-17 (1987).
2. Bukur, D. B., S. A. Patel, J. G. Daly, and M. Raphael, "Effect of Operating Conditions on Bubble Column Hydrodynamics Using Molten Waxes", Proceedings of International Meeting on Chem. Eng. and Biotechn. 22nd Exhibition-Congress, Frankfurt Am Main, W. Germany June 5-11 (1988).
3. Raphael, M., S. Rohani, and F. Sosulski, "Sunflower Protein Recovery in a Tubular Precipitator", Proceedings of 44th Can. Chem. Eng. Conference, Calgary 637-638, October 2-5 (1994).
4. Raphael, M., S. Rohani, and F. Sosulski, "Comparison of the PSD and Yield of Sunflower Proteins From the MSMRP and a Tubular Precipitator", Proceedings of the 1995 AIChE Annual Meeting, Miami Beach Florida, pg 34, Nov 12-17 (1995).
5. Raphael, M., S. Rohani, and F. Sosulski, "Recovery of Oil Seeds Protein by Precipitation: Isoelectric Precipitations of Canola and Sunflower Proteins", Proceedings of ACS Vol 584: Purification by Crystallization, 1995 International Chemical Congress of Pacific Basin Societies, PACIFICHEM, Honolulu, Hawaii, USA, Dec 17-22 (1995).
6. Raphael, M., S. Rohani, and F. Sosulski, "Isoelectric Precipitation of Sunflower Protein in Batch and Continuous Flow Precipitators", Proceedings of the 13th Symposium on Industrial Crystallization, Toulouse, France, Sept. 16-19 (1996).